STUDIES OF CRYSTALLIZATION OF NATURAL

FIBERS-POLYPROPYLENE COMPOSITES

Usa Somnuk

A Thesis Submitted in Partial Fulfillment of the Requirements for the

Degree of Doctor of Philosophy in Polymer Engineering

Suranaree University of Technology

Academic Year 2007

การศึกษาการตกผลึกของเส้นใยธรรมชาติ-พอลิโพรพิลีนคอมพอสิท

นางสาวอุษา สมนึก

STUDIES OF CRYSTALLIZATION OF NATURAL

FIBERS-POLYPROPYLENE COMPOSITES

Suranaree University of Technology has approved this thesis submitted in partial fulfillment of the requirements for the Degree of Doctor of Philosophy

Thesis Examining Committee

_____

(Asst. Prof. Dr. Utai Meekum)

Chairperson

_____

(Asst. Prof. Dr. Yupaporn Ruksakulpiwat)

Member (Thesis Advisor)

_____

(Asst. Prof. Dr. Nitinat Suppakarn)

Member

_____

(Asst. Prof. Dr. Wimonlak Sutapun)

Member

_____

(Assoc. Prof. Dr. Ittipol Jangchud)

Member

_____ _____

(Assoc. Prof. Dr. Saowanee Rattanaphani) (Assoc. Prof. Dr. Vorapot Khompis)

Vice Rector for Academic Affairs Dean of Institute of Engineering

USA SOMNUK : STUDIES OF CRYSTALLIZATION OF NATURAL FIBERS–

POLYPROPYLENE COMPOSITES. THESIS ADVISOR : ASST. PROF.

YUPAPORN RUKSAKULPIWAT, Ph.D 196 PP.

CRYSTALLIZATION/POLYPROPYLENE (PP)/INJECTION MOLDING/COMPOSITES

NATURAL FIBERS/NUCLEATION/SPHERULITES

In this research, polypropylene (PP) composites composed of natural fibers i.e., vetiver grass, rossells, and sisal were prepared using an injection molding machine. An alkalization treatment of vetiver grass was carried out to obtain alkali-treated vetiver grass. Thermal characteristics, chemical compositions, and surface morphology of the alkali-treated vetiver grass were examined. It was found that the alkali-treated vetiver grass exhibited higher thermal stability than untreated vetiver grass. The microstructure of injection-molded PP and PP composites showed a distinct skin layer due to shear-induced crystallization. The effect of vetiver size and vetiver content on rheological, thermal, and mechanical properties of the composites was elucidated. In addition, the effect of vetiver size and vetiver content on shear-induced crystallization layer was also examined. It was found that vetiver fiber-PP composites exhibited higher viscosity, tensile strength, and Young's modulus than vetiver powder-PP composites. On the other hand, normalized thickness of shear-induced crystallization layer of vetiver fiber-PP composites was lower than that of vetiver powder-PP composites. An increase in vetiver content led to an increase in viscosity, tensile strength, Young's modulus of PP composites. However, a decrease in normalized thickness of shear-induced crystallization layer was observed with increasing vetiver content.

In addition, the effect of types of natural fibers i.e., vetiver fiber, rossells, and sisal on shear-induced crystallization layer, rheological, thermal, and mechanical properties of

PP composites was also studied. It was observed that the viscosity of vetiver fiber-PP composite was higher than that of rossells-PP, and sisal-PP composites. Rossells-PP composite had higher Young's modulus and impact strength than those of PP composites from vetiver fiber and sisal. The normalized thickness of shear-induced crystallization layer of vetiver fiber-PP, rossells-PP, and sisal-PP composites showed insignificant differences. Additionally, Differential Scanning Calorimetry (DSC) curves of natural fiber-PP composites of the core region obviously showed more multiple and boarder peaks than those of the skin region. This indicated that several crystallographic forms could be taken place in the core region.

Furthermore, effect of processing conditions i.e., screw speed, injection speed, holding pressure, and mold temperature on shear-induced crystallization layer, degree of crystallinity, gapwise crystallinity distribution, and mechanical properties of vetiver fiber-PP composite were investigated. It was shown that injection speed and mold temperature affected the normalized thickness of shear-induced crystallization layer and degree of crystallinity of the composites. However, processing conditions had insignificant effect on the mechanical properties of vetiver fiber-PP composites. There was no distribution of the degree of crystallinity throughout the thickness direction of the PP composites.

Moreover, the effect of natural fibers on quiescent crystallization of PP composites was investigated. A decrease in equilibrium melting temperature (T_m^o), a decrease in half time of crystallization, and an increase in the rate of crystallization were observed in the PP composites compared to those of neat PP. The presence of natural fibers in the composites led to a decrease in Avrami exponent. Transcrystallization of PP could be observed on the fiber surface. Additionally, spherulitic growth rates of the PP composites were lower than that of neat PP. The shperulitic growth rates combined with the crystallization rates were used to calculate number of effective nuclei. It was found that the number of effective

nuclei of natural fiber-PP composites was higher than that of neat PP. This suggested that natural fibers could act as a nucleating agent in the composites.

School of <u>Polymer Engineering</u>   Student's Signature _____

Academic Year 2007   Advisor's Signature _____

                                                        Co-Advisor's Signature _____

                                                        Co-Advisor's Signature _____

อุษา สมนึก : การศึกษาการตกผลึกของเส้นใยธรรมชาติ—พอลิโพรพิลีนคอมพอสิท
(STUDIES OF CRYSTALLIZATION OF NATURAL FIBERS-
POLYPROPYLENE COMPOSITES) อาจารย์ที่ปรึกษา : ผู้ช่วยศาสตราจารย์ ดร. ยุพาพร
รักสกุลพิวัฒน์, 196 หน้า.

ในงานวิจัยนี้ พอลิโพรพิลีนคอมพอสิทจากเส้นใยธรรมชาติ ได้แก่ หญ้าแฝก ปอแก้ว และป่าน
ศรนารายณ์เตรียมโดยกระบวนการฉีดขึ้นรูป หญ้าแฝกที่ปรับปรุงโดยอัลคาไลน์ได้มาโดยวิธีอัลคาไลน์เซ-
ชัน จากการตรวจสอบสมบัติทางความร้อน องค์ประกอบทางเคมี และโครงสร้างทางสัณฐานวิทยาของ
พื้นผิวของหญ้าแฝกชนิดที่ปรับปรุงโดยอัลคาไลน์ พบว่าหญ้าแฝกที่ปรับปรุงโดยอัลคาไลน์มีความเสถียร
ทางความร้อนสูงกว่าหญ้าแฝกที่ไม่ได้ปรับปรุงโดยอัลคาไลน์   ลักษณะโครงสร้างเชิงจุลภาคของพอลิ
โพรพิลีนและพอลิโพรพิลีนคอมพอสิทที่ขึ้นรูปโดยกระบวนการฉีดแสดงให้เห็นลักษณะผิว อันเนื่องมา
จากการตกผลึกภายใต้แรงเฉือนอย่างชัดเจน นอกจากนี้ได้ศึกษาผลของขนาดและปริมาณของหญ้าแฝกต่อ
สมบัติทางกระแสวิทยา สมบัติทางความร้อนและสมบัติเชิงกลของคอมพอสิท รวมทั้งได้ศึกษาผลของ
ขนาดและปริมาณของหญ้าแฝกต่อการตกผลึกภายใต้แรงเฉือนของคอมพอสิท จากผลการทดลองพบว่า
เส้นใยหญ้าแฝก—พอลิโพรพิลีนคอมพอสิทมีความหนืด ความแข็งแรงต่อการดึง และค่ามอดุลัสของยัง
สูงกว่าผงหญ้าแฝก—พอลิโพรพิลีนคอมพอสิท ในทางตรงกันข้าม ค่าชั้นความหนาที่เกิดจากการตกผลึก
ภายใต้แรงเฉือนของเส้นใยหญ้าแฝก—พอลิโพรพิลีนคอมพอสิท มีค่าน้อยกว่าค่าชั้นความหนาที่เกิดจาก
การตกผลึกภายใต้แรงเฉือนของผงหญ้าแฝก—พอลิโพรพิลีนคอมพอสิท การเพิ่มปริมาณหญ้าแฝกในคอม
พอสิทจะนำไปสู่การเพิ่มขึ้นของความหนืด ค่าความแข็งแรงต่อการดึง และค่ามอดุลัสของยัง อย่างไรก็
ตามการลดลงของค่าชั้นความหนาที่เกิดจากการตกผลึกภายใต้แรงเฉือนจะสังเกตเห็นได้เมื่อปริมาณหญ้า
แฝกเพิ่มขึ้น

จากการศึกษาเพิ่มเติมถึงผลของชนิดเส้นใยธรรมชาติ ได้แก่ เส้นใยหญ้าแฝก ปอแก้ว และป่าน
ศรนารายณ์ต่อค่าชั้นความหนาที่เกิดจากการตกผลึกภายใต้แรงเฉือน สมบัติทางกระแสวิทยา สมบัติทาง
ความร้อน และสมบัติเชิงกลของคอมพอสิท พบว่าความหนืดของเส้นใยหญ้าแฝก—พอลิโพรพิลีนคอม
พอสิทมีค่าสูงกว่าความหนืดของปอแก้ว—พอลิโพรพิลีนคอมพอสิท   และป่านศรนารายณ์—พอลิโพรพิ
ลีนคอมพอสิท   ส่วนปอแก้ว—พอลิโพรพิลีนคอมพอสิทมีค่ามอดุลัสของยังและค่าความแข็งแรงต่อแรง
กระแทกสูงกว่าคอมพอสิทที่เตรียมจากเส้นใยหญ้าแฝกและป่านศรนารายณ์   ค่าชั้นความหนาที่เกิดจาก
การตกผลึกภายใต้แรงเฉือนของเส้นใยหญ้าแฝก—พอลิโพรพิลีนคอมพอสิท ปอแก้ว—พอลิโพรพิลีนคอม
พอสิท   และป่านศรนารายณ์—พอลิโพรพิลีนคอมพอสิทมีความแตกต่างกันอย่างไม่มีนัยสำคัญ นอก
จากนั้น เส้นกราฟที่ได้จากการทดสอบโดยวิธีดิฟเฟอเรนท์เชียล สแกนนิ่ง แคลอรีมิตรี้ หรือ ดีเอสซี
(Differential Scanning Calorimetry : DSC) ของเส้นใยธรรมชาติ—พอลิโพรพิลีนคอมพอสิทบริเวณ
แกนกลาง แสดงให้เห็นว่า มีจำนวนพีกที่มากกว่าและลักษณะกว้างกว่าพีกในบริเวณผิวอย่างชัดเจน สิ่งนี้
ชี้ให้เห็นว่ามีผลึกหลากหลายรูปแบบเกิดขึ้นในบริเวณแกนกลาง

ยิ่งไปกว่านั้น จากการศึกษาผลของสภาวะในการขึ้นรูป ได้แก่ ความเร็วของสกรู ความเร็วในการ ฉีด ความดันย้ำ และอุณหภูมิแม่พิมพ์ต่อค่าชั้นความหนาที่เกิดจากการตกผลึกภายใต้แรงเฉือน ปริมาณ ผลึก การกระจายตัวของปริมาณผลึกตามความหนา และสมบัติเชิงกลของเส้นใยหญ้าแฝ—พอลิโพรพิ ลีนคอม-พอสิท แสดงให้เห็นว่าความเร็วในการฉีดและอุณหภูมิของแม่พิมพ์มีผลกระทบต่อค่าชั้นความ หนาที่เกิดจากการตกผลึกภายใต้แรงเฉือน และปริมาณผลึก อย่างไรก็ตาม สภาวะในการขึ้นรูปไม่มีผลต่อ สมบัติเชิงกลของเส้นใยหญ้าแฝ—พอลิโพรพิลีนคอมพอสิทอย่างมีนัยสำคัญ

นอกจากนี้ จากการศึกษาผลของเส้นใยธรรมชาติต่อการตกผลึกในสภาวะที่ปราศจากแรงเฉือน พบว่าในพอลิโพรพิลีนคอมพอสิทมีการลดลงของอุณหภูมิการหลอมเหลวที่สภาวะสมดุล (T_m^0) การลด ลงของค่าครึ่งเวลาของการตกผลึก และการเพิ่มขึ้นของอัตราการตกผลึกเมื่อเทียบกับพอลิโพรพิลีน การ เติมเส้นใยธรรมชาติลงในคอมพอสิทนำไปสู่ การลดลงของค่ายกกำลังของแอฟรามี การตกผลึกแบบท รานส์คริสตัลไลเซชันของพอลิโพรพิลีนสามารถสังเกตเห็นได้บนพื้นผิวของเส้นใยธรรมชาติ ยิ่งไปกว่านั้น อัตราการเติบโตของผลึกของคอมพอสิทมีค่าต่ำกว่าของพอลีโพรพิลีน อัตราการเติบโตของผลึกรวมกับ อัตราการตกผลึกนำมาใช้ในการคำนวณหาจำนวนนิวคลีไอที่มีประสิทธิภาพ พบว่าจำนวนนิวคลีไอที่มี ประสิทธิภาพของเส้นใยธรรมชาติ—พอลิโพรพิลีนคอมพอสิทมีค่าสูงกว่าของพอลีโพรพิลีน สิ่งนี้แสดง ให้เห็นว่าเส้นใยธรรมชาติสามารถทำหน้าที่เป็นตัวก่อเกิดนิวคลีไอสำหรับการตกผลึกในคอมพอสิทได้

สาขาวิชา <u>วิศวกรรมพอลิเมอร์</u>   ลายมือชื่อนักศึกษา _____

ปีการศึกษา 2550   ลายมือชื่ออาจารย์ที่ปรึกษา _____

ลายมือชื่ออาจารย์ที่ปรึกษาร่วม_____

ลายมือชื่ออาจารย์ที่ปรึกษาร่วม_____

ACKNOWLEDGEMENTS

Usa Somnuk

TABLE OF CONTENTS

TABLE OF CONTENTS (Continued)

TABLE OF CONTENTS (Continued)

TABLE OF CONTENTS (Continued)

TABLE OF CONTENTS (Continued)

LIST OF TABLES

LIST OF FIGURES

LIST OF FIGURES (Continued)

LIST OF FIGURES (Continued)

LIST OF FIGURES (Continued)

LIST OF FIGURES (Continued)

LIST OF FIGURES (Continued)

LIST OF FIGURES (Continued)

LIST OF FIGURES (Continued)

FIGURE **PAGE**

SYMBOLS AND ABBREVIATIONS

%	=	Percent
°C	=	Degree Celsius
ΔH	=	Heat of fusion
μm	=	Micrometer
cm^3	=	Cubic centimeter
g	=	Gram
GPa	=	Gigapascal
J	=	Joule
kg	=	Kilogram
kJ	=	Kilojoule
m^2	=	Squaremeter
mg	=	Milligram
min	=	Minute
mm	=	millimeter
MPa	=	Megapascal
mW	=	Milliwatt
rpm	=	Revolution per minute
s	=	Second
v	=	Volume
wt	=	Weight

CHAPTER I

INTRODUCTION

1.1   Natural fibers and natural fiber-composites

During the last few years it has been an increasing environmental consciousness, which increased the interest to use natural fibers such as kenaf, jute, hemp, flax, and coir instead of man made fibers i.e. glass fibers, aramid fibers, and carbon fibers in composite materials. The advantages of natural fibers are low-density with high specific properties (properties per unit weight), abundance, inexpensive, and less tool wear. Furthermore, the natural fibers are recyclable, biodegradable, renewable, and locally available (Oksman, 2000).

Some properties of natural fibers and synthetic fibers are presented in Table 1.1 (Taylor, 2004). Although the tensile strength and tensile modulus of natural fibers are remarkably lower than those of synthetic fibers, natural fibers offer significant cost advantages. The differences in fiber structure and the overall environmental conditions during growth affect the mechanical properties of natural fibers. Natural fibers can be treated in different ways to yield reinforcing fillers having different mechanical properties. In some treatments, they could have mechanical properties comparable to those of glass fiber-polymer composites (Bledzki and Gassan, 1999). In addition, the lightweight natural fiber-polymer composites have a potential weight saving. On the contrary, the synthetic fibers have serious drawbacks in manners of high cost, non-recycle, non-renewable, non-biodegradable, and riskful. The shortcoming has been highly exploited by proponents of natural fiber composites. The use of natural fiber for composite applications has recently

been the subject of intensive research in several countries. Many automotive components have already produced by natural composites.

According to Al-Qureshi et al. (2001), they have developed, manufactured and assembled a small prototype car with all body panels made from jute fiber reinforced composite and hybrid composite as illustrated in Figure 1.1. In addition, an important step towards higher performance applications of automobiles was achieved with the door panels of E-Class Mercedes-Benz (Figure 1.2). This sector is of interest to developing the world. The door panels which consist of a flax/sisal mat embedded in an epoxy resin matrix has shown a remarkable weigh reduction of about 20%. Moreover, their mechanical properties that are important for passenger protection in the event of an accident have been improved. Furthermore, the flax/sisal material can be molded in complicated shapes (Schuh, 2004). A number of building components manufactured from agricultural materials have reached a production stage. They include low-density insulation boards, medium-density fiber boards, hard boards, particle boards, and other building system components such as walls and roofs. In Africa, it has been reported that a strong particle board was made from combinations of bagasses (sugar cane residue), mangrove bark, wood shavings, and corncobs (Taylor, 2004).

Table 1.1 Properties of natural and synthetic fibers (Taylor, 2004).

	Fibers	Density (g/cm³)	Tensile Strength (MPa)	Tensile Modulus (GPa)	Elongation at Break (%)	Decomposition Temperature (°C)	Price (Euros/kg)
Natural	Jute	1.3-1.5	187-540	3-55	1.4-3.1	270	0.7
	Ramie	-	585-900	33	2.0-3.5	260	-
	Hemp	1.4-1.5	580-1,110	3-90	1.3-4.7	258	-
	Bamboo	-	-	1.7-29	3.2	-	-
	Flax	1.4	250-1,000	12-100	1.3-40	280	0.15-0.76
	Sisal	1.4	507-855	24	2.9	270	0.7-1.02
	Cotton	1.5-1.6	350	11	2-10	-	0.35
	Banana	1.3	791	30	2.10	-	0.7-0.9
	Kenaf	1.4	930	53	-	270	-
	Coconut	-	544	14	-	-	0.36-0.45

Table 1.1 Properties of natural and synthetic fibers (Continued).

	Fibers	Density (g/cm^3)	Tensile Strength (MPa)	Tensile Modulus (GPa)	Elongation at Break (%)	Decomposition Temperature (°C)	Price (Euros/kg)
Natural	Wood	0.6	-	12	2.90	-	0.31-0.35
	Cellulose	1.2	-	2.1	-	-	-
	Wood flour	0.6	-	10	-	-	-
Synthetic	E-glass	2.5	1,625-3,400	72	2-5	756	1.6-2.0
	C-glass	2.5	2,800	69	-	756	9.3-16
	S-glass	2.5	4,600	87	-	946	8.3-20
	A-glass	2.5	2,400	68	-	696	2.5
	Aramid (Kevlar)	1.4	2,380-3,100	124	-	496	16.67
	Carbon	1.8-1.9	2,090-5,200	525	-	3,647	33-166
	Zirconia	5.6	700	100	-	2,497	41.7
	Alumina	2.8	1,000	100	-	1,997	-

Figure 1.1   A car made from jute fiber reinforced composite and hybrid composite in Brazil (Al-Qureshi, 2001).
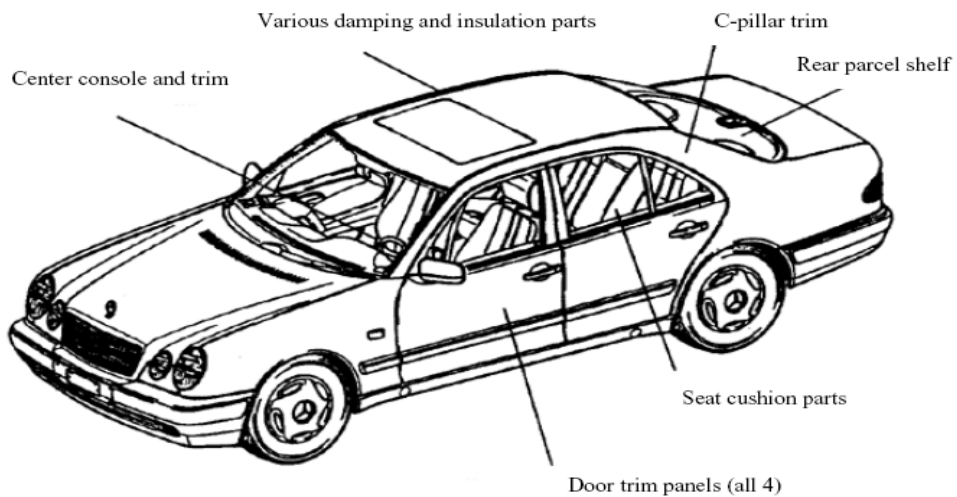
Figure 1.2   Plant fiber applications in the current E-class Mercedes-Benz (Schuh, 2004).

Natural fibers or plant fibers can be classified into five groups according to the part of the plant from which they are extracted as shown in Figure 1.3.

```
                        ┌──────────────┐
                        │ Plant Fibers │
                        └──────────────┘
    ┌───────────┬───────────┬───────────┬───────────┐
┌───────────┐ ┌───────────┐ ┌───────────┐ ┌───────────┐ ┌───────────┐
│Bast Fibers│ │Leaf Fibers│ │Seed Fibers│ │Fruit Fibers│ │Wood Fibers│
└───────────┘ └───────────┘ └───────────┘ └───────────┘ └───────────┘
      ↓             ↓             ↓             ↓             ↓
┌───────────┐ ┌───────────┐ ┌───────────┐ ┌───────────┐ ┌───────────┐
│ - Flax    │ │ - Agaves  │ │ - Cotton  │ │ - Coconut │ │ - Pinewood│
│ - Hemp    │ │   e.g.    │ │ - Kapok   │ └───────────┘ └───────────┘
│ - Jute    │ │   sisal,  │ └───────────┘
│ - Kenaf   │ │   curaua  │
│ - Rami    │ │ - Banana  │
└───────────┘ └───────────┘
```
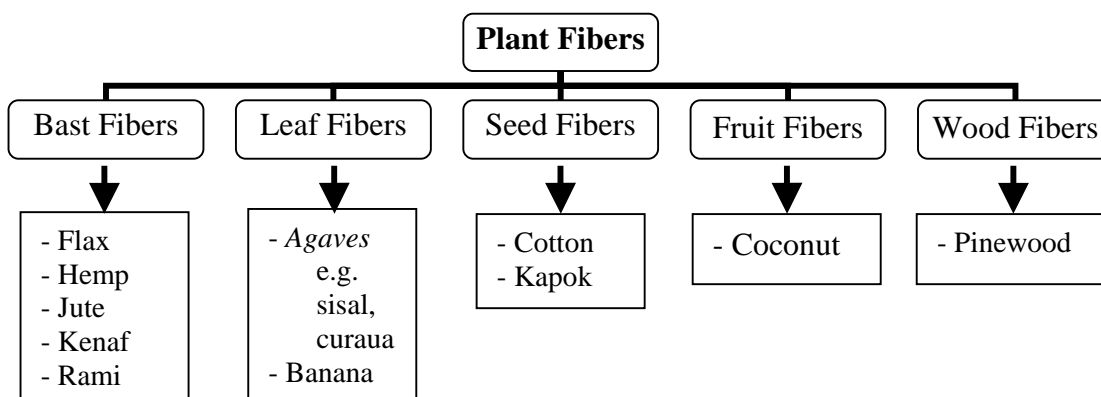
Figure 1.3   Classification of plant fibers (Schuh, 2004).

Typically, natural fibers are mainly composed of cellulose, hemicellulose, and lignin. In order to expand the use of agro-fibers for composites, it is useful to have the information on fiber characteristics and the factors, which affect performance of the fiber (Rowell et al., 2000). Vetiver grass (*Vetiveria zizanioides*) as shown in Figure 1.4 belongs to the same grass family as maize, sorghum, sugarcane and lemon grass. Vetiver grass is well known as a useful plant for erosion control. In Thailand, His Majestic the King Bhumipol Adulyadej has initiated and supported the use of vetiver grass for soil and water conservation since 1991. Various activities on other applications of this grass have been promoted since then (Roongtanakiat and Chairoj, 2002). Normally, leaves of the vetiver grass are cut every few months. Only a minor portion of the residues is reserved as animal feed or household fuel. On the other hand, huge quantities of the remaining residues are burnt in fields or on the side of road. Therefore, investigations aiming to improve the value

of such a residue by using it as a filler in polymer composites are challenging attempts (Thumthong et al., 2003 and 2004, Ruksakulpiwat et al., 2003, and Somnuk et al., 2004).

Figure 1.4 Photograph of a clump of vetiver grass (*Vetiveria zizanioides*) (The Chaipattana Foundation, 2005).

Sisal fiber is another one of the most widely used natural fibers, which is very easily cultivated. It has short renewal times and grows wild in the fields (Maurtherjee and Satyanarayana, 1984). Sisal plant as shown in Figure 1.5 is a hard fiber extracted from the leaves of the sisal plant (*Agave sisalana*). It is now widely grown in tropical countries of Africa, America, and Asia (Brisanda and Ansell, 1992). In Thailand, sisal is easily cultivated and found in many regions especially, in Nakornratchasima and Prachuabkirikhun. At present, sisal fiber is mainly used as ropes for the marine and agriculture industry (Maurtherjee and Satyanarayana, 1984). Other applications of sisal fibers include twine, cords, upholstery, padding and mat making, fishing nets, fancy

articles such as purses, wall hangings, table mats, etc (Chand et al., 1984). In Thailand, sisal fiber is used to produce many hand-made goods such as bag, handbag, hat, purse and so on which are supported and promoted by one tambon one product project (OTOP-Thaitambon, 2000). Hence, the use of sisal fiber as a reinforcement in composites has raised great interest and expectations. As a result, scientists and engineers have been carried out the study of sisal fiber reinforced composites.

Figure 1.5 Photograph of bushes of sisal plant (*Agave sisalana*) (ARC-Institute for Industrial Crops, 2006).

Rossells (*Hibiscus sabdariffa*) as illustrated in Figure 1.6 is in the same family *Malvaceae* as Kenaf (*Hibiscus cannabinus*). Rossells is one of the most widely used natural fibers, which is easily cultivated and found in the northeast of Thailand. Traditionally, it is used as a rope, canvas, and sacking. Recently, this plant is used as a raw material to be alternative to wood in pulp and paper industries for avoiding destruction of forest (Pande and Roy, 1998). It is also used as non-woven mats in the automotive industries (Magurno, 1999), textiles (Ramaswamy, Craft and Wartelle, 1995), fiber-board (Kawai et al., 2000).

The other interesting application to utilize rossells is as a reinforcement fiber to the composites.

Figure 1.6 Photograph of rossells plant (*Hibiscus sabdariffa*) and its pale yellow flowers during blossomy period (Thai Junior Encyclopedia Project by Royal Commanded of H.M. the King, 1999).

1.2 Processing of natural fibers-polypropylene composites

Polypropylene (PP) is a thermoplastic material that has been used for production of natural fiber-thermoplastic composites because it posses many advantages, such as its good processability, high cost-performance ratio, and low processing temperature. Injection molding is one of processing operations used to produce products from natural fiber-PP composites since the products can be easily formed into complex shapes and can be produced as mass productions. In order to determine the quality of polymers or fiber reinforced plastics, it is necessary to consider their processing properties and product properties. Typically, the processing properties are controlled by the primary structure of the raw material (such as MW, MWD, and tacticity) and by processing conditions. Also,

the product properties depend on both the primary and higher order structure (i.e. crystallinity, orientation, and dispersion of fillers). The higher order structures are formed during processing and are dependent on both the primary structure and the processing conditions. Therefore, the quality of a polymer product is decided basically by the material and processing conditions (Fujiyama, 1995). During injection molding, plastics undergo fountain flow (Figure 1.7). The molten polymer is subjected to high shear stress at the cavity wall which causes the preferential orientation of the molecular chains. As a result, a skin layer or normalized thickness of shear-induced crystallization layer with a high molecular orientation takes place at the surface of moldings. On the other hand, in the core of moldings, the relaxation of the molecular chain occurs due to the low cooling rates and low shear stress. Then, the effect of shear on crystallization can be neglected. At the core region, quiescent crystallization takes place. As a result, spherulites with a low molecular orientation are observed (Figure 1.8).

Although the shear-induced crystallization of PP has already been well understood (Churdpunt et al., 2000 and Isayev et al., 2000), the shear-induced crystallization of polymer composites has not been studied so far. Principally, the processing parameters determine the quality of the molded product. Injection molding control involves many aspects of both machine operation and the behavior of plastic. These controls are essential to produce products with good quality. Quality features include mechanical properties, dimensional accuracy, absence of distortion, and surface quality (Rosato et al., 2000). The experimental studies on the effect of processing parameters, especially injection molding parameters on the mechanical properties of natural fiber-polymer composites have not been published so far.
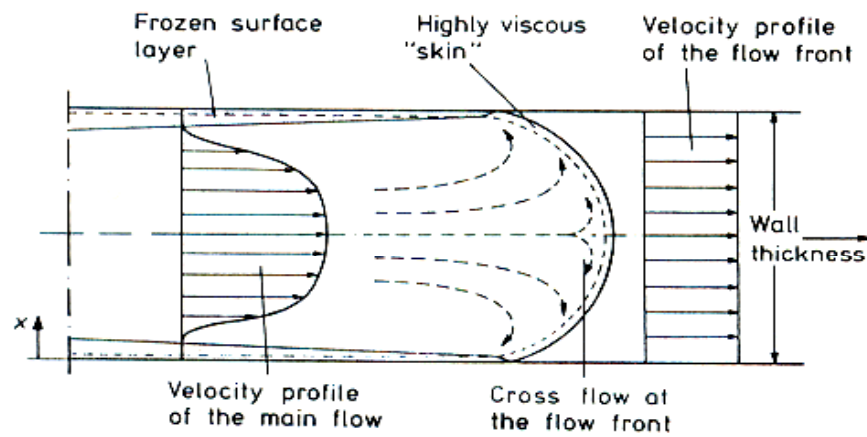
Figure 1.7 Velocity profile in a longitudinal cross section (Johannaber, 1994).
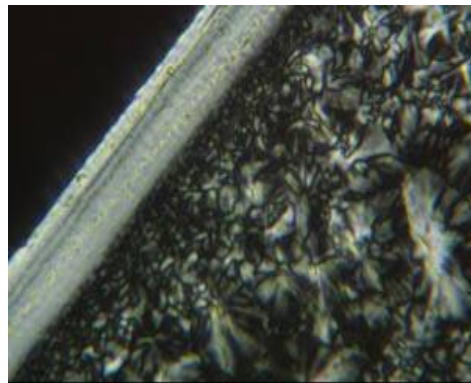
Figure 1.8 Polarized optical micrograph of skin-core morphology (Kornfield Laboratory, 2004).

1.3 Research objectives

The main objectives of this research can be classified as followings:

(i) To investigate the effect of chemical treatment by alkalization on thermal, rheological, and morphological properties of vetiver grass-PP composites.

(ii)   To study the effect of sizes and contents of vetiver grass on shear-induced crystallization, rheological, thermal, and mechanical properties of vetiver grass-PP composites.

(iii)   To study the effect of different kinds of natural fibers i.e. vetiver grass, rossells, and sisal on shear-induced crystallization, rheological, thermal, and mechanical properties of PP composites.

(iv)   To study the effect of processing conditions on shear-induced crystallization, degree of crystallinity, gapwise crystallinity distribution, and mechanical properties of vetiver grass-PP composites.

(v)   To study the quiescent crystallization kinetic of natural fiber-PP composites.

1.4   Scope and limitations of the study

Three types of natural fibers i.e., vetiver grass, rossells, and sisal were used in this study. Vetiver grass (ecotype of Songkhla 3) was cultivated by The Land Development Department, Nakhon Ratchasima. The age of vetiver grass was 6-8 months. Rossells was kindly supplied from The NEP Realty and Industry Public Co., Ltd. without concerning of the cultivation areas. Sisal was cultivated in Tumbol Bankao, Dan Khuntod, Nakhonratchasima. The age of sisal was 5-7 years.

Chemical treatment of vetiver grass was done by alkalization. Rossells and sisal were treated with methanol/benzene mixture and followed by alkalization. Mixing time and mixing speed were fixed at 13 min and 50 rpm, respectively. Processing parameters studied in this research were screw speed (rpm), injection speed (mm/s), holding pressure (kg/cm^2), and mold temperature (°C). Mechanical properties of test specimens were

considered on tensile strength, Young's modulus, elongation at break (%), and Izod impact strength. The quiescent crystallization was conducted under isothermal condition.

CHAPTER II

LITERATURE REVIEW

2.1   Chemically treated natural fibers

Currently, many research projects are devoted to the utilization of cellulose-based fibers as reinforcement for plastics. However, these fibers are mainly composed of cellulose, hemicellulose, and lignin. In order to expand the use of cellulose-based fibers for composites, it is useful to have the information on fiber characteristics and factors which affect performance of the fibers (Rowell, 1997).

Mwaikambo and Ansell (1999 and 2002) found that alkalization of plant fibers (hemp, sisal, jute and kapok) effectively changes the surface topologies of the fibers and their crystallographic structures. However, the concentration of sodium hydroxide (NaOH) for alkalization must be taken into consideration. Moreover, they have reported that removal of surface impurities on plant fibers may be an advantage for fiber to matrix adhesion. This may facilitate both mechanical interlocking and the bonding reaction due to the exposure of fibril to chemicals such as resins and dyes.

Bisanda (2000) also examined the effect of alkali treatment on the wetting ability and coherence of sisal-epoxy composites. Treatment of sisal fiber in NaOH solution resulted in more rigid composites with lower porosity and hence higher density. The treatment has been shown to improve the adhesion characteristics due to an increase in surface tension and surface roughness. The resulting composites showed improvements in the compressive strength and water resistance. It was suggested that the removal of intracrystalline and intercrystalline lignin and other surface waxy substances by the

alkalization substantially increases a possibility for mechanical interlocking and chemical bonding.

Ray and Sarkar (2001) conducted a research on the characterization of alkali-treated jute fibers for physical and mechanical properties. The alkali treatment of jute fibers with 5% NaOH solution showed that most of the changes occurred within 2-4 hours of treatment. The weight loss due to losing their cementing capacity in the fiber structure, separating the fibers from the strands, and dissolution of hemicellulose was maximized at these treatment hours. Thus, a sharp drop in the linear density was measured from 33.0 to 14.5 denier after 6 hours of treatment. The loss of hemicellulose led to closer packing of its cellulose chains. On further treatment with alkali solution from 4-8 hours, the crystallinity of the fibers has found to be improved. The tenacity and modulus of the fibers were improved by 45 and 79%, respectively, and the percent breaking strain was decreased by 23% after 8 hours of treatment. This indicated that fibers become stiffer and more brittle with increasing the crystallinity of the fibers. The rate of change of tenacity, modulus, and breaking strain showed the possibility of two different mechanisms before and after 4 hours of treatment. The first mechanism was the loss of hemicellulose as a cementing material at the beginning up to 4 hours of treatment contributed to the closer packing of the cellulose chains. The second mechanism was a slow improvement in crystallinity with further closer packing of the cellulose chains beyond 4 hours of treatment. This caused the fibers stiffer and stronger. A transition with a predominant chemical reactivity before 4 hours of treatment and a gradual development of crystallinity was apparent. Furthermore, Jähn et al. (2002) explained that when flax fibers were subjected to NaOH treatments, so called mercerization, the extent of polymorphic transformation of cellulose I to cellulose II was taken place within the crystalline domains of the fiber depending on the alkali concentration.

Zefeiropoulos et al. (2002(a)) studied two different surface modification treatments (acetylation and stearation) on two grades of flax fibers (green and dew retted flax). Acetylation has been found to increase the percent weight gain of fibers at high levels (around 15-17%), which implies that the treatments is affecting the bulk and not just the surface of flax fibers. An investigation of the acetylation condition indicated that the presence of moisture in the fibers is beneficial for the reaction, as it hydrolyses acetic anhydride to acetic acid, a compound that swells the fiber and facilitates the reaction. For stearation, the percent weight gain of the fiber after treatment indicated that only the surface is affected and not the bulk, as in the case for acetylation. It has been found that both treatments result in a removal of non-crystalline constituents of the fibers and alter the characteristics of the surface topology. Also, the results showed that both treatments change the fiber surface free energy. Acetylation increased fiber surface energy whereas stearation decreasing it (Zefeiropoulos, et al. 2002(b)). It was found that acetylation improved the stress transfer efficiency at the interface for both green and dew retted flax fibers. The optimum treatment time was 2 hours for acetylation of dew retted flax and 4 hours. for acetylation of green flax. The stearic acid treatment also improved the stress transfer efficiency at the interface but only for lower treatment times. The optimum treatment time was 36 hours for both green and dew retted flax fibers. It has also found that stearation for 90 hours deteriorated the interface in both green and dew retted flax fibers. The reasons were because the longer time of treatment deteriorated the fiber strength, and an excess of stearic acid present on the fiber surface may have acted as a lubricant more than as a compatibilizer.

The effect of fiber treatment on the mechanical properties of unidirectional sisal-reinforced epoxy composites was investigated by Rong et al. (2001). Treatment including alkalization, acetylation, cyanoethylation, silane coupling agent, and heating were carried out to modify the fiber surface and its internal structure. It was shown that chemical

methods usually led to an active surface by introducing some reactive groups, and provided the fibers with higher extensibility through partial removal of lignin and hemicellulose. In contrast, thermal treatment of the fibers could result in higher fiber stiffness due to the increased crystallinity of hard cellulose. Treatments of sisal fiber which increased fiber strength and the adhesion between the fiber bundles and the matrix, would favor an overall improvement of mechanical properties (especially tensile properties) of laminated sisal. However, the treatments of sisal fiber did not introduce any new bonding to the intercellular region to hinder cell pull-out. Similarly, Joseph et al. (1996(a)) studied the effect of chemical treatment on the tensile properties of sisal fiber-reinforced low density polyethylene (LDPE) composites. Treatment using chemicals such as NaOH, isocyanate, permanganate, and peroxide were carried out to improve the bonding at the fiber–polymer interface. Alkali treated fiber composites showed better tensile properties than untreated composites. This was because their rough surface topography and aspect ratio were increased. It was observed that cardinal derivative of toluene diisocyanate (CTDIC) treated composites exhibit superior mechanical properties. This may be due to the fact that the long chain structure of CTDIC linked to the cellulosic fibers makes the fiber hydrophobic, compatible and highly dispersible in the LDPE matrix. The SEM micrographs also showed the strong fiber matrix adhesion in sisal-LDPE composites. Peroxide treated composites showed an enhancement in tensile properties due to the peroxide induced grafting. Permanganate treated composite also showed similar result due to the permanganate induced grafting. Among the various types of treatments, CTDIC and DCP (dicumyl peroxide) treatments showed the maximum tensile properties. In addition, Paul et al. (1997) evaluated the electrical properties of short sisal reinforced LDPE composites. Various surface treatments such as alkali, CTDIC, stearic acid, peroxide, permanganate, and acetylation were carried out on the sisal fibers to improve interfacial bonding. The results showed that the dielectric constant increases progressively with

increase in fiber loading and decreases with increase in frequency for all composites. The dielectric constant values of the composites were found to decrease with chemical treatments. This was due to the fact that the hydrophilic nature of natural fiber decreases with treatment. Volume resistivity values of treated sisal fiber/LDPE composites were found to be greater than those of raw sisal fiber/LDPE composites. Volume resistivity values of permanganate-treated-sisal fiber/LDPE composites depend on the concentration of potassium permanganate solution used for treatment. The value of volume resistivity increase reaches a maximum and then decreases with increase in concentration of potassium permanganate solution. The dielectric loss factors of treated sisal fiber reinforced/LDPE composites were found to be lower than that of untreated sisal fiber/LDPE composites.

Fung et al. (2002) investigated the effect of matrix maleation and fiber content on the processability, mechanical properties, and morphology of sisal fiber-reinforced PP (PP) composites. To improve the interfacial bonding between sisal fiber and PP, the PP matrix was maleated (MAPP) by blending PP and maleic-anhydride-grafted-PP in the weight ratio of 9:1. It has been found that the sisal fiber/MAPP composites have lower melt viscosity (as reflected by torque rheometer measurements) than the sisal fiber/PP composites at 20 wt% sisal fiber contents. In term of mechanical properties, PP maleation showed an improvement in tensile strength. This can be explained in terms of the improved sisal fiber/matrix interfacial bonding when MAPP was used. However, the impact strength was reduced when the PP matrix was maleated. The improved sisal fiber/matrix interfacial bonding prevented fracture mechanisms such as fiber/matrix debonding and fiber pull-out. Another research work correlating to the use of meleic anhydride (MA) and maleic anhydride-polypropylene copolymer (MAPP) was done by Cantero et al. (2003). They studied the effects of different treatments on the fiber-matrix compatibility in terms of surface energy and mechanical properties of composites. The composites were

compounded with two kinds of flax fibers (natural flax and flax pulp) and PP. Three treatments were maleic anhydride (MA), maleic anhydride-polypropylene copolymer (MAPP) and vinyl trimethoxy silane (VTMO). The results indicated that wettability by PP matrix of both flax fibers and pulps can be improved by the action of chemical treatments, due to the reduction of the polar components of their fiber surfaces. MAPP treatment produced the best surface energy values for all percentages. Composites made with a 10 wt% MAPP treated fiber had the highest flexural and tensile strength, according to the surface energy values. Its effect was especially remarkable for flax pulps. However, the MA and VTMO treated fiber gave similar values to that for the untreated ones.

Valadez-Gonzalez et al. (1999(a)) used silane and alkaline treatment to enhance both the matrix fiber adhesion and the chemical surface modification in order to improve the physicochemical interactions at the fiber-matrix interphase. It was found that the alkaline treatment has two effects on the fiber: (1) it increases the surface roughness that results in a better mechanical interlocking; and (2) it raises the amount of exposed cellulose on the fiber surface, thus increasing the number of possible reactive sites. The fiber preimpregnation allowed a better fiber wetting which in a normal fiber-polymer mixing procedure would not be possible because of the high polymer viscosity. Thus, the preimpregnation enhanced the mechanical interlocking between fiber and matrix. The fiber-surface silanization resulted in a better interfacial load transfer efficiency, but it did not improve the wetting of the fiber.

Aziz and Ansell (2004) studied the effect of alkalization and alignment on the mechanical properties, and thermal properties of kenaf and hemp fiber composites. In their study, long hemp and kenaf fibers were used in as-received condition and alikalized in a 6% NaOH solution. They were combined with cashew nut shell liquid (CNSL) resin and hot-pressed to form natural fiber composites. It was apparent from the overall mechanical properties of the composites that treated long kenaf-CNSL and treated long hemp-CNSL

were fairly comparable to glass fiber reinforced polymer composites. However, maximum strength and maximum toughness cannot be simultaneously achieved. It was suggested that the composites must be considerably designed for suitable applications and desired mechanical properties. Moreover, wide endothermic DSC peaks were presented in all the thermograms of the composites indicating the presence of moisture. The presence of water in composites tends to develop plasticity in the material, thus reducing mechanical properties. From DMA analysis, the result showed that treated fiber composites posses a higher storage modulus E' and lower tan δ indicating greater interfacial bond strength and improved adhesion between the matrix and the fiber compared with untreated composites.

Sreekala and Thomas (2003) reported that oil palm fibers have been found to be an excellent reinforcement in phenolic materials, but its main disadvantage is hydrophilic nature. Thus they have investigated the effect of various fiber surface modifications such as mercerization, latex coating, gamma irradiation, silane treatment, isocyanate treatment, acetylation and peroxide treatment on water-sorption characteristic of oil palm fibers. Sorption behavior of distilled water at 30, 50, 70 and 90°C was evaluated. It was found that treatment reduces the water uptake at all temperatures. The decrease in water uptake was due to its physical and chemical changes occurred to the fibers on modifications. Treatment reduced the mechanical strength of the fibers. Strain at break of the fibers was considerably increased upon treatments except for silane treatment. Young's modulus shows enhancement on mercerized and silane treatment. In the swollen stage the stiffness of the fiber was considerably reduced.

Mohanty et al. (2000) conducted a research on surface modifications of two varieties of jute fabrics, i.e. hessian cloth (HC) and carpet backing cloth (CBC), involving dewaxing, alkali treatment, cyanoethylation, and grafting on performance of biodegradable jute-fabric/Biopol (poly(3-hydro-xybutyrate-co-8%-3-hydroxyvalerate) composites. The results showed that mechanical properties such as tensile strength, bending strength, and

impact strength increase in comparison to pure Biopol as a result of reinforcement with jute fabrics. More than 5% enhancement in tensile strength, 30% in bending strength and 90% in impact strength of the composites relative to pure Biopol sheets were observed. Furthermore, degradation study indicated that after 15 days of burial compost more than 50% weight loss of jute/Biopol composites was occurred.

Ichazo et al. (2000) studied the influence of acetylation on the mechanical, thermal and thermodegradative behavior of sisal fiber reinforced PP, PP/high density polyethylene (HDPE), and PP/HDPE with functionalized and non-functionalized ethylene-propylene copolymer (EPR) composites. Acetylation of fiber has been found to improve adhesion of the fiber to polyolefin matrix and to enhance the tensile strength and modulus of the resulting composites, except in some cases. It can be concluded that acetylated and non-acetylated short sisal fiber behaved as reinforcing loads in all the composites. It was suggested that the mixing and molding temperatures would lie between 160 and 230°C, respectively when acetylated fiber was mixed with polyolefins. In addition, PP with treated or untreated fibers can be replaced by a blend of PP/HDPE/non-functionalized EPR with acetylated sisal. This was because thermal stability of this blend was quite similar to that of filled PP.

One important chemical treatment on natural fibers is the chemical coupling method, which improves the interfacial adhesion. The fiber surface is treated with a compound that forms a bridge of chemical bonds between fiber and matrix. Moreover, another effective method of chemical modification of natural fibers is graft copolymerization. This reaction is initiated by free radicals of the cellulose molecule. The cellulose is treated with an aqueous solution with selected ions and is exposed to high energy radiation. Then the cellulose molecule cracks and radicals are formed. Afterward the radical sites of the cellulose are treated with suitable solution (compatible with the

polymer matrix), for example vinyl monomer, acrylonitrile, methyl methacrylate, and polystyrene (Bledzki and Gassan, 1999).

Singh et al. (2000(a)) used FT-IR microscope in reflectance mode (ATR) to study the effect of various coupling agents such as organosilane, zirconate, titanate and *N*-substituted methacrylamide on treated natural fibers (sisal). The results showed an irregular physisorption/chemisorption of coupling agents, their penetration beyond the surface, and a decrease in hydrophilicity of fibers. The difference in the properties of untreated and chemically treated fibers was also verified in the polymer composites.

According to Abdelmouleh et al. (2002), the adsorption of several prehydrolyzed alkoxysilanes onto the surface of cellulosic fibers in ethanol/water mixtures has been studied quantitatively. It was suggested that one should distinguish adsorption phenomena from actual chemical grafting when considering the interactions of silanes with the surface of cellulose. The quantitative assessment of the physicochemical equilibria for several silanes indicated that adsorption of monolayer and multi layers of prehydrolyzed silanes were readily achieved. However, it was emphasized that a simple extraction with ethanol to entirely remove these molecules should be done. Only a heat treatment can induce a condensation between the hydroxyl groups of the hydrolyzed silanes resulting in covalent bonding between substrate and silane monolayer.

Pickering et al. (2003) investigated the effect of two silane-based coupling agents, gamma-aminopropyltriethoxysilane (GS) and dichlrodiethylsilane (DCS), on radiata pine (*Pinus radiate*) wood fiber with and without pre-treatment using NaOH. The results showed that concentrations of silicon up to 3.2 wt% were obtained on the fiber surface due to silane coupling, however, pre-treatment was found to dramatically reduce this value. Nuclear Magnetic resonance (NMR) provided evidence that coupling had occurred between the fiber and DCS by reaction producing ether linkages between the hydroxyl groups on the wood fiber and silane. Pre-treatment and treatment have been found to have

an insignificant effect on fiber strength. Composite sheets were produced by blending fiber (5, 10, and 20 wt%) with polyethylene (PE) followed by extrusion. An increase in strength was obtained at fiber contents of 5 wt% for all treatments compared to composites with untreated fiber. This was mainly due to an increasing compatibility of the fiber surface to PE. However, there was no such improvement obtained at higher fiber contents. Evidence suggested that the production of void was limiting composite strength.

Graft copolymerization of methyl methacrylate (MMA) onto wood-fiber, in dispersed media, has been studied as function of temperature, concentration of redox initiator, and surfactant (Román-Aguirre et al., 2004). It was found that PMMA grafting onto wood-fiber was strongly dependent on variations in temperature and concentration of initiator and surfactant. Scanning Electron Micrograph (SEM) showed the presence of small agglomerates regularly distributed on the surface of the modified fiber. These agglomerates remained on the fiber surface after 24 hours of chloroform extraction and were presumably grafted PMMA. Infrared analysis of the acid hydrolysis products of the modified fiber showed a clear characteristic signal of carbonyl groups at 1734 cm^{-1}. Such signal indicated the presence of fiber-PMMA chemical links, since simple physical interactions would not remain after the cellulose hydrolysis. Mishra et al. (2001) also conducted the research on graft copolymerization of acrylonitrile (AN) on chemically modified sisal fibers using combination of $NaIO_4$ and $CuSO_4$ as initiator in an aqueous medium in the temperature range of 50-70°C. PAN grafting onto chemically modified sisal fiber was done to improve the surface and bulk mechanical properties for its potential use as reinforcing fiber for polymer composites. The optimum grafting condition was to use $NaIO_4$ and $CuSO_4$ concentrations of 0.008 mol/L and 0.002 mol/L, respectively with 0.1 g chemically modified sisal fiber, and 1 ml AN, at 60°C. The best tensile strength and modulus was obtained at 5% grafting of the fiber. The AN-grafted sisal fibers are expected

to act as compatible reinforcing fibers with several hydrophobic thermoplastics and thermosettings for preparation high performance composites.

Keener et al. (2004) reported that maleated coupling agents are widely used to strengthen composites containing fillers and fiber reinforcements. They have established role of MaPOs results from two main factors. Theses were economical manufacturing and the efficient interaction of maleic anhydride with the functional surface of fiber reinforcements. Peak performance was demonstrated in agro-fiber PP composites by selecting a maleated coupler that has the appropriate balance of molecular weight and maleic anhydride content. The flexural and tensile strengths of the 30% agro-fiber composites were increased by more than 60% with Epolene[TM] G-3015. Newly developed maleated polyethylene (MaPE) couplers for the wood-polyethylene market demonstrate superior performance compared against other potential polyolefin-coupling agents. Results indicated that the new polyethylene couplers at 3% loading can double the tensile strength and triple the impact properties compared to non-coupled blend of wood and polyethylene.

In the study of Thielemans and Wool (2004), butyrated kraft lignin was added to an unsaturated thermosetting resin, consisting of a mixture of acrylated epoxidized soybean oil and styrene. Composites were made by the Vacuum Assisted Transfer Molding process with varying amounts of butyrated kraft lignin dissolved in the unsaturated resin system. Butyrated kraft lignin improved the interface between the resin and reinforcing flax fibers. SEM images illustrated a clear improvement in the adhesion of the resin to the fibers by showing the fibers fracturing together with the resin, without fiber pullout. However, an increase in viscosity upon solubilization of butyrated kraft lignin in the unsaturated resin negatively affected the ability of the resin to flow through the fiber mats during mold filling. As a result, the amount of air bubble in the composites was increased. This led a decrease in the mechanical properties of the overall composites. On the other hand, strength improvement was seen for composites made from short wheat straw fibers, which

allow for better resin penetration and fiber wetting. The flexural strength increased by 40% for a 5 wt% butyrated lignin addition.

According to the study of Valadez-Gonzalez et al. (1999(b)), short henequen fibers were modified with a silane coupling agent in order to find out its deposition mechanism on the fiber surface and the influence of this chemical treatment on the mechanical properties of the composite. It was shown that the partial removal of lignin and other alkali soluble compounds from the fiber surface increases the adsorption of the silane-coupling agent whereas the formation of polysiloxanes inhibits this process. It has been further verified that the interaction between the fiber and the matrix is much stronger when the fiber surface topography was combined with the chemical modification of the fiber surface with a silane-coupling agent.

Jana and Prieto (2002(a)) investigated the effects of three coupling agents (Silquest® A-1100, Silquest® A-2120, and hydroxymethylated resorcinol) on the morphology of epoxy coating on wood flour particles and the mechanical and physical properties of the composite. They have found that all three coupling agents slowed the epoxy curing reactions and completely promoted the coverage of wood flour particles by crosslinked epoxy. Although a hydroxymethylated resorcinol coupling agent provided better morphology around wood flour particles, much smaller-size epoxy particles of a more uniform size were formed. Nevertheless, both tensile and impact strengths were reduced due to the use of coupling agents.

Karmaker and Youngquist (1996) conducted a research in short jute fiber reinforced PP composite, which prepared by injection molding. In their study, maleic anhydride-grafted PP was added as coupling agent to improve the adhesion between jute fiber and PP. The results revealed that injection molding caused a high fiber abrasion resulting in an average fiber length of 390 and 350 μm for formulations with and without coupling agent, respectively. The role of the average fiber length in strengthening of the

composites was interpreted with help of the critical fiber length. The effect of jute fibers on the tensile and bending strengths was poor when there was no coupling agent. The addition of MAPP as coupling agent improved the composite performance by enhancing the adhesion between jute fibers and PP. The improved adhesion did partially offset the fiber abrasion and the associated strength loss that resulted from injection molding. In addition it was found that fiber orientation occurred mainly in the melt-flow direction. Another interesting research concerning to the effectiveness of (graft copolymer of PP and maleic anhydride copolymers (MAH-PP) as coupling agents in jute-PP composites was done by Gassan and Bledzki (1997). It was observed that the MAH-PP concentration in solution, the treatment time, and the processing parameters were of considerable influence the mechanical properties of the composite. Flexural strength of the composite with MAH-PP treated fibers was higher than that of unmodified fibers, and increased with fiber loading. The cyclic dynamic values at an increasing load indicated that the coupling agent reduced the progress of damage. Therefore, dynamic strength (dynamic failure stress at load increasing test) of the MAH-PP modified composites was raised by about 40%. SEM investigations confirmed that the increase in properties was caused by improved fiber-matrix adhesion. Also, there was less tendency for fibers to pull out the matrix.

By using thermokinetic mixer and injection molding machine, Sanadi et al. (1995) prepared kenaf fiber-PP composites. A maleated PP was used to improve the interaction and adhesion between the non-polar matrix and the polar lignocellulosic fibers. The results indicated that the impact strength of the composite depended on the amount of fiber and the type of testing, i.e., whether the samples were notched or un-notched. In the case of notched samples, the impact strength increased with the amount of fibers added until a plateau is reached at about 45% fiber weight, irrespective of whether MAPP was used or not. The fiber bridges crack and increase the resistance of the propagation of the crack. In the case of the un-notched samples, impact values of the uncoupled composites and the

presence of the fibers decreased the energy absorbed by specimens. Addition of the fibers created regions of stress concentrations that required less energy to initiate a crack. Improving the fiber-matrix adhesion through the use of MAPP increased the resistance to crack initiation at the fiber-matrix interface, and the fall in impact strength with the addition of fibers was not as dramatic. The specific tensile and flexural moduli of a 50% by weight (39% by volume) of kenaf-PP composite favorably compared with a 40% by weight of glass fiber-PP injection-molded composite.

2.2   Polymer composites from natural fibers

2.2.1   The effects of natural fibers on the mechanical properties of polymer composites

Curvelo et al. (2001) used cellulosic fibers from *Eucalyptus urograndis* pulp as reinforcement for thermoplastic starch in order to improve its mechanical properties. The composites were prepared with regular cornstarch plasticized with glycerin and reinforced with short cellulosic fibers (16% w/w) from bleached pulp. The composite showed an increase of 100% in tensile strength and more than 50% in modulus with respect to non-reinforced thermoplastic starch. SEM of fractured surfaces revealed a very good adhesion between the fibers and the matrix. However, it was indicated that the main drawback involved in the use of pulp as a fiber was the tendency of fibers to self-agglomerate, which made it difficult for them to disperse in the matrix.

Nishino et al. (2003) investigated mechanical properties of friendly environmental composite made of kenaf fiber and poly-L-lactic acid (PLLA) resin. The results showed that young's modulus (6.3 GPa) and the tensile strength (62 MPa) of the kenaf/PLLA composite (fiber content was 70 vol%) were comparable to those of traditional composites. These properties were higher than those of the kenaf sheet and the PLLA film themselves. This was attributed to the strong interaction between the kenaf

fiber and PLLA. In addition, the storage modulus of the composite remained unchange up to the melting point of PLLA. Also, it was found that kenaf fiber could be a good candidate for the reinforcement fiber of high performance biodegradable polymer composites.

A new method for the development of natural fiber composites of high-performance thermoplastic polymers considering poly(phenylene ether) (PPE) and wood flour was established by Jana and Prieto (2002(b)). They have reported that thermosetting liquid epoxy resins could be a useful reactive solvent for combining wood flour particles with a high-temperature thermoplastic polymer, PPE. The new composite materials, especially the one cured with M-CDEA (4,4′-methylenebis(3-chloro-2,6-di-ethylaniline), showed lower water absorption and provided much higher strength than those of other natural fiber-filled composites. Moreover, its strength was comparable very well with some glass-filled engineering polymers.

Joseph et al. (1996(b)) evaluated the mechanical properties of sisal fiber composites (randomly oriented) of several thermoset resin matrices (polyester, epoxy, phenol-formaldehyde) and a thermoplastic matrix (low density polyethylene:LDPE) with respect to fiber length and fiber loading. It was observed that all composites showed an increase in properties with increasing fiber loading. However, the optimum length of the fiber required to obtain an increase in properties and varied with the type of matrix. Among polyester, epoxy, and phenol-formaldehyde composites of sisal fiber, a phenolic type resin performed as a better matrix than epoxy and polyester resins with respect to tensile and flexural properties. This was due to the high interfacial bonding in phenolic composites. However, sisal fiber-LDPE composites showed a better reinforcing effect as compared to thermoset resin composites. This was because the high matrix ductility and high strength/modulus ratio of sisal as compared to that of LDPE matrix. The interesting results of a relative research in short sisal fiber reinforced PP composites was done by

Joseph et al. (2003). In this study, the dynamic mechanical properties of short sisal fiber reinforced PP composites containing both untreated and treated fibers have been investigated with reference to fiber loading, fiber length, chemical treatments, frequency, and temperature. It was indicated that the addition of sisal fiber to pure PP increased the storage modulus, i.e. the E′ of sisal-PP system was higher than that of PP matrix. This was due to the reinforcement imparted by the fiber that allowed stress transfer from the matrix to the fiber. Both $E′$ and $E″$ were found to be increased with fiber loading. The influence of fiber length indicated that an optimum length of 2 mm was necessary to get maximum dynamic modulus. The loss modulus $E″$ was also maximum for 2 mm fiber length. The $E′$ and $E″$ of chemically treated composites were higher than those of untreated composites due to the improvement of fiber-matrix interfacial adhesion. Moreover, both storage and loss modulus decreased with increasing temperature. Reduction in modulus with increasing temperature was associated with softening of the matrix at higher temperature. Dynamic moduli increased with increasing frequency due to the reduction of segmental mobility.

Van de Velde and Kiekens (2003) studied unidirectional (UD) and multidirectional (MD) flax/PP composites. Flax with varying retting degree and boiled flax were used as reinforcements for the UD composites. Unmodified and maleic anhydride modified PP (MAA-PP) were used as matrix. MD flax/PP composites were manufactured on laboratory scale and on pilot scale. They were made from needle-punched hybrid flax/PP non-wovens. It was concluded that fiber treatment, such as boiling of flax, led to improvement on mechanical properties for UD and to complete compactness MD flax/PP composites. The use of MAA-PP increased the properties of all studied composites due to an increase in interaction between the anhydride functions and the hydroxyl functions on cellulose. A combination of boiled flax with MAA-PP gave the best mechanical properties.

Joseph et al. (2002) investigated the environmental degradation behavior on the physical and mechanical properties of short sisal/PP composites with respect to the influence of ageing conditions like treatment with water and UV radiation. The dependence of water uptake on the sorption characteristics of sisal/PP composites was evaluated by immersion in distilled water with respect to fiber loading, temperature, and chemical treatment. It was found that water uptake increased with increasing fiber loading due to an increase in cellulose content. The raise of temperature up to 70°C was accompanied by an increase in the rate and extent of sorption. Chemical treatments such as urethane derivative of polypropylene glycol (PPG), poly[(methylene) poly(phenyl isocyanate)] (PMPPIC), and maleic anhydride modified PP (MAPP) were given to sisal fiber. All chemically modified fiber composites showed lower uptake than the unmodified composites. This was because all chemical treatments given to sisal fiber reduced its hydrophilicity thereby favoring strong interfacial adhesion between the fiber and PP matrix. Tensile properties decreased with water uptake, time of immersion, and fiber loading. The behavior was strongly dependent on the chemical treatment and fiber orientation. Moreover, the tensile properties were found to decrease with increasing time of exposure to UV radiation. The reduction in properties was due to chain scission and degradation, which occurred to PP molecules and resulted from photooxidation promoted by UV radiation. As a result of UV irradiation, surface cracks could be seen on neat PP and PP composites, which could be evidenced from SEM. The retention of tensile properties increased with increasing fiber loading.

Gassan (2002) evaluated the tension-tension fatigue behavior of different natural fiber reinforced plastics, which made of flax, jute yarn, and jute wovens as reinforcements for epoxy resins, polyester resins, and PP. Fiber type, textile architecture, interphase properties, fiber properties, and fiber content were found to strongly affect the fatigue behavior as illustrated with damping versus applied maximum load curves. It was

found that natural fiber reinforced plastics with higher fiber strength and modulus, stronger fiber-matrix adhesion, and higher fiber fraction exhibited higher critical loads for damage initiation and higher failure loads. In addition, damage propagation rates were reduced. Furthermore, unidirectional composites were less sensitive to fatigue induced damage than woven reinforced ones.

According to Singh et al. (2000(b)), the physical and mechanical properties of jute composites were studied under various humidity conditions, hydrothermal, and weathering conditions. The aging-induced deteriorative effect of these conditions on the dimensional stability, surface topography, and mechanical properties of the composites were observed. The severity of aging was more detrimental in an accelerated water test than the other exposure conditions. SEM observation revealed the fiber accentuation along with fiber breakage/splitting, and surface discoloration in both natural and accelerated weathering of UV exposure. Some biological defacement in the form of fungal infestation appeared at the cut edges of weathered composites while extensive disfigurement was noticed on all surfaces under high humidity/water-immersion.

2.2.2 The effects of processing conditions on the mechanical properties of polymer composites

Baiardo et al. (2004) prepared composites of an aliphatic polyester (Bionolle) with natural flax fibers by batch mixing. The effect of processing conditions on fiber length distribution and the dependence on mechanical properties of the composite on fiber content were investigated. The tensile modulus changed with fiber content according to the modified rule-of-mixture equation, with a fiber orientation efficiency factor, $\eta_0 = 0.194$. The strength of Bionolle/flax composites tended to decrease with fiber loading. There was no adhesion between matrix and fibers. With the aim to improve fiber-matrix adhesion, surface chemically modified flax fibers were also tested as reinforcing agents. A

30% strength increase was observed when natural fibers (25 vol%) were substituted by fibers containing acetate groups. No significant strength changes were observed in composites containing fibers with valerate groups of polyethylene glycol chain grafted at the surface.

Wibowo et al. (2004) reported that cellulose esters (bioplastic made from cellulose) were potentially useful biosourced polymers. By embedding inexpensive plant-based cellulosic fibers (chopped hemp fiber) into a biopolymeric matrix (cellulose ester) novel biocomposites was made utilizing two different processing approaches. Powder impregnation (process I) and extrusion followed by injection molding (process II). It was indicated that cellulose acetate plasticized with 30% citrate plasticizer proved to be a better matrix compared to PP for hemp fiber reinforcements in terms of flexural and damping properties. Biocomposites with 30 wt% of industrial hemp fiber processed through extrusion and injection molding exhibited a flexural strength of ~78 MPa and modulus of elasticity of ~5.6 GPa. Cellulose acetate butyrate plastic (CABP) proved to be a better matrix than plasticized cellulose acetate (CAP) for biocomposite applications.

Jayaraman and Bhattacharyya (2004) produced composite specimens consisting of waste plastics obtained from Kerbside collection (high density polyethylene (HDPE) waste, Janitorial waste, Kerbside waste I, and Kerbside waste II) and *Pinus radiata* woodfibers (medium density fibers (MDF)), through melt blending and injection molding. It was found that the mechanical properties of these composites at room temperature and humidity depended on the amount of woodfibers, the mechanical properties of the waste plastics used, and the presence of a suitable coupling agent. The tensile strengths increased by about 25% compared to those of the corresponding waste plastics. Flexural strengths of MDF/waste plastic composites increased with the addition of MDF with the exception of MDF/Kerbside waste I composites. The tensile and flexural moduli of MDF/waste plastic composites mostly increased with increasing fiber content.

Lundquist et al. (2003) developed three pre-forming techniques to prepare pulp fiber reinforced cellulose diacetate (CDA) pre-forms, namely filtration-forming, solvent impregnation, and commingling with polymer fibers. These techniques eliminated all thermomechanical steps, prior to final processing. Nevertheless, the CDA polymer was found to be very sensitive to the specific process histories relevant to each technique, whereas the pulp fibers, whose size, shape, and mechanical properties were affected by neither of the pre-forming processes. The tensile properties of composites compression molded from solvent impregnated pre-forms were compared to those of ground china reed reinforced CDA. On the other hand, ground china reed particles were found to act merely as fillers increasing composites stiffness. A remarkable reinforcement effect was observed for the pulp fiber reinforced impregnated pre-forms. A combination of stiffness increased by a factor 5.2 and a strength increase by a factor of 2.3 relative to the pure polymer was achieved. In typical pulp fiber reinforced thermoplastics, the stiffness increase was frequently obtained at the expense of loss in strength. In addition, the properties achieved by optimizing the extraction and processing steps indicating that pulp fiber reinforced thermoplastics composites were appropriate materials for load bearing applications.

Karnani et al. (1997) conducted the research on biofiber-reinforced PP composites. The preparation of lignocellulosic composites by reactive extrusion processing with good interfacial adhesion was generated by a combination of fiber modification and matrix modification methods. It was indicated that the enhancement on properties of biofiber- reinforced composites could possibly performed through functionalization of the polymer matrix with maleic anhydride (MA) and fiber surface modification. It was mentioned that, in general, composites based on the modified matrix had superior mechanical properties to those containing the unmodified matrix, primarily as a result of improved adhesion and enhanced polar interactions at the fiber/matrix interface.

By using K-mixer and injection molding machine, Rana et al. (2003) prepared short jute fiber reinforced PP composites according to ASTM test pieces. In general, it was found that an increase in toughness was always with decreasing tensile/flexural properties. However, the extent of increase/decrease depended on the type of modifier, its dose and its compatibility with the jute-PP system. It revealed that both impact and tensile properties showed an increase trend with the compatibilizer but a reverse trend was found for the flexural properties. Effect of impact modifier on fiber loading, however, showed different results. There was an increase in impact strength with increasing fiber loading. Tensile and flexural properties were found to optimize at 40% fiber loading.

Lu et al. (2003) introduced self-reinforced melt processable composites of sisal. Through slight benzylation treatment, skin layers of sisal fibers were converted into thermoplastic material while the core of the fiber cell remained unchange. On the basis of these modified sisal fibers, self-reinforced composites were prepared using hot pressing, in which the plasticized parts of sisal serve as matrix and the unplasticized cores of the fibers as reinforcement. It was found that balances of melt processability and reinforcing effect to the benzylated sisal fibers should be considered. Therefore, structure, melt processability, mechanical properties of the treated fibers, and the self-reinforced composites could be accordingly tailored. Furthermore, it was suggested that as the self-reinforced sisal composites still consisted of cellulose, hemicellulose, and lignin, the biodegradatbility associated with plant fibers would be retained. Thus, fungi or enzyme could decompose the composites at the end of their lifetime rather than could incinerate for conventional composite materials.

Czvikovszky (1996) developed a reactive extrusion procedure for wood fiber reinforced thermoplastic composites. By applying a small amount of reactive additive that compatiblizes the synthetic and natural polymer components, with a subsequent

Electron Beam treatment, which is a productive method of creating active sites on both matrix polymer and fibrous reinforcement. It has been indicated that wood fiber and PP (PP) bound together through reactive additive results in a composite which has not only a high modulus of elasticity, but also significantly higher flexural and tensile strength and improved thermal tolerance over the conventional wood fiber-PP blends, and over the PP itself.

Jayaraman (2003) suggested that common methods for manufacturing natural fiber-reinforced thermoplastic composite, injection molding and extrusion, tend to degrade the fibers during processing. Hence, development of simple manufacturing technique for sisal fiber-reinforced PP composites that minimizes fiber degradation was investigated. The results showed that sprinkling the fibers successfully formed sisal fiber mats down a drop feed tower. This innovative fiber mat production method allowed the fiber to avoid much of the processing degradation that is often encountered during conventional shear mixing process. Composite sheets were manufactured from these sisal fiber mats interleaved with PP by vacuum forming of hot pressing. The best possible mechanical properties for the sisal fiber-reinforced PP composites were achieved when the fiber length was greater than 10 mm and the fiber mass fraction was in the range 15-35%.

Joseph et al. (1999) prepared sisal-fiber-reinforced PP composites by melt-mixing and solution-mixing methods. In the melt-mixing technique, the various conditions of mixing time, rotor speed and chamber temperature were investigated for optimal mixing parameters. It was found that a mixing time of 10 min, rotor speed of 50 rpm and a mixing temperature of 170°C were found to be the optimal mixing conditions. Under optimal mixing conditions melt-mixed composites showed better tensile properties than those of solution-mixed composites. Fiber length of 2 mm was found to be optimum for the best balances of properties in the case of melt mixed composites. Composites containing

longitudinally oriented fibers show superior mechanical properties than that of the transverse and random orientations.

Biodegradable composites based on treated and untreated sisal fiber and mater Bi-Z, which was used as matrix, were processed using internal batch mixer (Iannace et al. 2001). The effect of processing conditions (temperature, speed of rotation, and time of mixing) and alkaline treatment on the dimensions of sisal fiber was studied. It was indicated that the length and diameter of the initial fibers were reduced during mixing and this effect was correlated to the magnitude of shear stress developed in the mixer. An increase of the speed of rotation and/or a reduction of temperature resulted in fibers of smaller dimensions but with a higher aspect ratio l/d. Alkaline treatment speeded up the process of the fiber fragmentation and disaggregration but did not affect the final dimensions after a sufficient time of mixing.

2.3   Polymer crystallization

The microstructures of crystallizable polymer matrices play a very important role in thermoplastic composite characteristics. The solidification of semicrystalline polymers, such as PP, from the melt takes place through nucleation and crystal growth. When the process of solidification is completed, the entire volume of material is full of spherulites. Since the mechanical properties of polymeric materials strongly depend on their microstructures and crystallinity. Therefore, understanding the kinetics of crystallization is very important and useful to predict the most appropriate molding conditions and to correlate the developed microstructure with the kinetics of transformation (Avalos et al., 1998).

2.3.1 Kinetics of crystallization

Crystallization occurs in two stages: nucleation and growth. The overall crystallization kinetic has been largely analyzed by the Avrami analysis and the Hoffman and Lauritzen analysis (Gordon et al., 1993).

2.3.2 Avrami analysis

The overall crystallization rate can be monitored by thermal analysis through the evolution of heat of crystallization. Differential scanning calorimetry (DSC) can also be used to determine the crystallinity as a function of time. The enthalpy from DSC thermogram are used to obtain the relative degree of crystallinity, X(t), by using the following equation (Papageogiou et al., 2005).

$$X(t) = \frac{\int_0^t (dH/dt)dt}{\int_0^\infty (dH/dt)dt} \qquad (2.1)$$

Where *dH* denotes the measured enthalpy of crystallization during an infinitesimal time interval *dt*. The limits *t* and ∞ are used to denote the elapsed time during the course of crystallization and at the end of the crystallization process, respectively. The change in crystallinity with time can be readily expressed in the Avrami equation:

$$X(t) = 1 - \exp(-kt^n) \qquad (2.2)$$

Where X(t) is the volume fraction of material crystallized at time t, k is the temperature-dependent constant that contains nucleation and crystal growth rate (rate constant), and n is the crystal geometry information (Avrami exponent). The Avrami parameters, n and k, are

determined by taking the double logarithm of Equation (2.2) to yield a plot of log{-ln(1-X)} versus log t.

In isothermal crystallization, the crystals are grown at a constant temperature, For each temperature, the fraction of polymer crystallized at time t can be obtained from DSC thermograms and plotted in the form of log{-ln(1-X)} versus log t, where the slope of the plot is equal to n, and k is obtained from the intercept of the plot or from the expression:

$$k(T) = \frac{\ln 2}{(t_{1/2})^n} \tag{2.3}$$

Where the half time, $(t_{1/2})^n$ is the time taken for 50% of the total crystallization to occur.

During actual processing conditions the crystallization takes place under nonisothermal conditions. Therefore, numerous attempts have been made to extend the theory to nonisothermal conditions. The most accepted and used model was proposed by Nakamura et al. (1972 and 1973). On the basis of isokinetic conditions that assume the same temperature dependence for the radial growth rate, G, and the crystallization rate constant, k(T), Nakamura obtained the following model.

$$X(t) = 1 - \exp\left[\left(\int_0^t K(T(t'))dt'\right)\right]^n \tag{2.4}$$

Where X(t) is the relative degree of crystallinity at time t and K(T) is the nonisothermal crystallization rate constant. The differential form of the Nakamura equation is more useful for processing simulation and takes the form:

$$\frac{dX}{dt} = nK(T)(1-X)[-\ln(1-X)]^{(n-1)/n} \tag{2.5}$$

The nonisothermal rate constant is related to the isothermal one through the following equation proposed by Nakamura et al. (1972 and 1973).

$$K(T) = [k(T)]^{1/n} = \frac{(\ln 2)^{1/n}}{t_{1/2}} \tag{2.6}$$

Where K(T) is nonisothermal rate constant (Nakamura), and k(T) is isothermal rate constant (Avrami).

2.3.3   Hoffman and Lauritzen analysis

Kinetic theories, as opposed to theories that emphasize the characterization of the equilibrium aspects of polymer crystals, are essentially nucleation theories. These kinetic theories differ from classical nucleation theory in that the emphasis is not only on the formation of the nucleus but also on its subsequent growth. The well-established Hoffman and Lauritzen theory has been used to quantify the isothermal crystallization kinetics because of the applicability and straightforward quantitative nature of the theory.

Under normal circumstances, flexible linear molecules crystallize into the form of thin platelets whose upper and lower surface consist of an array of molecular folds. These folded structures in polymers crystallizing from the melt are referred to as "chain-folded lamellae" These lamellae grow to form spherulites, so commonly encountered in crystallized linear polymers. The growth rate of Hoffman and Lauritzen theory is based on surface or secondary nucleation theory. The following treatment does not consider the fluctuations of the fold but still predicts growth rates over a wide range of supercooling. The Hoffman and Lauritzen growth rate equation is given as (Hoffman et al., 1976):

$$G(T) = G_0 \exp\left[\frac{-U^*}{R(T_c - T_\infty)}\right] \exp\left[\frac{-K_g}{T_c(\Delta T)f}\right] \qquad (2.7)$$

Where

G(T)   is the radial growth rate.

G_0 is the pre-exponential factor containing quantities not strongly dependent on temperature.

U^* is a universal constant characteristic of the activation energy of chain motion (reptation) in the melt.

R   is the gas constant.

K_g is the nucleation constant.

T_∞ is the theoretical temperature at which all motion associated with viscous flow or reptation ceases, and is defined as $T_\infty = T_g - 30$ (K).

T_c is crystallization temperature.

f is the correction factor $f = 2T_c/(T_m^0 + T_c)$, which account for the temperature dependence of Δh_f, f has little effect at small supercoolings, but decreases Δh_f considerably near the glass transition temperature.

T_m^0 is the equilibrium melting temperature.

ΔT is the supercooling and is equal to $T_m^0 - T_c$.

Based on Equation (2.6) and Hoffman-Lauritzen theory the temperature dependence of the nonisothermal rate constant may be expressed as (Isayev et al., 2000).

$$K(T) = (\ln 2)^{1/n} \left(\frac{1}{t_{1/2}}\right)_o \exp\left[\frac{-U^*}{R(T_c - T_\infty)}\right] \exp\left[\frac{-K_k}{T_c(\Delta T)f}\right] \qquad (2.8)$$

Where $\left(\dfrac{1}{t_{1/2}}\right)_o$ is the pre-exponential factor that includes all terms independent of temperature, K_k is the nucleation exponent, and the remaining factors have the same meaning as outlined in Equation (2.7).

The growth rate, combined with the crystallization rate constants determined from isothermal and nonisothermal, will be used to estimate the number of effective nuclei for each material. For instantaneous nucleation for three dimensional spherulite growth rate, the Avrami exponent equal to 3, all potential nucleation sites are already in their activates state, N. If spherulites are assumed to grow in a free space without impingement, the total volume relative to the unit volume transformed by time, t, is given by the following equation (Nagasawa et al., 2005):

$$V_{free} = \sum_{i=1}^{\infty} n_i \left(\frac{4\pi}{3}\right)[G(t-t_i)]^3 \tag{2.9}$$

Where n_i is the number of nuclei per unit volume activated at time, t_i, and G is the radial growth rate. If the mode of nucleation is simultaneous then,

$$V_{free} = N\left(\frac{4\pi}{3}\right)[G(t)]^3 \tag{2.10}$$

Where N is the number of effective nuclei. For the real space in which a number of spherulites impinge with each other and their growth is restricted, the Avrami-Evans theory proposed,

$$1 - \frac{V}{V_{\infty}} = \exp(-V_{free}) \tag{2.11}$$

Where V_∞ is the transformable volume fraction and V is the volume fraction transformed by a certain time. By representing V/V_∞ by the degree of crystallization, X(t), and replacing Equation (2.10) by Kt^3, Equation (2.10) was transformed into the following equation:

$$1-X(t) = \exp(-Kt^3) \tag{2.12}$$

Where

$$N = \frac{3K}{4\pi G^3} \tag{2.13}$$

From Equation (2.13), the growth rates combined with the non-isothermal rate constants determined from Equations (2.7) and (2.8), respectively, were used to estimate the number of effective nuclei as a function of temperatures.

2.3.4 Crystallization of polypropylene composites

The physical properties of semi-crystalline polymeric materials strongly depend on their microstructure and crystallinity, because failure of the materials takes place at the microscopic level. The crystalline form can be obtained by slowly cooling the melt or by isothermal crystallization at a temperature between the crystalline melting point and the glass transition temperature. From this point of view, the crystallization kinetics of PP has been widely studied by different methods.

Xu et al. (2003) investigated the effect of nucleating agent (mainly contained sodium benzoate) on the crystalline morphology under different structure levels of PP material. It was reported that an increase in nucleating agent had an effect on both high and low levels of the crystalline structure. Nucleating agent showed a heterogeneous

nucleation effect. At the level of aggregation structure, crystallinity increased and spherulite size tended to decline with increasing nucleating agent. At the same time, the nucleating agent also effected on both the crystal grain structure and the unit cell structure.

Amash and Zugenmaier (2000) studied thermal, morphological and dynamic mechanical properties of PP-cellulose fiber (CF). Two types of CF and a compatibilizer were used. Calorimetric measurements exhibited an increase in the crystallization temperature and crystallinity of the PP component. This was attributed to the nucleating effects of the fiber surfaces, resulting in the formation of transcrystalline regions observed by an optical method. The dynamic mechanical spectra of the composites revealed an increase in the stiffness and reduction in the damping values with increasing CF content. The results were consistent with morphological observations, which verified and improved interfacial adhesion between fiber and matrix. The effects of drawing on structure and physical properties of PP-cellulose composites shown that increasing drawing ratio, the melting peak of PP component was shifted to higher temperatures suggesting a constrained melting, and the uniaxial elastic modulus was considerably enhanced. The biggest influence was observed for the samples of PP-spun cellulose and the lowest for neat PP. In addition to the fibrillar structure of the oriented PP, the highly CF orientation and the efficient compatibilization in composites were responsible for the effects observed in the drawn samples. Moreover, Quillin et al. (1994) found that the presence of treated and untreated cellulose fibers in PP has a dramatic effect on the kinetics crystallization. The addition of untreated cellulose fiber to PP, which was shown to produce a transcrystalline region, resulted in an exponent value of 2.7-2.9 for the initiation stage, followed by a value of 3.9 for the bulk stage. Treatment of cellulose with alkyl ketene dimmer, alkenyl succinic anhydride, or stearic acid resulted in intermediate exponent values from 2.7 to 3.9. These results verified the effectiveness of surface treatments in reducing the natural nucleating ability of cellulose.

In a study of Avalos et al. (1996), the effect of small additions (up to 20 wt %) of low-density polyethylene (LDPE) on the crystallization kinetics and thermodynamics of an isotactic polypropylene (iPP) was examined, including morphological studied of iPP/LDPE blends. It was shown that at LDPE percentages above 10% in the blend, the LDPE aggregated pass over the spherulitic limits and went into the intraspherulitic domains of the PP. The half-crystallization time ($t_{1/2}$) as well as Avrami exponent (n) and the chain folding energy for PP crystallization (σ_e) increased markedly at LDPE percentages above 10% in the blend. The isothermal radial growth, G, of the PP in the blends was one-third of the plain polymer, although it remained constant at any blend composition. However, the overall kinetic rate constant seemed to be influenced by the presence of the melt LDPE phase. In all case, and according to the obtained results, an instantaneous nucleation took place. Later on, the same research group of Avalos et al. (1997 and 1998) investigated the effect of only short glass fibers and simultaneously both short glass fibers (SGF) and LDPE, on PP crystallization kinetics and thermodynamics. In a case of short glass fibers, a marked decrease of the half time of PP crystallization, $t_{1/2}$, as well as a sensible increase of the overall crystallization rate, K_n, were observed in the presence of fibers. However, at any crystallization temperature, a maximum of $t_{1/2}$ was reached at 20% glass fiber content in the composite followed by a continuous decrease as fiber percentage increaseed. A nucleant effect of fibers was evident and no transcrystallinity was observed with these short glass fibers. In a case of ternary composites based on PP, LDPE, and short glass fibers, It was reported that glass fibers tended to initially compensate the delaying effect of LDPE on the PP crystallization as was shown by the values of $t_{1/2}$ as well as by K_n. However, at high glass fiber percentages in the composite (30-40%) a considerable increase of $t_{1/2}$ values was observed, although they remained always below the corresponding values of the plain polymer. The isothermal radial growth rate of PP spherulites was hardly affected by both the fibers and the LDPE.

According to the value of the Avrami exponents, it could be established that the spherulitic development arised from an athermal, instantaneous and heterogeneous nucleation with two-directional diffusion controlled growth. No transcrystallinity was observed. Next, López-Manchado and Arroyo (1999) studied the effect of short polyethylene terephthalate (PET) and nylon 66 (PA) fibers, and their chemical treatment with azide derivative, on the PP crystallization kinetics and thermodynamics. It was indicated that both fibers were effective nucleating agents for PP crystallization, giving rise to the phenomenon of PP transcrystallinity on their surface. However, the presence of azide groups on the chemical structure of the fibers produced a different effect on the PP crystallization kinetics. Azide-modified PET fiber gave rise to an additional increase of the global rate of the PP crystallization process, but in this case the transcyrstalline development of the PP was not as sensible as in the presence of the unmodified fibers. An opposite behavior was observed with the azide-modified PA fibers. In general, it could be established for the studied composites that the sperulitic development of the polymer matrix came from an instantaneous and athermal nucleation whose growth was not constant. It was also suggested that transcrystallinity and a good adhesion at the interface may take place independently one of each other.

Cho et al. (1999) studied the crystallization and melting behavior of PP and maleated PP (mPP) blends. It was found that either co-crystallization or phase separation in the blends could be obtained depending on the crystallization conditions. The half-life of crystallization ($t_{1/2}$) showed that incorporation of mPP in PP could either have little effect or greatly increased the crystallization rate of PP depending on the crystallization temperatures. At higher crystallization temperatures, the crystallization rate of the blends was higher than both the pure homopolymers, resulting in phase separation morphology. Similar research was done by Seo et al. (2000), who have investigated the crystallization kinetics of isotactc PP (iPP) and maleic anhydride grafted PP (MA-PP) and their blends,

crystallized both nonisothermally and isothermally by DSC. It was reported that during isothermal crystallization, relative crystallinity developed with the time dependence described by the Avrami equation with exponents n ≈ 2.7 for neat iPP and n ≈ 3.8 for MA-PP. The half crystallization time for MA-PP was much smaller than that for iPP. The half crystallization time for iPP depended more strongly on the crystallization temperature than that of MA-PP did. A kinetic equation for nonisothermal crystallization was employed to analyze the crystallization characteristics of iPP and MA-PP. The nonisothermal crystallization kinetic analysis for MA-PP at different cooling rates was possible. Assuming that the spherulitic growth was initiated by heterogeneous nucleation alone while that for iPP at high cooling rates was successfully done by assuming both homogeneous and heterogeneous nucleations. The diffusional activation energy was smaller for MA-PP than for iPP. The number of heterogeneous nuclei for MA-PP was larger than that for iPP. The presence of MA-PP in iPP affected the crystallization of iPP by acting as a nucleating agent.

Cyras et al. (2001) conducted a research on crystallization kinetics of polycaprolactone (PCL)/starch and their reinforced sisal fiber composites. The induction time of the crystallization and the crystallization rate were not influenced by the presence of sisal fiber as was expected in heterogeneous nucleation. Although it was able to physically produce this effect, the fibers perhaps acted as a retardant of nucleation. According to a research group of Joseph et al. (2003), the thermal and crystallization behavior of sisal/PP composites was studied by thermogravimetry (TG), DSC and polarizing optical microscopy. DSC measurements exhibited an increase in the crystallization temperature and crystallinity, upon the addition of fibers to the PP matrix. This was attributed to the nucleating effects of the fiber surfaces, resulting in the formation of transcrystalline regions. With increasing fiber content, the melting peak of the PP component was shifted to higher temperatures suggesting a constrained melting. The

thickness of the transcrystalline layer depended on crystallization temperature and time. The transcrystalline growth rate was slow in the quiescent state. On the other hand, upon the application of stress, transcrystallization developed quickly. In fact, the shear stress at the polymer/fiber interface initiated the nucleation. Fiber surface modification by urethane derivative of polypropylene glycol (PPG/TD) increased the nucleating ability of sisal fiber to a very small extent.

Crystallization and interfacial morphology of bamboo fiber-reinforced PP composites was examined by Mi et al (1997). PP and two maleated polpropylenes (s-MAPP and m-MAPP) were used as matrices. It was shown that the addition of bamboo fiber to any of the three polymers caused an increase in the overall crystallization rate. A considerable amount of β-form crystallinity was produced in the PP, s-MAPP, and m-MAPP by mixing bamboo fibers; and all the bamboo fiber-filled samples contain both the α- and the β-forms. In addition, transcrystalline growth of s-MAPP and m-MAPP on the bamboo fiber surface was observed.

The effect of different kinds of fibers on the crystallization of iPP was analyzed by López-Manchado et al. (2000). Results revealed a dramatic decrease of the half-time of crystallization, $t_{1/2}$, as well as a sensible increase of the overall crystallization rate, K_n, for all the composites compared to neat iPP. The crystallization peak temperature was shifted tohigher temperature in the presence of fibers and was more noticeable for the aramid fibers. On the other hand, no differences were observed in the melting temperature. The determination of the spherulitic growth confirmed the positive effects of fibers on nucleation and crystallization kinetics. An increase of the nucleation density was observed for all the analyzed samples and in particular for the aramid fibers.

Mucha et al. (2000) studied the effect of carbon black on the properties and kinetics of crystallization of iPP. It was found that both the nature of nucleation and growth mechanism of crystalline PP changed depending on the crystallization temperature

and carbon black content. The rates of nucleation and crystallization significantly increased confirming the nucleating effect of carbon back, particularly, in the case of samples with a small content of carbon black.

The crystallization of nanocomposites of iPP with organo modified montmorillonite compatibilized by maleic anhydride grafted PP was studied by Nowacki et al. (2004) using light microscopy in isothermal conditions, in quiescent, and in shear state. The isothermal and nonisothermal crystallization of the composites were also investigated by DSC method. It was found that only weak nucleation activity of montmorillonite was observed during crystallization in static conditions. The clay nucleation activity was greatly enhanced in shear-induced crystallization and resulted in a drastic decrease of spherulite sizes. In nanocomposites films isothermally crystallized, the intense nucleation of iPP spherulites was observed when the polymer was forced to flow to compensate the volume shrinkage due to crystallization. It was also found that the presence of glass support enhanced spherulitic nucleation in nanocomposites. This was possibly caused by shear due to a difference in thermal shrinkage of polymer matrix and a glass support.

Maiti et al. (2002) prepared intercalated nanocomposites of PP/clay (PPCNs) by a melt extrusion process using maleic anhydride modified PP (PP-MA) and organophilic clay. Further, they have studied the influence of crystallization on intercalation, morphology, and mechanical properties of PP/clay nanocomposites. It has been found that the extent of intercalation of PP-MA chains in the space between silicate galleries increased with crystallization temperature, T_c, and decreased with increasing clay content. As compared to matrix PP-MA, the dispersed clay particles in the PP-MA matrix acted as a nucleating agent and lowered the spherulie dimension with increasing clay content as revealed by light scattering experiments and polarizing optical microscopy. The PPCNs crystallized at high T_c showed that a certain extent of segregation of the dispersed

clay particles took place around the boundary of the spherulites (interspherulite). Extensive intercalation occurred during crystallization, especially at high T_c due to the long time for full solidification of the melt. The degree of intercalation of PP-MA chains in the silicate galleries strongly depended on the time in the molten state. The effect of the intercalation through organophilic interaction on the dynamic storage modulus of the PPCNs crystallized in the temperature range of 70-130 °C was emphasized.

Isothermal and non-isothermal crystallization kinetics of PP/surface-treated SiO_2 nanocomposites were investigated by Pagageorgious et al. (2005). Isothemal crystallization rates of iPP-fumed silica nanocomposites increased with increasing filer content up to 7.5wt%. In the case of non-isothermal crystallization, it was found that the Ozawa analysis was rather inapplicable for the nanocomposites. In contrast, the modified Avrami method was applied giving satisfactory results, together with the analysis of Mo and co-workers. The nucleation activity of the silica nanoparticles was found to increase with the silica amount up to 7.5wt%. Another study on silica nanoparticle-filled poly(ethtylene 2,6-naphthalate) (PEN) composites was done by Kim et al.(2003). The melt viscosity and total torque values of the composites were reduced by the silica content. The crystallization exothermic peak shifted to a higher temperature and overall crystallization time was reduced as the silica content increased. Moreover, the spherulite growth rate increased with increasing silica content. It was also revealed that silica nanoparticles acted as nucleation agents in the PEN matrix. Esteves et al. (2005) also investigated the crystallization behavior of polyamide-based nanocomposites containing surface-modified SiO_2 nanofillers. The nanocomposites microstructure showed a high degree of dispersion of the filler. The isothermal crystallization kinetics was shown a strong influence of the nanofillers morphology on the poly(tetramethyleneterephthalamide) crystallization behavior. The strong nucleating effect of the inorganic substrate was interpreted as the

combined result of a lower activation energy for the primary nucleation and a higher activation energy for the transport of chain stems to the growing lamellae.

Wang et al (2003) determined the effect of barium sulfate ($BaSO_4$) on the spherulite radial growth rates of iPP. The PP-$BaSO_4$ interface was modified by treating the fillers with different couple agents. The addition of $BaSO_4$ depressed the spherulite growth rate and the effect was more dramatic when the interfacial interaction between PP and $BaSO_4$ was enhanced. In addition, the enhancement of PP-$BaSO_4$ interaction promoted the particles to serve as physical crosslink points, which hindered the movement of the polymer chains and resulted in a decrease of the pre-exponential factor, G_0.

Blom et al. (1998) presented the results from their investigation in the crystallization behavior of PP. The crystallization process was followed by hot-stage optical microscopy, DSC, and dynamic mechanical methods. Also, NMR spin-spin relaxation techniques were employed to prove the morphology of the PP. Nucleation in this iPP was athermal and appeared to be heterogeneous. The dependence of the onset temperature of crystallization on the annealing temperature and on the annealing time indicated that PP nuclei were able to survive the melting process. NMR spin-spin relaxation experiments indicated that the PP melt contained a significant proportion of regions of high segment density. It was postulated that these ordered regions acted as nucleation sites for PP crystallization, and the number and size of these regions was determined by the annealing time and temperature. Addition of HDPE to PP resulted in melting-point depression and plasticization of the PP phase at lower HDPE contents. HDPE was able to sufficiently penetrate the PP phase at lower HDPE contents to reduce the number and size of regions of high segment density. As a result, the nucleation and subsequent crystallization of the PP phase was delayed.

2.4   Shear-induced crystallization

It is generally agreed that the properties of an injection molded part partially depend on its morphology. During injection molding, plastics undergo fountain flow. The molten polymer is subjected to high shear stress at the cavity wall which causes the preferential orientation of the molecular chains. As a result, a skin layer or normalized thickness of shear-induced crystallization layer with a high molecular orientation takes place at the surface of moldings. On the other hand, in the core of moldings, the relaxation of the molecular chain occurs due to the low cooling rates and low shear stress. Then the effect of shear on crystallization can be neglected. At the core region, quiescent crystallization takes place. As a result, spherulites with a low molecular orientation are observed. In reality, injection molded parts are frequently composed of many layers of varying orientation depending on the materials, flow pattern, and molding conditions. Extensive work has been done to identify and measure the layered structure of injection molded parts.

Kantz (1972) found a multilayer structure in injection molded bars of PP. It could be observed four different layers and demonstrated that the skin thickness was proportional to the melt temperature during molding. It was also showed that the modulus and yield strength were greater for the skin than for the core, assuming that higher orientation and density led to higher modulus. Jarus (1996) identified five different layers within the injection molded bars and showed that the core have a higher modulus than the skin.

According to the study of Strebel et al. (2004), the injection molded parts from TPOs which were produced by blending PP homopolymers, PP impact copolymers and poly(ethylene-propylene) copolymer rubbers, had up to five distinct layers of varying orientation between the outer edge and the center of the sample. In both the PP and TPO formulations, the skin thickness of the moldings increased as the polymer molecular weight increased. Similarly, Son et al. (2000(b)) investigated the morphology of injection

molded poly(phenylene oxide)/polyamide-6 blends. A distinct skin layer, sub-skin layer, and core region were observed across the part thickness, and the morphology of the skin layer was clearly seen.

Viana (2004) investigated the condition affecting the development of the skin layer in injection molding. For all moldings the skin thickness decreased with the increase in the thermal and shear stress levels, although with distinct contributions for the different molding geometries. The development of the skin layer was interpreted in the light of a phenomenological model involving two time variables: the time allowed for relaxation of the highly oriented melt until the crystallization temperature was reached and the relaxation time of the material.

Murhy et al. (2002 and 2003) studied the effect of melt temperature (T_m) and skin-core morphology on the mechanical properties of nylon 6. Rapid quenching of the surface produced a skin with lower crystallinty than the core, which was cooled more slowly. There was an optimal melt temperature to achieve the desired mechanical properties. This was because microstructure near the skin and core changed in opposite directions as the T_m was changed. As T_m was increased, the crystallintiy at the skin increased. This, for instance, gave rise to a minimum in flexural modulus and a maximum in the elongation at break.

A novel approach for the numerical simulation of the flow-induced crystallization and frozen-in birefringence in moldings of semi-crystalline polymers was proposed by Kim et al. (2005). The approach was based on the calculation of elastic recovery that becomes frozen when the flow-induced crystallization occurred. In agreement with experiments, the calculation indicated that the melt temperature, injection speed, molecular weight, and wall temperature affected the flow-induced crystallization and the amount of frozen-in birefringence in molding. However, the present calculations showed that these processing conditions including holding pressure and holding time had less effect on the calculated frozen-in birefringence than the experiments indicated.

In the study of Schrauwen et al. (2004), results from optical micrographs showed layers of different level of orientation. Layer thickness in injection molded sample was found to decrease along the flow path and increased for lower melt temperature and longer filling time. For all polymer studied, an increase of extended chains (shish) in the loading direction was proposed to cause an increase in the yield stress and a lamellar structure oriented perpendicular to loading direction. This led to an increase in strain hardening. In the extruded samples, where a low level of extended chains and a high level of oriented lamellae were found, the resulting combination of yield stress and strain hardening led to homogeneous deformation.

Kumaraswany et al. (2000) conducted a research on shear-enhanced crystallization in iPP. In-situ synchrotron wide angle ray diffraction (WAXD) was used to follow crystallization in a polydisperse iPP during and after a brief interval of shear under isothermal conditions. A specific flow history was selected from the range that induced a highly oriented skin core morphology. At the chosen crystallization temperature ($T_{cryst} = 141$ °C, characteristic time quiescent crystallization, $t_Q \sim 10^4$ s), crystalline WAXD peaks emerged during the brief interval of shear ($\sigma_w = 0.06$ MPa, $t_s = 12$ s) showing a highly oriented fiber-like diffraction pattern. Primary lamellae with c-axis orientation were present, along with their associated crosshathched daughter lamellae. The crystallinity grew rapidly during the first 100 s ($\sim 10^{-2} t_Q$) after cessation of shear, and very slowly after that. Further, for the first 1200 s, the orientation distribution did no change from that generated during the shear pulse. Ex-situ transmission electron microscopy showed a characteristic skin-core morphology with a thin skin region consisting of oriented crystallites near the walls of the shear device, adjacent to weakly anisotropic spherulites farther from the walls. This indicated that the in-situ WAXD at the early stages of crystallization arose mainly from crystallites in the oriented skin. The skin consisted of densely nucleated thread-like line structures from which α-phase crystalline lamellae

radiate. The spacing between the row nuclei in the skin increased as a function of distance from the wall of the shear device. It was suggested that the lamellae grew from a central thread until they impinge at about 100 s to from the dense crystalline structure in the skin.

Seki et al. (2002) studied the role of long chains in shear-mediated crystallization by in situ rheo-optical measurements and ex situ microscopic observations. To elucidate the effects of long chains, they have prepared model blends in which fractionated iPP (denoted L-PP) with high molecular weight (MW) and narrow molecular weight distribution was blend with a metallocene iPP (Base-PP) with low molecular weight. The concentration of L-PP (c) was varied ranging from 0 to twice the concentration (c^*) at which L-PP coil overlap. The crystallization kinetics were not affected by the addition of L-PP. A distinctive change in the development of birefringence after shearing was observed when the wall shear stress (σ_w) exceeded a critical value (σ^*). Below σ^* and irrespective of c, the birefringence after transient shearing gradually increased and reached a small value at the end of crystallization. Above σ^*, a brief interval of shear induced highly oriented growth, manifested in the birefringence after cessation of flow and growing stronger and reaching a large value as crystallization proceeded. Further, the growth rate of the birefringence exhibited a strong, nonlinear c dependence. The morphology of the skin layer showed a shish kebab type structure observed by TEM for samples subjected to stresses above σ^*. The number density and thickness of shish were affected by c and drastically changed at c near the overlap concentration of the long chains. This indicated that the role of long chains in shear-induced oriented crystallization was cooperative (rather than a single chain effect), enhanced by long chain-long chain overlap.

2.5　Transcrystallization in polymer composites

It is well known that when fibers are incorporated in semicrystalline polymers, under appropriate conditions, a highly oriented layer is developed at the fiber/matrix interface. This distinct morphology is called transcrystalline layer (TCL) and is a consequence of high nucleating ability of the fibers, compared to that of the bulk matrix. In contrast, isotropic spherulites are normally found in the bulk. Owing to its better mechanical properties, compared to the bulk matrix, (Kewi et al., 1967 and Hata et al., 1993) TCL has drawn much attention recently in studying fiber reinforced semi-crystalline polymer composites.

2.5.1　Structure of transcrystallization

Varga and Karger-Kocsis (1995) found that in the quiescent melt, the high modulul-carbon fiber (HMCF) generated α-transcrystallization due to its strong α-nucleation ability. In the isothermally crystallized sheared melt, achieved by pulling the HMCF slightly above the crystallization temperature, a transcrystalline-like supermolecular structure developed. It was evidenced that this shear-induced supermolecular structures composed of two crystalline phases: α and β. The α-layer, generated by melt shearing along the CF surface (α-row nuclei), triggered the growth of the β-modification of PP under the selected crystallization condition. This shear-induced polymorphous interfacial morphology should be correctly term 'cylindrite'. The basic different between transcrystallization and cylindritic crystallization was related to the fact that transcrystallization was induced by heterogeneous nucleation, whereas cylindritic growth was induced by self (homogeneous) nucleation (Figure 2.1).
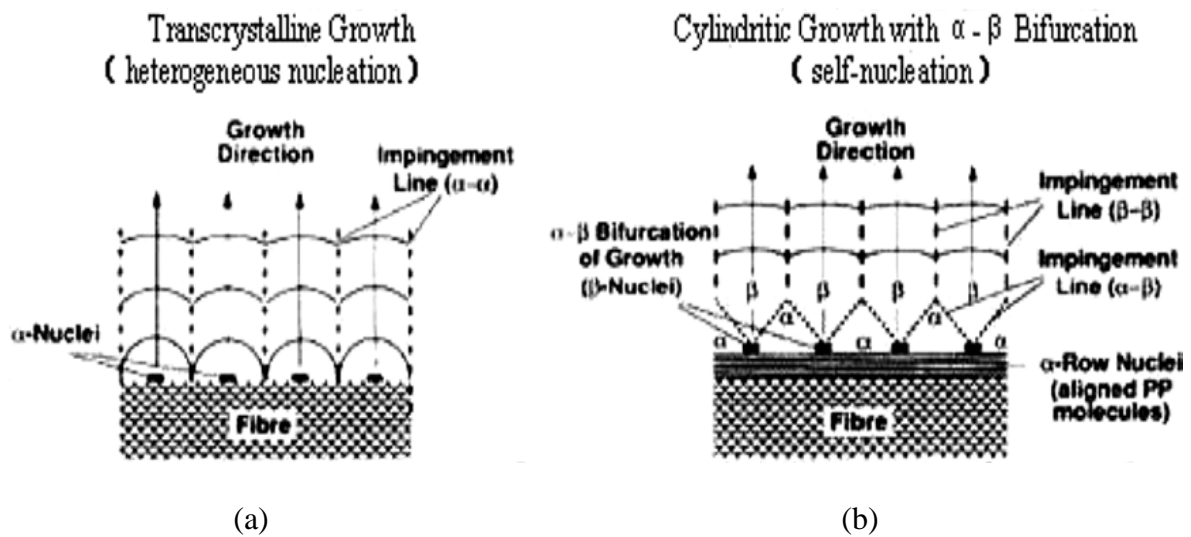
Figure 2.1 Schematic diagram of the difference between transcrystallization and cylindritic crystallization (Varga and Karger-Kocsis, 1995).

Kitayama et al. (2003) studied TC in iPP fiber reinforced iPP composites and found that TC layers were often composed of two regions. That was in one region close (<300 nm) to the fibers, lamellae existed very densely and the c-axes of the crystal lattices were oriented along the longitudinal direction of the fiber. In the other region, a little away (>300 nm) from the fiber, a cross-hatched structure composed to the parent lamellae (whose c-axes were parallel to the fiber surface) and the daughter lamellae (whose c-axes were perpendicular both to the fiber and the parent lamellae), was observed. A schematic illustration of the lamellae orientation near the fiber surface was shown in Figure 2.2.
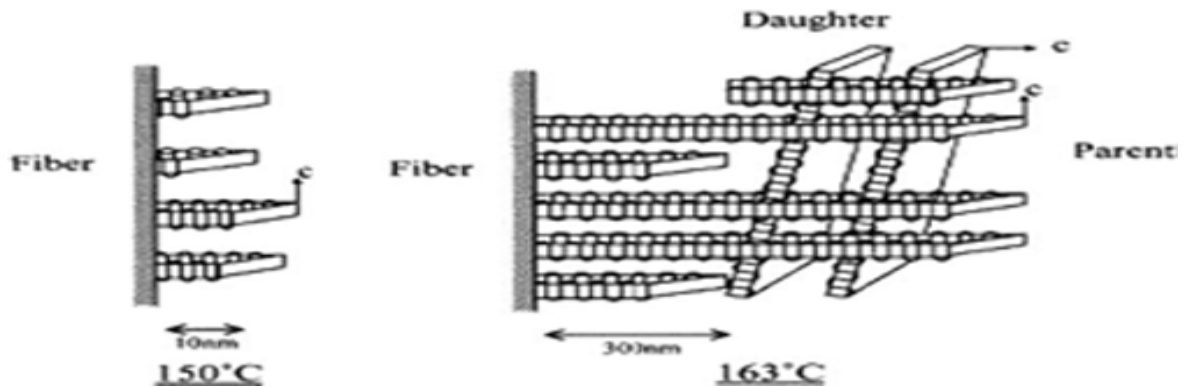
Figure 2.2   Schematic illustration of lamellae orientation near the fiber surface (Kitayama et al., 2003).

2.5.2   Transcrystalliztion in natural fiber-PP composites

Several natural fibers such as sisal (Schonhorn et al., 1968), jute (Joseph et al., 2003 and Mildner and Bledzki, 1999), cellulose (Quillin et al., 1993 and 1994, Son et al., 2000(a), Amash and Zugenmaier, 1998 and 2000, Felix and Gatenholm, 1994), flax (Zafeiropoulos et al., 2001), kenaf (Sanadi and Caulfield, 2000), bamboo (Mi et al., 1997) fibers could be used for the formation of TC. Joseph et al. (2003) found that when chemical modifications were treated to sisal fiber using urethane derivative of polypropylene glycol (PPG/TDI), MA-PP, and KMnO$_4$ in order to improve the interfacial adhesion between the fiber and matrix, a TC layer occurred at the interface. The thickness of the TC layer depended on crystallization temperature and time. The TC growth rate was slow in the quiescent state, on the other hand, upon the application of stress, TC developed quickly. Fiber surface modification by PPG/TDI increased the nucleating ability of sisal fiber to a very small extent.

In the study of jute fiber (untreated and alkali treated)/iPP and jute fiber/MA-PP by Mildner and Bledzki (1999), it was found that the thickness of the TC

layer varied with the cooling rate, with the system jute/MA-PP having the thickest TC layer at the lowest crystallization temperature (115°C). Furthermore, no TC was induced on regenerated cellulose fibers, whereas the fibers which exposed a clean natural cellulose surface induced TC rapidly. The presence of lignin or hemicellulose on the fiber's surface inhibited TC. When PP was allowed to isothermally crystallize at different temperatures (125-133°C), a TC layer was generated around the cotton fibers (Felix and Gatenholm, 1994). The thickness reached 80-120 μm when crystallized for 15 min at 131°C. The TC layer of different thickness was observed by interrupting the isothermal crystallization at certain intervals and quenching the melt.

Zafeiropoulos et al. (2001) examined isothermal crystallization (range of 137-155°C) from the melt of two different iPP in the presence of flax (*Linum usitatissinum*) fibers with four different type (green flax, dew retted flax, Duralin® treated flax, and stearic acid sized flax). It was reveled that the fiber surface micro-roughness seemed to be an important factor affecting the morphology of the TC and the ability of the fiber to induce it. Stearic treated flax fibers inducing a TC layer was a new finding and the cooling rate from the melt to the crystallization temperature was found not to affect the morphology of the TC layer. If MAPP coupling agent was used to improve the stress-transfer efficiency in the kenaf fiber-PP composites (Sanadi and Caulfield, 2000), TC was observed for both uncoupled and coupled composites. Although the growth rate of the coupled composites was higher than that of the uncoupled ones.

2.5.3   Transcrystalliztion in synthetic fiber-PP composites

Synthetic fibers, such as PTFE fiber (Wang and Liu, 1998, Wang and Hwang, 1996(a) and 1996(b), Amitay-Sadovsky et al., 1999, and Hata et al., 1994), aramid fiber (Assoulline et al., 1999 and 2002, Barber et al., 2002, Arroyo et al., 2000, Wu et al., 2001, and Dean and Register, 1998), PET fiber (Saujanya et al., 2001(a) and 2001(b), Li

et al., 2004(a), and 2004(b)), PI fiber (Sukhanova et al., 1995, Amitay-Sadovsky et al., 1999, and Ton-That and Jungnickel, 1999), aluminum (Lin et al., 2001, and Fitchmun and Newman, 1970), and talc (Naiki et al., 2001), were reported to induce TC of iPP.

Dean and Register (1998) obtained a mixture of α and γ TC by inserting a high weight fraction of HMCF or Kevlar 49 aramid fibers in iPP at atmospheric pressure. The proportion of the γ form depended on the fiber concentration. Wherein 90% of fibers were required to obtain a significant proportion of γ which decreased rapidly as the fiber concentration decreased.

Li et al. (2002(a)-(c), 2003, and 2004(a)-(b)) studied the crystal morphology of PET/iPP in-situ MFC, prepared by a slit extrusion-hot stretching-quenching progress. It was found that TC was formed around the PET in-situ microfibers, and a shish-kebab structure could be observed as well. Three nucleation origins were proposed in the microfibrillar composite under a flow field: (a) the classical row-nuclei model; (b) fiber nuclei; and (c) nuclei induced by fiber assistant alignment. The last model provided a natural explanation for the case that TC only occurred in some fiber-reinforced composites under flow rather than without an external field.

The TC of iPP was reported to be induced by PI fiber with different nucleation ability (Sukhanova et al., 1995). The TC layer had a composed structure, with a characteristic layer adjacent to the fiber surface. The layer was about 1 μm thick and had a crosshatched lamellar morphology. At the interface between iPP and the PI fiber which could induce TC, the nuclei from which the TC zone grow were observed. The nuclei consisted of sheaves of closely packed parallel needle-shaped lamellae of uniform thickness. The TC could be explained by the epitaxial crystallization of iPP matrix on the surface fragments (domains) formed by extended chains of PI fibers. The TC layer of iPP could only be produced if the alumina fiber was pulled through the supercooled matrix (Peron et al., 1996), both α-monoclinic and β-hexagonal crystal structures were identified

in the TC. The β crystal could be only induced in areas which existing α crystals. The α region transformed into β crystals except for a small region at the fiber/matrix interface. The β crystals grew at a faster rate than α crystals and were found to melt at 157°C, compared to 170°C for the α crystals.

Some researchers compared the nucleation ability of different fibers (Thomason and Van Rooyen, 1992, Cai et al., 1997, Wang and Liu, 1999, López-Manchado and Arroyo, 1999, Assouline et al., 2000, Amitay-Sadovsky et al., 1999, Arroyo et al., 2000, Ton-That and Jungnickel, 1999, and López-Manchado et al., 2000). López-Manchado et al. (2000) studied the effects of the incorporation of different types of fibers, such as PET, aramid fiber, GF and sisal fiber, on the crystallization kinetics and thermodynamics of iPP. The crystallization kinetics of composites was successfully described by the Avrami model. The fibers behaved as effective nucleating agents and TC took place in all kind of fibers studied, but aramid fibers were the most effective in promoting TC. Ton-That and Jungnickel (1999) found that TC developed between all polymeric substrates PI, PTFE, and PET. Metallic substrates like steel, copper, and aluminum yielded, in no case, TC, and GF did not promote TC either. The thicknesses of the TC layers increased severely with decreasing cooling rate if they did develop. By suitable choice of the cooling rate, the structure could then be controlled between purely spherulitic and completely TC.

Cai et al. (1997) studied the TC of iPP on different fibers (CF, GF, and aramid fiber) conducted in a temperature gradient. The UHMCF, the HMCF, and the aramid fiber showed sufficient nucleation ability to form TC of iPP in certain temperature ranges. Among them, the UHMCF showed the best nucleation ability. On the contrary, the intermediatemodule CF, the high-tenacity CF, and the E-GF showed too low nucleation ability to form TC. One efficient way to induce TC on these fibers was proved by pulling the fibers in supercooled iPP melts. The interface shear and temperature gradient between

fiber and supercooled matrix melt on crystallization were considered to be two important factors for the formation of TC. Thomason and Van Rooyen (1992) found that the occurrence of TC depended on the type of fiber used and the crystallization temperature. The aramid fibers and HMCF did induce TC, whereas high-strength CF and GF did not. However, the ability of aramid fibers and HMCF to induce TC in PP was dependant on the crystallization temperature, and no TC was observed in quiescently crystallized PP above 138°C.

CHAPTER III

EXPERIMENTAL

3.1 Materials and chemical reagents

Three types of natural fibers i.e., vetiver grass, rossells, and sisal were used in this study. Vetiver grass (ecotype of Songkhla 3) was cultivated by The Land Development Department, Nakhon Ratchasima. The age of vetiver grass was 6-8 months. Rossells was kindly supplied from The NEP Realty and Industry Public Co., Ltd. without concerning of the cultivation areas. Sisal was cultivated in Tumbol Bankao, Dan Khuntod, Nakhon Ratchasima. The age of sisal was 5-7 years. A commercial grade of isotactic PP (700J) was obtained from Thai Polypropylene Co., Ltd. Sodium hydroxide (NaOH), laboratory grade, was purchased from Merck. Analytical grade of methanol and benzene were purchased from Carlo Erba Reagents.

3.2 Sample preparation

3.2.1 Natural fibers preparation

In a case of vetiver grass, it was firstly washed by water to eliminate dirt and dried in an oven at 100°C for 24 hours. After that, it was prepared into two forms: (a) vetiver fibers, with 2 mm in length and its aspect ratio of 6.15 and (b) vetiver powder, with its mean particle size of 57.48 μm. For rossells and sisal, they were cleaned and dried in an oven at 100°C for 24 hours. Then, they were cut into a length of 2 mm. The aspect ratios of rossells and sisal were 27.82 and 14.28, respectively.

3.2.2 Chemical treatment of natural fibers

Alkalization was used to treat vetiver grass by immersing the vetiver grass in 4% (by weight) NaOH solution at 40°C for 2 hours. The alkali-treated vetiver grass was then washed thoroughly with water and dried in an oven at 100°C for 24 hours. The rossells and sisal were treated as follows. The fibers were weight about 700 grams and put into a reactor. Methanol/benzene mixture (1:1) was then added into the reactor and the mixture was heated to 80°C for 3 hours. After that, the fibers were immersed in 2% (by weight) NaOH solution for 2 hours at room temperature, subsequently washed by water, and then dried overnight in an oven at 100°C.

3.2.3 Preparation of natural fiber-PP composites

PP was mixed with each natural fiber at 170°C in an internal mixer (Haake Rheomix 3000P model 557-1306). Mixing speed and mixing time were 50 rpm and 13 minutes, respectively. In order to examine the effect of types and processing conditions on properties of PP composites the ratio of natural fibers to PP matrix was fixed at 20:80 (by weight). In order to study the effect of vetiver contents on properties of PP composites the ratio of vetiver fiber was varied within the range of 10%-30% (by weight). After that, natural fiber-PP composites were ground and dried before molding.

Natural fiber-PP composites (Figure 3.1) were molded by injection molding (Chuan Lih Fa Machine model CLF-80T). Processing conditions used in this study were summarized in Table 3.1. Processing conditions 1, 2, and 3 were used to study the effect of screw speed on shear-induced crystallization and mechanical properties of the composites. Processing conditions 1, 4, and 5 were used to examine the effect of injection speed on shear-induced crystallization and mechanical properties of the composites. Processing conditions 1, 8, and 9 were used to elucidate the effect of holding pressure on shear-induced crystallization and mechanical properties of the composites. Additionally,

processing conditions 4, 6, and 7 were used to investigate the effect of mold temperature on shear-induced crystallization and mechanical properties of the composites.

(a)   (b)
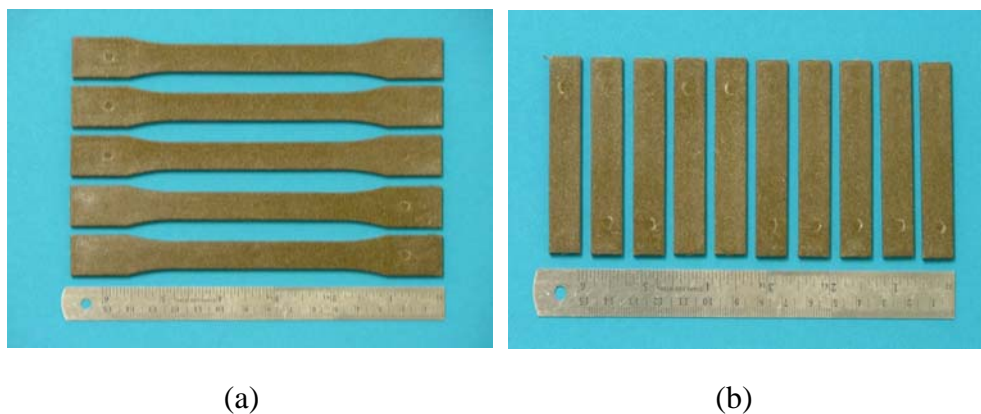
Figure 3.1   Specimens of vetiver fiber-PP composites obtained from injection molding (a) tensile specimens and (b) unnotched impact test specimens.

Table 3.1   Processing conditions for injection molding of vetiver fiber-PP composites.

Processing Condition	Screw Speed (rpm)	Injection Speed (mm/s)	Holding Pressure (kg/cm^2)	Mold Temperature (°C)
1	130	46	1.400	25
2	65	46	1.400	25
3	195	46	1.400	25
4	130	18.4	1.400	25
5	130	82.8	1.400	25
6	130	18.4	1.400	45
7	130	18.4	1.400	65
8	130	46	840	25
9	130	46	2.240	25

3.2.4   Preparation of natural fiber-PP thin films

Thin films of neat PP and of each composite with the thickness of 50 μm were prepared by compression molding at 180°C (Figure 3.2). These thin films were used to determine the equilibrium melting temperatures (T_m^o) and rate of crystallization of PP composites by differential scanning calorimetry (DSC). In addition, these thin films were used to obtain aspect ratios of natural fibers after processing and spherulitic growth rate of PP composites by polarized light optical microscope.
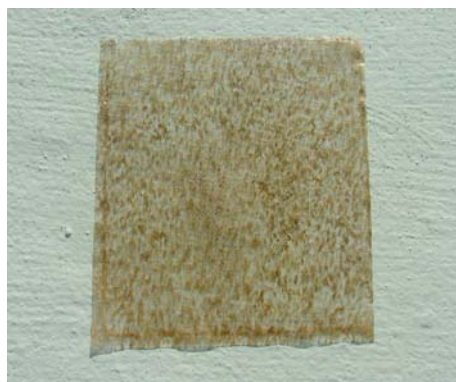
Figure 3.2   Specimen of vetiver fiber-PP composite with a thickness of 50 μm obtained from compression molding.

3.3   Characterization of natural fiber-PP composites

3.3.1   Rheological property

Shear viscosities at the shear rate range of 10 to 10,000 s^{-1} of neat PP and of natural fiber-PP composites were measured using Kayeness capillary rheometer at 180°C.

3.3.2 Thermal properties

Thermogravimetric analysis (TGA model SDT 2960) was performed by heating neat PP or natural fiber-PP composites from 30 to 800°C at a heating rate of 20°C/min under a nitrogen atmosphere.

3.3.3 Functional group analysis

DRIFT spectra of vetiver grass were recorded by a Perkin-Elmer FT-IR spectrometer (model Spectrum GX: FT-IR). DRIFT spectrum was collected in mid-IR region (4,000-400 cm^{-1}) against a background of pure KBr powder. One hundred and twenty eight scans were co-added at a resolution of 4 cm^{-1} to achieve better signal-to-noise ratio.

3.3.4 Scanning electron microscopy

Surface morphology of vetiver grass was investigated by a scanning electron microscope (SEM model JSM 6400). The specimens were coated with gold prior to the examination,

3.3.5 Mechanical properties

Tensile testing was performed according to ASTM D638 using an Instron Universal Testing Machine (Instron: model 5569), at a crosshead speed of 10 mm/min and a gauge length of 80 mm. Izod impact tests were performed according to ASTM D256 using an impact tester (basic pendulum tester, Atlas model BPI).

3.4 Shear-induced crystallization of natural fiber-PP composites

3.4.1 Normalized thickness of shear-induced crystallization layer

Tensile specimens of natural fiber-PP composites were cut perpendicular to machine direction (MD) and parallel to transverse direction (TD) at the center of the

specimens. Subsequently, the specimen was cut throughout the center plane parallel to MD using Rotary Microtome (RMC: model MT 960) into a thin film of 50 μm-thickness. The cutting procedure was illustrated in Figure 3.3. The morphology of the specimens was investigated using a polarized light optical microscope (Nikon: model Eclipes E600 POL). Normalized thickness of shear-induced crystallization layer was determined using the following equation:

Normalized thickness of shear-induced crystallization layer (%)

$$= \frac{\text{Skin layer thickness}}{\text{Total thickness of test specimen}} \times 100 \quad\quad (3.1)$$

3.4.2 Degree of crystallinity and degree of crystallinity distribution

Injection molded specimens were cut into various depths (Y) in thickness direction (H) by a rotary microtome to obtain a thin film of 50 μm-thickness (Figure 3.4). The weight of each film was approximately 5 mg. The depth of the composite specimen was varied into four zones, which were referred to different Y/H value. The Y/H value was ranged from 0-1. In a case of Y/H=1, it referred to skin of the specimen, whereas Y/H = 0 referred to core (center) of the specimen. Degree of crystallinity of injection molded composites at various depths was determined by differential scanning calorimetry (DSC: Mettler Toledo Version STAR[e] SW 8.1).
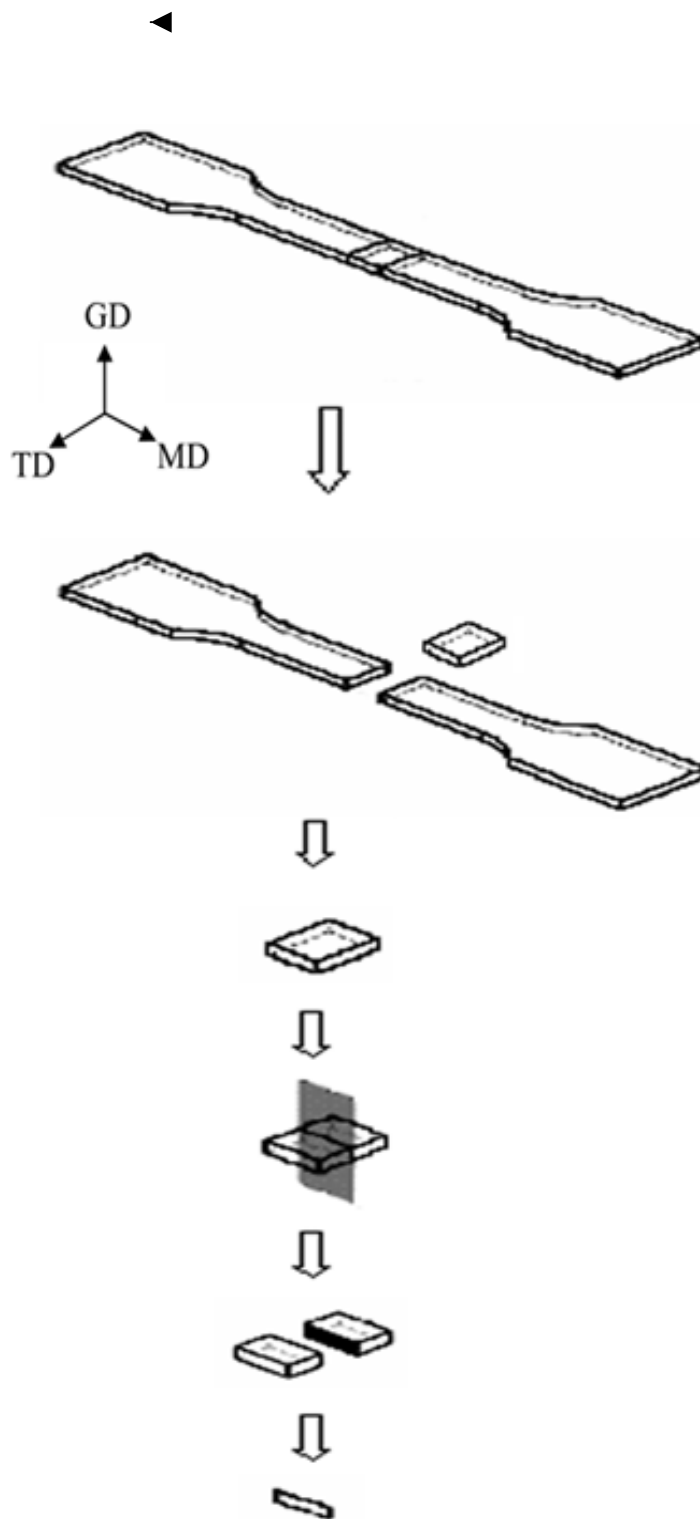
Figure 3.3   Cutting procedure to investigate the shear-induced crystallization layer.
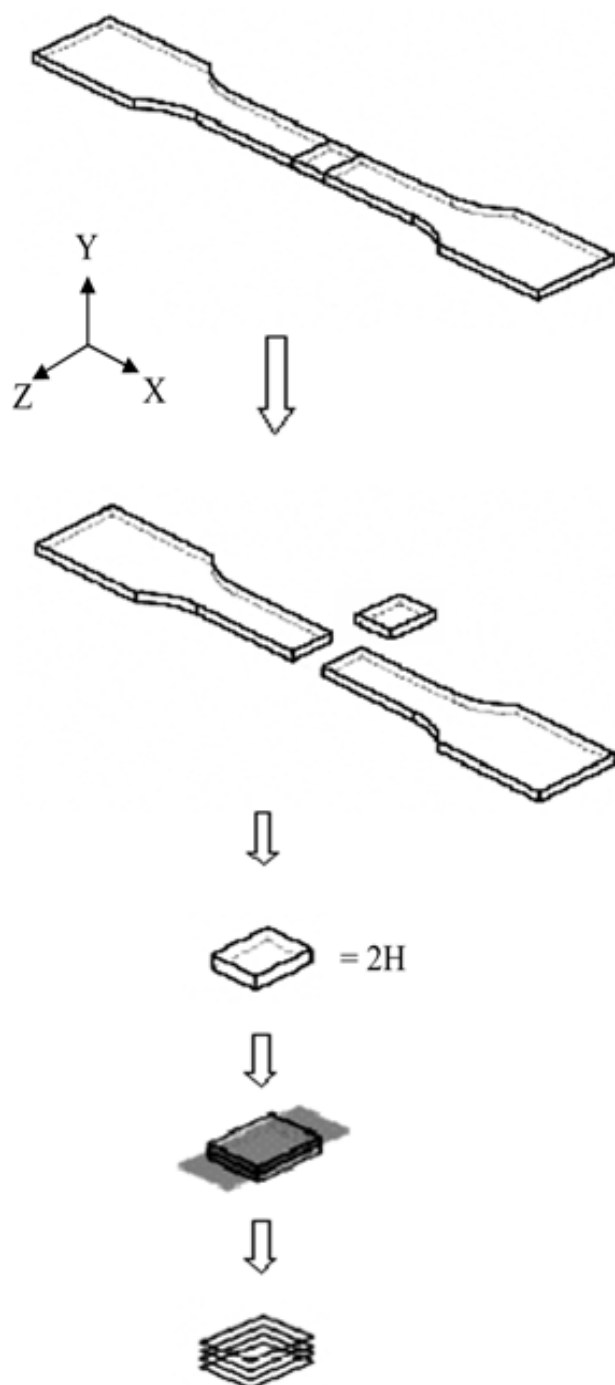
Figure 3.4 Cutting procedure to examine the degree of crystallinity.

Thermal programming for DSC experiments was divided into 3 stages as followed (Figure 3.5):
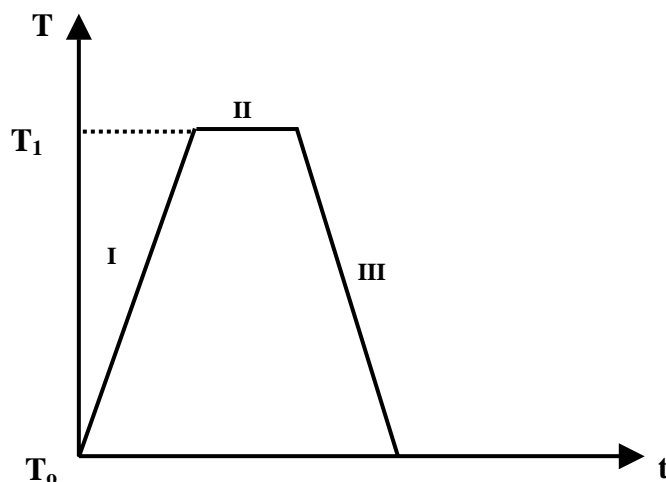
Figure 3.5 Thermal programming for DSC experiments $T_o = 25°C$ and $T_1 = 200°C$.

Stage I: Heating a sample in the calorimeter at a heating rate of 10°C/min from 25°C to 200°C.

Stage II: Isothermally annealing the sample at the temperature, $T_1 = 200°C$ for 5 min (to remove thermal history of sample).

Stage III: Cooling the sample in the calorimeter to 25°C at a cooling rate of 10°C/min.

To measure the degree of crystallinity of a sample, the sample was heated from 25°C to 200°C with a heating rate of 10°C/min (heating scan) under a nitrogen atmosphere, and was held at 200°C for 5 min to remove thermal history. Then, the sample was cooled to 25°C with a cooling rate of 10°C/min (cooling scan). The degree of crystallinity (X_c) was determined using the following equation (Amash and Zugenmaier, 2000):

$$X_c \text{ (Degree of crystallinity)} = \frac{\Delta H_f}{\Delta H_f^o W} \times 100 \qquad (3.2)$$

Where ΔH_f is a latent heat of fusion of a sample (area under a crystallization peak), ΔH_f° is the latent heat of fusion of a 100% crystalline PP (207.1 J/g (Krevelen, 1997)) and W is the weight fraction of PP in the composite.

3.5 Crystallization of natural fiber-PP composites

3.5.1 Isothermal crystallization of natural fibers-PP composites

Isothermal crystallization of PP composites was determined using a Differential Scanning Calorimeter (DSC, Perkin-Elmer: model DSC7). Thermal program for rate of crystallization measurements was divided into 5 stages as followed (Figure 3.6):
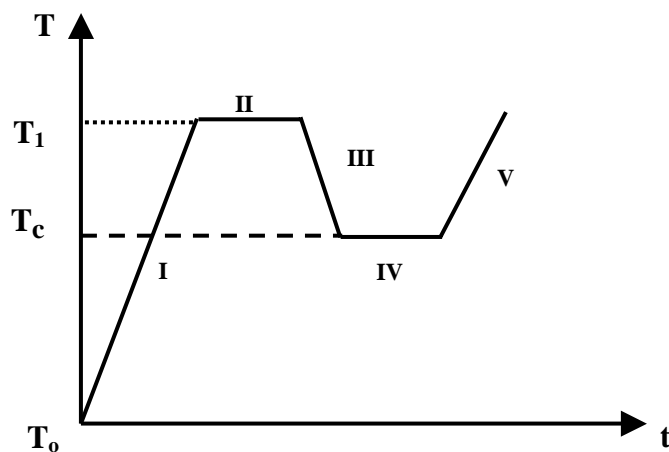
Figure 3.6 Thermal programming for rate of crystallinity measurements $T_o = 25°C$, $T_1 = 200°C$, and $T_c = $ isothermal crystallization temperature.

Stage I: Heating a sample in the calorimeter with a heating rate of 10°C/min from 25°C to 200°C.

Stage II: Isothermally annealing the sample at the temperature, $T_1 = 200°C$ for 5 min (to remove thermal history of sample).

Stage III: Cooling the sample in the calorimeter to the T_c with a cooling rate of 40°C/min.

Stage IV: Performing isothermal crystallization at various crystallization temperatures ranging from 122°C to 134°C.

Stage V: Heating the sample in the calorimeter again from studied crystallization temperatures to 200°C with a heating rate of 10°C/min.

To measure rate of crystallization of the sample, the sample was heated from 25°C to 200°C and held at 200°C for 5 minutes under a nitrogen atmosphere in order to eliminate the thermal history of sample. Then, the sample was cooled down with a rate of 40°C/min to various predetermined crystallization temperatures (T_c) and maintained at that temperature until the crystallization was completed. The enthalpy from DSC thermogram was determined in order to obtain the relative degree of crystallinity, X(t), by using the following equation (Papageogiou et al., 2005).

$$X(t) = \frac{\int_0^t (dH/dt)dt}{\int_0^\infty (dH/dt)dt} \qquad (3.3)$$

Where dH denotes the measured enthalpy of crystallization during an infinitesimal time interval dt. The limits t and ∞ are used to denote the elapsed time during the course of crystallization and at the end of the crystallization process, respectively.

After the completion of crystallization, the samples were heated to 200°C at a rate of 10°C/min. The melting temperature (T_m) of the samples was obtained from the maximum of the endothermic peaks. The equilibrium melting temperatures ($T_m°$) was determined from Hoffman-Weeks plot (the extrapolation plot of T_c versus T_m) (López-Manchado et al, 1999).

3.5.2 Isothermal crystallization rate constant by Avrami plots

The relative degree of crystallinity, X(t), is related to the crystallization time, t, according to Avrami equation as shown in the following equation (Avrami, 1939, 1940, and 1941):

$$X(t) = 1-\exp(-kt^n) \tag{3.4}$$

Where n is the Avrami exponent which is a function of the nucleation process and k is the isothermal rate constant of crystallization. The values of n and k can be calculated by fitting experimental data using the double logarithmic form as shown in Equation (3.5)

$$\log\{-\ln[1-X(t)]\} = \log k + n \log t \tag{3.5}$$

A plot of $\log\{-\ln[1-X(t)]\}$ as a function of log t yields a straight line with slope n and intercept log k called an Avrami plot.

3.5.3 Isothermal crystallization rate constant by half time of crystallization

The half time of crystallization, $t_{1/2}$, which is the elapsed time from the crystallization onset until the relative degree of crystallinity reaches a value of 0.5, was

determined. The half time of crystallization also used to calculate the isothermal rate of crystallization from the following equation (Avrami, 1939, 1940, and 1941):

$$k(T) = \frac{\ln 2}{(t_{1/2})^n} \qquad (3.6)$$

Where n is assumed to be 3.

3.5.4 Non-isothermal crystallization rate constant from isothermal experiment

Non-isothermal crystallization rate constant was obtained by using Nakamura expression (Nakamura et al., 1972 and 1973):

$$X(T) = 1 - \exp\left[-\int_0^t K(T)dt\right]^n \qquad (3.7)$$

Where K(T) is non-isothermal crystallization rate constant which is related to the isothermal crystallization rate constant as shown in Equation (3.8).

$$K(T) = [k(T)]^{1/n} \qquad (3.8)$$

3.5.5 The overall rate of non-isothermal crystallization

The non-isothermal rate constant K(T), obtained from Equation (3.8) can be expressed by Hoffman-Lauritzen equation (Isayev et al., 2000).

$$K(T) = (\ln 2)^{1/n}\left(\frac{1}{t_{1/2}}\right)_o \exp\left[\frac{-U^*}{R(T_c - T_\infty)}\right]\exp\left[\frac{-K_k}{T_c(\Delta T)f}\right] \qquad (3.9)$$

From the expression, the kinetic model has four parameters: $\left(\dfrac{1}{t_{1/2}}\right)_o$ is the pre-exponential factor that includes all terms independent of temperature, K_k is the nucleation exponent, U^* and T_∞ are the Vogel-Fulcher-Tamman-Hesse (VFTH) parameters describing the transport of polymer segments across the liquid/crystal interphase, ΔT denotes the supercooling ($\Delta T = T_m^o - T_c$) and $f = 2T_c/(T_c + T_m^o)$ is a correction factor accounting for the temperature dependence of the latent heat of fusion. R is the gas constant. The universal values used for the VFTH parameters are $U^* = 1500$ cal/mol (6280 J/mol) and $T_\infty = (T_g - 30)$ K (Papageorgiou et al., 2005). In this study, the T_g of PP was 270 K (ATHAS Databank) and the equilibrium melting temperature, T_m^o would be obtained from this study.

3.5.6   Spherulitic growth rate and number of effective nuclei

A thin film (the thickness of 50 μm) of natural fibers-PP composites and neat PP were used to measure the spherulitic growth rate (G) by using a Hot Stage (Linkam TH600) under a Polarized Light Optical Microscope attached with CCD video camcorder system (Sony) as illustrated in Figure 3.7. The sample was heated from room temperature to 200°C with a heating rate of 10°C/min and held at that temperature for 5 min. Then, the sample was cooled down with a rate of 50°C/min to various T_c. The radius of spherulite was measured as a function of time. The growth rate (G) at various T_c was obtained from the slope of the plots of spherulite diameter versus time.
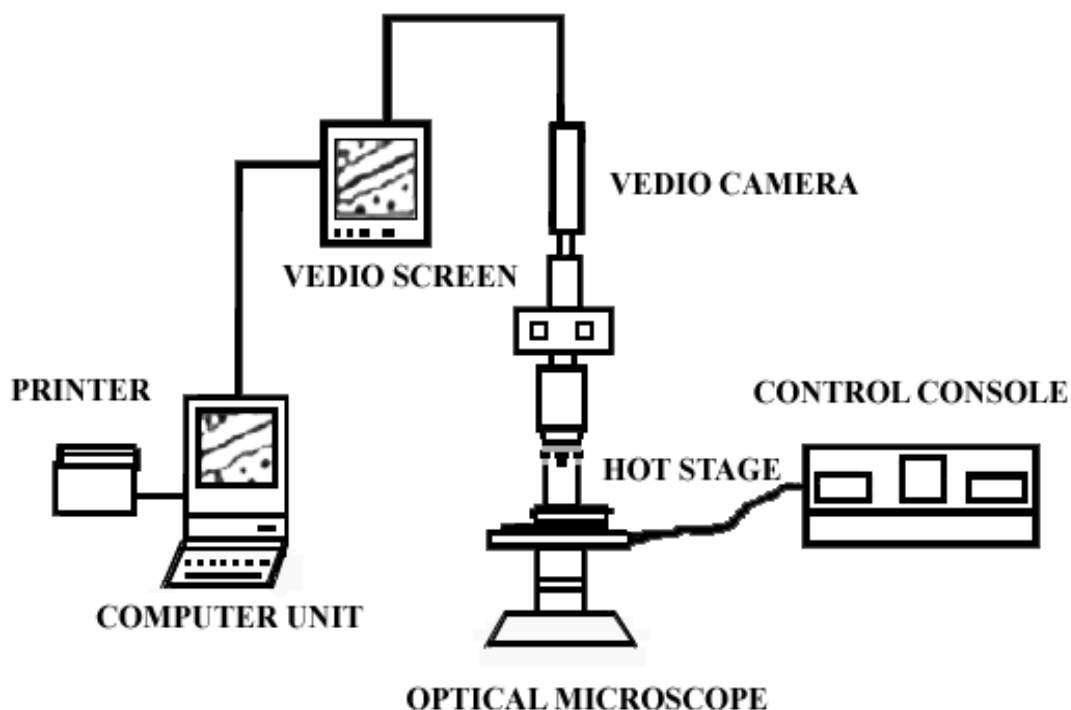
Figure 3.7   Schematic of experiment set-up for the hot stage polarized optical microscope.

The kinetic data of isothermal crystallization can be analyzed using the spherulitic growth rate in the context of Hoffman-Lauritzen secondary nucleation theory. Accordingly, the growth rate G(T) is given as a function of the crystallization temperature by the following bi-exponential equation (Hoffman et al., 1976):

$$G(T) = G_o \exp\left[\frac{-U^*}{R(T_c - T_\infty)}\right] \exp\left[\frac{-K_g}{T_c(\Delta T)f}\right] \tag{3.10}$$

Where G_o is the pre-exponential factor independent of temperature. K_g is a nucleation parameter. The remaining factors have the same meaning as described in Equation (3.9).

If spherulites are assumed to grow in a free space without impingement, the total volume relative to the unit volume transformed by time, t, is given by the following equation (Nagasawa et al., 2005):

$$V_{free} = \sum_{i=1}^{\infty} n_i \left(\frac{4\pi}{3} \right) [G(t - t_i)]^3 \tag{3.11}$$

Where n_i is the number of nuclei per unit volume activated at time, t_i, and G is the radial growth rate. If the mode of nucleation is simultaneous then,

$$V_{free} = N \left(\frac{4\pi}{3} \right) [G(t)]^3 \tag{3.12}$$

Where N is the number of effective nuclei. For the real space in which a number of spherulites impinge with each other and their growth is restricted, the Avrami-Evans theory proposed,

$$1 - \frac{V}{V_\infty} = \exp(-V_{free}) \tag{3.13}$$

Where V_∞ is the transformable volume fraction and V is the volume fraction transformed by a certain time. By representing V/V_∞ by the degree of crystallinity, X(t), and replacing Equation (3.12) by Kt^3, Equation (3.12) was transformed into the following equation:

$$1 - X(t) = \exp(-Kt^3) \tag{3.14}$$

Where

$$N = \frac{3K}{4\pi G^3} \tag{3.15}$$

From Equation (3.15), the growth rates combined with the non-isothermal rate constants determined from Equation (3.9) and (3.10), respectively, were used to estimate the number of effective nuclei as a function of temperatures.

CHAPTER IV

RESULTS AND DISCUSSION

4.1   Characterization of untreated and alkali-treated vetiver grass

4.1.1   Thermal properties

TGA and DTG curves of untreated vetiver grass and alkali-treated vetiver grass were displayed in Figure 4.1. The TGA curve of each sample showed an initial transition around 100°C due to moisture evaporation. The DTG curve of untreated vetiver grass showed the second decomposition peak around 333°C. This peak was an integral peak derived from the decomposition of both hemicellulose and α-cellulose components. However, the decomposition of hemicellulose was observed in the DTG curve of alkali-treated vetiver grass as a shoulder peak around 310°C. In addition, the decomposition of α-cellulose was clearly observed at 365°C in DTG curve of the alkali-treated vetiver grass. The decomposition temperatures of hemicellulose and α-cellulose of vetiver grass were in the same range as those of jute, hemp, and sisal (Albano et al., 1999, Ray et al., 2002, and Joseph et al., 2003). Moreover, TGA curve of the alkali-treated vetiver grass exhibited higher onset of decomposition temperature (320°C) than that of the untreated vetiver grass (275°C). This indicated that the alkali-treated vetiver grass has higher thermal resistance than the untreated vetiver grass. This might be due to the removal of some components degraded at lower temperatures such as lignin, pectin, hemicellulose, and waxy substances from the vetiver grass.
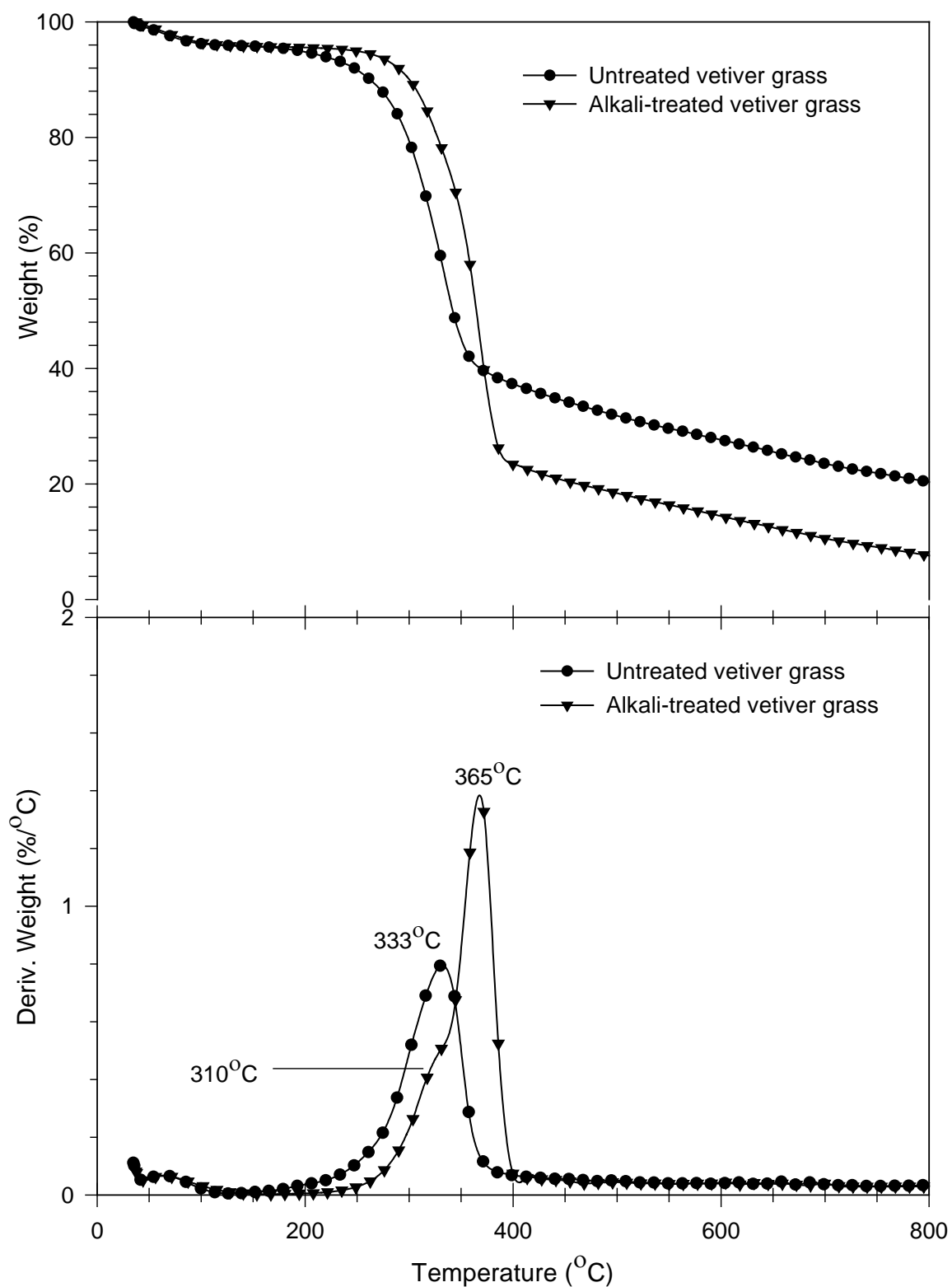
Figure 4.1   TGA and DTG curves of untreated vetiver grass and alkali-treated vetiver

grass.

4.1.2 Functional group analysis

DRIFT spectra of untreated and alkali-treated vetiver grass were shown in Figure 4.2. Significant changes of DRIFT spectra were observed from three peaks at 1734, 899 and 832 cm^{-1}, respectively. The peak at 1734 cm^{-1} is due to the C=O stretching of hemicellulose. The intensity of this peak was considerably reduced for the alkali-treated vetiver grass indicating the removal of the hemicellulose by the alkali treatment. Other two peaks at 899 and 832 cm^{-1} are due to the O-C-O stretching in β-glucosidic linkage (Mwaikambo and Ansell, 2002 and Ray et al., 2002). However, the peak at 832 cm^{-1} disappeared in the case of alkali-treated vetiver grass. This may be because sodium hydroxide (NaOH) solution tends to react with the cementing materials, i.e., hemicellulose. In particular, the removal of cementing materials led to destruction of the mesh structure and splitting of the fibers into finer filaments (Ray et al., 2002). Mwaikambo and Ansell (1999 and 2002) reported that NaOH is the most commonly used for bleaching and/or cleaning the surface of the plant fibers. It also changes the fine structure of the native cellulose I to cellulose II by a process known as alkalization. However, the extent of polymorphic transformation of cellulose I into cellulose II taking place within the crystalline domain of the fiber cellulose was dependent on NaOH concentration (Jähn et al., 2002).
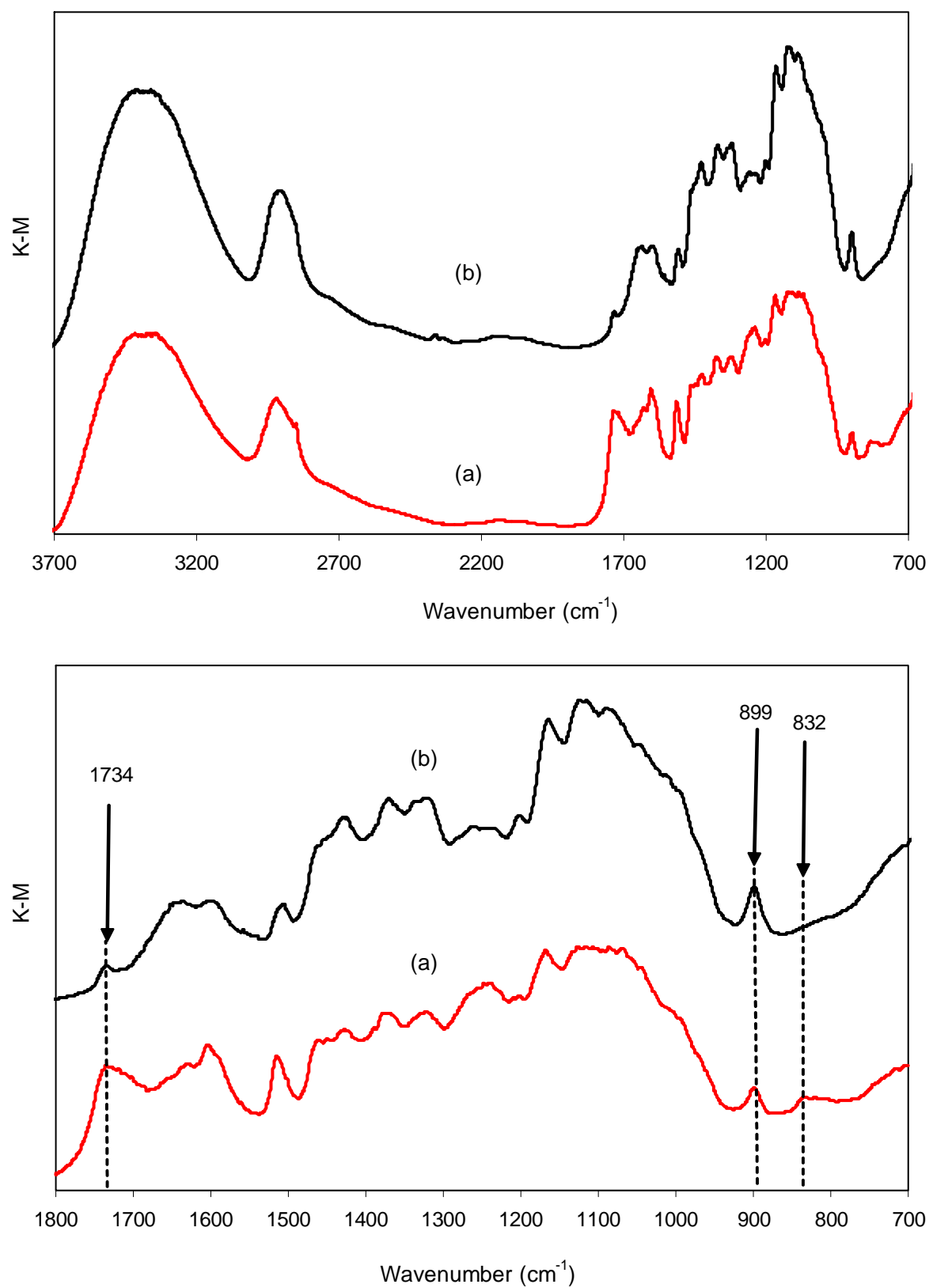
Figure 4.2 DRIFT Spectra of (a) untreated vetiver grass, and (b) alkali-treated vetiver grass.

4.1.3 Morphological property

SEM micrographs of untreated vetiver grass and alkali-treated vetiver grass were represented in Figure 4.3. The SEM micrograph of the alkali-treated vetiver grass revealed fibrils with a rough surface topography. This may be due to the leach out of alkali-soluble fractions like waxy layer, lignin and hemicellulose, etc. during alkalization (Albano et al., 1999 and Jayaraman, 2003), which was confirmed by DRIFT spectra as previously mentioned in section 4.1.2. According to a study of Valadez-Gonzalez et al. (1999), it has been found that alkaline treatment affects natural fibers in the following ways: (1) it increases the surface roughness of the fiber that results in a better mechanical interlocking and (2) it raises the amount of exposed cellulose on the fiber surface thus increasing the number of possible reactive sites.

(a)   (b)
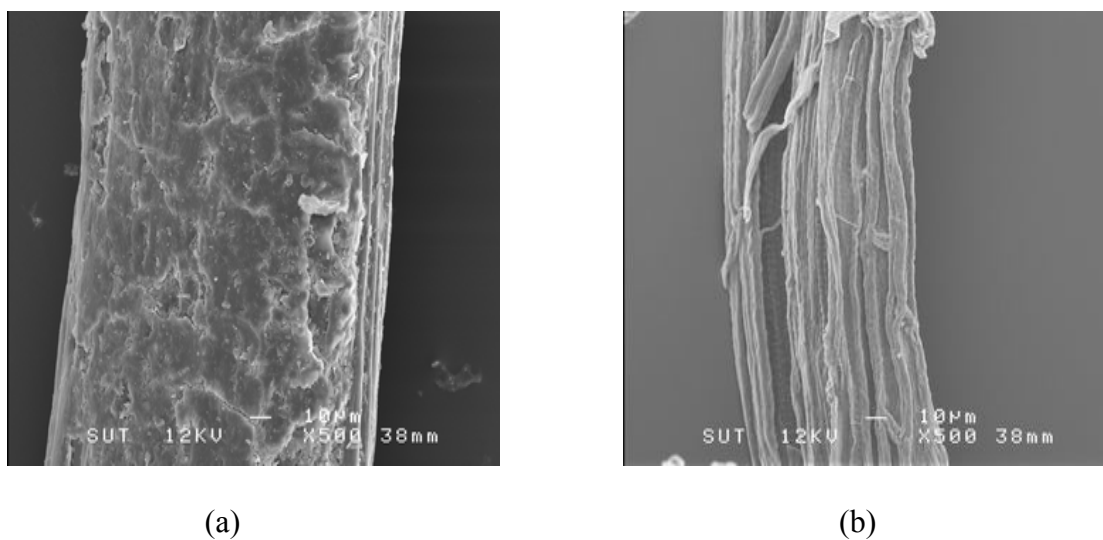
Figure 4.3 SEM micrographs of (a) untreated vetiver grass, and (b) alkali-treated vetiver grass.

4.2 The effect of sizes of vetiver grass on PP composites

4.2.1 Rheological property

Shear viscosities of both vetiver fiber-PP and vetiver powder-PP composites were higher than that of neat PP as shown in Figure 4.4. This was possibly because vetiver particles perturbed normal flow of PP and hindered the mobility of chain segments in the melt flow. In addition, viscosity of vetiver fiber-PP composites was slightly higher than that of vetiver powder-PP composites. Since the larger particle of vetiver was able to obstruct normal flow of polymer and impede the mobility of chain segments in the flow more than the smaller particles of vetiver.
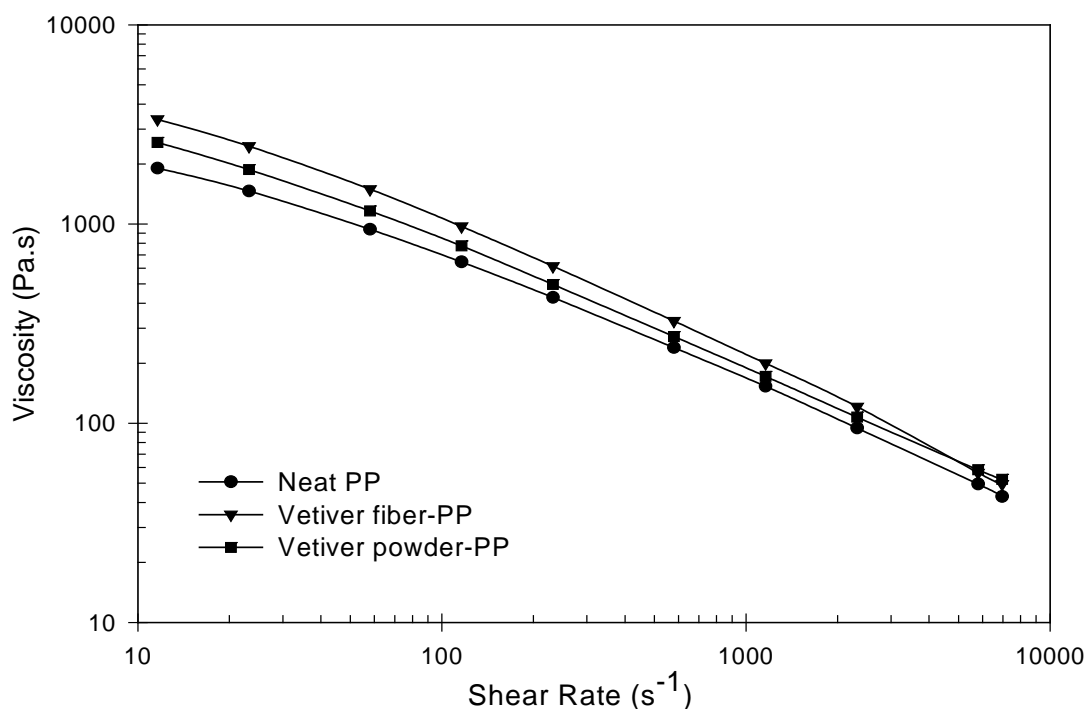
Figure 4.4 Plot of shear viscosity and shear rate of neat PP, vetiver fiber-PP composite and vetiver powder-PP composite.

4.2.2 Thermal properties

TGA and DTG thermograms revealed that the onset of the decomposition temperature of vetiver grass-PP composite was lower than that of neat PP (Figure 4.5). This was due to the lower thermal stability of vetiver grass than that of neat PP. Vetiver grass-PP showed the first decomposition peak around 365°C due to α-cellulose decomposition of vetiver grass (Ruksakulpiwat et al., 2007) of vetiver grass. The second decomposition peak around 460°C indicated the degradation of saturated and unsaturated carbon atoms in polypropylene (Joseph et al., 2003). Both vetiver fiber-PP and vetiver powder-PP composites showed similar TGA and DTG patterns.

DSC curves (heating scan) of neat PP, vetiver fiber-PP, and vetiver powder-PP composites at core layer and skin layer were illustrated in Figure 4.6(a)-(b), it can be seen that DSC curves of the core region exhibited obviously more multiple and broader than those of the skin region. This indicated that several crystallographic forms could be taken place in the core.

Figure 4.5 TGA and DTG curves of neat PP, vetiver fiber, vetiver powder, vetiver fiber-

PP composite, and vetiver powder-PP composite.
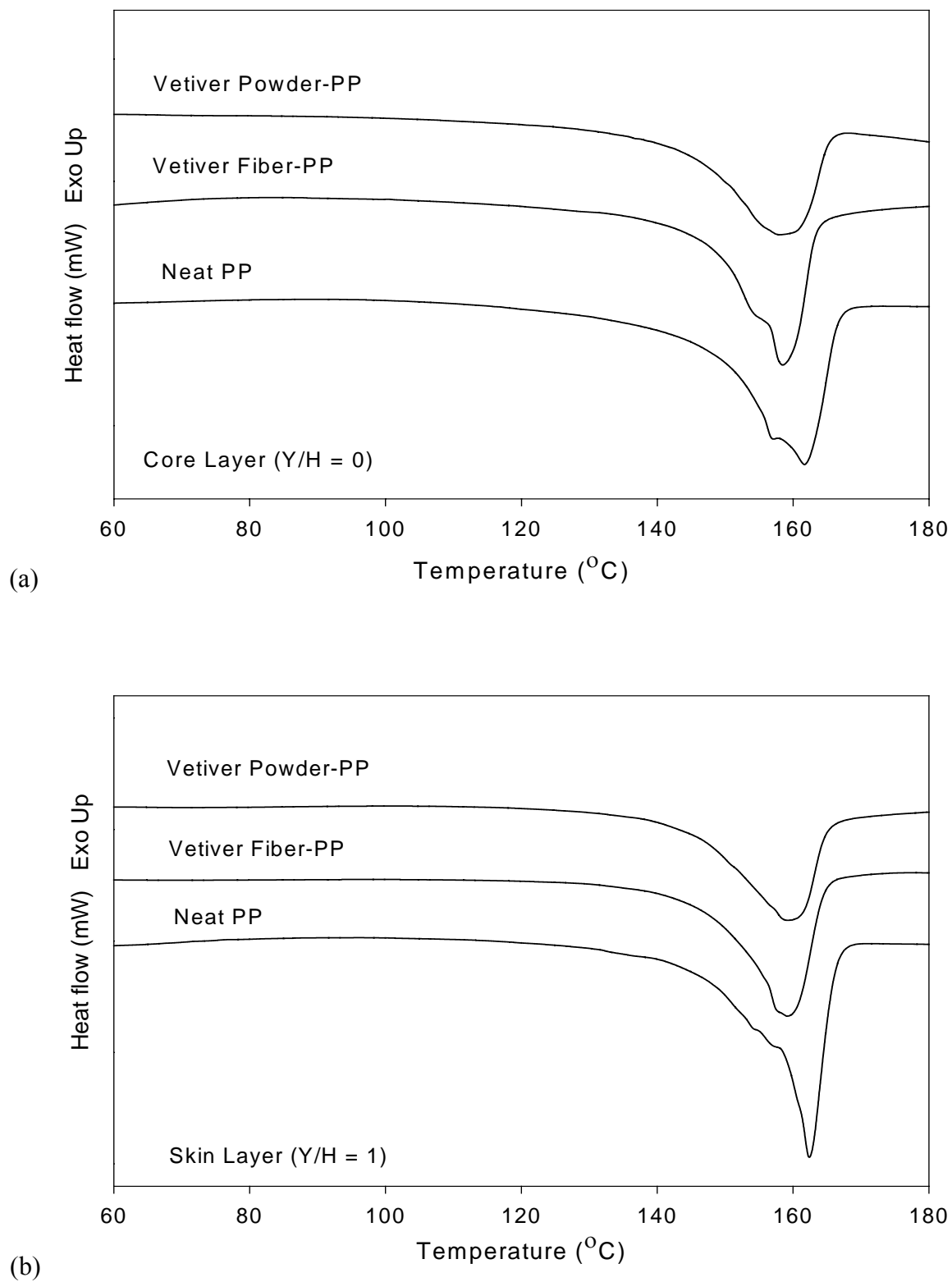
Figure 4.6 DSC curves corresponding to the heating scans of (a) core layer (Y/H = 0) and

(b) skin layer (Y/H = 1) of neat PP, vetiver fiber-PP composite and vetiver

powder-PP composite.

4.2.3 Normalized thickness of shear-induced crystallization layer

The optical micrograph of injection molded PP sample was shown in Figure 4.7. From this figure, the distinct skin layer due to shear-induced crystallization was observed. Figure 4.8 showed the effect of vetiver particle sizes on normalized thickness of shear-induced crystallization layer. It was observed that normalized thickness of shear-induced crystallization layer of neat PP was higher than those of vetiver fiber-PP and vetiver powder-PP composites. This was because vetiver fiber possibly restricted molecular orientation of polymer chain during shear-induced crystallization leading to a decrease in normalized thickness of shear-induced crystallization layer. In addition, vetiver fiber-PP composite exhibited lower normalized thickness of shear-induced crystallization layer than vetiver powder-PP composite. This was because the larger vetiver particles were able to obstruct normal flow of polymer and impede the mobility of chain segments in melt flow more than the smaller ones.

Skin layer (Shear-induced crystallization layer)
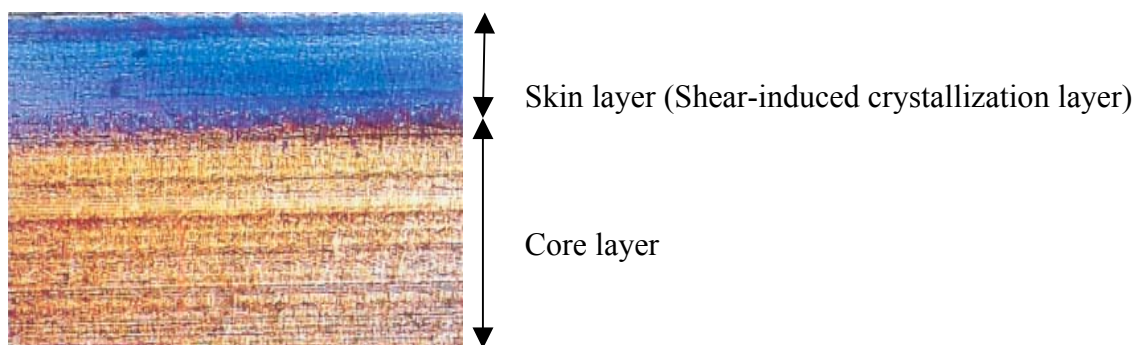
Core layer

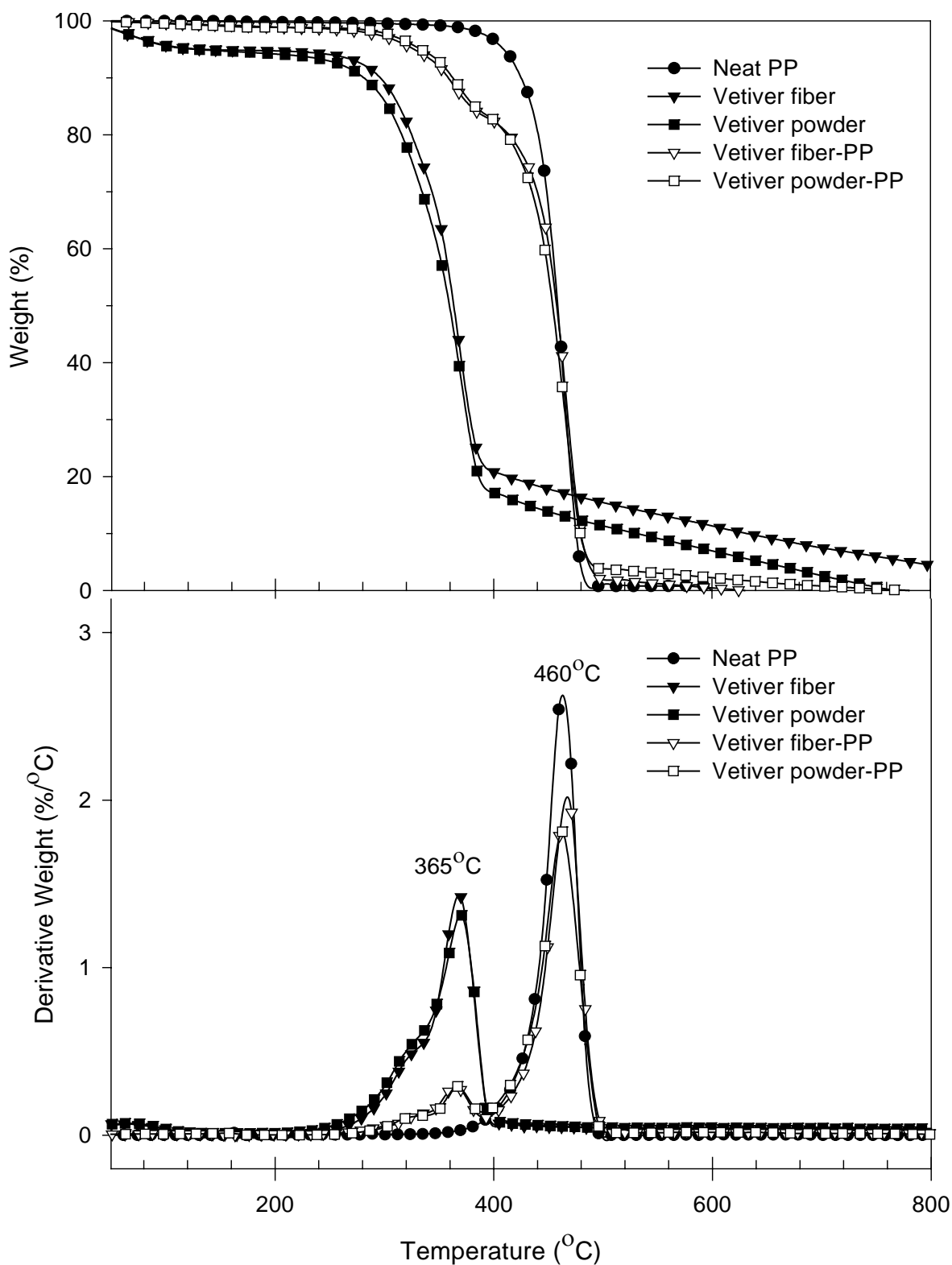**Figure 4.7** Optical micrograph of injection molded PP representing skin layer (shear-induced crystallization layer) and core layer.
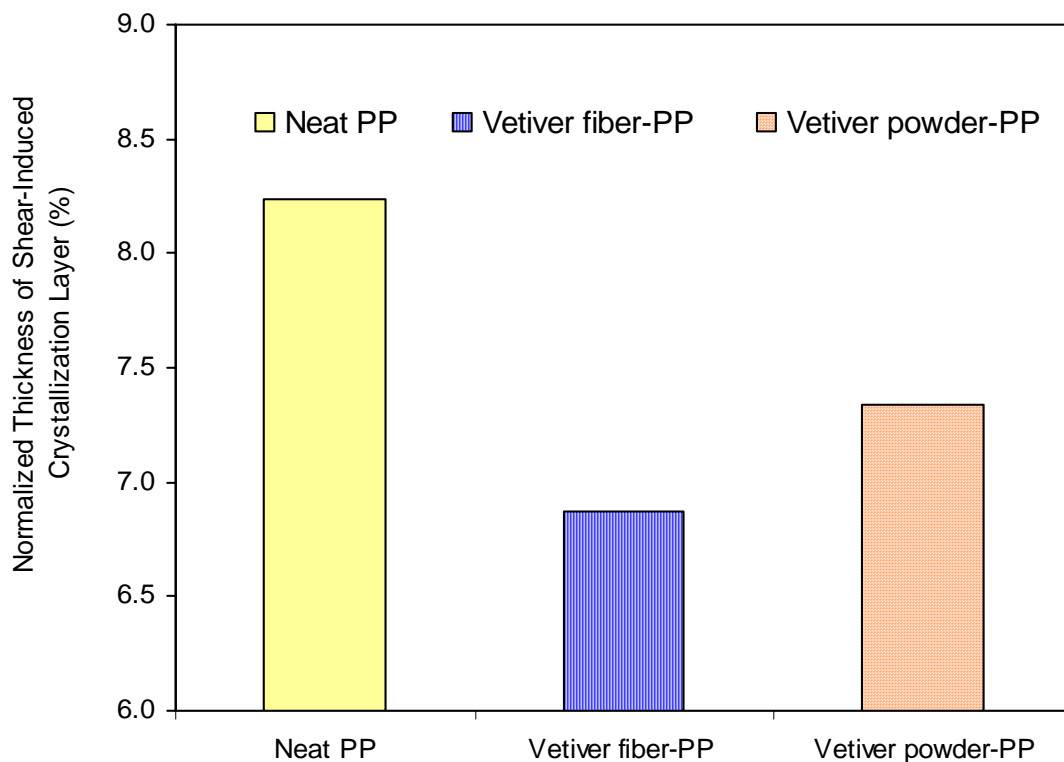
Figure 4.8   Plot of normalized thickness of shear-induced crystallization layer of neat PP, vetiver fiber-PP composite, and vetiver powder-PP composite.

4.2.4 Mechanical properties

Mechanical properties of neat PP and PP composites were shown in Figure 4.9(a)-(d). Both vetiver fiber-PP and vetiver powder-PP composites exhibited higher tensile strength and Young's modulus than those of neat PP. This was because the tensile strength and Young's modulus of vetiver fiber are much higher than that of neat PP. The tensile strength and Young's modulus of vetiver fiber used in this study were in the range of 247-723 MPa and 12.0-49.8 GPa, respectively (Ruksakulpiwat et al, 2007). According to Figure 4.9(c)-(b), elongation at break and impact strength of both vetiver fiber-PP composites and vetiver powder-PP composites were lower than that of neat PP. Yielding and necking phenomena were observed in neat PP. As a result, neat PP exhibited higher elongation at break than PP composites. Moreover, an introduction of vetiver grass into PP matrix results

in a heterogeneous system, which induces stress concentration from external loading. Heterogeneous stress distribution developing in the composites obviously affects its deformation and failure behavior (Pukánsky, 1995). It is widely accepted that fillers enhance the stiffness by sacrificing the ductility (yield and elongation behavior) and toughness performance of the matrix polymer, resulting in an apparently brittle material (Karger-Kocsis, 1995).

In addition, vetiver fiber-PP composites showed slightly higher tensile strength and Young's modulus than vetiver powder-PP composites. This was because vetiver fiber was able to transfer load applied to composites more than vetiver powder. However, the elongation at break and the impact strength of both vetiver fiber-PP and vetiver powder-PP showed insignificant difference. The strength of fiber-reinforced composites depends not only on the tensile strength of the fiber, but also on the degree to which an applied load is transmitted to the fibers. It was known that the extent of load transmittance is a function of fiber length and the magnitude of the fiber-matrix interfacial bond (George and Thomas, 1997). Under applied tension, load is transferred by shear at the matrix-fiber interface. The load transfer mechanism resulted in end effects which may reduce the fiber stress. When a stiff fiber is embedded in a relatively flexible matrix, shear strain is maximum at the fiber end. On the other hand, the tensile stress in the fiber is zero at the fiber ends and increases towards the center. The critical length of a fiber can be obtained if a fiber is long enough for tensile stress to reach maximum values.
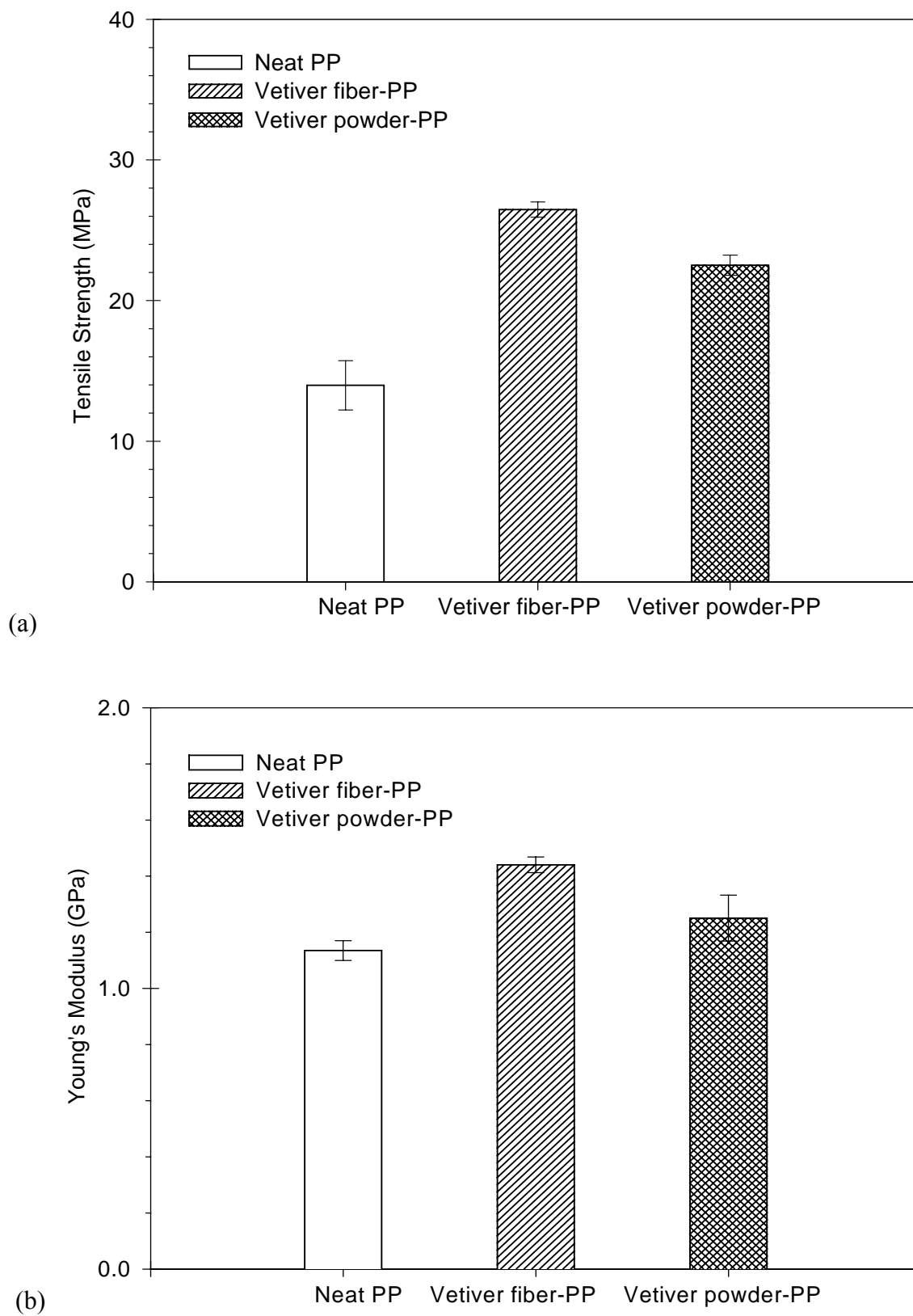
Figure 4.9   Plot of (a) Tensile strength and (b) Young's modulus of neat PP, vetiver fiber-PP composite, and vetiver powder-PP composite.

(c)

(d)
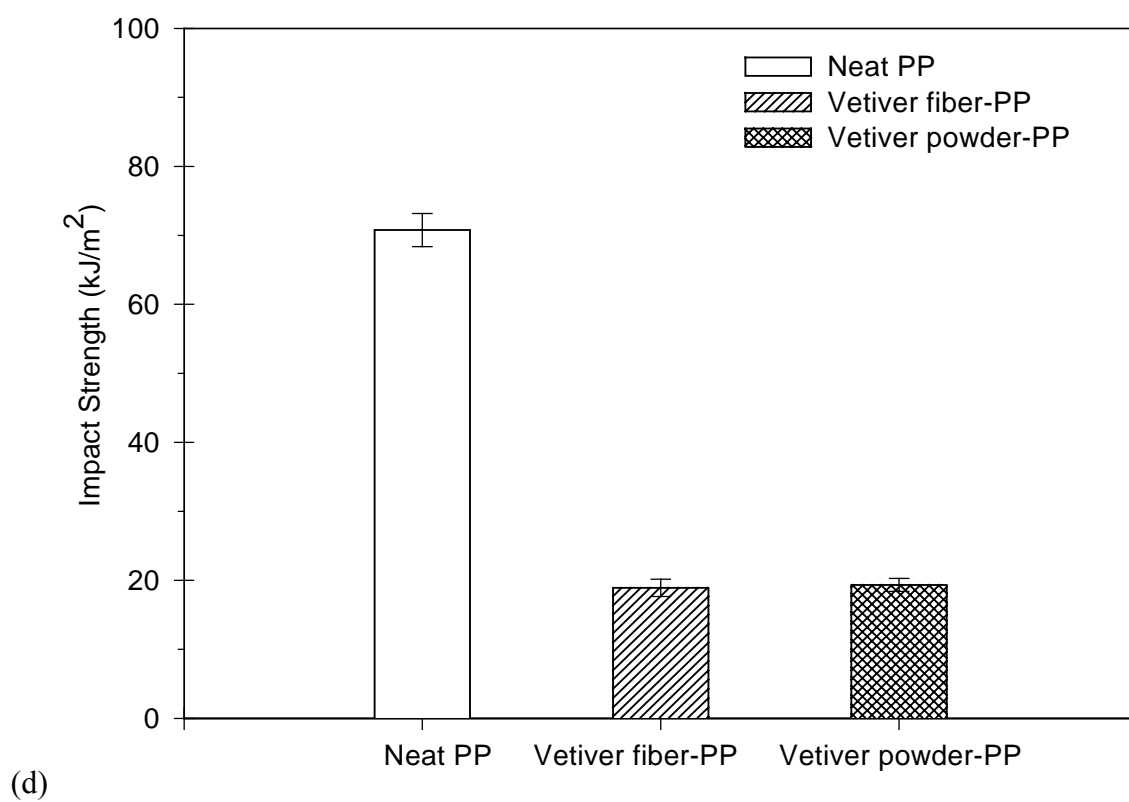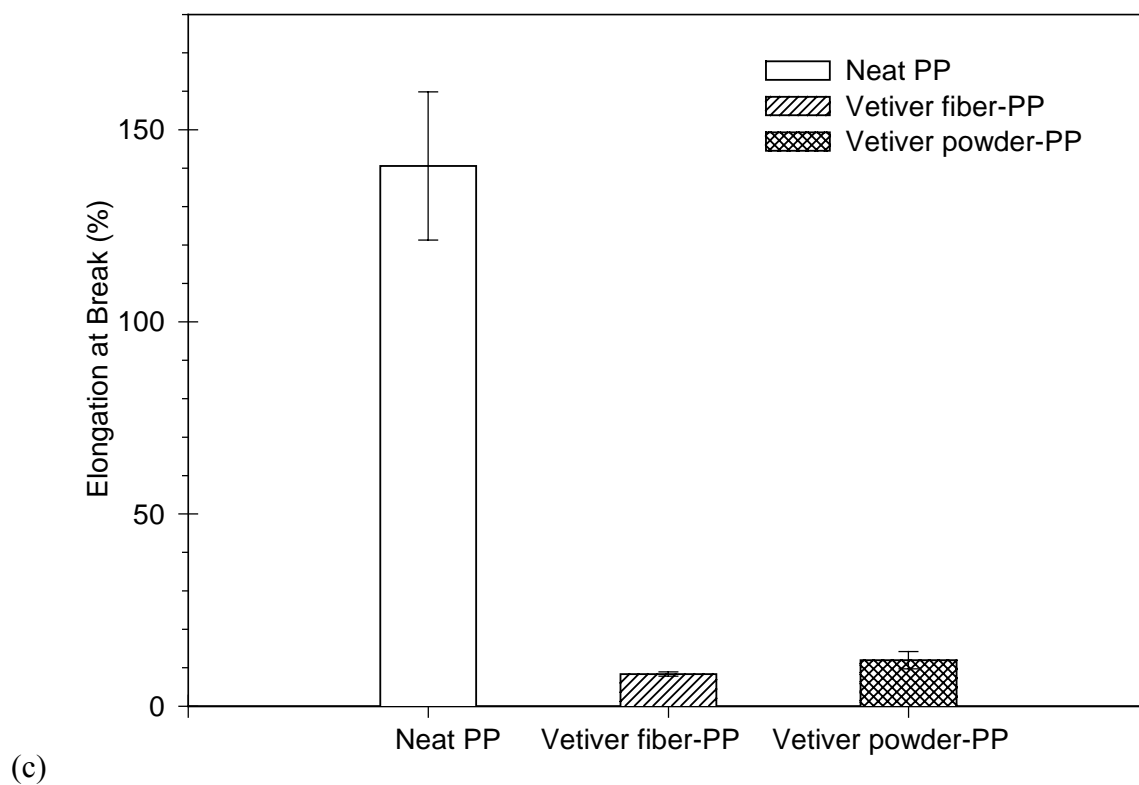
Figure 4.9   **(Continued)** Plot of (c) Elongation at break and (d) Impact strength of neat

PP, vetiver fiber-PP composite, and vetiver powder-PP composite.

4.3   The effect of vetiver contents on vetiver fiber-PP composites

4.3.1   Rheological property

As previously described in section 4.2.4, vetiver fiber-PP composites showed higher tensile strength and Young's modulus than those of vetiver powder-PP composites. Hence, vetiver fiber-PP composite was used to study effect of fiber contents, fiber types, and processing conditions on properties of PP composites hereafter. It revealed that viscosity of vetiver fiber-PP composite was considerably higher than that of neat PP matrix and markedly increased with the fiber content (Figure 4.10). Because of the higher content of vetiver fiber, the more perturbed the normal flow of polymer and the more hindered mobility of chain segments in the melt flow was occurred. Particularly, an increase in viscosity of vetiver fiber-PP composites with increasing vetiver content was more predominant at lower shear rate. However, the shear viscosity of vetiver fiber-PP composite at 10%, 20%, and 30% (by weight) vetiver content were insignificantly different at high shear rate.
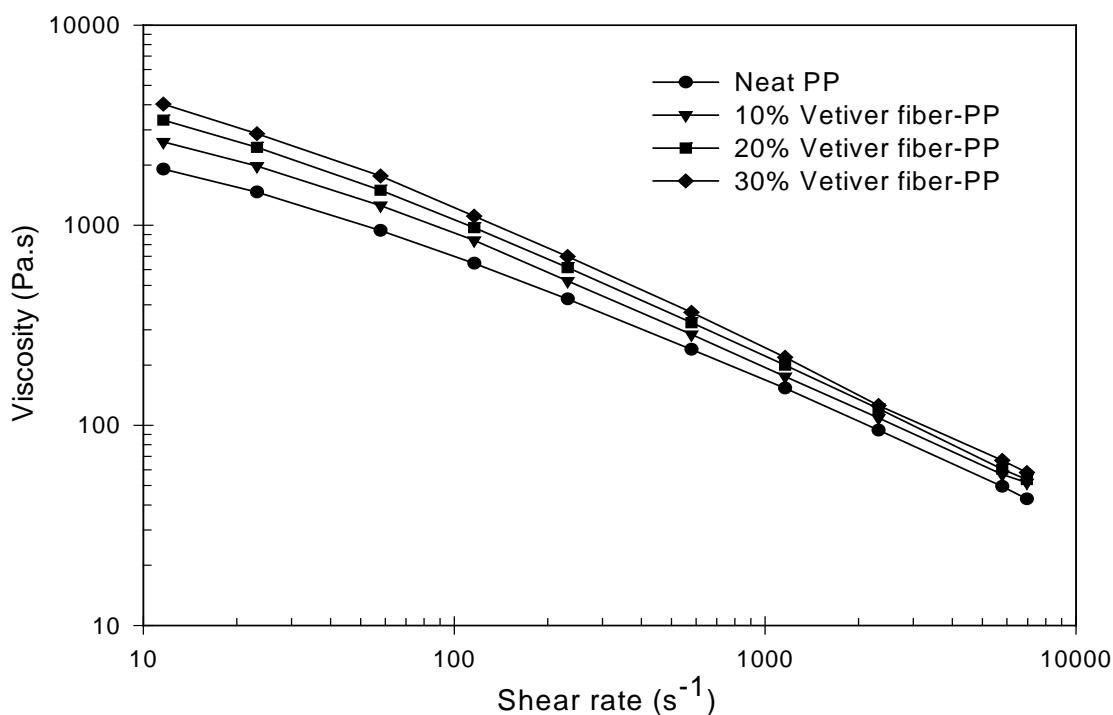
Figure 4.10 Plot of shear viscosity and shear rate of vetiver fiber-PP composites at 10%, 20%, and 30% (by weight) vetiver contents.

4.3.2 Thermal properties

Figure 4.11 showed TGA and DTG curves of neat PP and vetiver fiber-PP composites at various vetiver contents. The decomposition temperatures of hemicellulose (around 310°C) and α-cellulose (around 365°C) were clearly observed when the vetiver content was increased from 10% to 30% (by weight). Moreover, the beginning of decomposition of PP composites decreased with increasing vetiver contents due to the low thermal stability of vetiver fiber. The decomposition temperature of PP was around 460°C and PP was completely decomposed about 500°C. However, the decomposition temperature of PP slightly increased with an increase in vetiver contents. Avérous and Digabel (2006) also found that the decomposition temperature of polybutylene adipate-co-terephthalate, PBAT, as a matrix in biocomposites based on lignocellulose fillers (by

product of an industrial fractionation process of wheat straw) slightly increased with the filler contents.

DSC curves (heating scan) of neat PP and vetiver fiber-PP composites with 10%, 20%, and 30% (by weight) vetiver content at skin layer and core layer were illustrated in Figure 4.12(a)-(b). It was apparent from these figures that endotherms in the core exhibited more obviously multiple and broader than those in the skin. This characteristic was observed in both neat PP and PP composites. It implied that the presence of several crystallogrphic forms could be taken place in the core. However, these poorly resolved peaks may be classified into two types: 1) an unstable pseudo-hexagonal β form of lower melting temperature as well as less perfect form, and 2) a more stable monoclinic α form of higher ordering and higher melting temperature (Mucha et al., 2000).
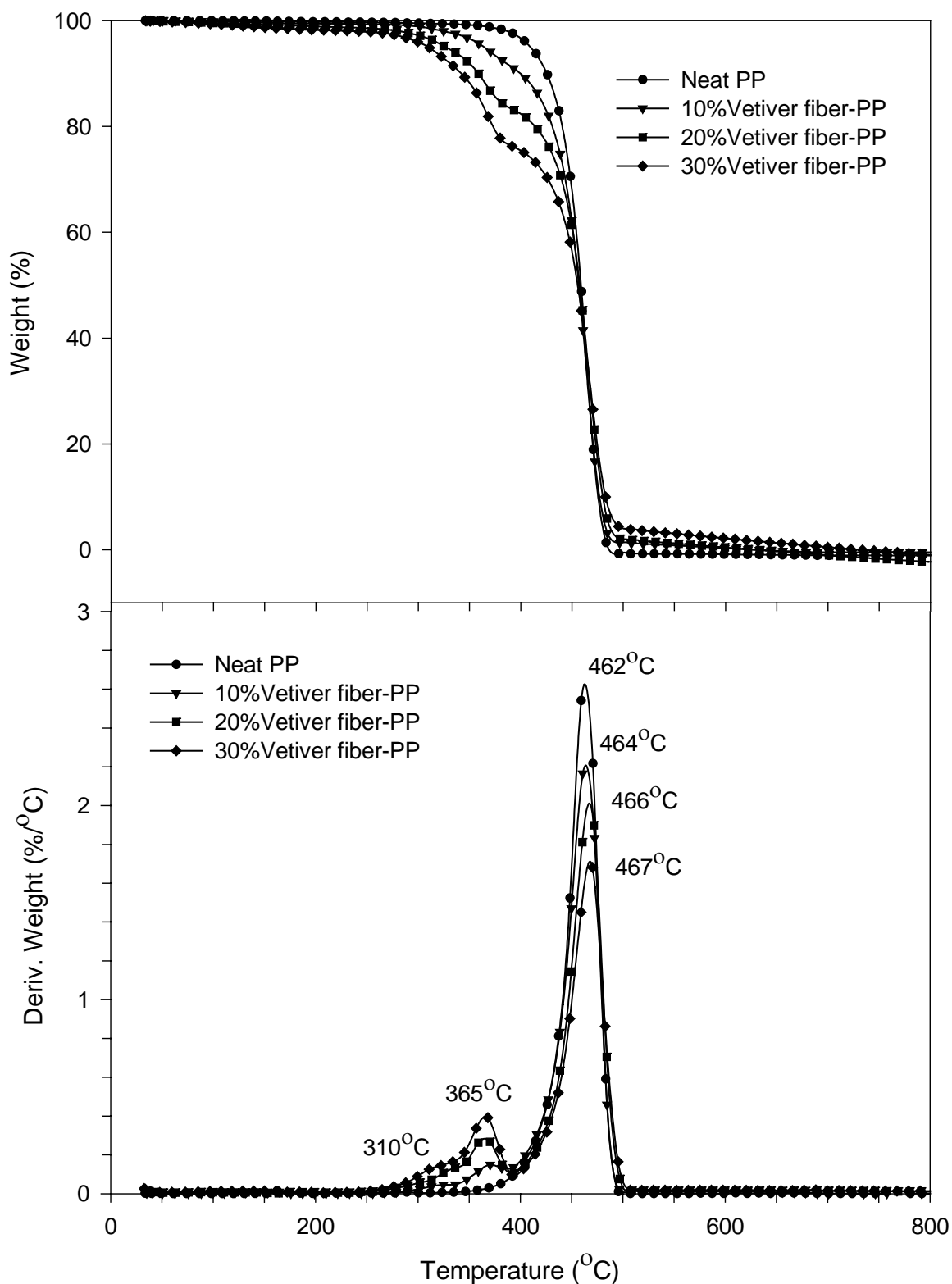
Figure 4.11   TGA and DTG curves of neat PP and vetiver fiber-PP composites at 10%, 20%, and 30% (by weight) vetiver contents.
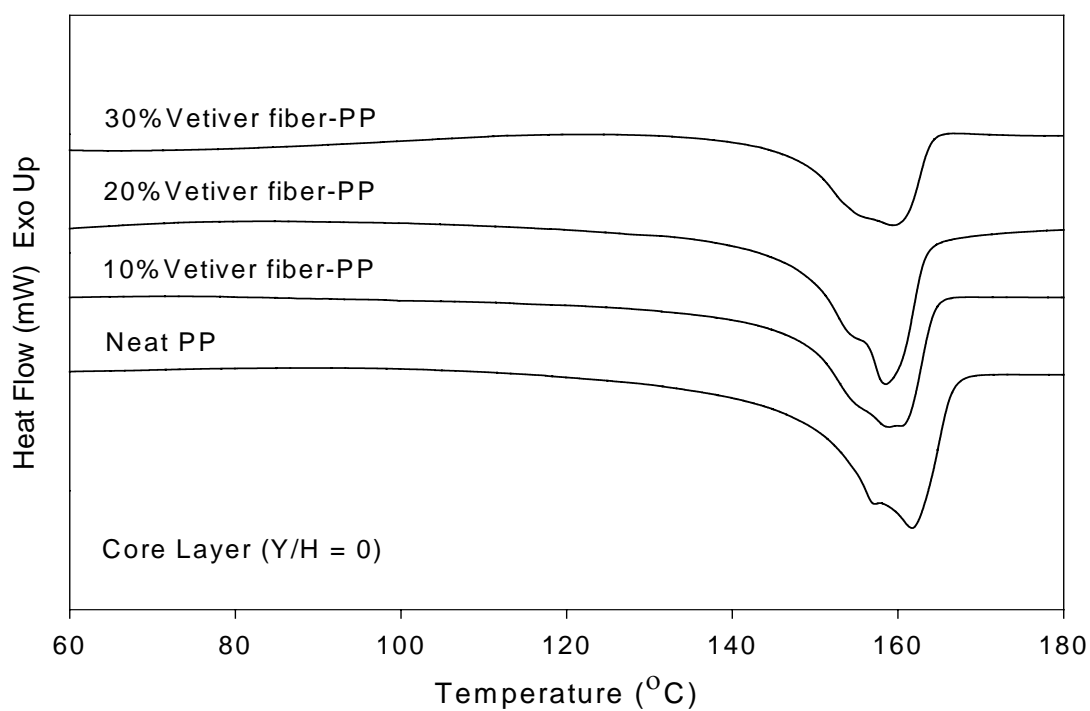
(a)
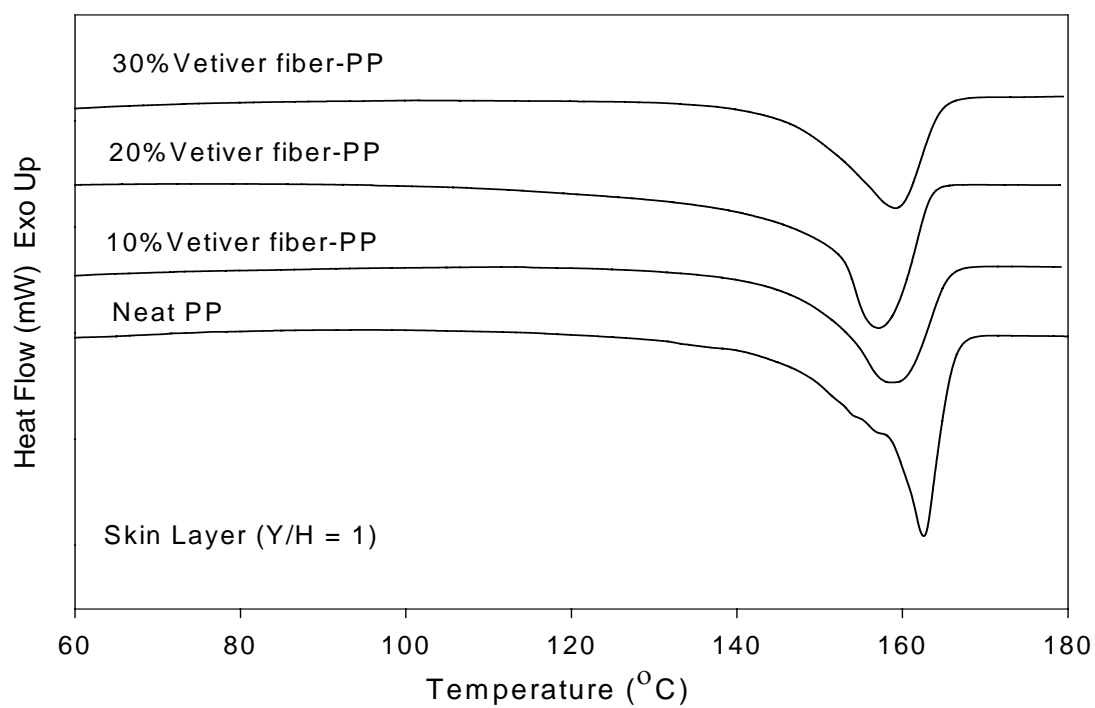
(b)

Figure 4.12   DSC curves corresponding to the heating scan of (a) core layer (Y/H = 0) and (b) skin layer (Y/H=1) of neat PP and vetiver fiber-PP composites with 10%, 20%, and 30% (by weight) vetiver content.

4.3.3 Normalized thickness of shear-induced crystallization layer

For vetiver fiber-PP composite, an increase in vetiver content in the composite led to a decrease in normalized thickness of shear-induced of crystallization layer of vetiver fiber-PP composite (Figure 4.13). This was because vetiver fibers acted as an obstruction to the normal flow of the polymer melt. Moreover, vetiver fibers could interfere the mobility of chain segments in melt flow. As a result, the molecular orientation of polymer chains in the composite with higher vetiver content was less than that of the composite with lower vetiver content. Therefore, the lower thickness of the shear-induced crystallization layer was observed in the composite with higher vetiver contents.
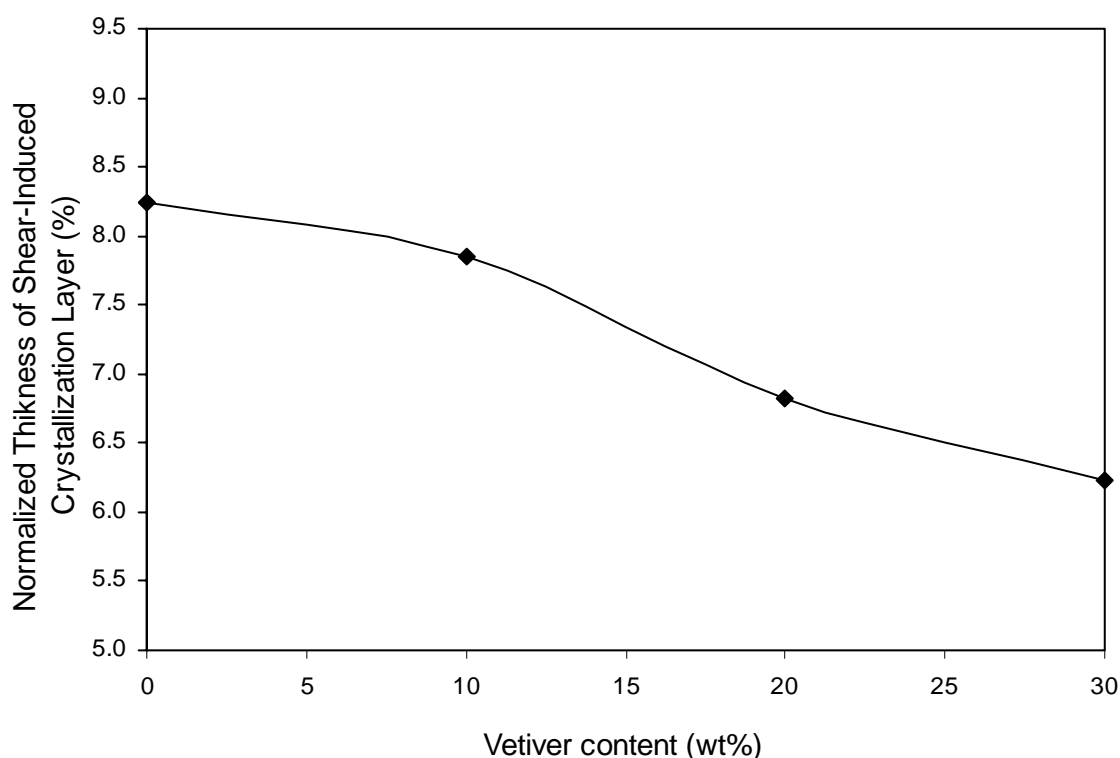
Figure 4.13 Plot of normalized thickness of skin layer of vetiver fiber-PP composite as a function of vetiver content.

4.3.4 Mechanical properties

The influence of vetiver content on the mechanical properties of the composite was displayed in Figure 4.14(a)-(d). As the fiber contents were increased, the vetiver fiber-PP composite exhibited higher Young's modulus but lower elongation at break and impact strength. However, tensile strength of vetiver fiber-PP composite increased as vetiver content increased up to 10% (wt). When the vetiver content was more than 10% (by weight), tensile strength of PP composite reached the plateau. This indicated that the reinforcing effect of vetiver fiber in the composite limiting at 10% (wt). An increase in vetiver content was possibly increased the number of void and agglomeration in PP composites. Hence, these void and agglomeration were served as a local area for crack initiation and caused the failure at lower stress. In addition, the improvement of strength and stiffness of PP composite was sacrificed by a decrease of strain at break. As a result, the composites were more brittle than neat PP matrix.
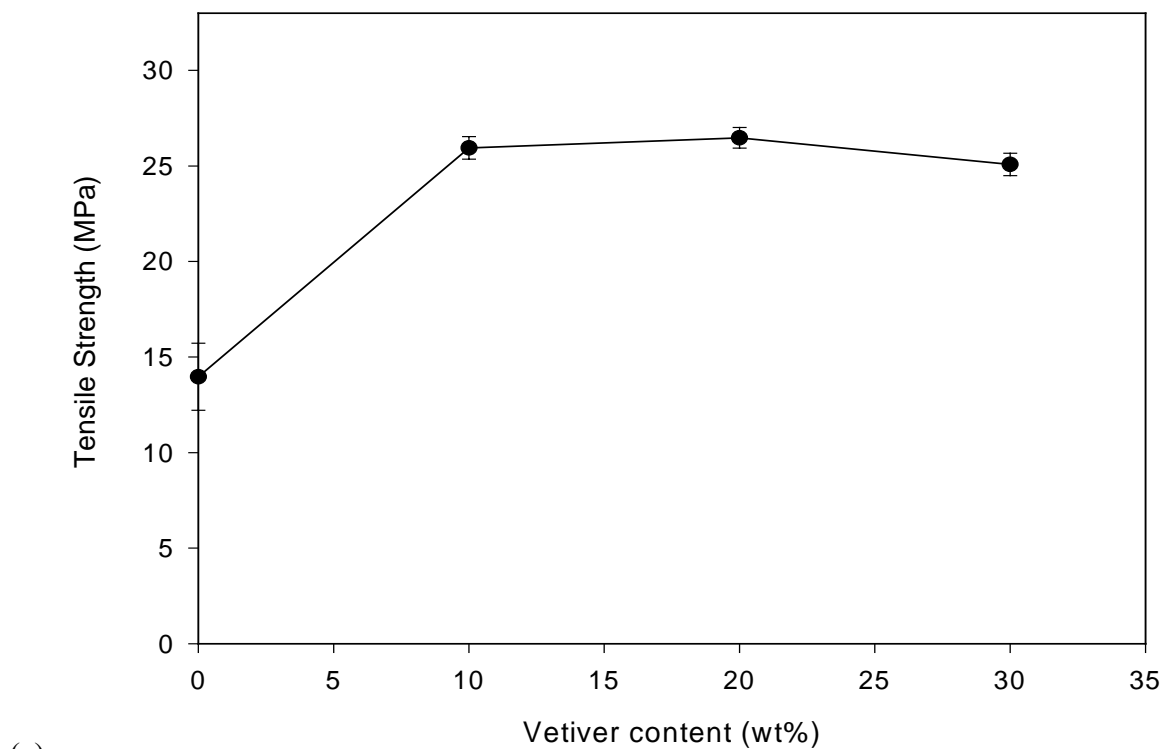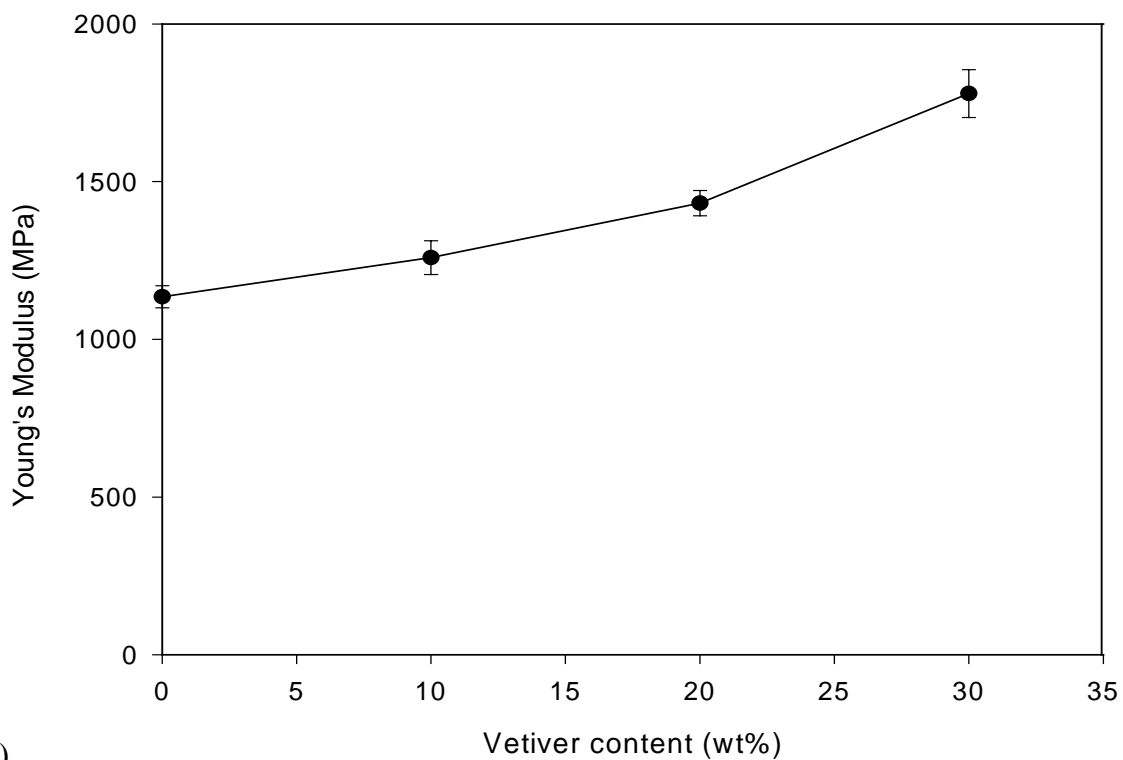
Figure 4.14 Plot of (a) Tensile strength and (b) Young's modulus of vetiver fiber-PP

composite as a function of vetiver content.
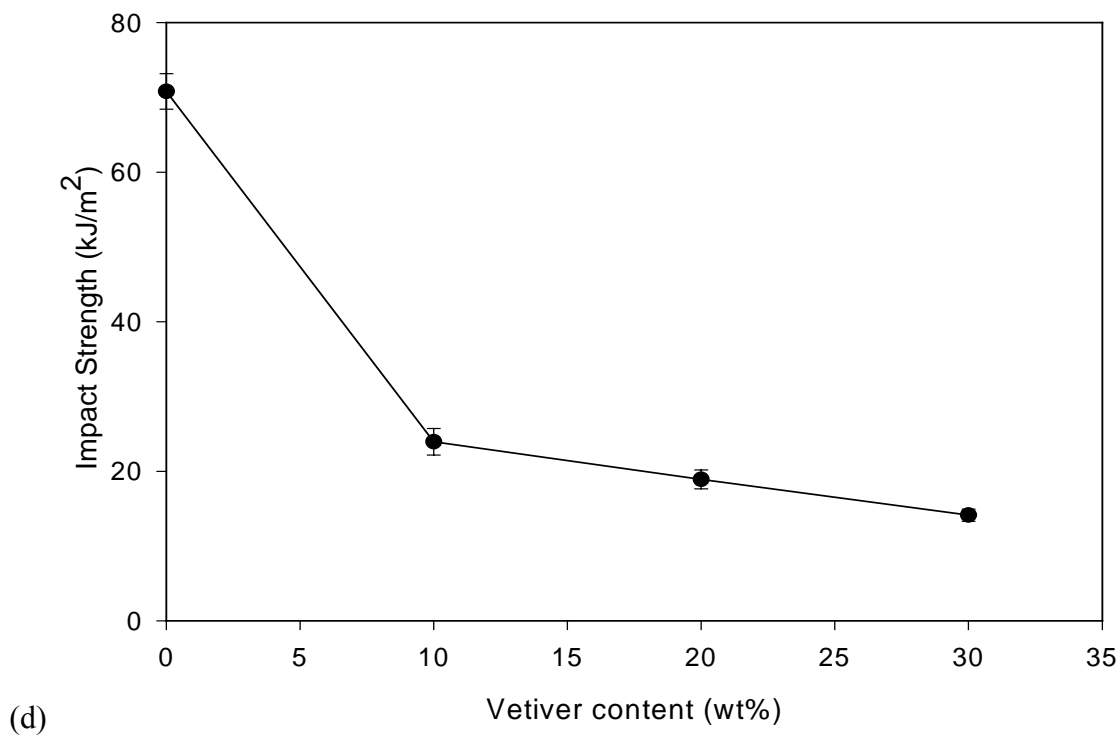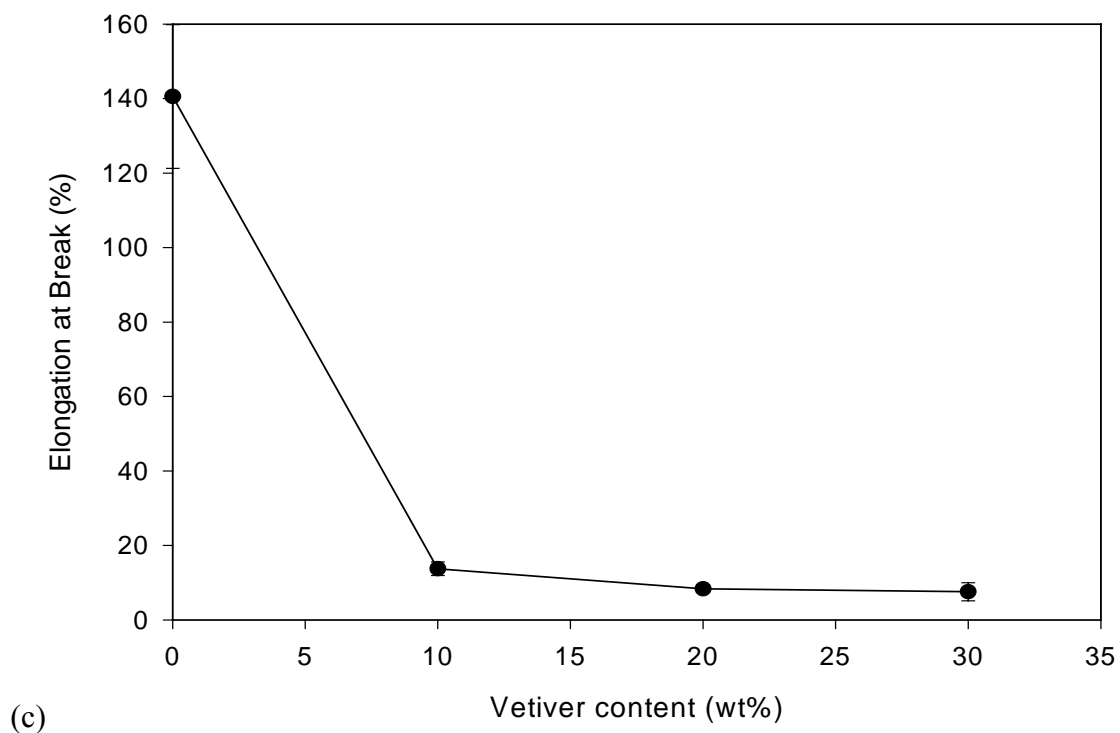
Figure 4.14 **(Continued)** Plot of (c) Elongation at break and (d) Impact strength of vetiver fiber-PP composite as a function various vetiver content.

4.4 The effect of various types of natural fibers on PP composites

4.4.1 Rheological property

Shear viscosity of neat PP and PP composites from various types of natural fiber were shown in Figure 4.15. It can be seen that vetiver fiber-PP, rossells-PP, and sisal-PP composites had higher shear viscosity when compared to neat PP. This was possibly because natural fibers i.e. vetiver fiber, rossells, and sisal can perturb normal flow of polymer and hinder the mobility of chain segments in the melt flow. Moreover, PP composite from vetiver fiber exhibited higher shear viscosity than rossells-PP and sisal-PP composites. This may be due to the different of sizes and shapes of vetiver, rossells, and sisal fibers. It was found that vetiver fiber had lower aspect ratio than rossells and sisal fibers. Hence, vetiver fiber was able to obstruct melt flow of polymer more than rossells, and sisal.
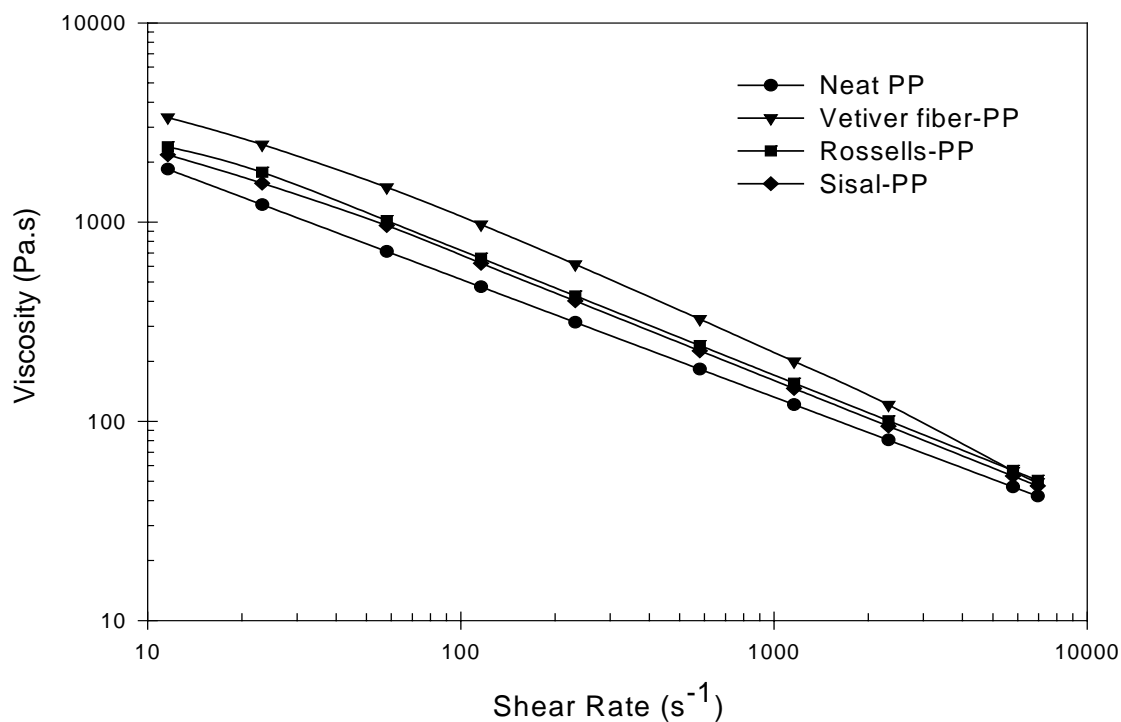
Figure 4.15 Plot of shear viscosity and shear rate of PP composites from vetiver fiber, rossells, and sisal at 20% (by weight) fiber content.

4.4.2 Thermal properties

Thermal properties of PP composites from vetiver fiber, rossells, and sisal at 20% (by weight) fiber content were displayed in Figure 4.16. Results revealed that the onset of the decomposition temperature of all composites was lower than that of neat PP. This may be due to the fact that vetiver fiber, rossells, and sisal had lower thermal stability than neat PP. However, there was no significant difference in α-cellulose decomposition temperature (around 365°C) of vetiver fiber, rossells, and sisal in the PP composites. The addition of natural fibers into the PP matrix did not significantly affect the decomposition temperature of PP. It was in a range of 461-466°C. Moreover, the residue weight of vetiver fiber-PP, rossells-PP, and sisal-PP around 800°C were not significantly different.

DSC curves (heating scan) of neat PP and PP composites from vetiver fiber, rossells, and sisal at 20% (by weight) fiber content at core layer and skin layer were illustrated in Figure 4.17(a)-(b). It was noticed that endotherms in the core of PP composites obviously exhibited more multiple and broader than those in the skin. This characteristic was also observed in neat PP. It implied that the presence of several crystallographic forms could be taken place in the core. These crystallites may be classified into two types: 1) an unstable pseudo-hexagonal β form of lower melting temperature as well as less perfect form, and 2) a more stable monoclinic α form of higher ordering and higher melting temperature (Mucha et al., 2000).
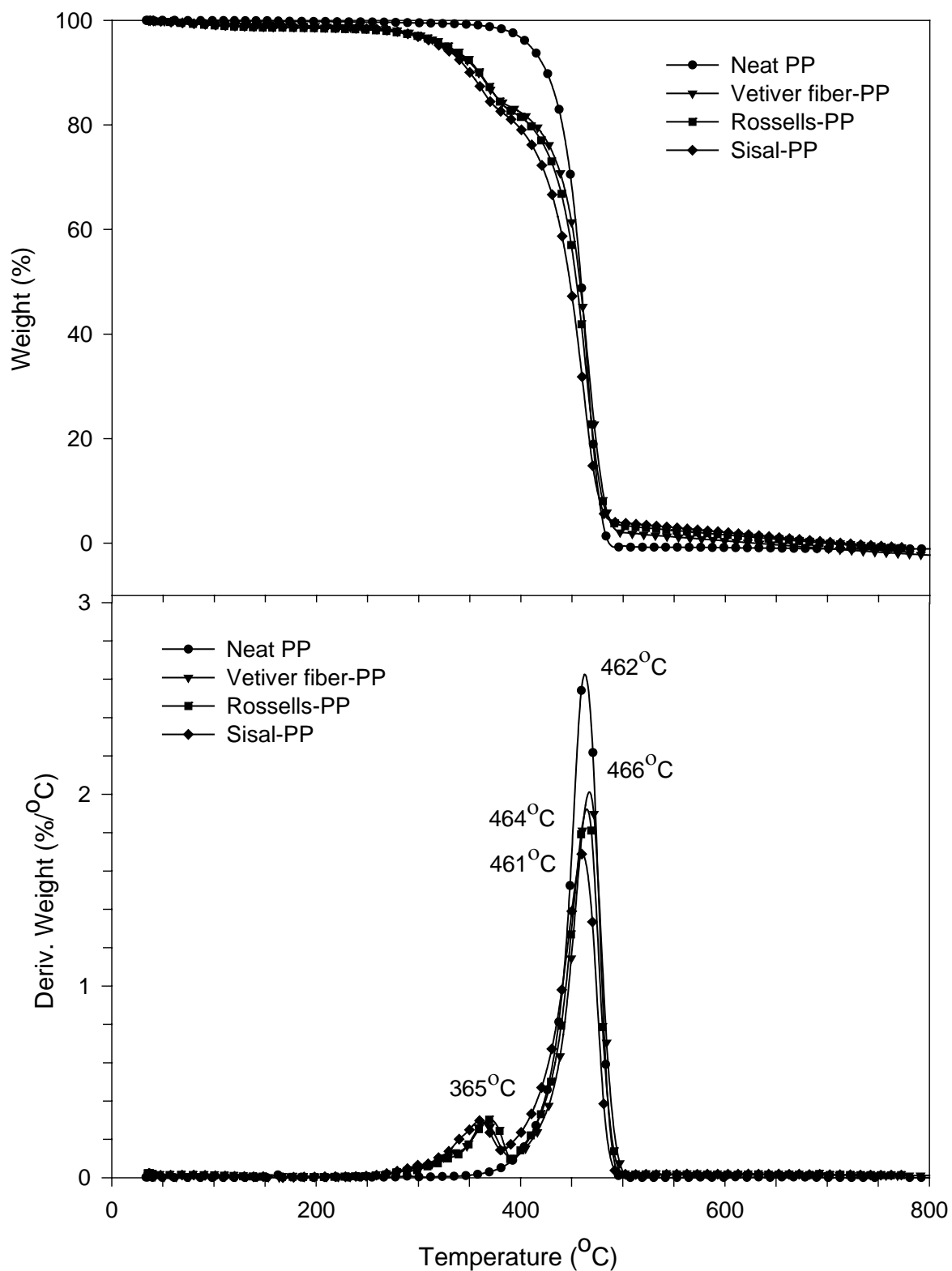
Figure 4.16   TGA and DTG curves of neat PP and PP composites from vetiver fiber, rossells, and sisal at 20% (by weight) fiber content.
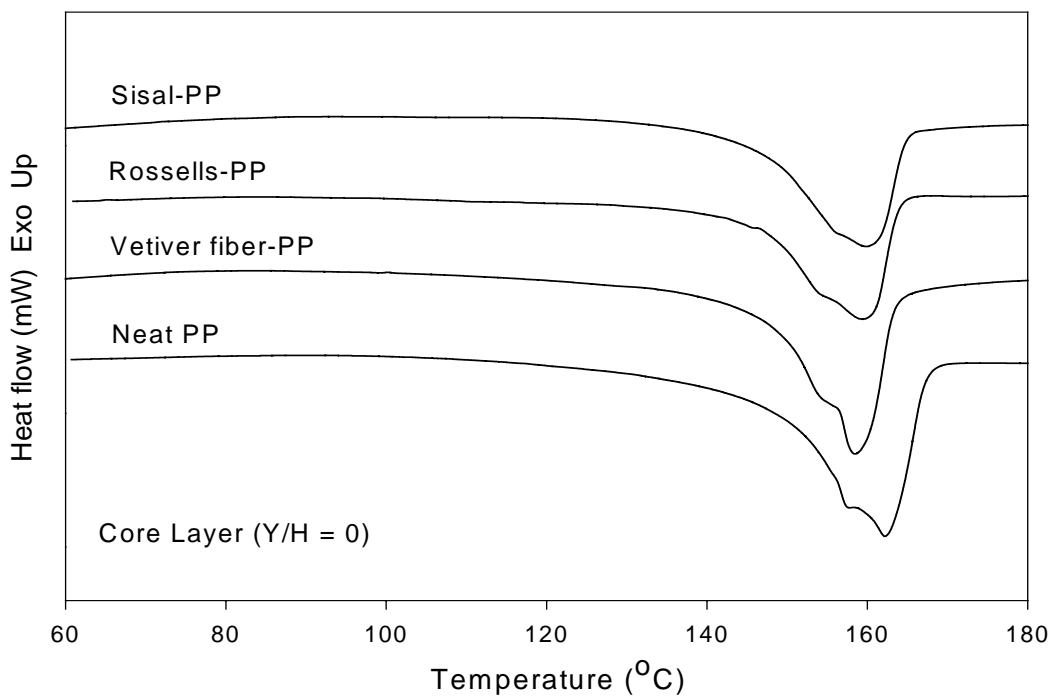
(a)
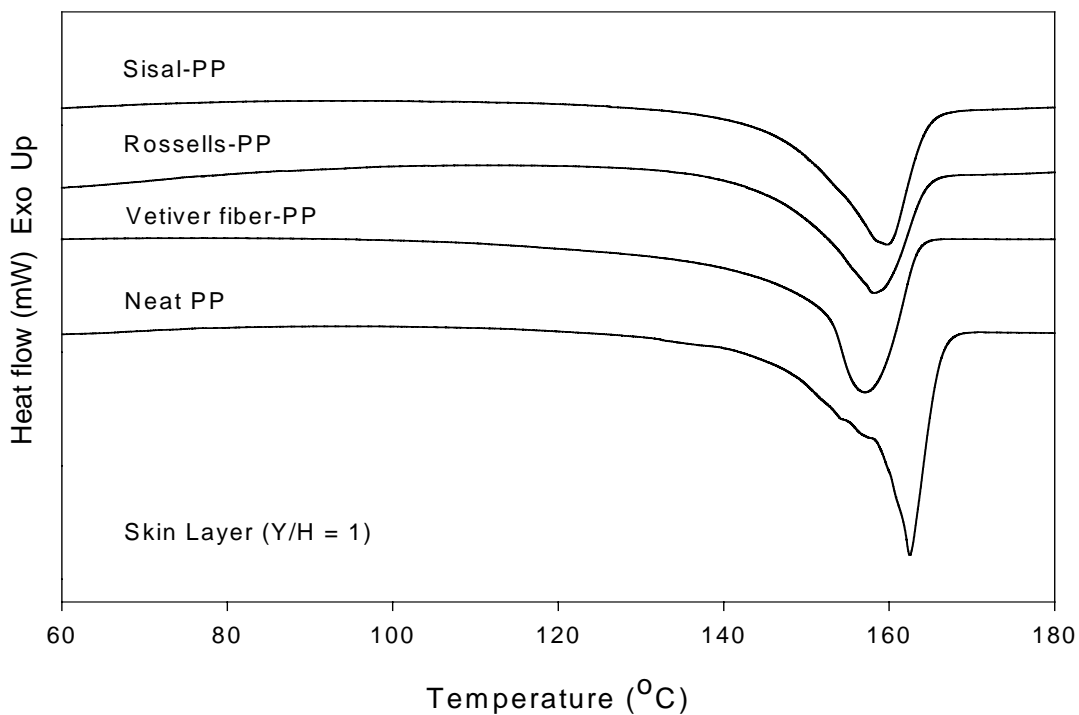
(b)

Figure 4.17 DSC curves corresponding to the heating scan of (a) core layer (Y/H = 0) and (b) skin layer (Y/H =1) of neat PP and vetiver fiber-PP, rossells-PP, and sisal-PP composites.

4.4.3 Normalized thickness of shear-induced crystallization layer

The effect of fiber types on normalized thickness of shear-induced crystallization layer of natural fiber-PP composites was represented in Figure 4.18. It was revealed that vetiver fiber-PP, rossells-PP, and sisal-PP composites had lower normalized thickness of skin layer than neat PP. This was because the shear viscosities of PP composites were higher than that of neat PP. It can be suggested that natural fibers i.e. vetiver fiber, rossells, and sisal possibly restricted or obstructed molecular orientation of polymer chain leading to a decrease in normalized thickness of shear-induced crystallization layer. In addition, it was noticed that normalized thickness of shear-induced crystallization layer among vetiver fiber-PP (6.82%), rossells-PP (6.37%), and sisal-PP (6.03%) composites were not significantly different.

4.4.4 Degree of crystallinity and gapwise crystallinity distribution

Figure 4.19 showed the gapwise crystallinity distribution at the midway of PP composites from vetiver fiber, rossells, and sisal at 20% (by weight). When take the consideration on the degree of crystallinity in various types of natural fiber-PP composites, it can be seen that the degree of crystallinity of vetiver fiber-PP composite was higher than those of rossells-PP and sisal-PP composites. This situation may possibly due to the more suitable surface topology and surface area of vetiver fiber for crystallization of PP than those of rossells and sisal fibers. However, there was no gapwise crystallinity distribution at the midway of moldings for all specimens.

4.4.5 Mechanical properties

Mechanical properties of PP composites from vetiver fiber, rossells, and sisal at 20% (by weight) fiber content were represented in Figure 4.20(a)-(d). It was found that tensile strength of vetiver fiber-PP composite was slightly higher than those of

rossells-PP and sisal-PP composites. This was because vetiver fiber-PP composite had higher degree of crystallinity than rossells-PP and sisal-PP composites as mentioned in section 4.4.4. Moreover, the aspect ratio of rossells and sisal were higher than that of vetiver fiber resulting in an increase in number of void and agglomeration in PP composites. This was served as a local area for crack initiation and caused the failure at lower stress.

However, rossells-PP composite exhibited slightly higher Young's modulus and impact strength than those of vetiver fiber-PP and sisal-PP composites. Elongation at break of rossells-PP composite was lower than those of vetiver fiber-PP and sisal-PP composites. This was because the aspect ratio and surface property of vetiver fiber, rossells, and sisal were different. The higher aspect ratio of natural fiber, the more defect was possibly increased. For natural fibers in this study, the aspect ratio of rossells was higher than those of sisal and vetiver fibers. Furthermore, it was found that during the processing of PP composites, some fiber damage resulting in the reduction in length and aspect ratio was considerable occurred. The final aspect ratio of vetiver fiber, rossells, and sisal in the composites were 4.94, 12.83, and 9.96, respectively (see Appendix A). In addition, the mechanical properties of the fibers played more important role on the mechanical properties of PP composites. The mechanical properties of vetiver fiber, rossells, and sisal have been known. The average tensile strength of vetiver fiber, rossells, and sisal were 485.0, 434.7 and 377.8 MPa, respectively. Moreover, the average Young's modulus of vetiver fiber, rossells, and sisal were, 30.9, 41.7, and 19.6 GPa, respectively. It can be seen that vetiver fiber had the highest average tensile strength whereas rossells exhibited the highest average Young's modulus. Hence, the results of mechanical properties of PP composites as early described were reasonable and expectable. The impact strength of sisal-PP composite was lower than those of vetiver fiber-PP and rossells-PP composites. This implied that the interfacial adhesion between natural fiber and PP matrix

is crucial to the performance of PP composites, in particular fracture behavior. The weak

interface would promote failure by fiber debonding and fiber pull-out.
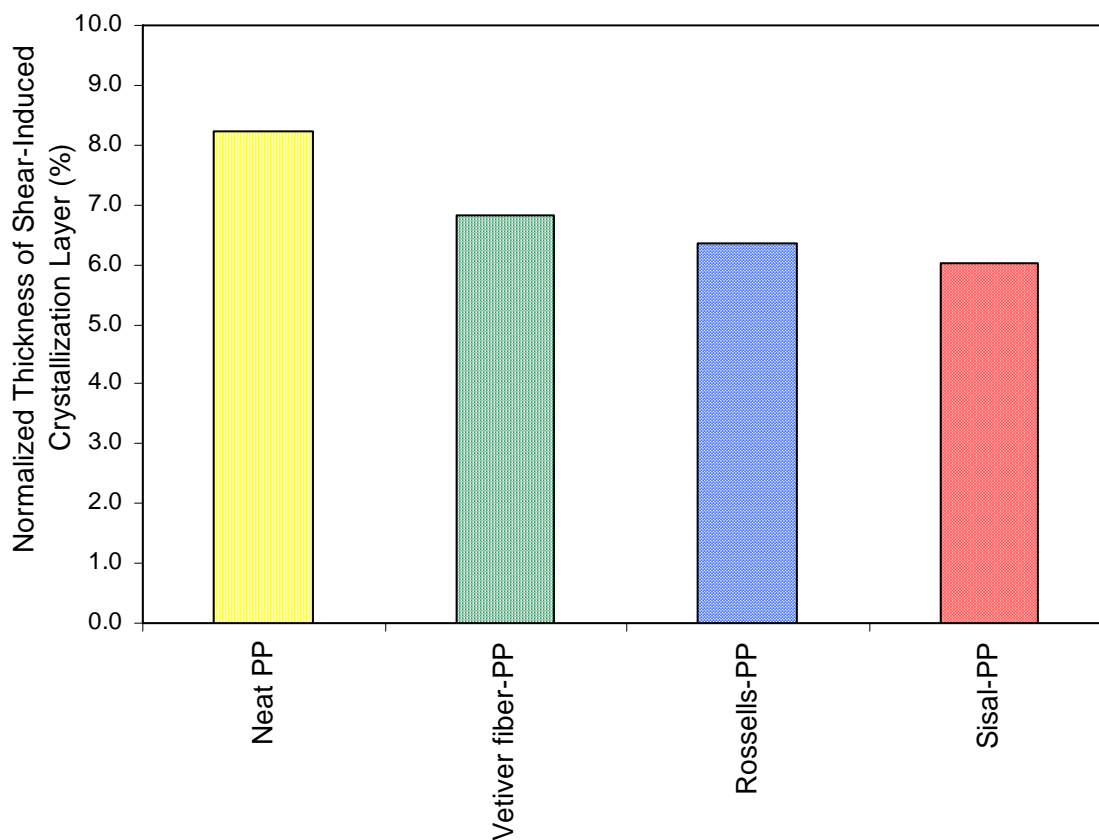
Figure 4.18 Plot of normalized thickness of shear-induced crystallization layer of neat

PP and PP composites from vetiver fiber, rossells, and sisal at 20% (by

weight) fiber content.
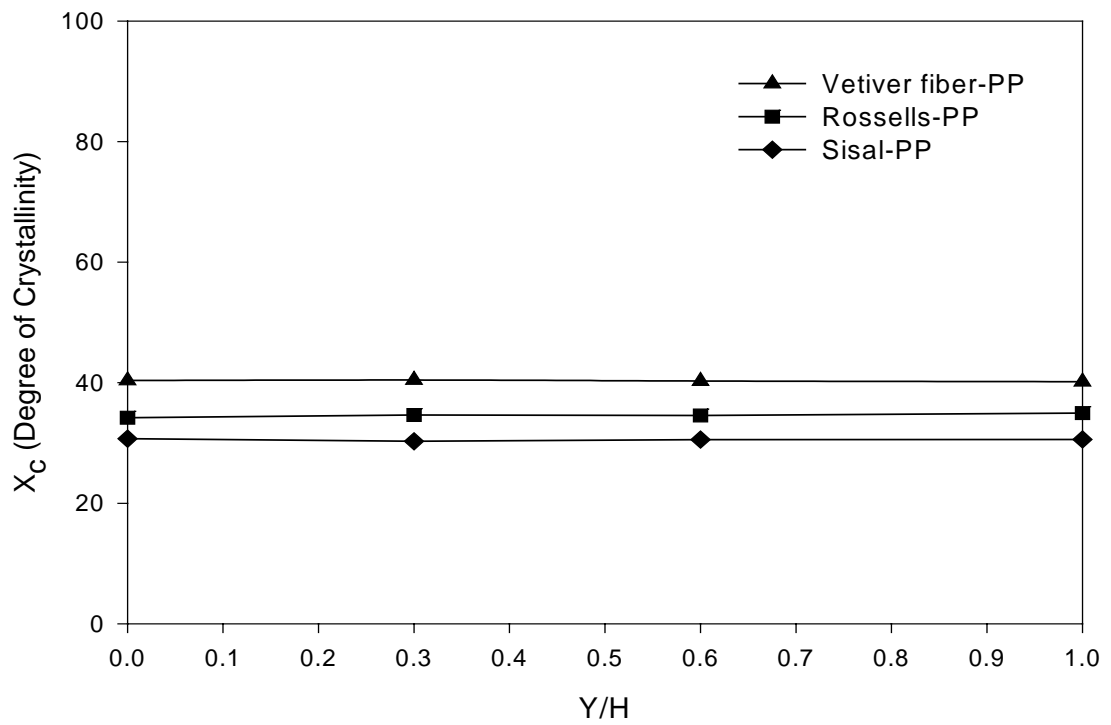
Figure 4.19 Gapwise crystallinity distribution at the midway of moldings of PP composites from vetiver fiber, rossells, and sisal at 20% (by weight).
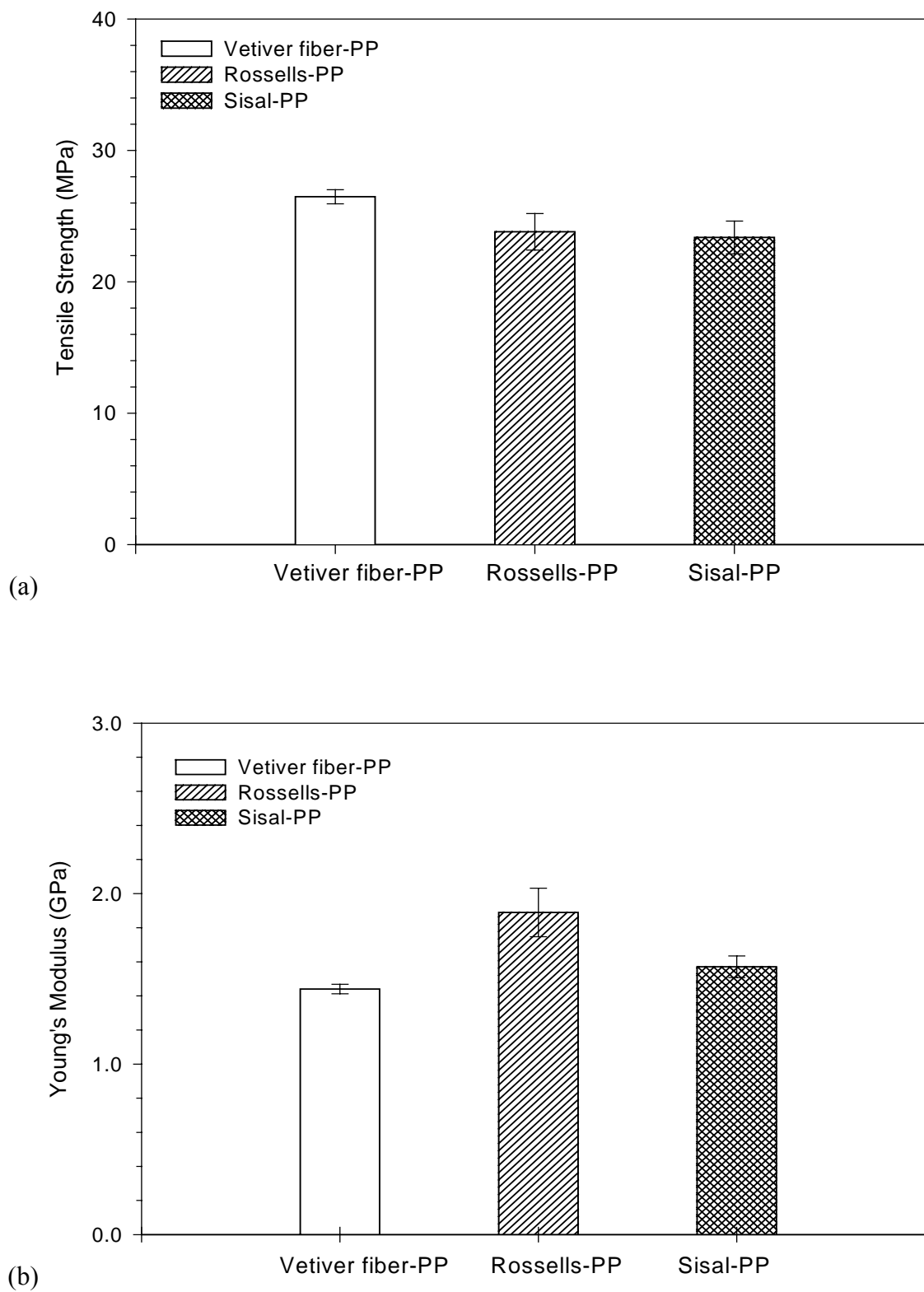
Figure 4.20 Plot of (a) Tensile strength and (b) Young's modulus of PP composites from

vetiver fiber, rossells, and sisal at 20% (by weight) fiber content.

(c)

(d)
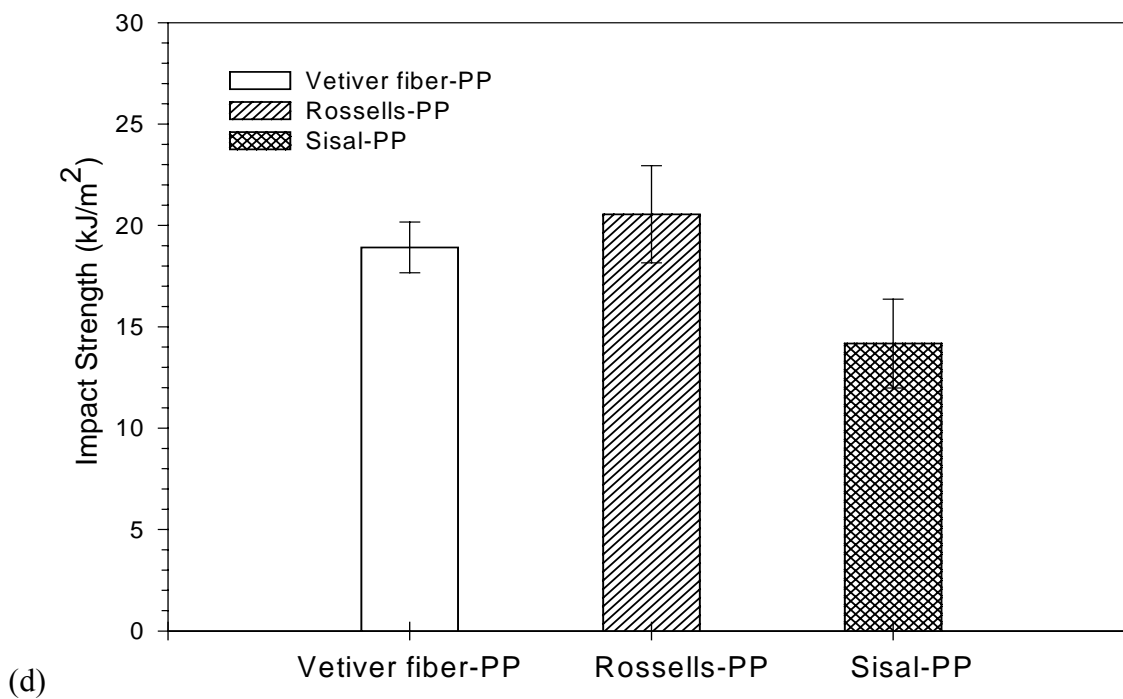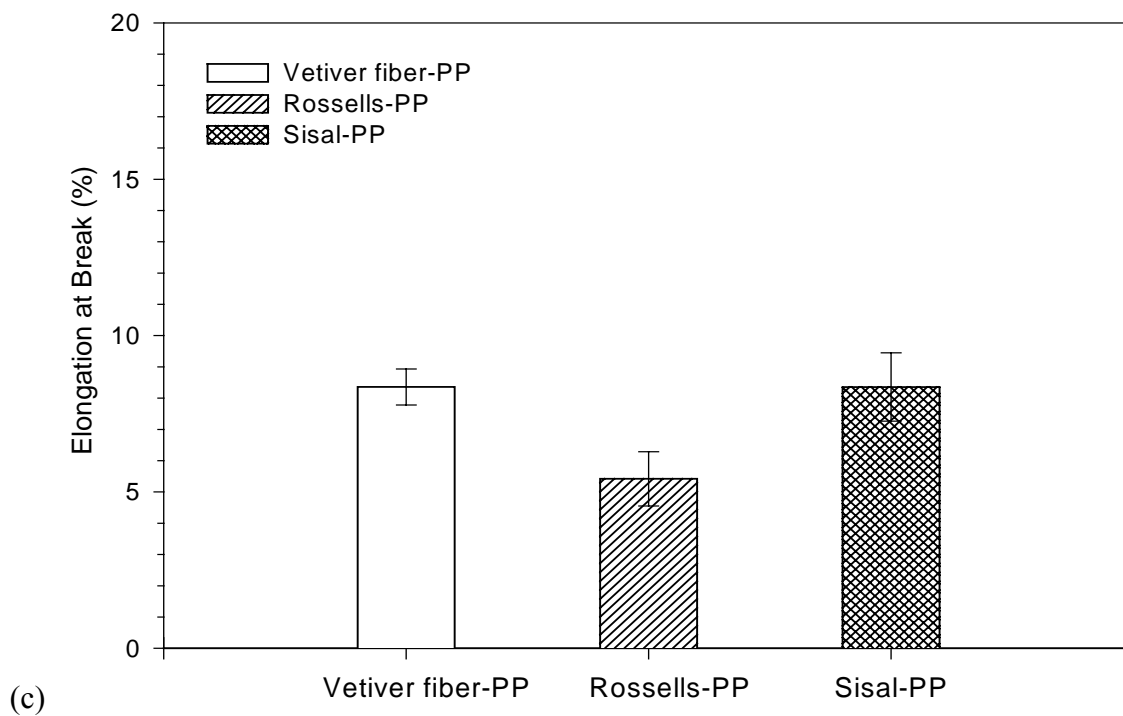
Figure 4.20 **(Continued)** (c) Elongation at break and (d) Impact strength of PP composites from vetiver fiber, rossells, and sisal at 20% (by weight) fiber content.

4.5   The effect of processing conditions on vetiver fiber-PP composites

4.5.1   Normalized thickness of shear-induced crystallization layer

The normalized thickness of shear-induced crystallization layer of both PP and vetiver fiber-PP composites slightly decreased with increasing screw speed as illustrated in Figure 4.21. Generally, screw speed refers to the rate at which the screw turns backward to accumulate the melt for the next injection shot; some of the heat necessary to plasticize the plastic comes as a result of rotating the screw. Basically, the faster the screw rotates, the higher melt temperature is generated because the amount of shear increases. As a result, the growth of shear-induced crystallization layer could possibly minimize as observed at higher screw speed.

From Figure 4.22, it was revealed that both normalized thickness of shear-induced crystallization layer of PP and vetiver fiber-PP composites gradually increased when holding pressure increased up to 1400 kg/cm^2, and remained unchanged after that. An increase in holding pressure resulted in the retardation of molecular relaxation. Consequently, the shear induced molecular orientation had no enough time to relax. This caused higher normalized thickness of shear-induced crystallization layer at higher holding pressure. Trotignon and Verdu (1990) also hypothesized that the holding pressure acted as a quenching phenomenon to the crystallization and perturbed relaxation of molecular chains. Furthermore, Sjönnell et al. (1995) reported that the holding pressure clearly affected the orientation of molecules especially in the shear zone of injection-molded PP discs. The average orientation was higher further in the sample molded with increasing holding pressure while the sample molded with zero holding pressure showed a much faster relaxation of oriented chains. However, Čermák et al. (2005) found that the holding pressure did not affect the shear-induced crystallization layer and morphology of iPP specimen.

Moreover, normalized thickness of shear-induced crystallization layer of both PP and vetiver fiber-PP composites decreased with increasing injection speed as shown in Figure 4.23. The injection speed refers to the speed of mold filling when the screw is acting as a ram. Thus, the injection speed controls the shear rate level imposed to the material during a filling stage (Johannaber, 1994). However, the effect of injection speed on normalized thickness of shear-induced crystallization layer was contributed by both the extent of shear (increased with increasing injection speed) and the shearing time (increased with decreasing injection speed). In this study, it was found that the shearing time showed much more influence on the development of shear-induced crystallization layer than the extent of shear. Hence, at higher injection speed, the shearing time was lower resulting in the thinner shear-induced crystallization layer.

In addition, it was shown that the normalized thickness of shear-induced crystallization layer of both neat PP and vetiver fiber-PP composites decreased with increasing mold temperature (Figure 4.24). Generally, an increase in mold temperature leads to less oriented chains due to the more possible relaxation. This result showed a well agreement with Fujiyama (1995), Kim et al. (2005), and Čermák et al. (2005). In comparison, vetiver fiber-PP composites showed lower normalized thickness of shear-induced crystallization layer than that of PP. This may be due to the vetiver fiber acting as an obstruction to the normal flow of polymer melt. As a result, the molecular orientation of vetiver fiber-PP composite was less than that of PP leading to the thinner normalized thickness of shear-induced crystallization layer.
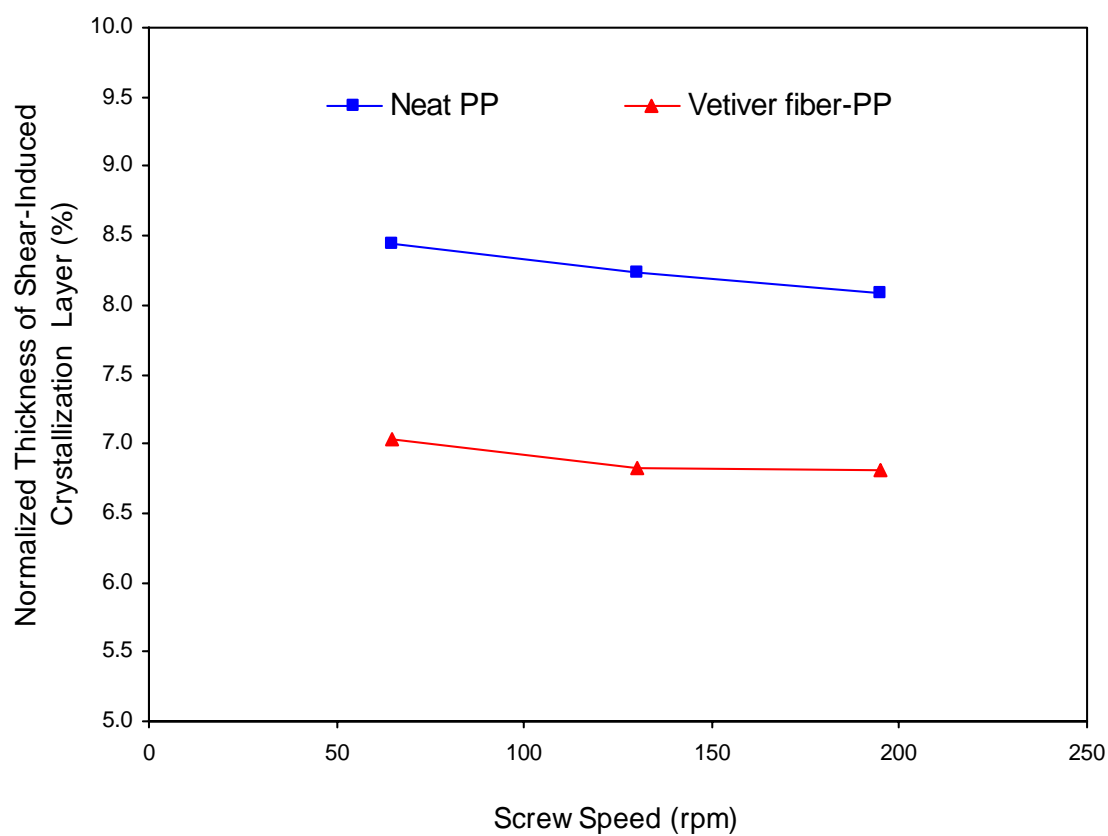
Figure 4.21 Plot of normalized thickness of shear-induced crystallization layer of neat PP and vetiver fiber-PP composites as a function of screw speed.
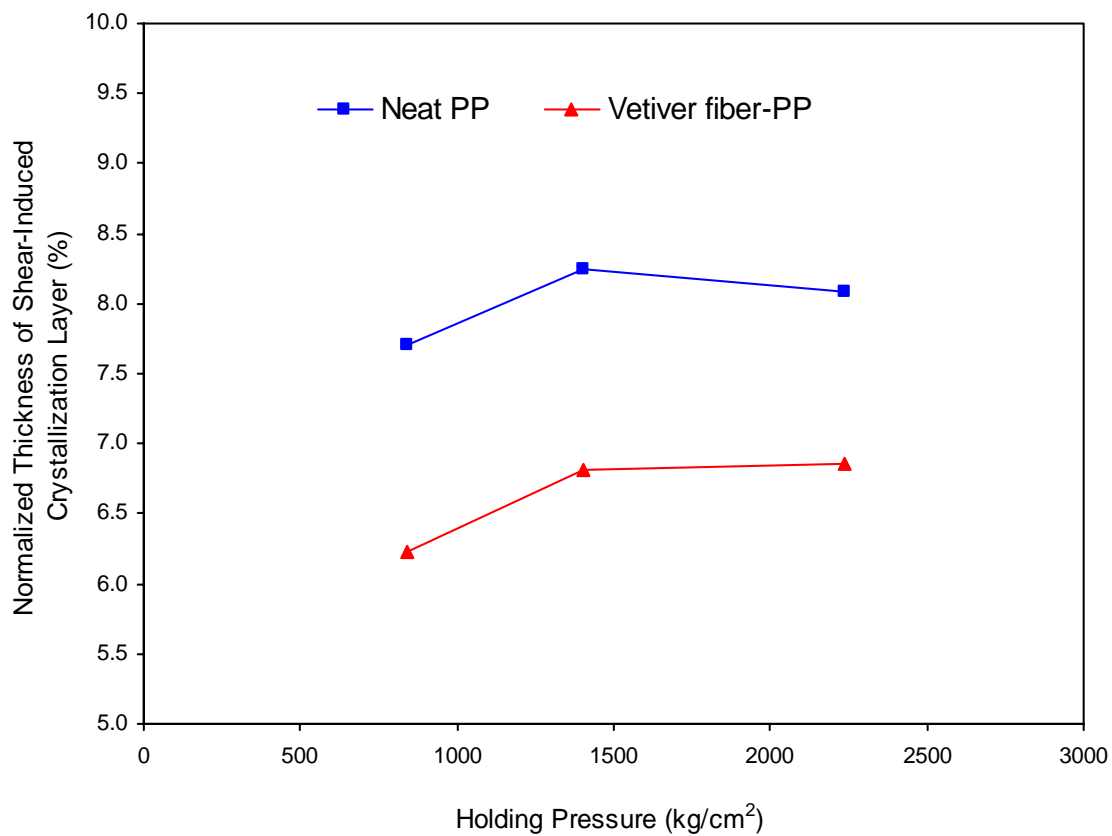
Figure 4.22   Plot of normalized thickness of shear-induced crystallization layer of PP and

vetiver fiber-PP composites as a function of holding pressure.
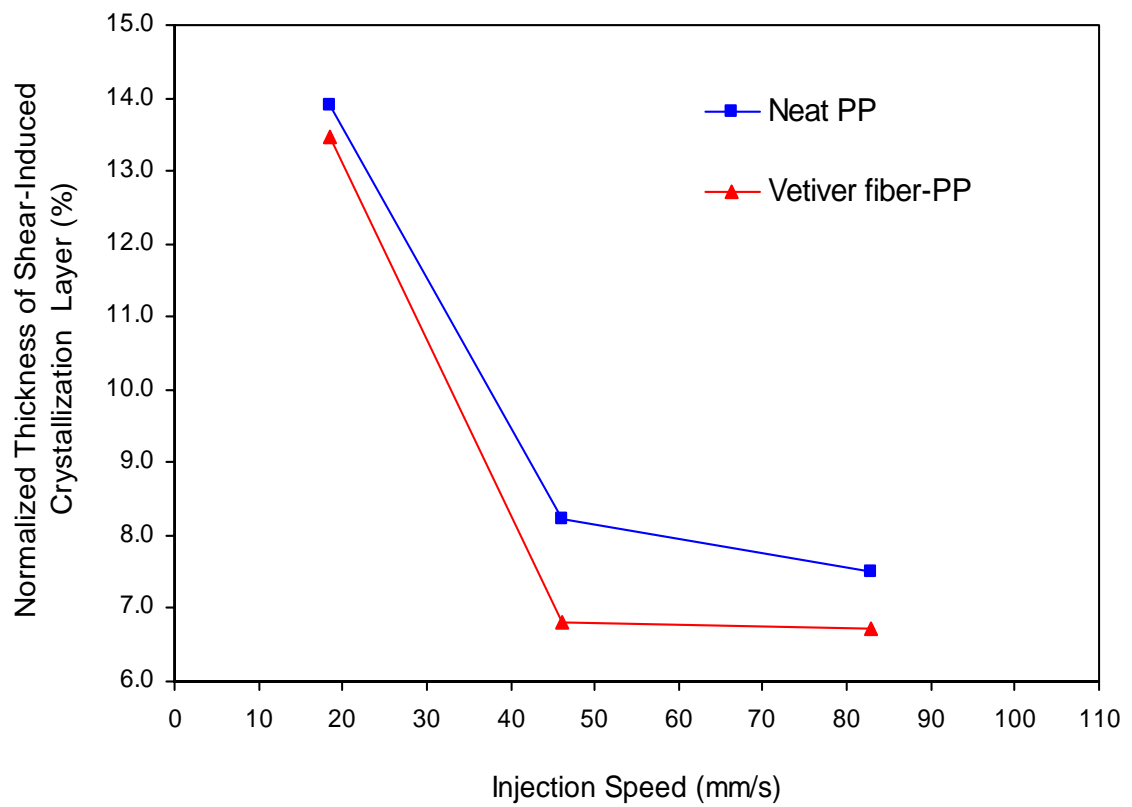
Figure 4.23   Plot of normalized thickness of shear-induced crystallization layer of neat

PP and vetiver fiber-PP composites as a function of injection speed.
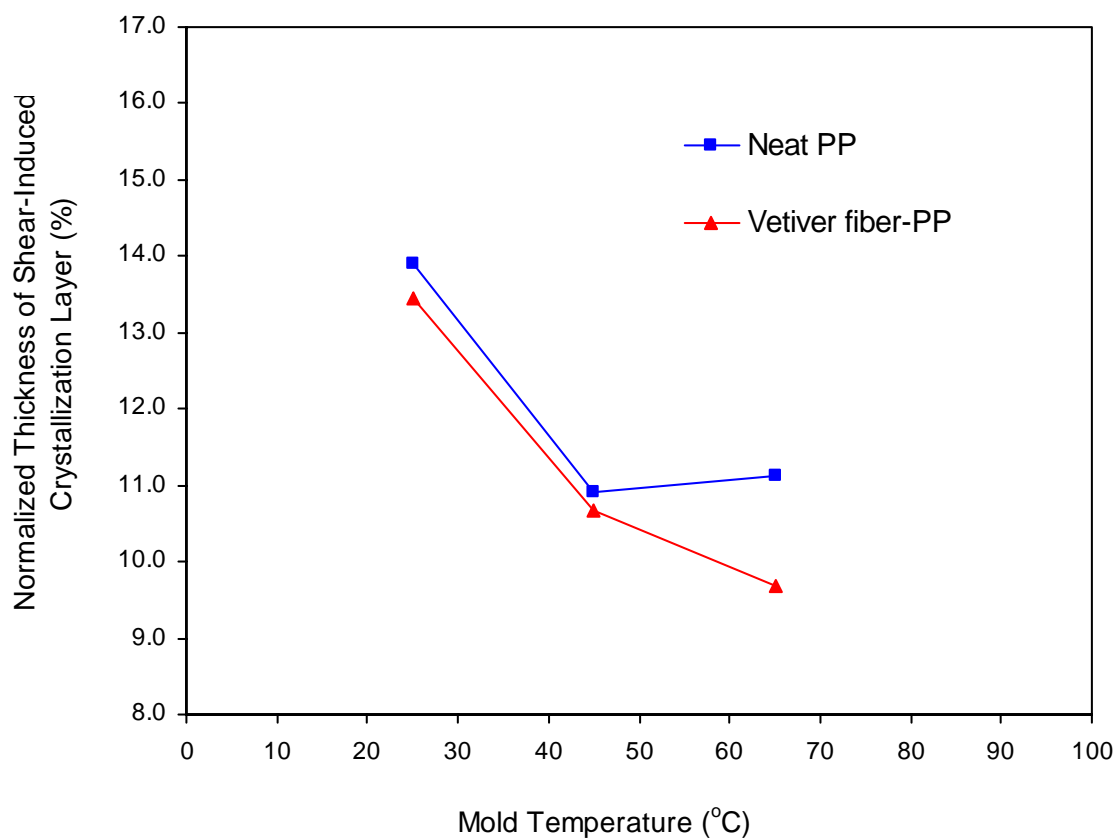
Figure 4.24 Plot of normalized thickness of shear-induced crystallization layer of neat PP and vetiver fiber-PP composites as a function mold temperature.

4.5.2 Melting behavior and crystallization temperature

Melting behavior and crystallization temperature were studied and compared between core layer and skin layer of the vetiver fiber-PP composite at 20% (by weight) fiber content. DSC curves of core layer and skin layer of vetiver fiber-PP composites at various screw speeds, holding pressures, injection speeds, and mold temperatures were displayed in Figure 4.25-4.28 respectively. In the case of screw speed, there was no significant difference in melting range of PP composites. However, the endothermic curves of PP composites at various screw speeds were noticeable multiple and remarkable complex. These characteristics were also observed in DSC curves of PP composites at various holding pressures, injection speeds, and mold temperatures. Hence,

the processing conditions had no influence on the pattern of endothermic curves and the melting range of the composites. Furthermore, it was noticed that vetiver fiber-PP composites obviously exhibited more multiple and broader endotherms in the core layer than those in the skin layer. This indicated that several crystallographic forms could be taken place in the core layer. However, these poorly resolved peaks may be classified into an unstable pseudo-hexagonal β form and a more stable monoclinic α form. The β form of PP has lower melting temperature and less perfection than α form of PP (Mucha et al., 2000).
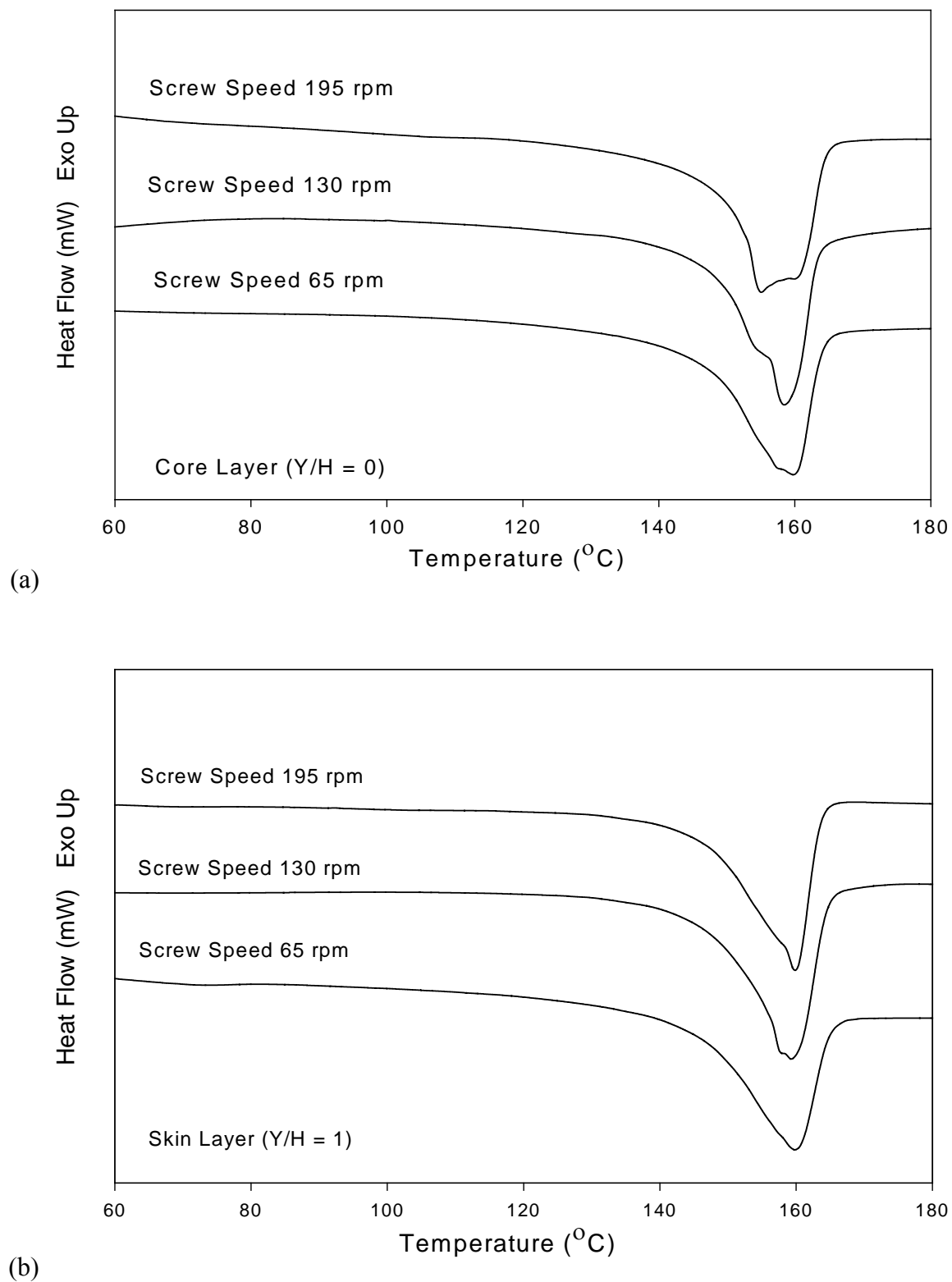
Figure 4.25 DSC curves corresponding to the heating scan of veiver fiber-PP composite

at (a) core layer (Y/H = 0) and (b) skin layer at screw speeds of 65, 130, and

195 rpm.
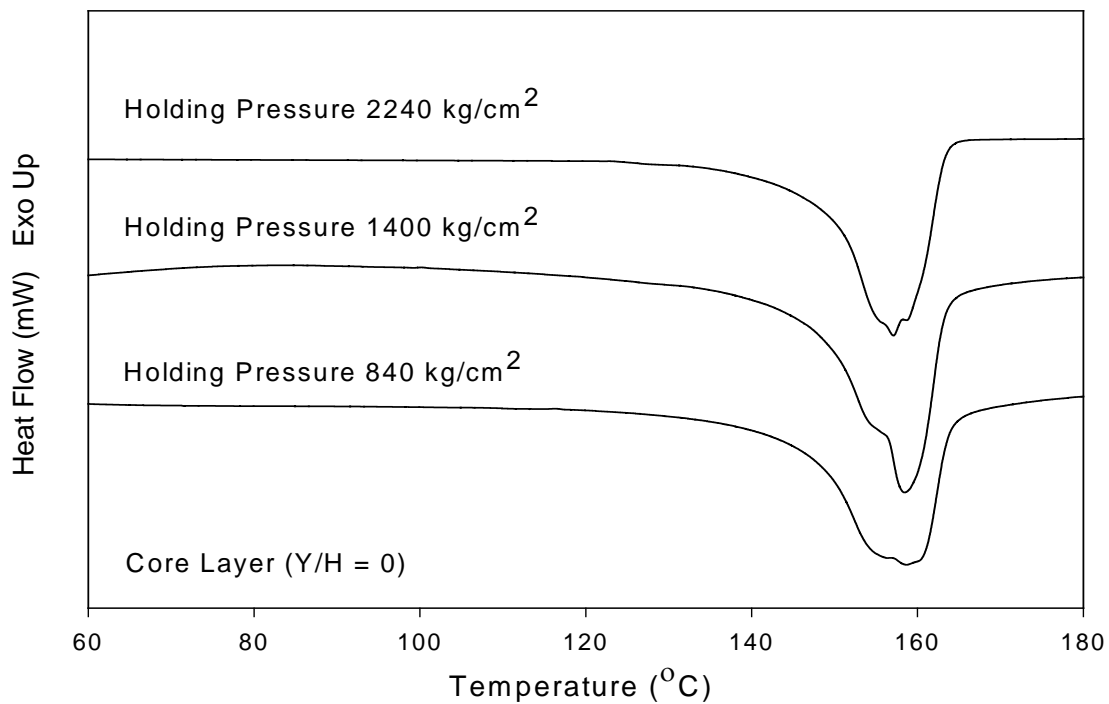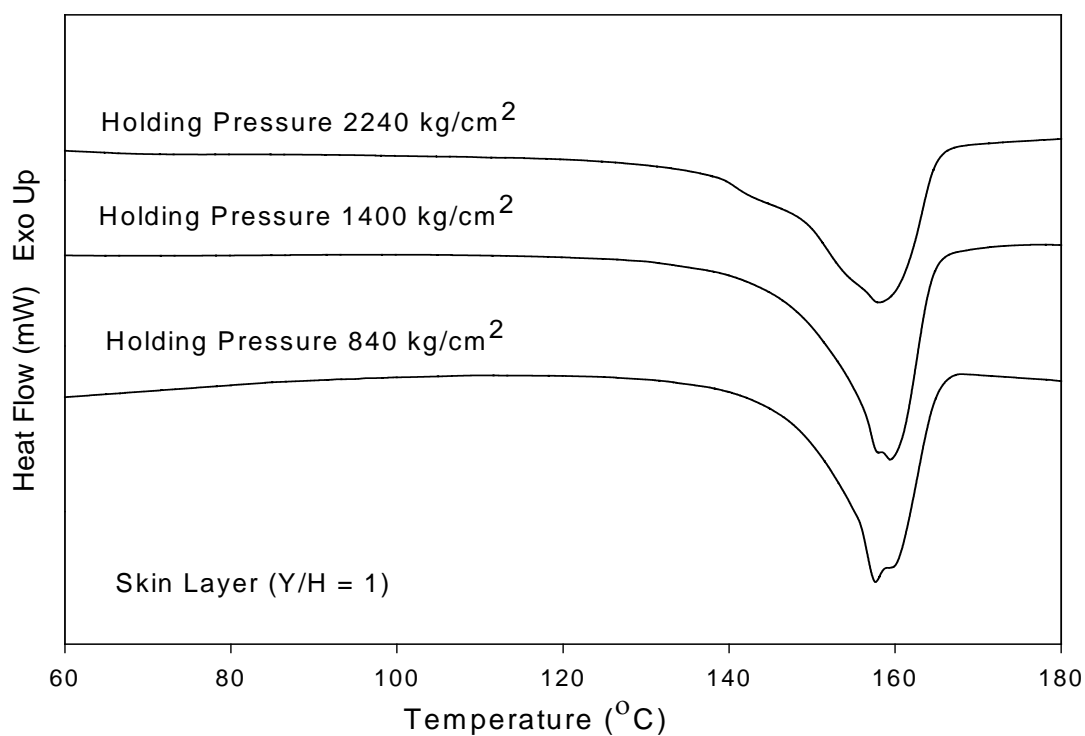
Figure 4.26   DSC curves corresponding to the heating scan of veiver fiber-PP composite at (a) core layer (Y/H = 0) and (b) skin layer at holding pressure of 840, 1,400, and 2,240 kg/cm^2.

(a)

(b)
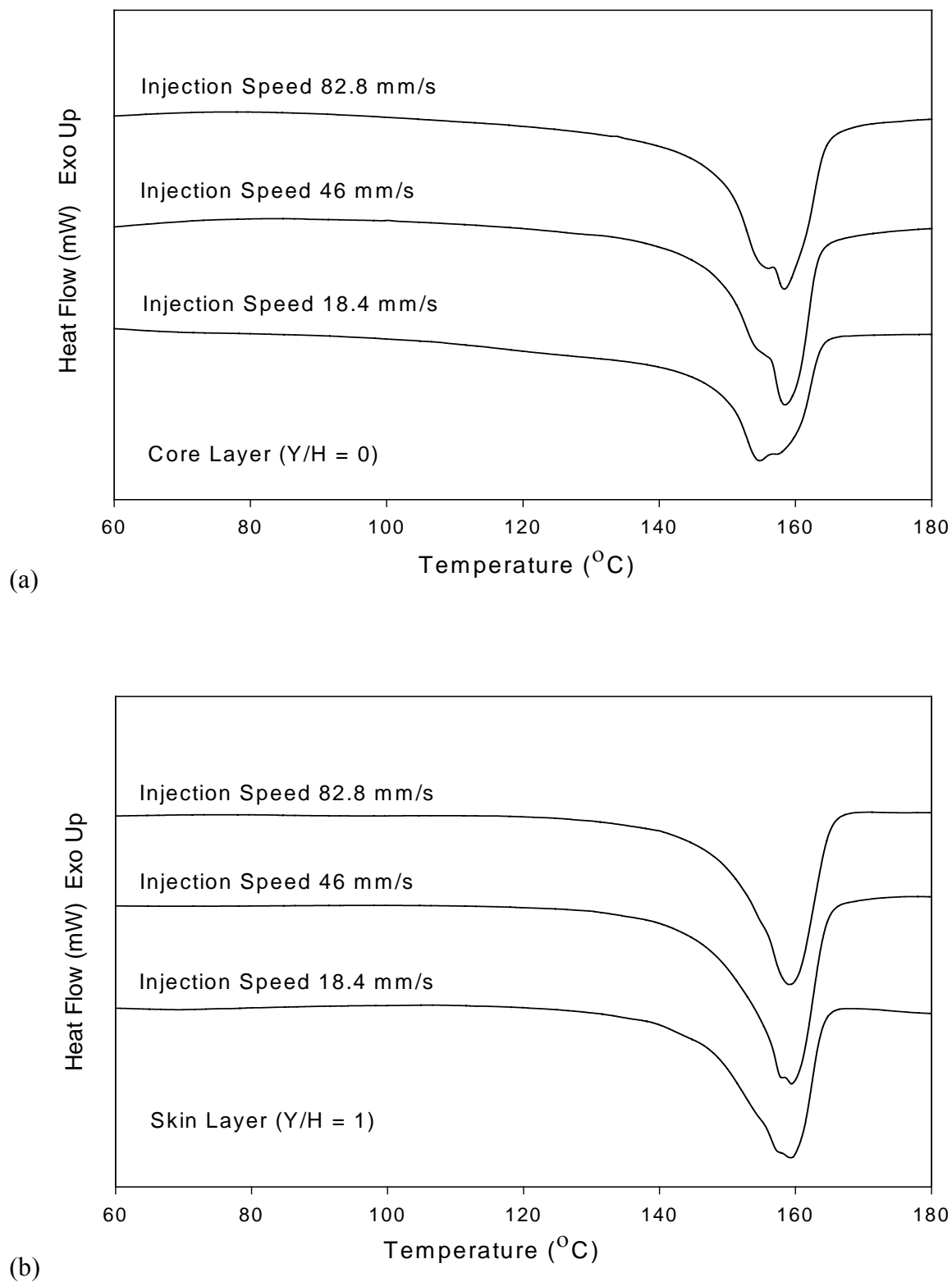
Figure 4.27   DSC curves corresponding to the heating scan of veiver fiber-PP composite

at (a) core layer (Y/H = 0) and (b) skin layer at injection speed of 18.4, 46,

and 82.8 mm/s.
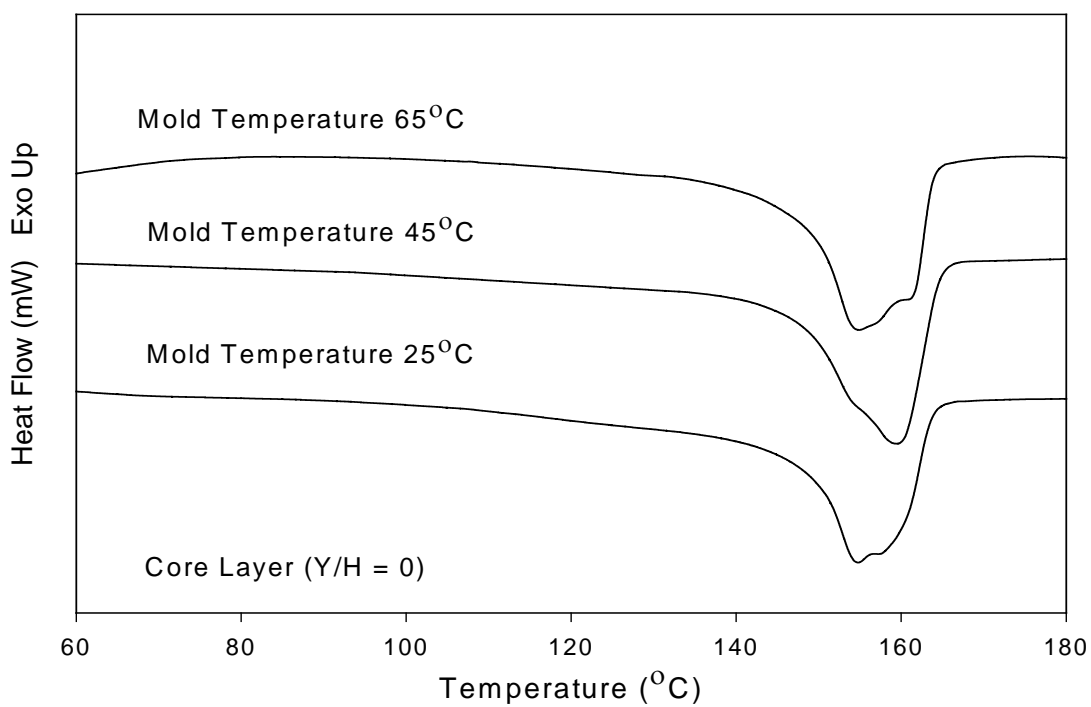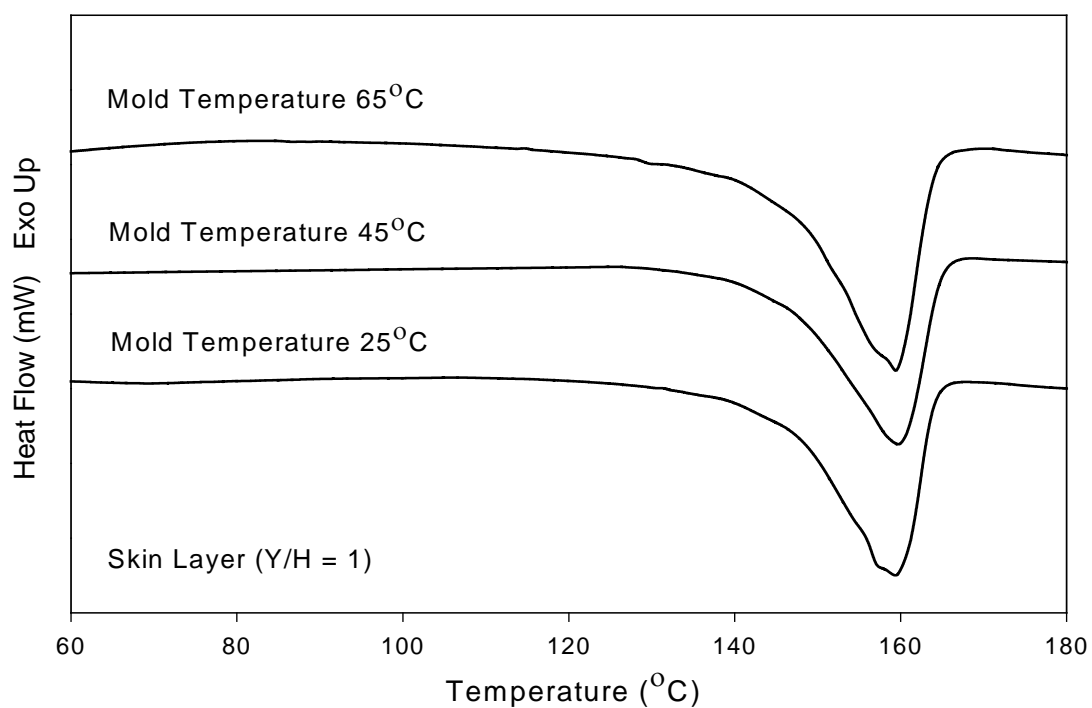
Figure 4.28   DSC curves corresponding to the heating scan of veiver fiber-PP composite

at (a) core layer (Y/H = 0) and (b) skin layer at mold temperature of 25, 45,

and 65°C.

4.5.3 Degree of crystallinity and gapwise crystallinity distribution

Gapwise crystallinity distribution at the midway of moldings of vetiver fiber-PP composites at various screw speeds, holding pressures, injection speeds, and mold temperatures were represented in Figure 4.29(a)-(d), respectively. It was found that screw speeds and holding pressures had no effect on degree of crystallinity of the composites. However, injection speed and mold temperature slightly affected the degree of crystallinity of the composites. The degree of crystallinity slightly increased with increasing injection speeds and mold temperatures. This could be suggested that the melt temperature was possibly increased due to the increasing extent of shear with increasing injection speed. Hence, the polymer molecules exhibited longer relaxation time leading to an increase in degree of crystallinity of the composites. In a case of mold temperature, an increase in mold temperature led to the longer solidification time for polymer. As a result, degree of crystallinity of the composites increased according to an increase in relaxation time of polymer chains. This observation showed a similar result with injection molded PP studied by Li and Cheung (1997). In addition, it was interesting to point out that there was no gapwise crystallinity distribution at the midway of moldings for all specimens. This phenomenon has been observed in the case of PP studied by Isayev et al. (2000).

(a)

(b)
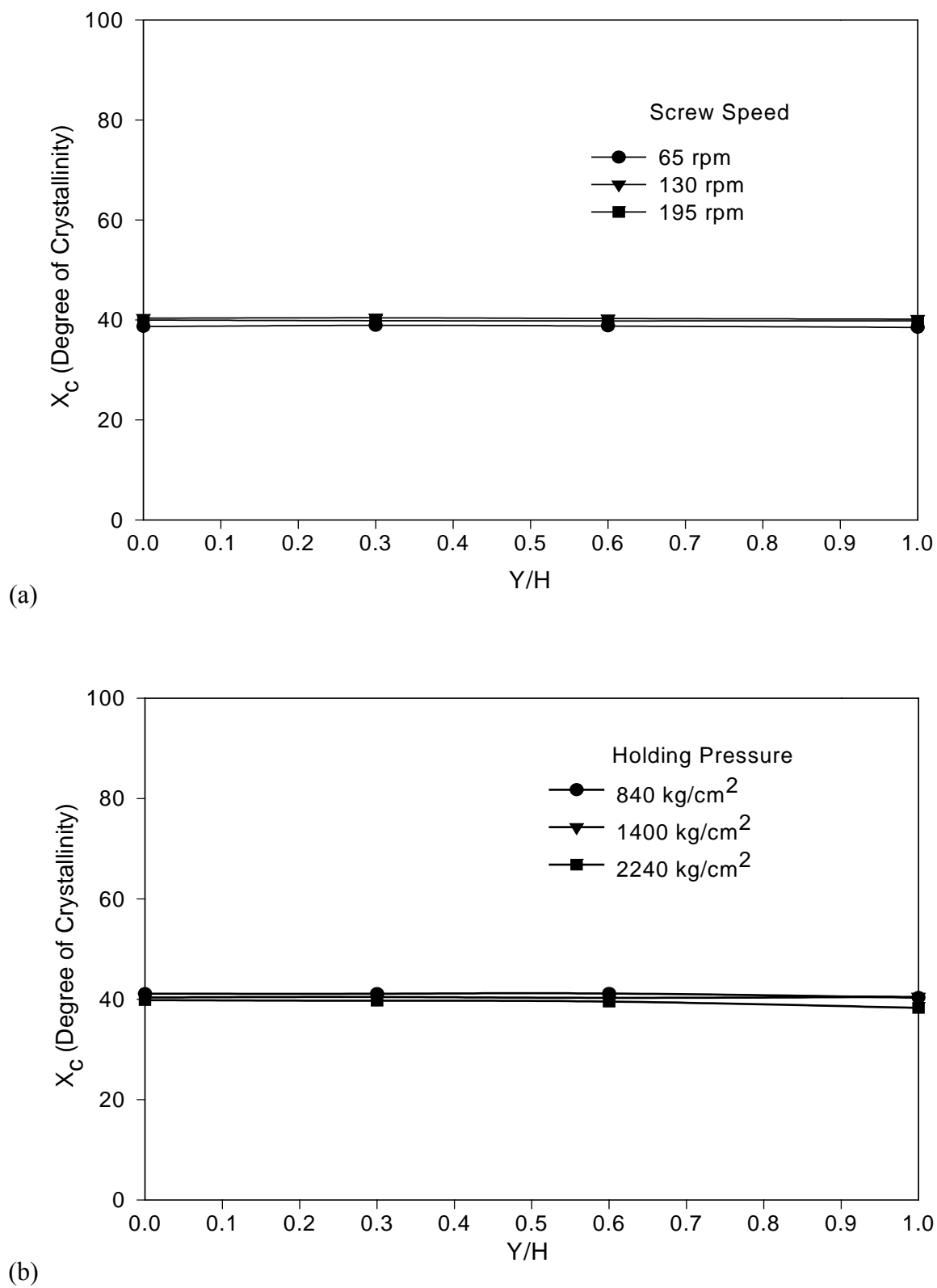
Figure 4.29 Gapwise crystallinity distribution at the midway of moldings of vetiver fiber-PP composites at (a) screw speeds and (b) holding pressures (according to Table 3.1).
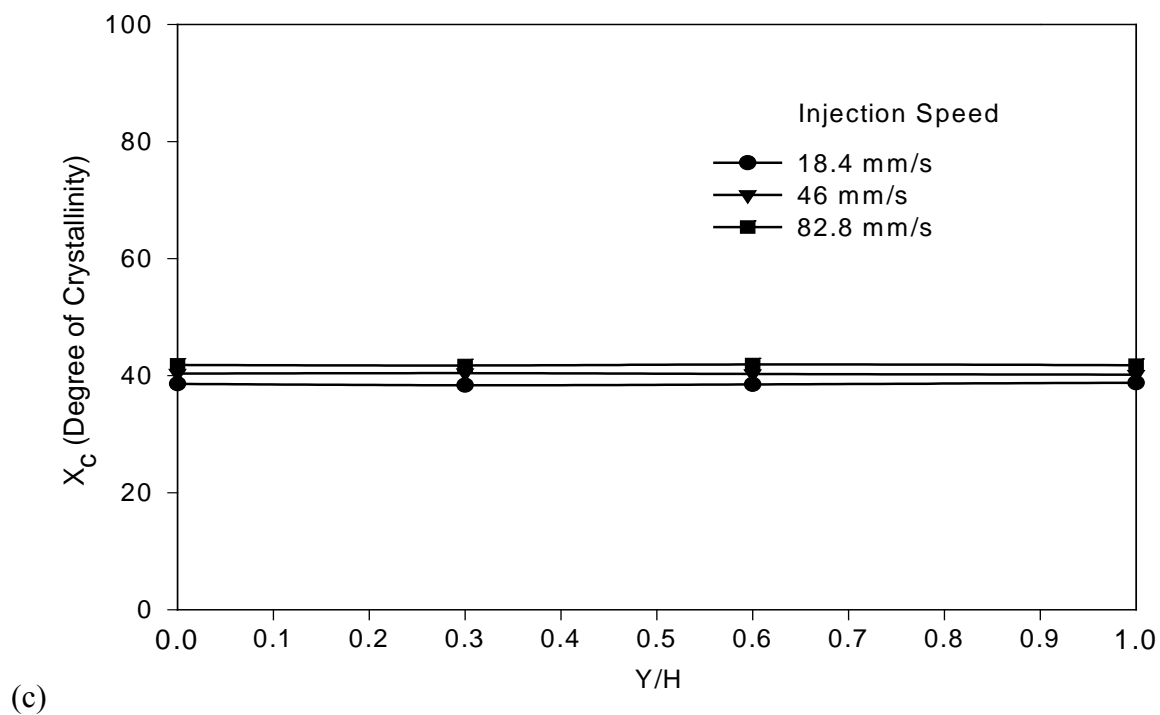
(c)
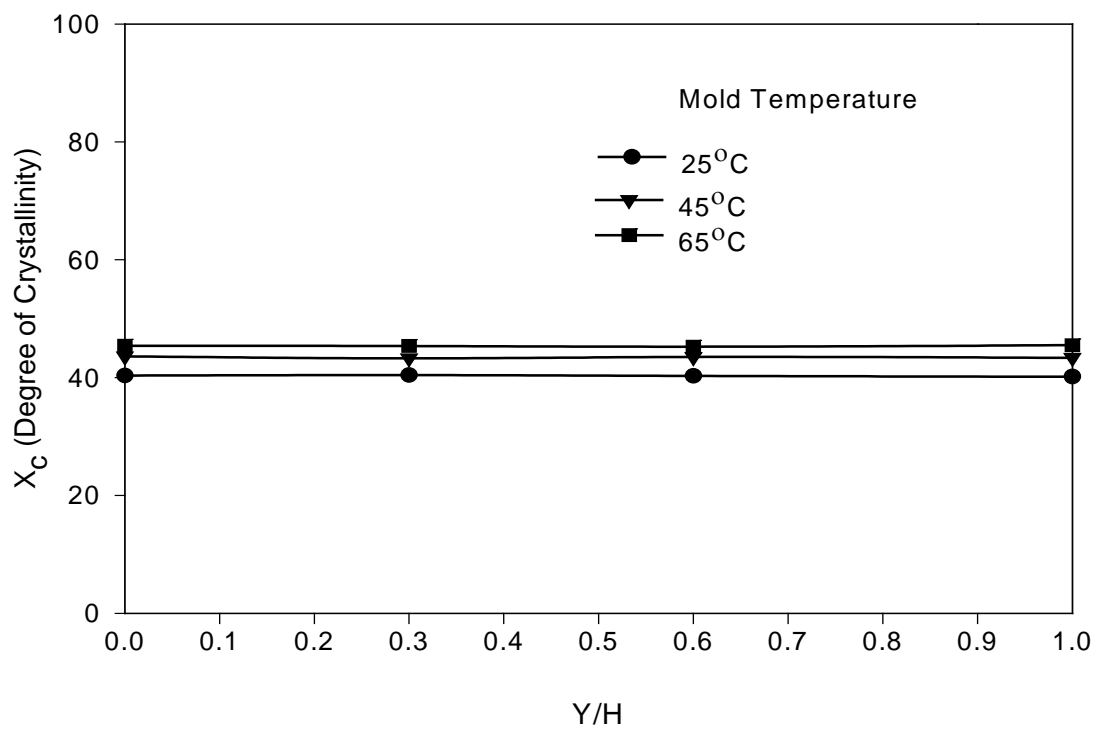
(d)

Figure 4.29 **(Continued)** Gapwise crystallinity distribution at the midway of moldings of vetiver fiber-PP composites at (c) injection speeds and (d) mold temperatures (according to Table 3.1).

4.5.4 Mechanical properties

Mechanical properties of 20% (by weight) vetiver fiber-PP composites prepared at various processing conditions according to Table 3.1 were summarized in Table 4.1. It was found that processing conditions i.e., screw speed, injection speed, holding pressure, and mold temperature showed no significant effect on mechanical properties of vetiver fiber-PP composite. This result is in contrast with other studies on PP homopolymer. In a case of PP, the processing conditions had influences on mechanical properties (Fujiyama, 1995 and Nagaoka et al., 2005). Fujiyama (1995) reported that properties such as flexural modulus, flexural strength, Izod impact strength, heat distortion temperature, and mold shrinkage of injection-molded PP increased as the cylinder temperature decrease. This was because the degree of molecular orientation is higher. Additionally, Nagaoka et al. (2005) found that in injection molding of PP, the strengths of the specimens decreased as the mold temperature increased, particularly in terms of bending properties.

The mechanical properties of the composites could be influenced by many factors such as the matrix intrinsic properties, fiber volume fraction, and interfacial bond strength. Particularly, the interfacial bond strength between fibers and the surrounding matrix is a crucial factor for many mechanical and physical properties of composites. Hence, the interfacial bond strength between vetiver fiber and PP matrix may play an important role on the mechanical properties of PP composites more than the processing conditions.

Table 4.1 Mechanical properties of vetiver fiber-PP composites prepared at various processing conditions according to Table 3.1.

Processing Condition	Impact Strength (kJ/m^2)	Tensile Strength (MPa)	Young's Modulus (GPa)	Elongation at Break (%)
1	18.91 ± 1.25	26.48 ± 0.54	1.43 ± 0.04	8.36 ± 0.57
2	18.58 ± 1.08	26.18 ± 0.65	1.49 ± 0.05	8.71 ± 0.97
3	18.80 ± 1.41	26.73 ± 0.58	1.44 ± 0.08	8.07 ± 0.59
4	18.19 ± 1.08	26.44 ± 0.42	1.42 ± 0.07	8.11 ± 0.41
5	17.65 ± 0.95	26.45 ± 0.42	1.38 ± 0.06	8.48 ± 0.68
6	19.20 ± 0.77	24.59 ± 0.68	1.27 ± 0.04	8.32 ± 0.43
7	21.45 ± 0.97	24.52 ± 0.53	1.16 ± 0.04	7.99 ± 0.56
8	18.80 ± 0.94	26.57 ± 0.60	1.40 ± 0.05	8.13 ± 0.56
9	18.24 ± 0.66	26.85 ± 0.43	1.35 ± 0.06	8.70 ± 0.35

4.6 Quiescent crystallization of natural fiber-PP composites

4.6.1 Equilibrium melting temperatures

The equilibrium melting temperature ($T_m°$) of neat PP, vetiver fiber-PP, rossells-PP, and sisal-PP composites with 20% (by weight) fiber content was 179.03°C, 168.42°C, 171.83°C, and 175.34°C respectively (Figure 4.30). The addition of natural fibers to the PP caused a decrease in $T_m°$. This may be because the presence of natural fibers in the composite led to the formation of unstable as well as less perfect spherulites. It was observed that vetiver fiber-PP composite exhibited lower $T_m°$ than rossells-PP, and sisal-PP composites. López-Manchado et al. (1999) also have found that the addition of

synthetic fibers to PP resulted in a decrease of $T_m°$. Additionally, Arroyo et al. (1997) has reported that adding more than 10% of glass fiber into PP composites resulted in decreasing $T_m°$ of the composites.
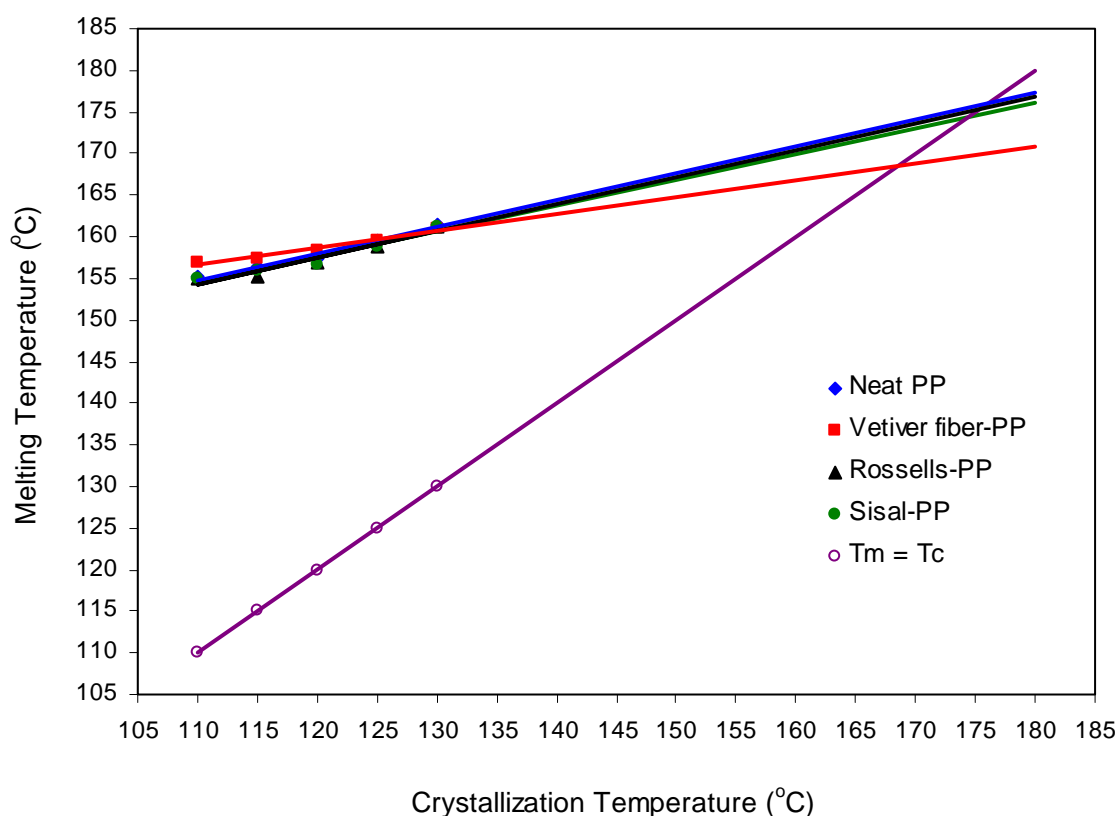
Figure 4.30 Hoffman-Weeks plots of neat PP and natural fibers-PP composites with 20% (by weight) fiber content.

4.6.2 Isothermal crystallization kinetics

DSC thermograms at various crystallization temperatures for neat PP, vetiver fiber-PP, sisal-PP and rossells-PP composites with 20% (by weight) fiber content were shown in Figure 4.31-4.34, respectively. Plot of relative crystallinity at various crystallization temperatures of neat PP, vetiver fiber-PP, rossells-PP, and sisal-PP composites were also presented in Figure 4.35-4.38, respectively. Half time of

crystallization, obtained from the time by which the relative degree of crystallization reached the value of 0.5, was shown in Figure 4.39. The half time of crystallization increased when the crystallization temperature increased. It can be seen that the composites showed a noticeable decrease in the half time of crystallization compared to that of neat PP. This may be attributed to the nucleating effect of the natural fibers on PP crystallization. For the natural fiber-PP composites, rossells-PP composite gave the lowest half time of crystallization.
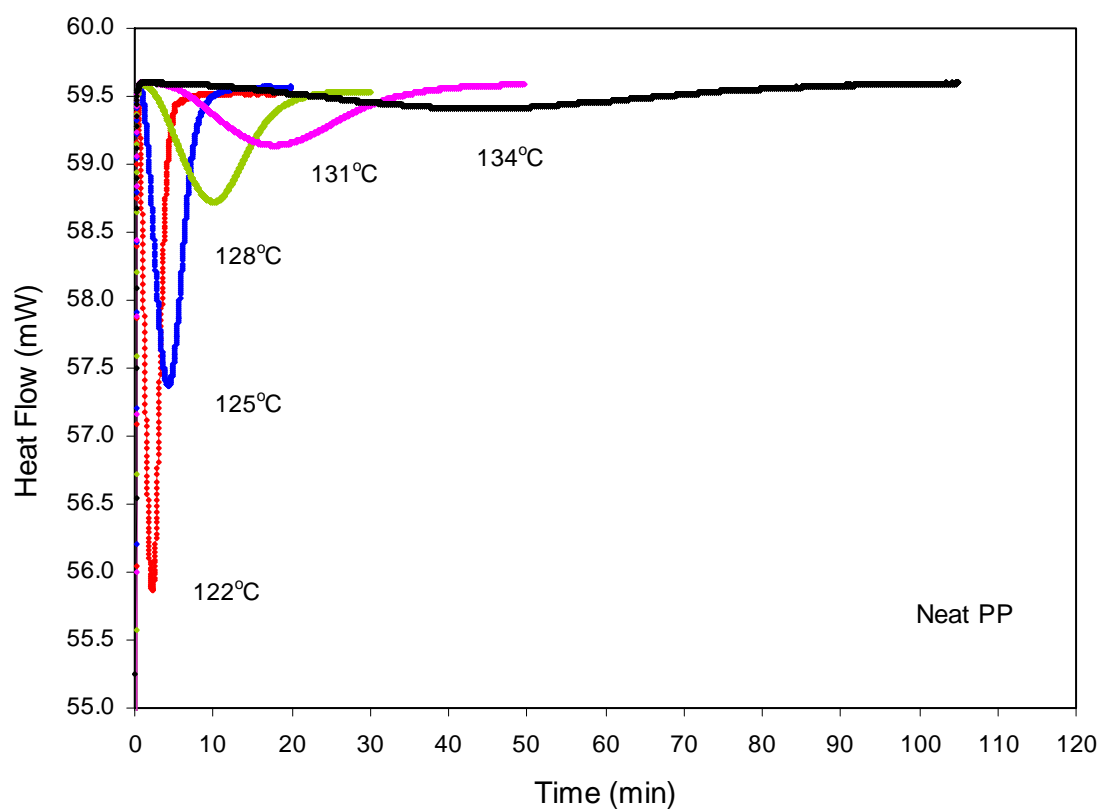
Figure 4.31　DSC thermograms of neat PP at various crystallization temperatures.
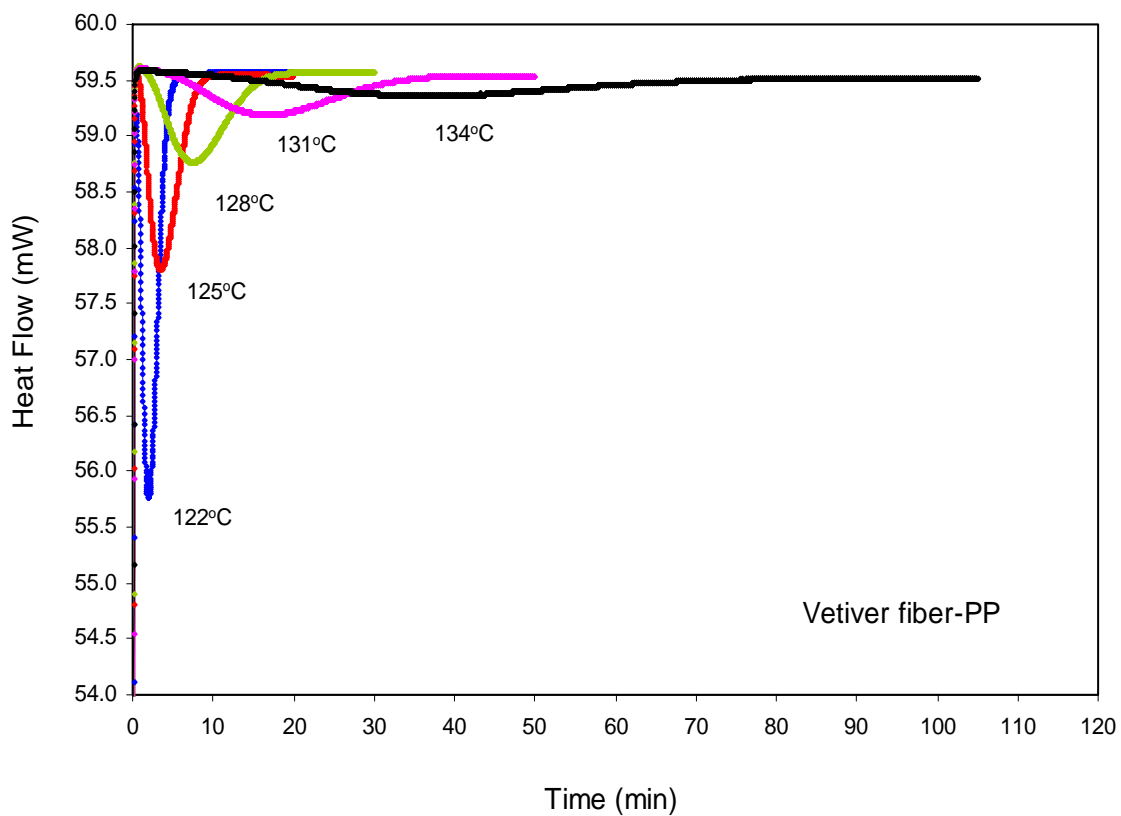
Figure 4.32   DSC thermograms of vetiver fiber-PP composite with 20% (by weight) fiber

content at various crystallization temperatures.
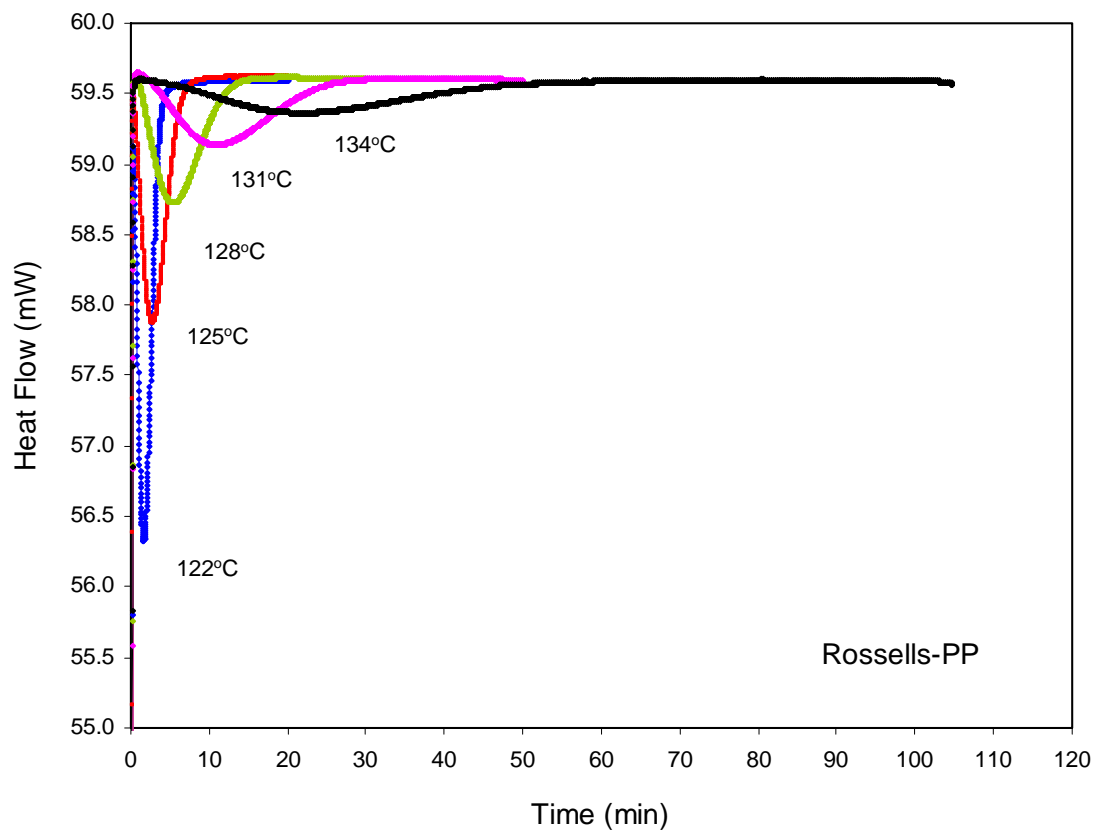
Figure 4.33   DSC thermograms of rossells-PP composite with 20% (by weight) fiber

content at various crystallization temperatures.
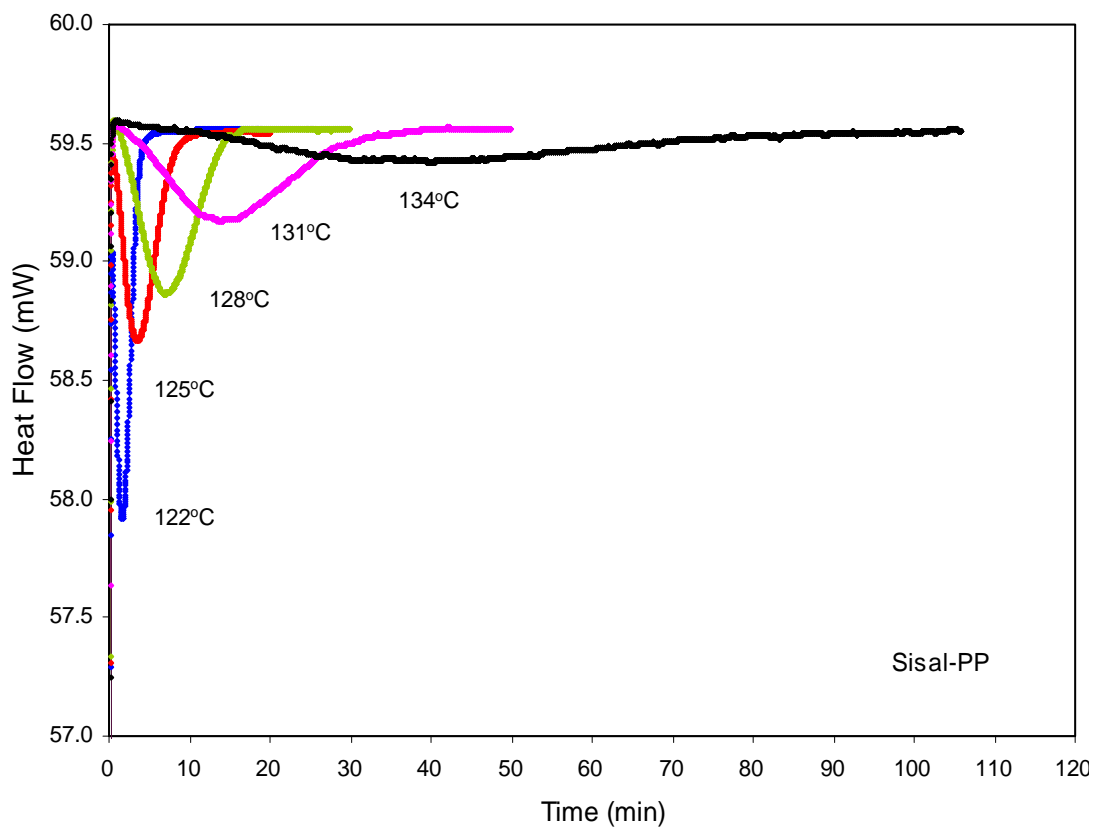
Figure 4.34   DSC thermograms of sisal-PP composite with 20% (by weight) fiber content

at various crystallization temperatures.
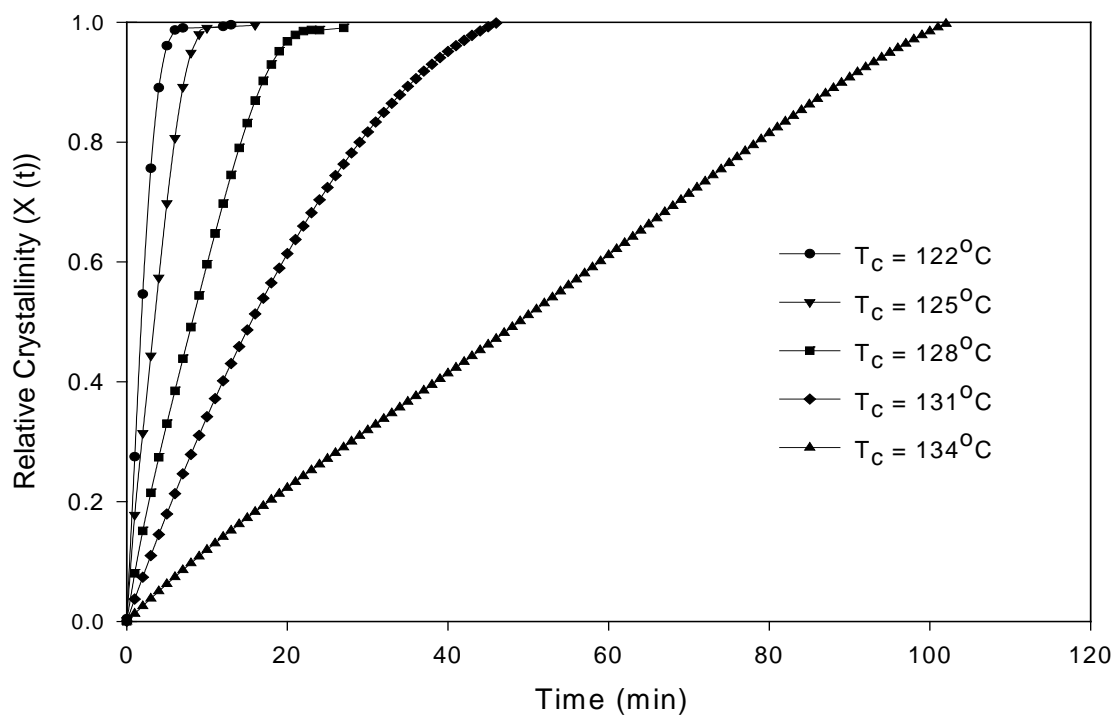
Figure 4.35   Plot of relative crystallinity (X(t)) of neat PP as a function of time at various

crystallization temperatures.
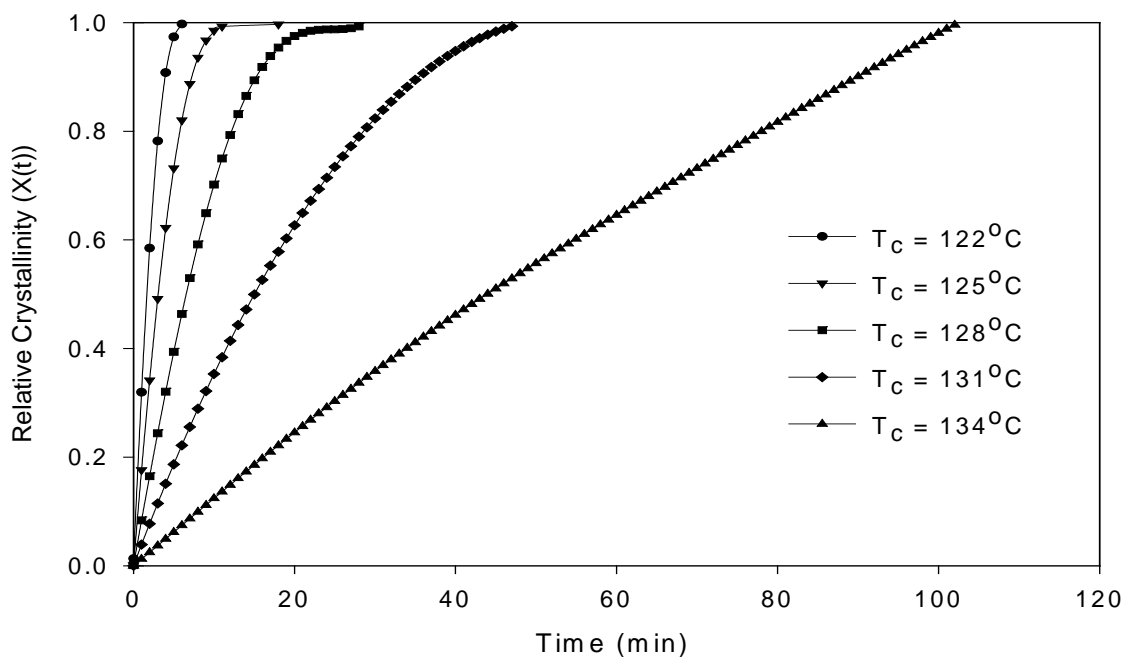
Figure 4.36   Plot of relative crystallinity (X(t)) of 20% (by weight) vetiver fiber-PP

composite as a function of time at various crystallization temperatures.
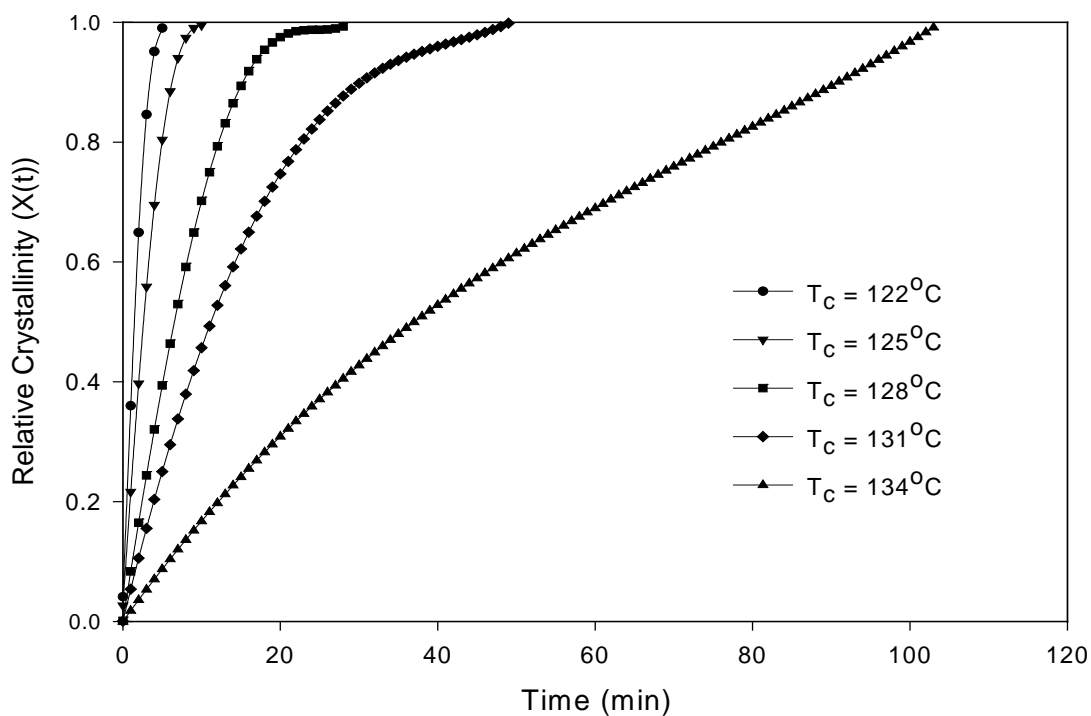
Figure 4.37   Plot of relative crystallinity (X(t)) of 20% (by weight) rossells-PP composite as a function of time at various crystallization temperatures.
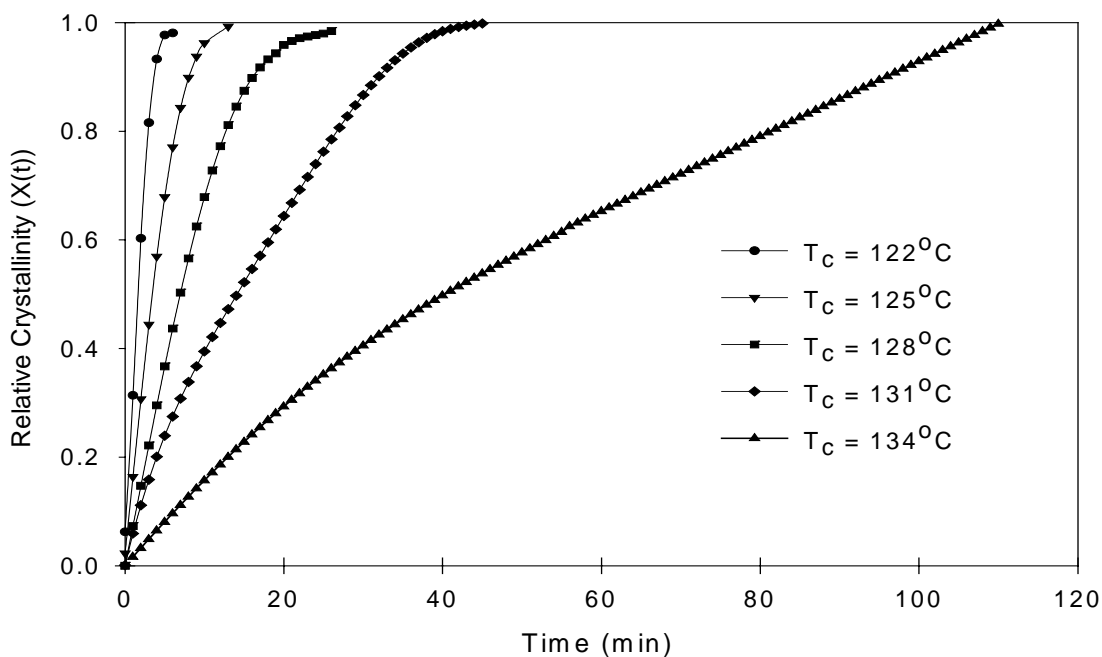
Figure 4.38   Plot of relative crystallinity (X(t)) of 20% (by weight) sisal-PP composite as a function of time at various crystallization temperatures.
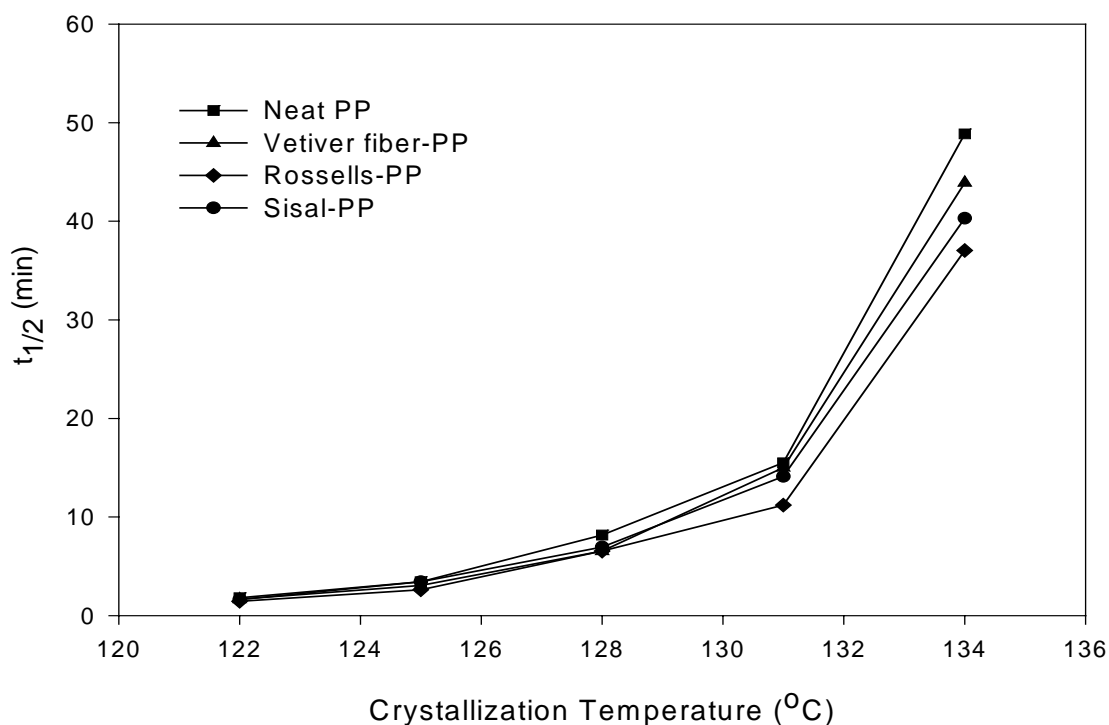
Figure 4.39 Plot of half time of crystallization ($t_{1/2}$) as a function of crystallization temperature for neat PP and natural fiber-PP composites.

In addition, the relative crystallinity shown in Figures 4.35-4.38 was used to determine Avrami exponent using Avrami equation (Equation (3.5)). The plots of Avrami exponent of neat PP, vetiver fiber-PP, rossells-PP, and sisal-PP composites were illustrated in Figure 4.40. The Avrami exponent (n) of neat PP was in a range of 1.57 to 2.66. The natural fiber-PP composites had lower n values than neat PP. When the natural fibers were used in the PP composites, sisal-PP composite exhibited the highest n values ranging from 1.33 to 1.50. Whereas vetiver fiber-PP and rossells-PP composites showed n values in the same ranges, 1.21 to 1.32. In this study, it was observed that all Avrami exponents were non-integer values. The difference of n values may be attributed to the secondary crystallization process, complex nucleation modes and the change in the material density. Moreover, a study of cellulose-thermoplastic composites by Quillin et al. (1994) showed that the presence of a transcrystalline layer (TCL) changes the n exponent obtained from

the Avrami analysis. In their study, the change in n value related to the change in shape of crystallites because of changes in nuclei concentration with the inclusion of cellulose fiber. For the heterogeneous nucleation case, the shape lies between a diffusion-controlled sphere (n = 3.0) and a truncated sphere (n = 1.5) (Harper and Wolcott, 2004). The addition of natural fibers tended to push the crystallites towards the truncated shaped. This shift was likely resulted from the increased nucleation sites on the fiber surface, but not from a change in the crystal growth. The increased nuclei concentration caused the impinging nuclei to be truncated rather than to be complete spherulitic forms
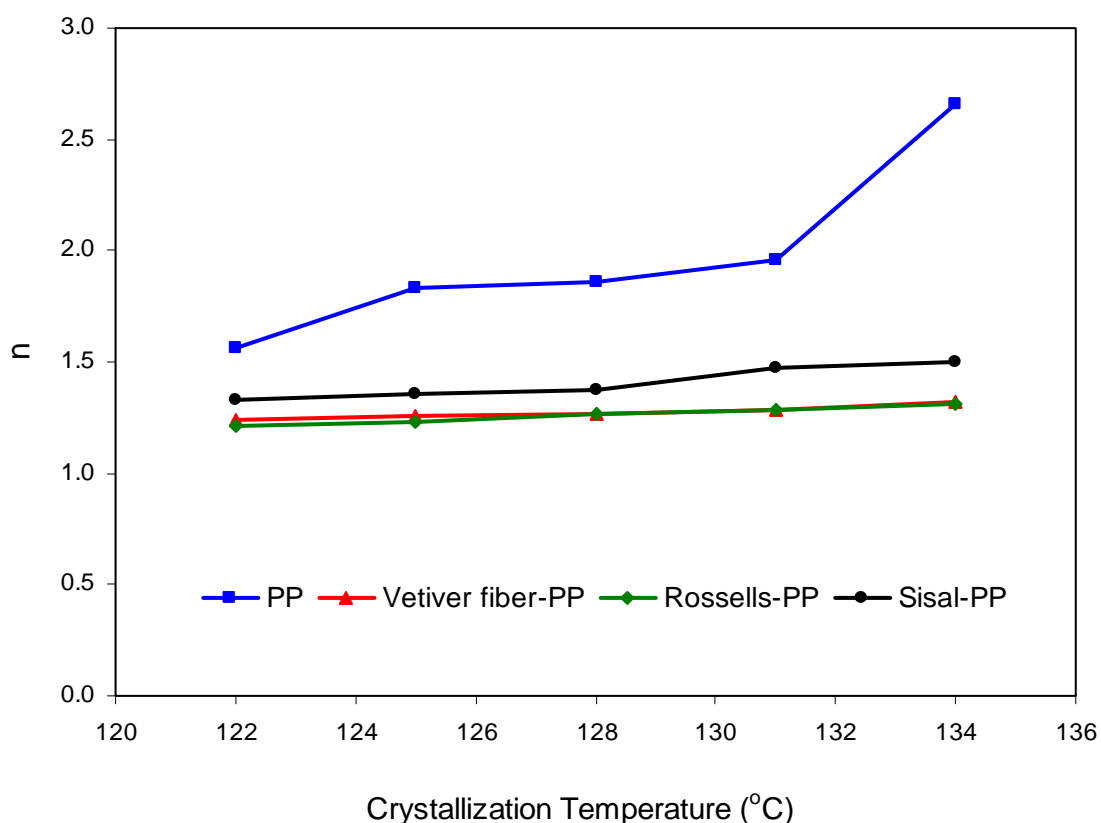
Figure 4.40 Plot of Avrami exponent (n) as a function of crystallization temperature for neat PP and natural fiber-PP composites.

The half time of crystallization in Figure 4.39 was used to calculate the isothermal rate constant according to Equation (3.6). Also, the relative crystallinity in Figure 4.35-4.38 was used to determine crystallization rate constant from Avrami equation referred to Equation (3.5). The isothermal rate constant from half time of crystallization and from Avrami plot as a function of crystallization temperature were shown in Figure 4.41. It was observed that the isothermal crystallization rate constant of the samples decreased when the crystallization temperature increased. Additionally, the rate constants of the composites obtained from both Avrami plot and half time of crystallization were higher than those of neat PP. The Avrami exponent, rate constant by Avarami plot, half time of crystallization, and rate constant by half time of crystallization of neat PP and natural fiber-PP composites at various crystallization temperatures were summarized in Table 4.2. For natural fiber-PP composites, rossells-PP composite showed the highest rate constant. This result was in good agreement with the lowest half time of crystallization of rossells-PP composite as shown in Table 4.2. López-Manchado et al. (1999) have also observed that the addition of synthetic fibers to PP resulted in the higher rate of crystallization. They have reported that both unmodified and modified synthetic fibers led to the rise in rate of crystallization due to the nucleating effect of fibers on the PP crystallization.
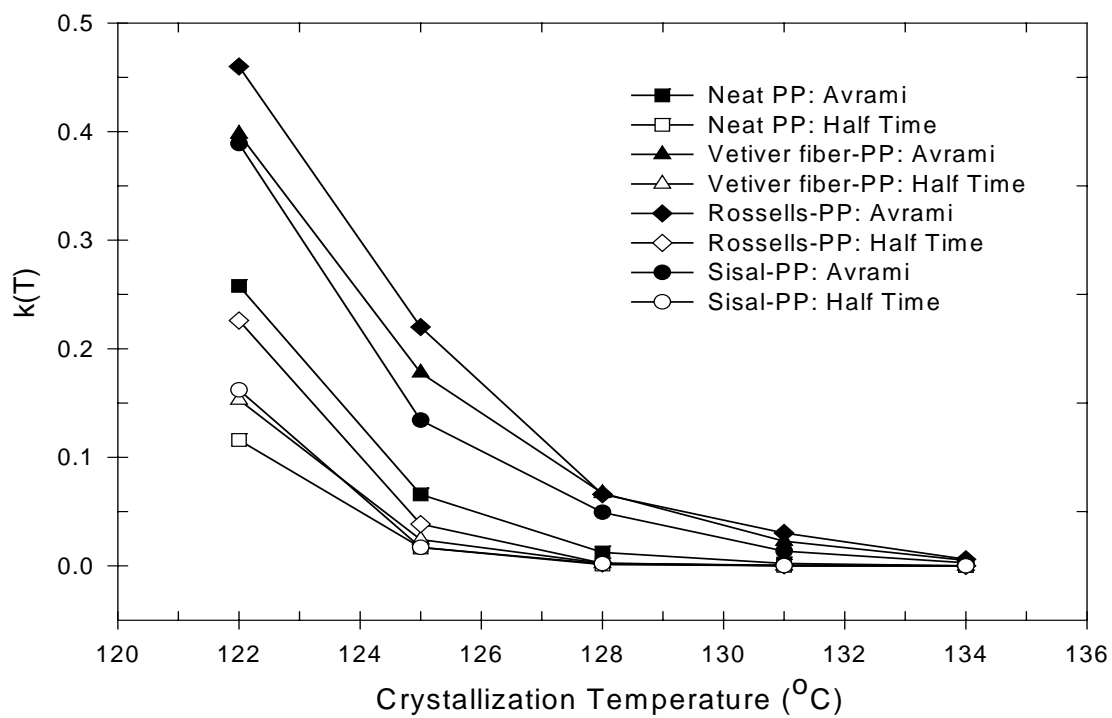
Figure 4.41   Plot of isothermal rate constant, k(T) obtained from half time of crystallization and Avrami plot as a function of crystallization temperature for neat PP and natural fiber-PP composites.

Table 4.2 Summary on Avrami exponent (n), rate constant by Avrami plot (k), half time of crystallization ($t_{1/2}$), and rate constant by half time of crystallization (k) of neat PP and natural fiber-PP composites at various crystallization temperatures.

Samples	T_c (°C)	Avrami Exponent (n)	Rate Constant by Avrami Plot (k)	$t_{1/2}$ (min)	Rate Constant by Half Time of Crystallization (k)
Neat PP	122	1.57	2.58×10^{-1}	1.817	1.16×10^{-1}
	125	1.83	6.59×10^{-2}	3.432	1.17×10^{-2}
	128	1.86	1.25×10^{-2}	8.162	1.27×10^{-3}
	131	1.96	2.30×10^{-3}	15.506	1.86×10^{-4}
	134	2.66	1.65×10^{-5}	48.870	5.94×10^{-6}
Vetiver fiber-PP	122	1.24	3.98×10^{-1}	1.654	1.53×10^{-1}
	125	1.26	1.78×10^{-1}	3.061	2.42×10^{-2}
	128	1.27	6.70×10^{-2}	6.541	2.48×10^{-3}
	131	1.28	2.28×10^{-2}	15.016	2.05×10^{-4}
	134	1.32	5.10×10^{-3}	43.920	8.18×10^{-6}
Rossells-PP	122	1.21	4.60×10^{-1}	1.452	2.26×10^{-1}
	125	1.23	2.20×10^{-1}	2.620	3.85×10^{-2}
	128	1.27	6.61×10^{-2}	6.541	2.48×10^{-3}
	131	1.28	3.04×10^{-2}	11.200	4.93×10^{-4}
	134	1.31	6.17×10^{-3}	37.040	1.36×10^{-5}
Sisal-PP	122	1.33	3.89×10^{-1}	1.625	1.62×10^{-1}
	125	1.36	1.34×10^{-1}	3.433	1.71×10^{-2}
	128	1.38	4.94×10^{-2}	6.952	2.06×10^{-3}
	131	1.47	1.38×10^{-2}	14.115	2.46×10^{-4}
	134	1.50	2.89×10^{-3}	40.290	1.06×10^{-5}

4.6.3 The overall rate of non-isothermal crystallization

In order to compare the rate constants obtained from the Avrami plot and half time of crystallization, the isothermal rate constants were converted to non-isothermal rate constants by Equation (3.8). The non-isothermal rate constant derived from both methods were presented in Figure 4.42. The result from the plots showed that the non-isothermal rate constant obtained from Avrami plots and half time of crystallization was not significantly different. Therefore, assuming an Avrami exponent of 3.0 and calculating the isothermal rate constant by Equation (3.5) seems to be valid for neat PP and natural fiber-PP composites.

The non-isothermal rate constant from half time of crystallization obtained from Figure 4.42 was then fitted to Equation (3.9) to obtain the non-isothermal rate constant in a wide range of crystallization temperatures of neat PP and natural fiber-PP composites as illustrated in Figure 4.44. The fitting parameters for non-isothermal rate constants (K_k, and $(1/t_{1/2})_o$ according to Equation (3.9) were obtained from Figure 4.43 and summarized in Table 4.3, respectively. The non-isothermal rate constant in the wide range of crystallization temperature would be combined with the growth rate in order to determine the number of effective nuclei which would be discussed in next section.
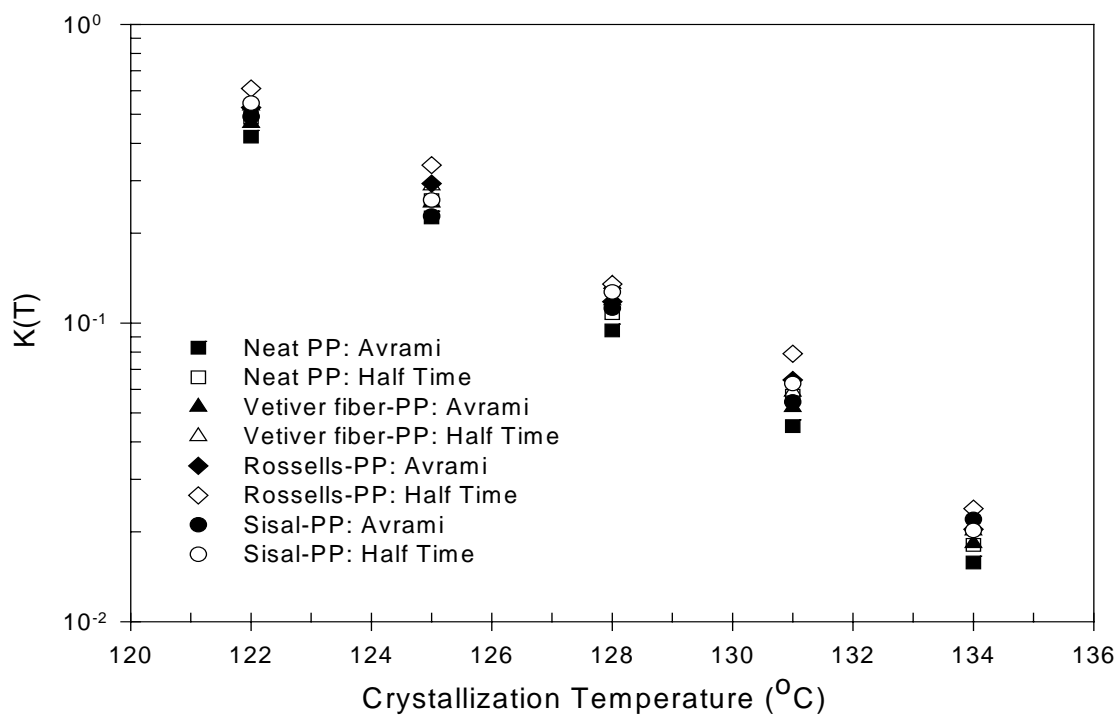
Figure 4.42 Plot of non-isothermal rate constant, K(T) obtained from half time crystallization and Avrami plot as a function of crystallization temperature for neat PP and natural fiber-PP composites.
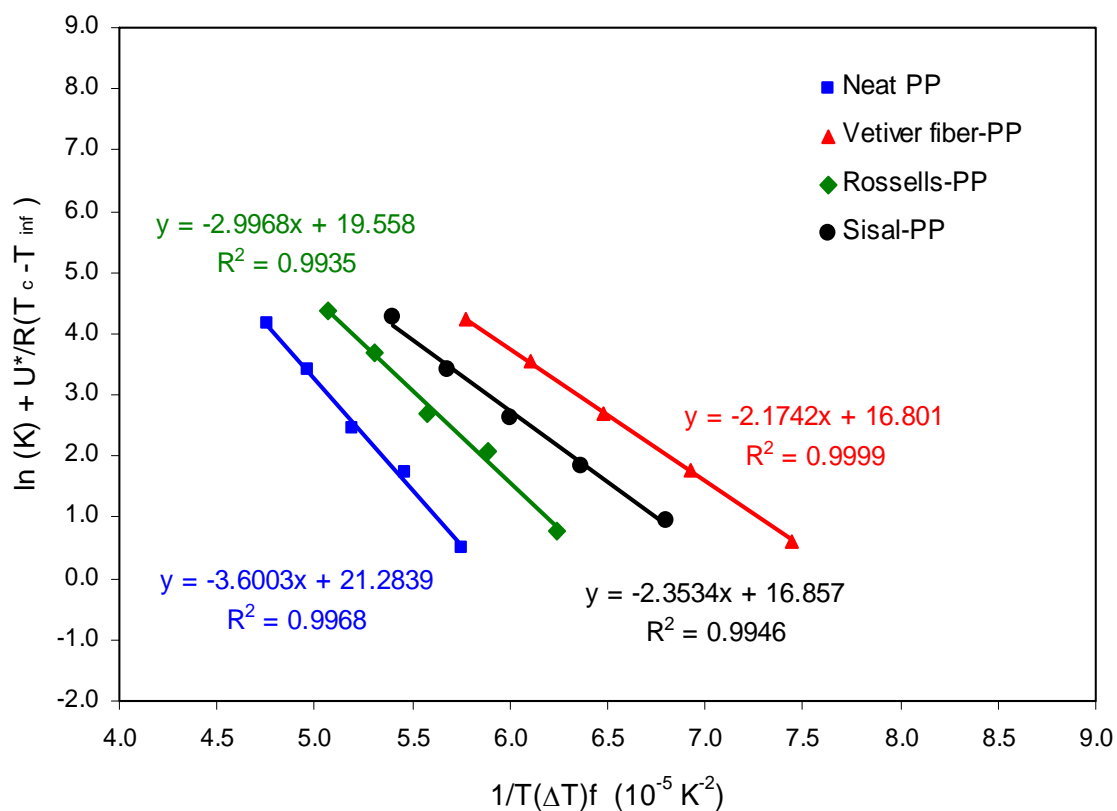
Figure 4.43   Hoffman-Lauritzen plots for determining $(1/t_{1/2})_o$ and K_k of neat PP and natural fiber-PP composites.

Table 4.3   Hoffman-Lauritzen fitted parameters for non-isothermal rate constants.

Sample	K_k (K^2)	$\left(\dfrac{1}{t_{1/2}}\right)_o$
Neat PP	3.60×10^5	1.98×10^9
Vetiver fiber-PP	2.17×10^5	2.24×10^7
Rossells-PP	3.00×10^5	3.52×10^8
Sisal-PP	2.35×10^5	2.37×10^7
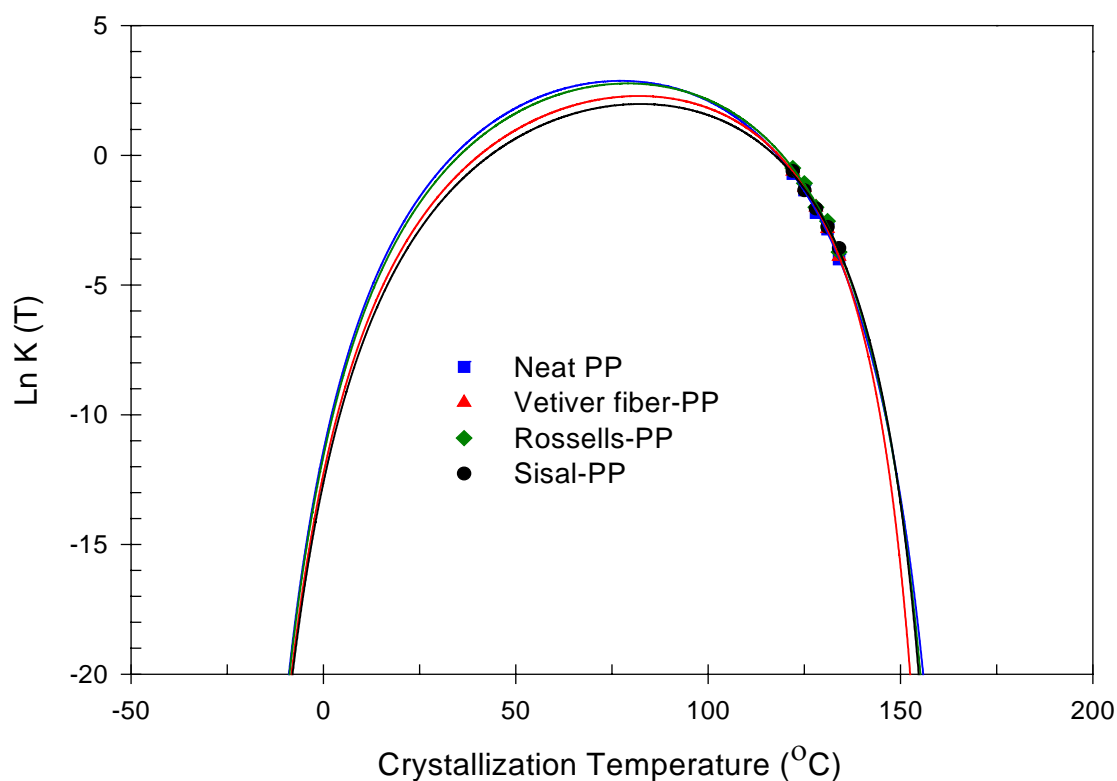
Figure 4.44 Plot of non-isothermal crystallization rate constants of neat PP and natural fiber-PP composites as a function of crystallization temperature. Symbols represent experimental data while lines indicate the fitting data to Hoffman-Lauritzen expression, Equation (3.9).

4.6.4 Spherulitic growth rate and number of effective nuclei

Examples of optical micrographs of crystallized PP in the bulk and on vetiver fiber taken during a crystallization process at T_c = 131°C were shown in Figure 4.45 and Figure 4.46, respectively. Spherulitic growth rate of PP in the bulk was determined by measuring diameter of spherulites against time as the crystallization isothermally proceeded. Growth rate of transcrystallization (TC) on the fiber surface was evaluated by measuring a width of the TC region perpendicularly proceeded to the fiber surface as a function of time. From the spherulitic growth rate study, it was observed that embedding natural fiber into the polymer melt, the fibers might act as nucleating sites for

the spherulitic growth as well. As a result, the growing spherulites would be restricted in the lateral direction so that a columnar layer, known as transcrystalline region, was developed on the fiber surface as seen in Figure 4.46. The TC is possible if the energetic conditions of nucleation are more favorable on the fiber surface than in the bulk of the melt (Varga, 1995). The growth of TC perpendicularly proceeded to the fiber until the growing front impinged with other spherulites nucleated in the bulk. The mechanism of TC was not fully understood and there was no rule for predicting the appearance of TC in a particular fiber-matrix system. Besides, its effect on the mechanical properties of the composites and on interfacial properties remained controversial (Quan et al., 2005). The ability of cellulose-based fibers such as wood, flax, and sisal, to induce transcrystallization in PP composites has been reported (Zafeiropoulos et al., 2001, Harper and Wolcott, 2004, Joseph et al., 2003, Arbelaiz et al., 2006, and Amash and Zugenmaier, 2000).

| t = 10 s | t = 30 s | t = 50 s |

| t = 70 s | t = 90 s | t = 110 s |
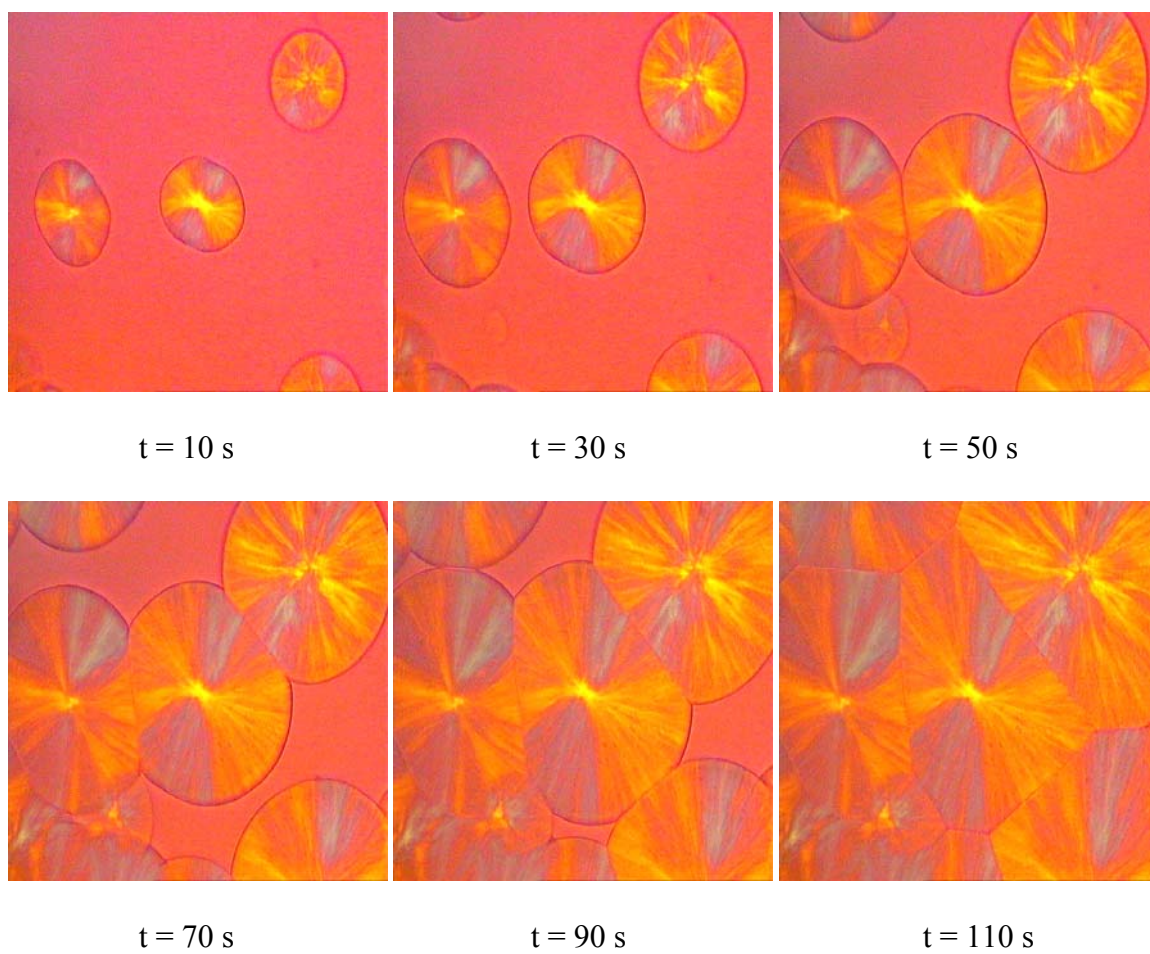
Figure 4.45 Optical micrographs of PP crystallized in the bulk of neat PP taken during the crystallization process at $T_c = 131°C$.

| t = 10 s | t = 30 s | t = 50 s |

| t = 70 s | t = 90 s | t = 110 s |
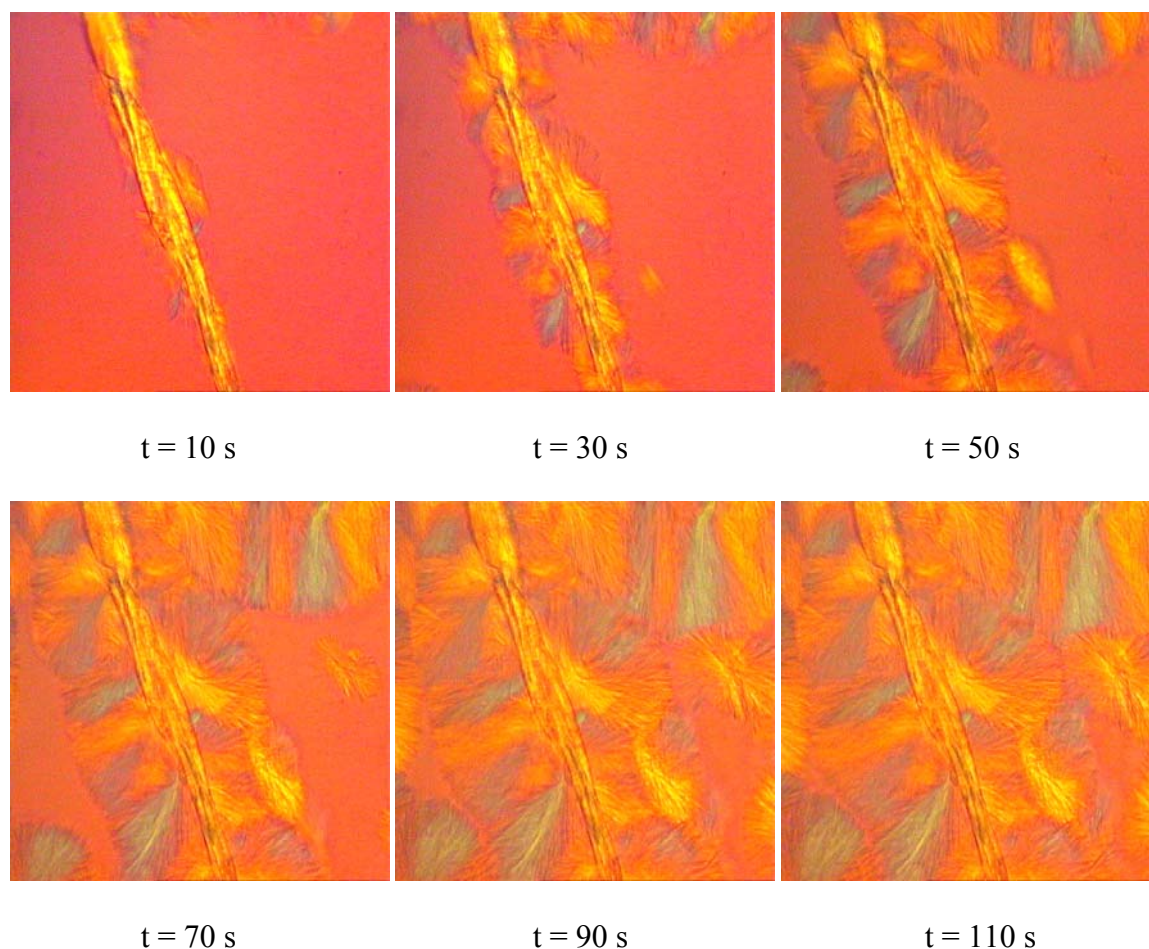
Figure 4.46 Optical micrographs of transcrystallization of PP on vetiver fiber taken during the crystallization process at $T_c = 131°C$.

The experimental data of spherulitic growth rate of PP in the bulk and on the fiber were represented as filled and unfilled symbols in Figure 4.47. In a case of the bulk, it was found that the growth rate of neat PP was noticeably higher than those of natural fiber-PP composites. This may be due to the restriction of the natural fiber on crystallization process. The crystallized PP in the bulk of vetiver fiber-PP, rossells-PP, and sisal-PP composites were not much different. In addition, it was observed that the growth rate of crystallized PP in the bulk of PP and the PP composites were greater than that of crystallized PP in a transcrystalline region. For natural fiber-PP composites, rossells-PP composite had the highest growth rate in the TC region. This implied that the fiber

topography of rossells fiber was more favorable for the nucleation of TC than that of vetiver fiber and sisal fibers. In addition, TC strongly depended on thermodynamic condition such as crystallization temperature or cooling rate due to its nucleation-controlled process.

The fitting parameters for the spherulitic growth rate, K_g and G_o, in the bulk and in TC region were elucidated from Figures 4.48-4.49 and then listed in Tables 4.4 and 4.5, respectively. From Tables 4.4 and 4.5, it was found that both K_g of natural fiber-PP composites in the bulk and on fiber surfaces were lower than that of neat PP in the bulk. It is well known that a foreign surface frequently reduces the nucleus size needed for crystal growth. This is because the creation of the interface between polymer crystal and substrate may be less hindered than the creation of the corresponding free polymer crystal surface. A heterogeneous nucleation path makes use of a foreign pre-existing surface to reduce the free energy opposing primary nucleation (Papageorgiou et al., 2005). Additionally, it revealed that the G_o of natural fiber-PP composites were lower than that of neat PP. According to a study by Wang et al. (2003), it has been observed that the incorporation of the $BaSO_4$ into PP caused a decrease of free volume available for PP chains to move, which certainly resulted in a decrease in G_o. Moreover, the interfacial modification improved the adsorption effects of macromolecular chains on particle surface, which resulted in an addition barrier for the motion of the macromolecules. This situation is quite similar to the polymer matrix with very high molecular weight leading to very high entanglement density. Therefore, a decrease in G_o with improved interfacial adhesion is possibly due to retardant mechanism similar to the molecular weight dependence of G_o.
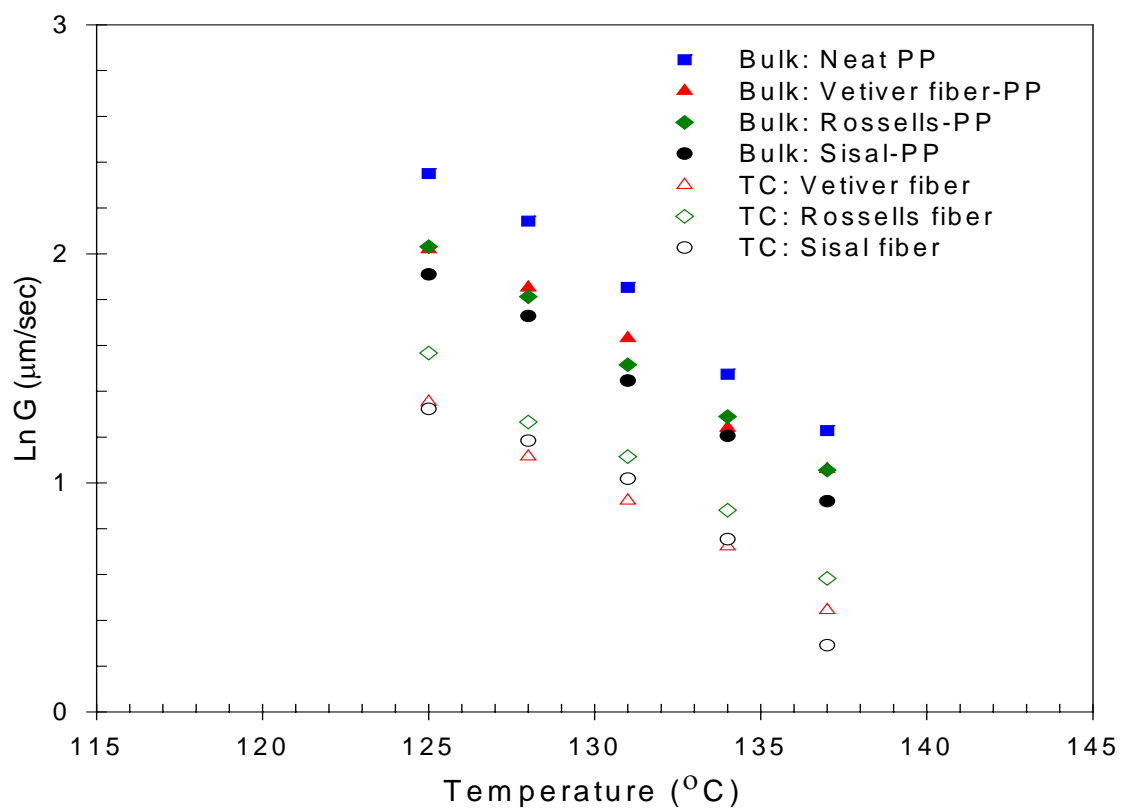
Figure 4.47 Plot of experimental growth rates of crystallization of PP in the bulk and transcrystallization of PP on natural fibers as a function of crystallization temperature.
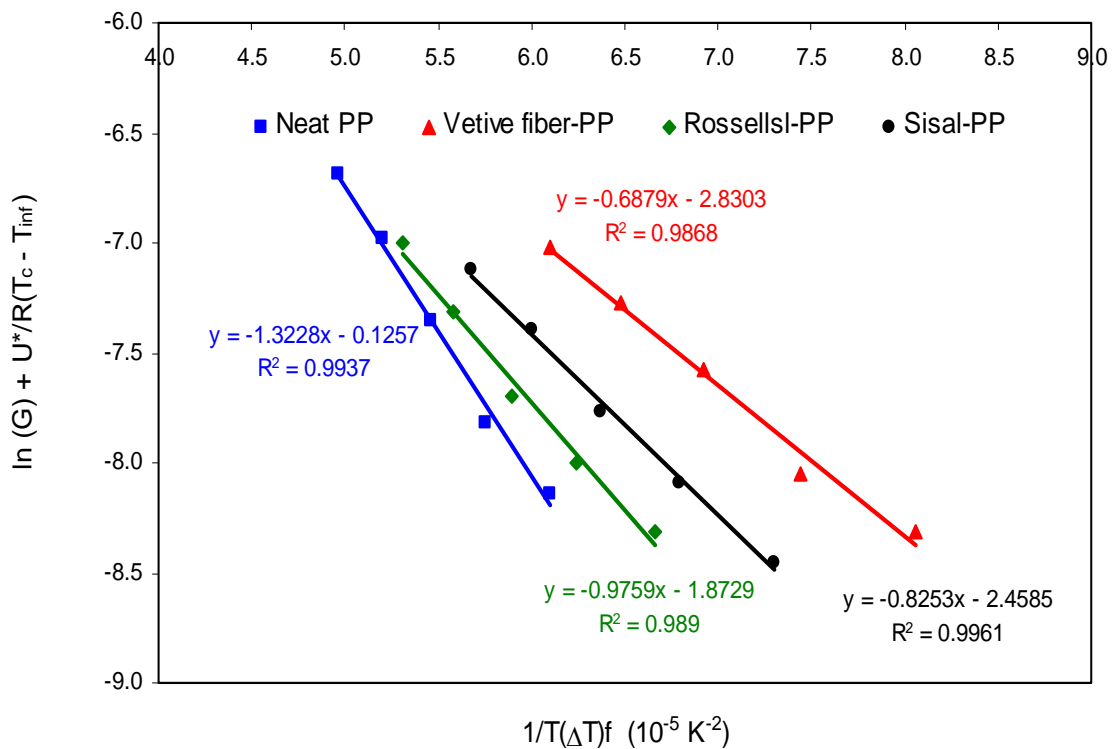
Figure 4.48   Plot of Hoffman-Lauritzen plots for determining G_o and K_g of neat PP and bulk PP of natural fiber-PP composites.
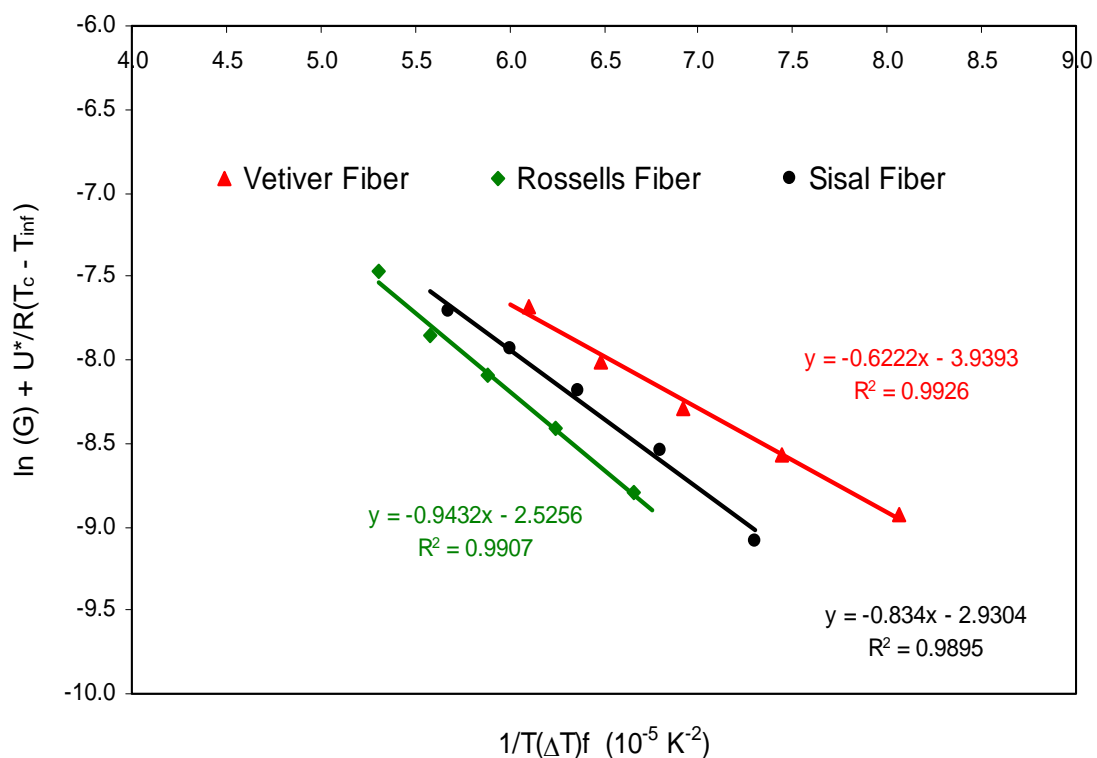
Figure 4.49 Plot of Hoffman-Lauritzen plots for determining G_o and K_g of transcrystallization of PP on natural fibers in natural fiber-PP composite.

Table 4.4 Nucleation constant (K_g) and pre-exponent factor (G_o) of neat PP and natural fiber-PP composites in the bulk region.

Sample	K_g (K^2)	G_o (m/s)
Neat PP	1.32×10^5	8.82×10^{-1}
Vetiver fiber-PP	6.88×10^4	5.90×10^{-2}
Rossells-PP	9.76×10^4	1.54×10^{-1}
Sisal-PP	8.25×10^4	8.56×10^{-2}

Table 4.5 Nucleation constant (K_g) and pre-exponent factor (G_o) of natural fiber-PP composites in TC region.

Sample	K_g (K^2)	G_o (m/s)
Vetiver fiber-PP	6.22×10^4	1.95×10^{-2}
Rossells-PP	9.43×10^4	8.00×10^{-2}
Sisal-PP	8.34×10^4	5.43×10^{-2}

The experimental spherulitic growth rates of PP and PP composites at various T_c were then fitted to Equation (3.10) as shown in Figure 4.50. It can be verified in this study that the Equation (3.10) used for determining the spherulitic growth rate in the bulk could also be applied to the growth rate in TC region. From Figure 4.50, it was found that growth rates of both neat PP and natural fiber-PP composites were represented by a bell-shaped curve as a function of temperature. The spherulitic growth rates were zero at the glass transition temperature, T_g (the molecular movements of polymer were too slow to allow crystallization). Also, at the equilibrium melting temperature, growth rates were zero. In this study, it can be seen that the maximum growth rate of neat PP was approximately at 100°C. The spherulitic growth rates combined with the non-isothermal rate constants, determined by Equations (3.9) and (3.10), respectively, were used to estimate the number of effective nuclei as a function of temperature. Figure 4.51 displayed the change of the number of effective nuclei (N) as a function of crystallization temperature for neat PP and natural fiber-PP composites according to Equation (3.15). Typically, the number of effective nuclei decreased with increasing T_c. It was seen that the number of effective nuclei of natural fiber-PP composites was higher than that of neat PP. Moreover, rossells-PP composite showed the highest number of effective nuclei. This result gave good

corresponding to the highest growth rate in the TC region of rossells-PP composite as discussed earlier.

Basically, the rate of crystallization depends on both nucleation rate and growth rate. In this study, it was found that the crystallization growth rate of the composites were lower than that of neat PP. However, the higher rate of crystallization of the composites was observed in all samples of natural fiber-PP composites. This implied that the nucleation rate dominated the growth rate of crystallized PP in the natural fiber-PP composites. Furthermore, it appeared that the number of effective nuclei of natural fiber-PP composites was higher than that of neat PP. This suggested that natural fibers may act as nucleating agents in the composites. Wang and Hwang (1996) showed that fiber topography, chemical compositions of the surface, and surface energy influenced the nucleation on the fiber surface.

However, it was worth to mention that the number of effective nuclei strongly depended on the fitting parameters of rate constant equation (according to Table 4.2) and growth rate equation (according to Table 4.3). Due to the fact that, the low crystallization temperatures or very rapid cooling rates can not be achieved in the DSC and the spherulitic growth rate experiments; therefore, the fitting of number of effective nuclei at the low temperature range may not be accurate. At the low temperature range, some errors might be introduced in the prediction of number of effective nuclei.
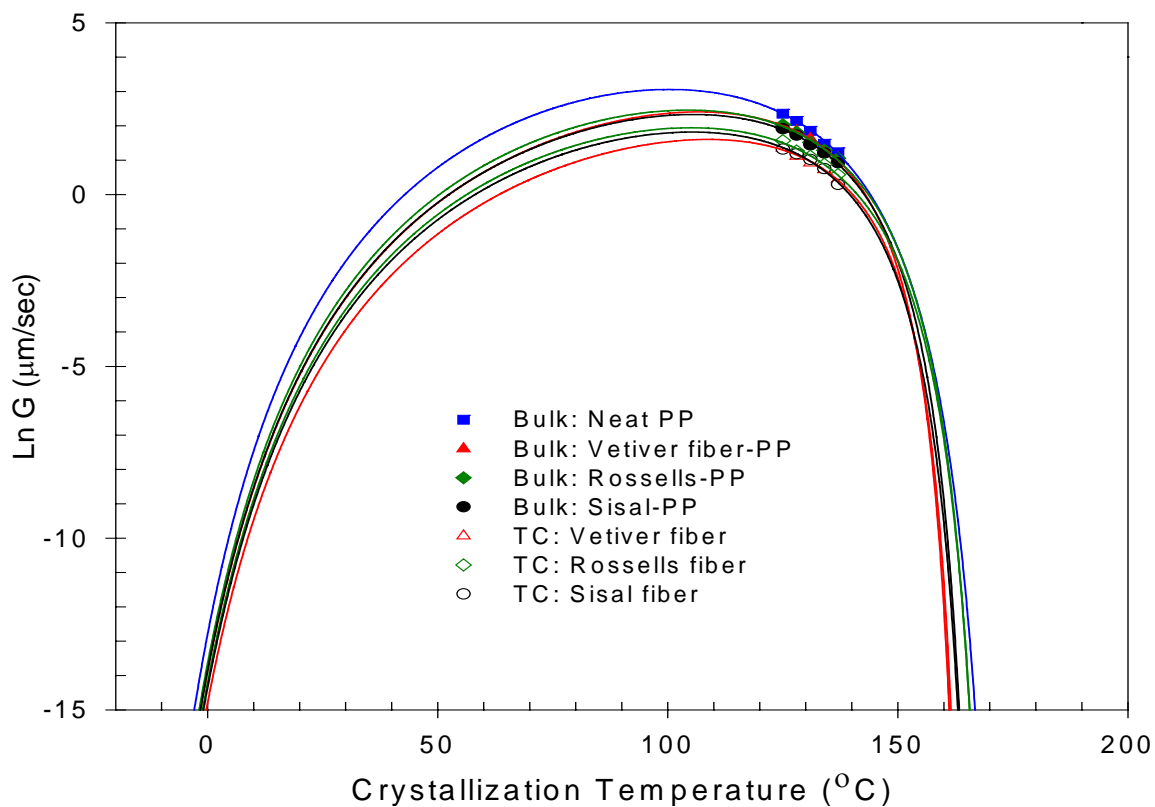
Figure 4.50   Plot of growth rates of PP crystallized in the bulk and transcrystallization of PP on natural fibers as a function of crystallization temperature. Filled symbols represent experimental data obtained in the bulk, and unfilled symbols indicate experimental data obtained on the fiber (TC). Lines refer to fitting data to the Hoffman-Lauritzen growth equation, Equation (3.10).
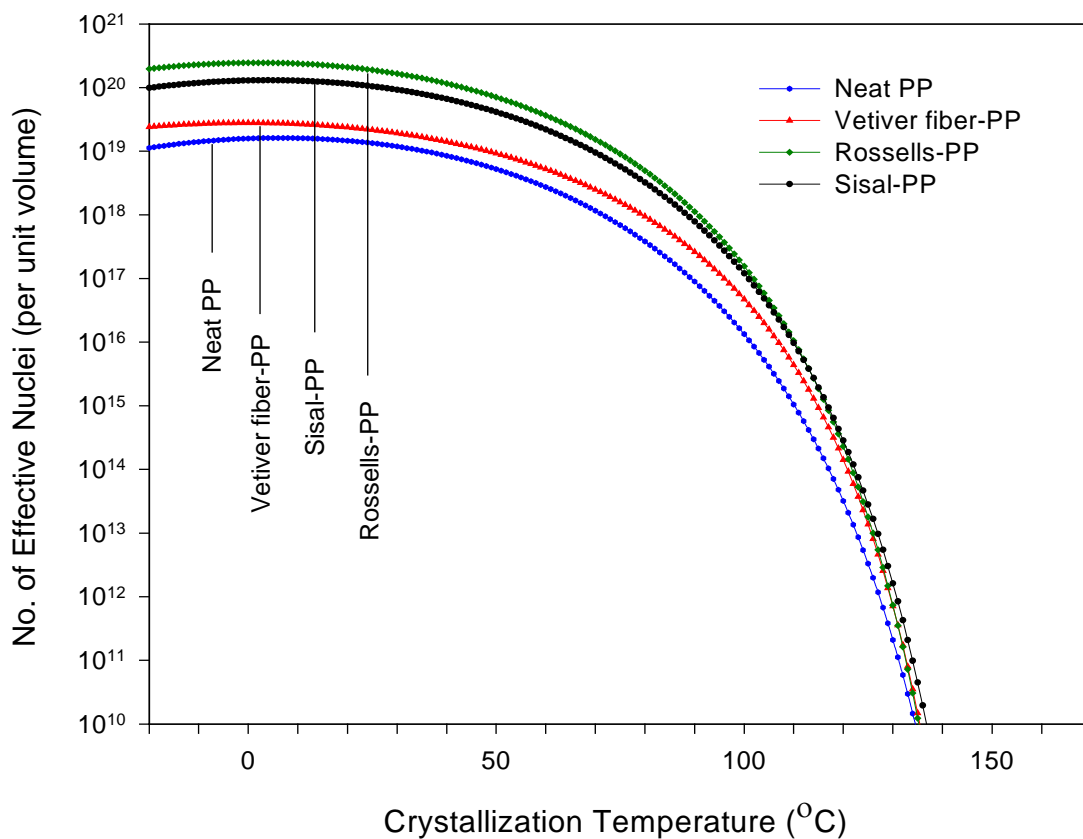
Figure 4.51 Plot of number of effective nuclei as a function of crystallization temperature for neat PP and natural fiber-PP composites, calculated according to Equation (3.15).

CHAPTER V

CONCLUSIONS

Alkali-treated vetiver grass exhibited higher thermal stability than that of untreated vetiver grass. DRIFT spectra and SEM micrographs of the alkali-treated vetiver grass revealed that low molecular weight substances in vetiver grass were removed after the alkalization. In addition, SEM morphology of alkali-treated vetiver grass revealed fibrils with a rough surface topology. The microstructure of injection molded vetiver fiber-PP composites showed a distinct skin layer due to shear-induced crystallization. It was shown that rheology, mechanical properties, and normalized thickness of shear-induced crystallization layer were affected by size and contents of vetiver grass. Vetiver fiber-PP composites had higher viscosity, tensile strength, and Young's modulus than those of vetiver powder-PP composites. On the contrary, vetiver fiber-PP composites exhibited lower normalized thickness of shear-induced crystallization layer than vetiver powder-PP composites. Moreover, with increasing vetiver content in PP composites, the viscosity, tensile strength, and Young's modulus were increased. It was also found that an increase in vetiver content led to a decrease in normalized thickness of shear-induced crystallization layer.

Furthermore, the effect of different types of natural fibers on shear-induced crystallization layer, rheological, thermal, and mechanical properties were also studied. It was revealed that the addition of natural fibers into the PP matrix did not significantly affect the decomposition temperature of α-cellulose (around 365°C) and neat PP (around 460°C). The viscosity of vetiver fiber-PP composite was higher than that of rossells-PP, and sisal-PP composites. Rossells-PP composite had higher Young's modulus and impact

strength than PP composites from vetiver fiber and sisal. However, the normalized thickness of shear-induced crystallization layer of vetiver fiber-PP, rossells-PP, and sisal-PP composites showed insignificant differences. In cases of the effect of processing conditions on PP composites, it was observed that injection speeds and mold temperatures affected the normalized thickness of shear-induced crystallization layer and degree of crystallinity of PP composites. However, processing conditions showed insignificant effect on the mechanical properties of vetiver fiber-PP composites. Additionally, it was found that the degree of crystallinity showed no distribution across the gapwise direction of the PP composites preparing at various processing conditions

In addition, the effect of natural fibers on quiescent crystallization of PP composites was examined. A decrease in equilibrium melting temperature (T_m^o), half time of crystallization, and an increase in the rate of crystallization were observed in the PP composites compared to those of neat PP. For natural fiber-PP composites, vetiver fiber-PP composite had the lowest T_m^o. Spherulitic growth rates of crystallized PP in bulk and growth rate of transcrystallization on the natural fibers were investigated under a polarized light optical microscope. Spherulitic growth rates of the composites were lower than that of neat PP. It was noticed that rossells-PP composite had the highest growth rate of transcrystallization. The shperulitic growth rates combined with the crystallization rates were used to calculate number of effective nuclei. It was found that the number of effective nuclei of the natural fiber-PP composites was higher than that of neat PP. The highest number of effective nuclei was found in rossells-PP composite. This suggested that natural fibers could act as nucleating agents for crystallization in the PP composites.

REFERENCES

Abdelmouleh, M., Boufi, S., Salah, A.B., Belgacem, M.N., and Gandini, A. (2002). Interaction of coupling agents with cellulose. **Langmuir.** 18: 3203-3208.

Albano, C., González, J., Ichazo, M., and Kaiser, D. (1999). Thermal stability of blends of polyolefins and sisal fiber. **Polym. Deg. Stab.** 66: 179-190.

Al-Qureshi., H.A. (2001). The application of jute fibre reinforced composites for the development of a car body. **UMIST Conference UK.**

Amash, A. and Zugenmaier, P. (1998). Study on cellulose and xylan filled polypropylene composites. **Polym. Bull.** 40(2-3): 251-258.

Amash, A. and Zugenmaier, P. (2000). Morphology and properties of isotropic and oriented samples of cellulose fiber-polypropylene composites. **Polymer.** 41: 1589-1596.

Amitay-Sadovsky, E., Cohen. S.R., and Wagner H.D. (1999). Anisotropic nanoindentation of transcrystalline polypropylene by scanning force microscope using blade-like tips. **Appl. Phys. Lett.** 74: 2966-2968.

Arbelaiz, A., Fernández, B., Ramos, J.A., and Mondragon, I. (2006). Thermal and crystallization studies of short flax fibre reinforced polypropylene matrix composites: Effect of treatments. **Thermochimica Acta.** 440: 111-121.

ARC-Institute for Industrial Crops (2006). **Sisal plant** [Online].Available: http://www.arc.agric.za/institutes/iic/main/topprojects/story.htm.

Arroyo, M., Lopez-Manchado, M.A., and Avalos, F., (1997). Crystallization kinetics of polypropylene: II. Effect of the addition of short glass fibers. **Polymer.** 38: 5587-5593.

Assouline, E., Pohl, S., Fulchiron, R., Gérard, J.-F, Lustiger, A., Wagner, H.D. and Marom, G., (1999). γ-transcrystallization in isotactic polypropylene-based composites promoted by aramid fibers. **J. Polym. Sci. Part B: Polym. Phys.** 37: 2534-2538.

Assouline, E., Pohl, S., Fulchiron, R., Gérard, J.-F, Lustiger, A., Wagner, H.D. and Marom, G., (2000). The kinetics of α and β transcrystallization in fiber-Reinforced polypropylene. **Polymer.** 41: 7843-7854.

Assouline, E., Wachtel, E., and Grigull, S. (2002). Lamellar orientation in transcrystalline γ isotactic polypropylene nucleated on aramid fibers. **Macromolecules.** 35: 403-409.

Avalos, F., Lopez–Manchado, M.A., and Arroyo, M. (1996). Crystallization kinetics of polypropylene: 1. Effect of small additions of low-density polyethylene. **Polymer.** 37: 5681-5688.

Avalos, F., Lopez-Manchado, M.A., and Arroyo, M. (1998). Cryatallization kinetics of polypropylene III. Ternary composite based on polypropylene/low density polypropylene blend matrices and short glass fibers. **Polymer.** 39: 6173-6178.

Avérous, L. and Boquillon, N. (2004). Biocomposites based on plasticized starch: Thermal and mechanical behaviours. **Carbo. Polym.** 56(2): 111-122.

Avérous, L. and Digabel, F. L. (2006). Properties of biocomposites based on lignocellulosic fillers. **Carbo. Polym.** 66(4): 480-493.

Avrami, M. (1939). Kinetics of phase change. I. General theory **J. Chem. Phy.** 7: 1103-1112.

Avrami, M. (1940). Kinetics of phase change. II. Transformation-time relations for random distribution of nuclei. **J. Chem. Phy.** 8: 212-224.

Avrami, M. (1941). Kinetics of phase change. III. Granulation, phase change, and microstructure. **J. Chem. Phy.** 9: 177-184.

Aziz, S.H. and Ansell, M.P. (2004). The effect of alkalization and alignment on the mechanical and thermal properties of kenaf and hemp bast fiber composites: Part 2-cashew nut shell liquid matrix. **Compos. Sci. Technol.** 64: 1231-1238.

Baiardo, F., Zini, E., and Scandola, M. (2004). Flax fiber-polyester composites. **Compos: Part A: Appl. Sci. Manufact.** 35: 703-710.

Barber, A.H., Wiesel, E., and Wagner, H.D. (2002). Crack deflection at a transcrystlline junction. **Compos. Sci. Technol.** 62: 1957-1964.

Bisanda, E.T.N. (2000). The effect of alkali treatment on the adhesion characteristics of sisal fibres. **Appl. Compos. Mater.** 7: 331-339.

Bisanda, E.T.N. and Ansell, M.P. (1992). Properties of sisal-CNSL composites. **J. Mater. Sci.** 27: 1690-1700.

Bledzki, A.K. and Gassan, J. (1999). Composites reinforced with cellulose based fibres. **Prog. Polym. Sci.** 24:221-274.

Blom, H.P., The, J.W., Bremner, T., and Rudin, A. (1998). Isothermal and non-Isothermal crystallization of PP: Effect of annealing and of the addition of HDPE. **Polymer.** 39: 4011-4022.

Cai, Y.Q., Petermann, J., and Wittich, H. (1997). Transcrystallization in fiber-reinforced isotactic polypropylene composites in a temperature gradient. **J. Appl. Polym. Sci.** 65: 67-75.

Cantero, G., Arbelaiz, A., Liano-Ponte, R., and Mondragon, I. (2003). Effect of fiber treatment on wettability and mechanical behaviour of flax/polypropylene composites. **Compos. Sci. Technol.** 63: 1247-1254.

Čermák, R., Obadal, M., Ponížil, P., Polášková, M., Stoklasa, K., and Lengálová, A. (2005). Injection-molded α- and β-polypropylenes: I. Structure vs. processing parameters. **Euro. Polym. J.** 41: 1838-1845.

Chand, N., Sood, S., Rohatgi, P.K., and Sayanarayana, K.G. (1984). Resources, structure, properties and uses of natural fibres of madhya pradesh. **J. Sci. Ind. Res**. 43: 489-499.

Cho, K., Li, F., and Choi, J. (1999). Crystallization and melting behavior of polypropylene and maleated polypropylene blends. **Polymer.** 40: 1719-1729.

Chual, C., Almdal, K., Poulsen, L., and Plackett, D. (2000). Conifer fibers as reinforcing materials for polypropylene-based composites. **J. Appl. Polym. Sci.** 80: 2833-2841.

Churdpunt, Y. and Isayev, A.I. (2000). Comparison of birefringence and mechanical properties of injection molded metallocene and Ziegler-Natta based isotactic polypropylenes. **J. Polym. Eng.**, 20:77-96.

Curvelo, A.A.S., De Cravalho, A.J.F., and Agnelli, J.A.M. (2001). Thermoplastic starch-cellulosic fibers composites: Preliminary results. **Carbo. Polym.** 45: 183-188.

Cyras, V.P., Kenny, J.M., and Vázqoez, A. (2001). Crystallization kinetics by differential scanning calorimetry for PCL/starch and their reinforced sisal fiber composites. **Polym. Eng. Sci.** 41: 1521-1528.

Czvikovszky, T. (1996). Electron-beam processing of wood fiber reinforced polypropylene. **Radiat. Phys. Chem.** 47: 425-430.

Dean, D.M.and Register, R.A. (1998). Oriented γ-isotactic polypropylene crystallized at atmospheric pressure. **J. Appl. Sci. Part B: Polym. Phys.** 36: 2821-2827.

Esteves, A.C.C, Borros-Timmons, A.M., Martins, J.A., Zhang, W., Cruz-Pinto, J., and Trindade, T. (2005). Crystallization behaviour of new poly(tetramethyleneterephthalamide) nanocomposites containing SiO_2 fillers with distinct morphologies. **Compos. Part: B** 36: 51-59.

Felix, J.M. and Gatenholm, P. (1994). Effect of transcrystalline morphology on interfacial adhesion in cellulose polypropylene composites. **J. Mater. Sci.** 29(11): 3043-3049.

Fitchmun, D.R. and Newman, S. (1970). Surface crystallization of polypropylene. **J. Polym. Sci. Part A-2: Polym. Phys.** 8: 1545-1564.

Fujiyama, M. (1995) In: J. Karger-Koscis editor. **Polypropylene Structure, Blends and Composites Vol. 1: Structure and Morphology** Chapman & Hall (Chapter 6).

Fung, K.L., Li, R.K.Y., and Tjong, S.C. (2002) Interface modification on properties of sisal fiber-reinforced polypropylene composites. **J. Appl. Polym. Sci.** 85: 169-176.

Gassan, J. (2002). A study of fibre and interface parameters affecting the fatigue behaviour of natural fiber composites. **Compos: Part A: Appl. Sci.Manufact.** 33: 369-374.

Gassan, J. and Bledzki, A.K. (1997). The influence of fiber-surface treatment on the mechanical properties of jute-polypropylene composites. **Compos. Part A: Appl. Sci. Manufact.** 28A: 1001-1005.

George, J. and Thomas, S. (1997). Short fiber-reinforced plastic composites. **Handbook of engineering polymeric materials.** In: Cheremisinoff NP. editor, Marcel Dekker Inc., New York, 811-837.

Gordon, B., Lim, A., and Douglas, R. L (1993). Isothermal crystallization of isotactic polypropylene in dotriacontane. I: Effect of nucleating agent addition on overall crystallization kinetics. **Polym. Eng. Sci.** 33:513-521.

Harper, D. and Wolcot, M. 2004. Interaction between coupling agent and lubricants in wood-polypropylene composites. **Compos. Part A: Appl. Sci. Manufact.** 35: 385-394.

Hata, T., Ohsaka, K., and Yamasa, T. (1994). Transcrystalline region of polypropylene-its formation, structure, and mechanical-properties. **J. Adhesion** 45: 125-135.

Hoffman, J.D., Davis, G.T., and Lauritzen, L.I. **Treatise on solid state chemistry: Crystalline and non-crystalline solids Vol. 3** In: Hannay JB Editor. Plenum, New York, 1976 (Chapter 7).

Iannace, S., Ali, R. and Nicolais, L. (2001). Effect of processing conditions on dimensions of sisal fibers in themoplastic biodegradable composites. **J. Appl. Polym. Sci.** 79: 1084-1091.

Ichazo, M.N., Albano, C., and González, J. (2000). Behavior of polyolefin blends with acetylaed sisal fibers. **Polym. Intern.** 49: 1409-1416.
iecred/pdf.

Isayev, A.I. and Catignani, B.F. (1996). Crystallization and microstructure in quenched slabs of various molecular weight polypropylene. **SPE ANTEC Tech. Papers**, 1815-1818.

Isayev, A.I., Churdpunt, Y., and Guo, X. (2000). Comparative study of Ziegler-Natta and metallocene based polypropylenes in injection molding. **Intern. Polym. Process.** 15: 72-82.

Jähn, A., Schröder, M.W., Füting, M., Schenzel, K., and Diepenbrock, W. (2002). Characterization of alkali treated flax fibres by means of FT raman spectroscopy and environmental scanning electron microscopy. **Spectrochem. Acta. Part A: Appl. Sci. Manufact.** 58: 2271-2279.

Jana, S.C. and Prieto, A. (2002(a)). Natural fiber composites of high-temperature thermoplastic polymers: Effects of coupling agents. **J. Appl. Polym. Sci.** 86: 2168-2173.

Jana, S.C. and Prieto, A. (2002(b)). On the development of natural fiber composites of high-temperature thermoplastic polymers. **J. Appl. Polym. Sci.** 86: 2159-2167.

Jarus, D., Scheibelhoffer, A., Hiltner, A., and Baer, E. (1996). The effect of skin-core morphology on the heat-deflection temperature of polypropylene. **J. App. Polym. Sci.** 60:209-219.

Jayaraman, K. (2003). Manufacturing sisal-polypropylene composites with minimum fiber degradation. **Compos. Sci. Technol.** 63: 367-374.

Jayaraman, P. and Bhattacharyys, D. (2004). Mechanical performance of woodfibre-waste plastic composite materials. **Resources, Conservation, and Recycling**. 41: 307-319.

Johannaber, F. (1994). **Injection Molding Machines: A User's Guide**, 3rd Edition, Hanser Publishers (Chapter 2).

Joseph, K. and Thomas, S. (1996). Effect of chemical treatment on the tensile properties of short sisal fibre-reinforced polyethylene composites. **Polymer.** 23: 5139-5149.

Joseph, K., Varghese, S., Kalaprasad, G., Thomas, S., Prasannakumari, L., Koshy, P., and Pavithran, C. (1996(a)). Influence of interfacial adhesion on the mechanical properties and fracture behaviour of short sisal fibre reinforced polymer composites. **Euro. Polym. J.** 32: 1243-1250.

Joseph, P.V., Joseph, K., and Thomas, S. (1999(b)). Effect of processing variables on the mechanical properties of sisal-fiber-reinforced polypropylene composites. **Compos. Sci. Technol.** 59: 1625-1640.

Joseph, P.V., Joseph, K., Thomas, S., Pillai, C.K.S., Prasad, V.S., Groeninckx, G., and Sarkissova, M., (2003). The thermal and crystallization studies of short sisal fibre reinforced polypropylene composites. **Compos. Part A: Appl. Sci. Manufact.** 34: 253-266.

Joseph, P.V., Mathew, G., Joseph, K., Groeninckx, G., and Thomas, S. (2003). Dynamic mechanical properties of short sisal fiber reinforced polypropylene composites. **Compos. Part A: Appl. Sci. Manufact.** 34: 275-290.

Joseph, P.V., Rabello, M.S., Mattoso, L.H.C., Joseph, K., and Thomas, S. (2002). Environmental effects on the degradation behaviour of sisal fibre reinforced polypropylene composites. **Compos. Sci. Technol.** 62: 1357-1372.

Kantz, M., Newman, H.D., and Stigale, F.H. (1972). The skin-core morphology and structure-property relationships in injection-molded polypropylene. **J. App. Polym. Sci.** 16:1249-1260.

Karger-Kocsis, J. (1995). **Polypropylene: Structure Blends and Composites, Vol. 1, Structure and Morphology**, Chapman & Hall, London (Chapter 3).

Karmaker, A.C. and Youngquist, J.A. (1996). Injection molding of polypropylene reinforced with short jute fibers. **J. Appl. Polym. Sci.** 62: 1147-1151.

Karnani, R., Krishnan, M., and Narayan, R. (1997). Biofiber-reinforced polypropylene composites. **Polym. Eng. Sci.** 37: 476-483.

Kawai, S., Ohnishi, K., Okudaira, Y., and Zhang, M. (2000). Manufacture of oriented fiberboard from kenaf bast fibers and its application to the composite panel. **Intern. Kenaf Symp.** 2000: 144-148.

Keener, T.J., Stuart, R.K., and Brown, T.K. (2004). Maleated coupling agents for natural fibre composites. **Compos. Part A: Appl. Sci. Manufact.** 35: 357-362.

Kim, K.H., Isayev, A.I., Kwon, K., and Sweden, C.V. (2005). Modeling and experimental study of birefringence in injection molding of semicrystalline polymers. **Polymer.** 46: 4183-4203.

Kim, S.H., Ahn, S.H., and Hirai, T. (2003). Crystallization kinetics and nucleation activity of silica nanoparticle-filled poly(ethylene 2,6-naphthalate). **Polymer.** 44: 5625-5634.

Kitayama, T., Utsumi, S., and Hamada, H. (2003). Interfacial propreties of PP/PP composites. **J. Appl. Polym. Sci.** 88: 2875-2883.

Kornfield Laboratory (2004). **Flow-induced crystallization.** [Online]. Available: http://cheme.che.caltech.edu/groups/jak/research/crystallization/images/skin-core.jpg.

Koscher, E. and Fulchiron, R. (2002). Influence of shear on polypropylene crystallization: Morphology development and kinetics. **Polymer.** 43:6931-6942.

Krevelen van DW. **Properties of polymer.** Elsevier Science, New York, 1997: 109-127.

Kumaraswamy, G., Verma, R.K., Issaian, A.M., Wang, P., Kornfield, J.A., Yeh, F., Hsiao, B.S., and Olley, R.H. (2000). Shear-enhanced crystallization in isotactic polypropylene Part 2. Analysis of the formation of the oriented skin. **Polymer.** 41: 8931-8940.

Li Y., Mai Y-W., and Ye, L. (2000). Sisal fibre and its composites: A review of recent developments. **Compos. Sci. Technol.** 60: 2037-2055.

Li, J.X. and Cheung, W.L. (1997). Effect of mould temperature on the formation of α/β polypropylene blends in injection molding. **J. Mater. Process. Tech.** 63: 472-475.

Li, Z.M., Li. L.B, and Shen, K.Z.(2004(a)). Transcrystalline morphology of an in situ microfibrillar poly(ethylene terephthalate)/polypropylene blend fabricated through slit-extrusion, hot stretch quenching process. **Macromol. Rapid Commun.** 25: 3275-3285.

Li, Z.M., Yang, M.B., and Feng, J.M. (2002(a)). Morphology of in-situ poly(ethylene terephthalate)/polyethylene microfiber reinforced composite formed via slit die extrusion and hot stretching. **Mater. Res. Bull.** 37: 2185-2198.

Li, Z.M., Yang, M.B., and Huang, R. (2002(b)). Poly(ethylene terephthalate)/polyethylene composite based on in-situ microfiber formation. **Polym. Plast. Eng. Technol.** 41: 19-32.

Li, Z.M., Yang, M.B., and Lu, A. (2002(c)). Tensile properties of poly(ethylene terephthalate) and polyethylene in-situ microfiber reinforced composite formed via slit die extrusion and hot-stretching. **Mater. Lett.** 56: 756-62.

Li, Z.M., Yang, W., and Li. L.B. (2004(b)). Morphology and nonisothermal crystallization of in situ microfibrillar poly(ethylene terephthalate)/polypropylene blend fabricated through slit-extrusion, hot stretch quenching. **J. Polym. Sci. Part B: Polym Phys.** 42: 374-385.

Lin, C.W., Lai, Y.C., and Liu, S.S. (2001). Effect of the surface roughness of sulfuric acid-anodized aluminium mold on the interfacial crystallization behavior of isotactic polypropylene. **J. Ashes Sci. Technol.** 15: 929-944.

López-Manchado, M.A. and Arroyo, M. (1999). Crystallization kinetics of polypropylene Part 4: Effect of unmodified and azide-modified PET and PA short fibres. **Polymer.** 40: 487-495.

López-Manchado, M.A., Biagiotti, J., Torre, L., and Kenny, M. (2000). Effects of reinforcing fibers on the crystallization of polypropylene. **Polym. Eng. Sci.** 40: 2194-2204.

Lu, X., Zhang, M.Q., Rong, M.Z., Shi, G., and Yang, G.C. (2003). Self-reinforced melt processable composites of sisal. **Compos. Sci. Technol.** 63:177-186.

Lundquist, L., Marque, B., Hagstrand, P.-O., Leterrier, Y., and Manson, J.-A.E. (2003). Novel pulp fibre reinforced thermoplastic composites. **Compos. Sci. Technol.** 63: 137-152.

Magurno, A. (1999). Vegetable fibres in automotive interior components. **Angew. Makromol. Chem.** 272: 99-107.

Maiti, P., Nam, P.H., and Okamoto, M. (2002). Influence of crystallization on intercalation, morphology, and mechanical properties of polypropylene/clay nanocomposites. **Macromolecules.** 35:2042-2049.

Martuscelli, E., Pracella, M., Volpe, G.D., and Greco, P. (1984). Morphology, crystallization, and thermal behaviour of isotactic polypropylene/low density polyethylene blends. **Makromol. Chem.** 185:1041-1061.

Mi, Y., Chen, X., and Guo, Q. (1997). Bamboo fiber-reinforced polypropylene composites: crystallization and interfacial morphology. **J. Appl. Polym. Sci.** 64: 1267-1273.

Midldner, I., and Bledzki, A.K. (1999). In: Proceedings of the Second International, **Wood Nat. Fiber Compos. Symposium.** Kassel, Germany, 17.

Mishra, S., Misra, M., Tripathy, S.S., Nayak, S.K., and Mohanty, A.K. (2001). Graft copolymerization of acrylonitrile on chemically modified sisal fibers. **Macromol. Mater. Eng.** 286: 107-113.

Mohanty, A.K., Khan, M.A., and Henrichsen, G. (2000). Surface modification of jute and its influence on performance of biodegradable jute-fabric/biopol composites. **Compos. Sci. Technol.** 60: 1115-1124.

Mucha, M., Marszalek, J., and Fidrych, A. (2000). Crystallization of isotactic polypropylene containing carbon black as a filler. **Polymer.** 41: 4137-4142.

Murherjee, P.S. and Satyanrayana, K.G. (1984). Structure and properties of some vegetable fibres, Part 1. Sisal fibre. **J. Mater. Sci.** 19: 3925-3934.

Murthy, N.S., Kagan, V.A., and Bray, R.G. (2002). Effect of melt temperature and skin-core morphology on the mechanical performance of nylon 6. **Polym. Eng. Sci.** 42: 940-950.

Murthy, N.S., Kagan, V.A., and Bray, R.G. (2003). Optimizing the mechanical performance in semi-crystalline polymers: Role of melt temperature and skin-core crystalline morphology of nylon. **J. Reinfo. Plast. Compos.** 22:685-694.

Mwaikambo, L.Y. and Ansell, M.P. (1999). The effect of chemical treatment on the properties of hemp, sisal, jute, and kapok for composite reinforcement. **Die. Angew. Makromol. Chem.** 272: 108-116.

Mwalkambo, L.Y. and Ansell, M.P. (2002). Chemical modification of hemp, sisal, jute, and kapok fibers by alkalization. **J. Appl. Polym. Sci**. 84: 2222-2234.

Nagaoka, T., Ishiaku, U.S., Tomari, T., Hamada, H., and Takashima, S. (2005). Effect of molding parameters on the properties of PP/PP sandwich injection moldings. **Polym. Test.** 24: 1062-1070.

Nagasawa, S., Fujimori, A., Masuko, T., and Iguchi, M. (2005). Crystallization of polypropylene containing nucleators. **Polymer.** 46: 5241-5250.

Naiki, M., Fukui, Y., and Matsumura, T. (2001). The effect of talc on the crystallization of isotactic polypropylene. **J. Appl. Polym. Sci.** 79: 1693-1703.

Nakamura, K., Katayama, K., and Amano, T. (1973). Some aspects of non-isothermal crystallization of polymers. II. Consideration of the isokinetic condition **J. Appl. Polym. Sci.** 17: 1031-1041.

Nakamura, K., Watanabe, T., Katayama, K., and Amano, T. (1972). Some aspects of non-isothermal crystallization of polymers. I. Relationship between crystallization temperature, crystallinty, and cooling condition. **J. Appl. Polym. Sci.** 16: 1077-1091.

Nishino, T., Hirao, K., Kotera, M., Nakamae, K., and Inagak, H. (2003). Kenaf reinforced biodegradable composite. **Compos. Sci. Technol.** 63: 1281-1286.

Nitta, K.H. and Yamamoto, Y. (2003). Morphology and mechanical properties of transcrystalline isotactic polypropylene. **E-Polymers. No.024:1-11.** [Online]. Available: http://www.epolymers.org.

Nowacki, R., Monasse, B., Piorkowska, E., Galeski, A., and Haudin, J.M. (2004). Spherulite nucleation in isotactic polypropylene based nanocomposites with montmorillonite under shear. **Polymer.** 45: 4877-4892.

Oksman, K. (2000). Mechanical properties of natural fibre mat reinforced thermoplastic. **Appl. Compos. Mater.** 7: 403-414.

OTOP-Thaitambon (2000). **OTOP 5 Stars.** [Online].Available: http://www.thaitambon.com.

Pande, H. and Roy, D.N. (1998). Influence of fibre morphology and chemical composition on the potential of kenaf fibers. **Pulp Paper Can.** 99: 31-34.

Papageorgious, G.Z., Achilias, D.S., Bikiaris, D.N., and Karayannidis, G.P. (2005). Crystallization kinetics and nucleation activity of filler in polypropylene/surface-treated SiO_2 nancomposites. **Thermochimica Acta.** 427: 117-128.

Paul, A., Joseph, K., and Thomas, S. (1997). Effect of surface treatments on the electrical properties of low-density polyethylene composites reinforced with short sisal fibers. **Compos. Sci. Technol.** 57: 67-79.

Peron, B., Lowe, A., and Baillie, C., (1996). The effect of transcrystallinity on the interfacial characteristics of polypropylene/alumina single fibre composites. **Compos. Part A: Appl. Sci. Manufact.** 27A: 839-845.

Pickering, K.L., Abdalla, A., Ji, C., McDonald, A.G., and Franich, R.A. (2003). The effect of silane coupling agents on radiata pine fibre for use in thermoplastic matrix composites. **Compos: Part A: Appl. Sci. Manufact.** 34: 915-926.

Pompe, G. and Mäder, E., (2000). Experimental detection of transcrystalline interphase in glass-fiber/polypropylene composites. **Compos. Sci. Technol.** 60: 2159-2167.

Pukánsky, B. (1995). **Polypropylene: Structure Blends and Composites, Vol. 3, Composites.** In: Karger-Kocsis J. Editor, Chapman & Hall, London (Chapter 1).

Quan, H., Li, Z., Yang, M., and Huang, R. (2005). On transcrystallinity in semi-crystalline polymer composites. **Compos. Sci. Technol.** 65: 999-1021.

Quillin, D.T., Caulfield, D.F., and Koutsky, J.A. (1993). Crystallinity in the polypropylene/cellulose system. I. Nucleation and crystalline morphology. **J. Polym Sci. Part B: Polym. Phys.** 50: 1187-1194.

Quillin, D.T., Caulfield, D.F., and Koutsky, J.A. (1994). Crystallinity in the polypropylene/cellulose system. II. Crystallization kinetics. **J. Polym Sci. Part B: Polym. Phys.** 52: 605-615.

Ramaswamy, G.N., Craft, S., and Wartelle, L. (1995). Uniformity and softness of kenaf fibres for textile products. **Textile. Res. J.** 65: 755-770.

Rana, A.K., Mandal, A., and Bandyopadhyay, S. (2003). Short jute fiber reinforced polypropylene composites: Effect of compatibiliser, impact modifier, and fiber loading. **Compos. Sci. Technol.** 63: 801-806.

Ray, D. and Sarkar, B.K. (2000). Characterization of alkali-treated jute fibers for physical and mechanical properties. **J. Appl. Polym. Sci.** 80: 1013-1020.

Ray, D., Sakar, B.K., and Rana, A.K. (2002). Study of the thermal behavior of alkali treated jute fibers. J**. Appl. Polym. Sci.** 85: 2594-2599.

Román-Aguirre, M., Márquez-Lucero, A., and Zaragoza-Contreras, E.A. (2004). Elucidating the graft copolymerization of methyl methacrylate onto wood-fiber. **Carbo. Polym**. 55: 201-210.

Rong, M.Z., Zhang, M.Q., Liu, Y., Yang, G.C., and Zeng, H.M. (2001). The effect of fiber treatment on the techanical properties of unidirectional sisal-reinforced epoxy composites. **Compos. Sci. Technol.** 61: 1437-1447.

Roongtanakiat, N. and Chairoj, P. (2002). Vetiver grass for remedying soil contaminated with heavy metals. **Presentation: Poster 17th WCSS, 14-12 August 2002, Thailand**. 1962: 1-8.

Rosato, D.V., Rosato, D.V., and Rosato, M.G. (2000). **Injection molding handbook**, 3rd Edition. Springer-Verleg (Chapter 4).

Rowell, R.M. (1997). Agro-fiber composites: Exploring the limits. **Proceedings of the 18th Risø International Symposium on Materials Science: Polymeric Composites–Expanding the Limits Denmark**.127-133.

Rowell, R.M., Hun, J.S., and Rowell, J.S. (2000). Characterization and factors effecting fiber properties. **Nat. Polym. Agrofibers Compos.** San Carlos-Brasil. 115-134.

Ruksakulpiwat, Y., Suppakarn, N., Sutapun, W., and Thomthong, W. (2003). The study of using vetiver grass as a filler in polypropylene composites. **SPE Tech. Paper.** 1641-1645.

Ruksakulpiwat, Y., Suppakarn, N., Sutapun, W., and Thomthong, W. (2007). Vetiver-polypropylene composites: Physical and mechanical properties. **Compos. Part A: Appl. Sci. Manufact.** 38: 590-601.

Ruseckaite, C.R. and Jiménez, A. (2003). Thermal degradation of mixtures of polycaprolactone with cellulose derivatives. **Polym. Deg. Stab.** 81(2): 353-358.

Sain, M., Park, S.H., Suhara, F., and Law, S. (2004). Flame retardant and mechanical properties of natural fibre-PP composites containing magnesium hydroxide. **Polym. Deg. Stab.** 83: 363-367.

Sanadi, A.R. and Caulfield, D.F. (2000). Transcrystalline interphases in natural fiber-PP composites: Effect of coupling agent. **Compos. Interface.** 7: 31-43.

Sanadi, A.R., Caulfield, D.F., Jacobson, R.E., and Rowell, R.M. (1995). Renewable agricultural fibers as reinforcing fillers in plastics: Mechanical properties of kenaf fiber-polypropylene composites. **Ind. Eng. Chem. Res.** 34: 1889-1896.

Saujanya, C. and Radhakrishnan, S. (2001(a)). Development of a transcrystalline phase in polypropylene at the PET interface. **Macromol. Mater. Eng.** 286:1-4.

Saujanya, C. and Radhakrishnan, S. (2001(b)). Structure development and properties of PET fiber filled PP composites. **Polymer.** 42: 4537-4548.

Schonhorn, H., Ryan, F.W. (1968). Effect of morphology in the surface region of polymers on adhesion and adhesive joint strength. **J. Polym. Sci.** 6: 231-240.

Schrauwen, B.A.G., Breemen, L.C.A.V., Spoelstra, A.B., Govaert, L.E., Peters, G.W.M., and Meijer, H.E.H. (2004). Structure, deformation, and failure of flow-oriented semicrystalline polymers. **Macromolecules.** 37: 8618-8633.

Schuh, T.G. (2004). **Renewable materials for automotive applications** [Online]. Available: www.ienica.net/fibresseminar/schuh.pdf.

Seki, M., Thurman, D.W., Oberhauser, J. P., and Kornfield, J.A. (2002). Shear−mediated crystallization of isotactic polypropylene: The role of long chain−long−chain overlap. **Macromolecules.** 35:2583-2594.

Seo, Y., Kim, J., Kim, K.U., and Kim, Y.C., (2000). Study of the crystallization behaviors of polypropylene and maleic anhydride grafted polypropylene. **Polymer.** 41: 2639-2646.

Singh, B, Gupta, M., Verma A., and Tyagi, O. (2000(a)). FT-IR microscopic studies on coupling agents: Treated natural fibres. **Polym. Intern.** 49: 1444-1451.

Singh, B., Gupta M., and Verma, A. (2000(b)). The durability of jute fibre-reinforced phenolic composites. **Compos. Sci. Technol.** 60: 581-589.

Sjönell, Y., Terselius, B., and Jansson, J-F. (1995). Injection molding of polypropylene discs, I: Effect of holding pressure on orientation distribution. **Polym. Eng. Sci.** 35: 950-956.

Somnuk, U., Ruksakulpiwat, Y., Suppakarn, N., and Sutapun, W. (2004). Characterization of chemical treated vetiver grass. **3rd Thailand Materials Science and Technology Conference Bangkok Thailand**. PP17: 420-422.

Son, S.J., Lee, Y.M., and Im, S.S. (2000(a)). Transcrystalline morphology and mechanical properties in polypropylene composites containing cellulose treated with sodium hydroxide and cellulose. **J. Mater. Sci.** 35:5767-5778.

Son, Y., Ahn, K.H., and Char, K. (2000(b)). Morphology of injection molded modified poly(phenylene oxide)/polyamide-6 blends. **Polym. Eng. Sci.** 40: 1376-1384.

Sreekala, M.S. and Thomas, S. (2003). Effect of fibre surface modification on water-sorption characteristics of oil palm fibres. **Compos. Sci. Technol.** 63: 861-859.

Strebel, J.J., Mirabella, F., Blythe, C., and Pham, T. (2004). Injection molded automotive TPO-A mulitlayer composite structure of varied orientations. **Polym. Eng. Sci.** 44: 1588-1593.

Sukhanova, T.E., Lednicky, F., and Urban, J. (1995). Morphology of melt crystallized polypropylene in the presence of polyimide fibers. **J. Mater Sci.** 30: 2201-2214.

Taylor, J. (2004). **Agricultural fibres for product design and development** [Online].Available: http://jasont.media.mit.edu/papers.

Thai Junior Encyclopedia Project by Royal Commanded of H.M. the King (1999). ปอแก้ว ปอกระเจา [Online].Available:http://www.kanchanapichek.or.th/ kp6/Book17/

The Chaipattana Foundation (2005). **Vetiver grass** [Online].Available: http://www.chaipat.or.th/intranet/article/vetiver/vetiver_t.html

Thielemans, W. and Wool, R.P. (2004). Butyrated kraft lignin as compatibilizing agent natural fiber reinforced thermoset composites. **Compos: Part A: Appl. Sci. Manufact.** 35: 327-338.

Thomason, J.L. and Van Rooyen, A.A. (1992). Transcrystallized interphase in thermoplastic composites. I. Influence of fiber type and crystallization temperature. **J. Mater. Sci.** 27: 889-896.

Thuamthong, W., Ruksakulpiwat, Y., Suppakarn N., and Sutapun, W. (2004). Effect of vetiver contents and vetiver lengths on mechanical and morphological properties of vetiver-polypropylene composite. **3rd Thailand Materials Science and Technology Conference Bangkok Thailand**. P17: 167-169.

Thuamthong, W., Ruksakulpiwat, Y., Suppakarn, N., and Sutapun, W. (2003). Thermal, rheological, mechanical and morphological properties of vetiver-polypropylene composite. **8th Pacific Polymer Conference Bangkok Thailand**. 194: 118.

Ton-That, T.M. and Jungnickel, B.J. (1999). Water diffusion into transcrystalline layers on polypropylene. **J. Appl. Polym. Sci.** 74:3275-3285.

Trotignon, J. P. and Verdu, J. (1990). Effect of the holding pressure on the skin-core morphology of injection-molded polypropylene parts. **J. Appl. Polym. Sci.** 39: 1215-1217.

Valadez-Gonzalez, A., Cervantes-Uc, J.M., Olayo, R., and Herrera-Franco, P.J. (1999(a)). Effect of fiber treatment fiber surface treatment on the fiber-matrix bond strength of natural fiber reinforced composites. **Compos. Part B: Eng**. 30: 309-320.

Valadez-Gonzalez, A., Cervantes-Uc, J.M., Olayo, R., and Herrera-Franco, P.J. (1999(b)). Chemical modification of henequén fibers with an organosilane coupling agent. **Compos. Part B: Eng**. 30: 321-331.

Van De Velde, K. and Kiekens, P. (2003). Effect of material and parameters on the mechanical properties of unidirectional and multidirectional flax/polypropylene composites. **Compos. Structures.** 62: 443-448.

Varga, J. (2005). **Polypropylene: Structure Blends and Composites, Vol. 1, Structure and Morphology.** In: Karger-Kocsis J. editor. Chapman & Hall, London (Chapter 3).

Varga, J. and Karger-Kocsis, J., (1995). Interfacial morphologies in carbon fiber-reinforced polypropylene microcomposites. **Polymer.** 36: 4877-4881.

Viana, J.C. (2004). Development of the skin layer in injection moulding: Phenomenological model. **Polymer.** 45: 993-1005.

Wang, C. and Hwang, L.M. (1996(a)). Transcrystallization of PTFE fiber/PP composites. I. Crystallization kinetics and morphology. **J. Polym. Sci. Part B: Polym. Phys.** 34: 47-56.

Wang, C. and Liu, C.-R. (1997). Transcrystallization of polypropylene on carbon fibers. **Polymer.** 38: 4715-4718.

Wang, C. and Liu, C-R. (1998). Transcrystallization of PTFE fiber PP composites. III. Effect of fiber pulling on the crystallization kinetics. **J. Polym. Sci. Part B: Polym. Phys.** 36: 1361-1370.

Wang, C. and Liu, C-R. (1999). Transcrystallization of polypropylene composites: Nucleating ability of fibers. **Polymer.** 40: 289-298.

Wang, H. and Hwang, L.M. (1996(b)). Transcrystallization of PTFE fiber/PP composites. II. Effect of transcrystallinity on the interfacial strength. **Polym. Sci. Part B: Polym. Phys.** 34: 1435-1442.

Wang, K., Wu, J., and Zeng, H. (2003). Radial growth rate of spherulites in polypropylene/barium sulfate composites. **Euro. Polym. J.** 39: 1647-1652.

Wibowo, A., Mohanty, A.K., Misra, M., and Drzal, L.T. (2004). **Chopped industrial hemp reinforced cellulosic plastic biocomposites: Thermomechanical and morphological Properties.** [Online].Available: http//pubs.acs.org/cgibin/asap.cgi/

Wu, C.M., Chen, M., Karger-Kocsis, J. (2001). Effect of micromorphologic features on the interfacial strength of iPP/Kevlar fiber microcomposites**. Polymer.** 42: 199-208.

Xu, T., Lei, H., and Xie, C.S. (2003). The effect of nucleating agent on the crystalline morphology of polypropylene (PP). **Material Design.** 24: 227-230.

Zafeiropoulos, N.E, Baillie, C.A., and Matthews, F.L. (2001). A study of transcrystallization and its effect on the interface in flax fibre reinforced composite materials. **Compos. Part A: Appl. Sci. Manufact.** 32: 525-543.

Zafeiropoulos, N.E., Baille, C.A., and Hodgkinson, J.M. (2002(a)). Engineering and characterisation of the interface in flax fibre/polypropylene composite materials. Part II. The effect of surface treatments on the interface. **Compos. Part A: Appl. Sci. Manufact.** 33: 1185-1190.

Zafeiropoulos, N.E., Williams, D.R., Baille, C.A., and Matthews, F.L. (2002(b)). Engineering and characterisation of the interface in flax fibre/polypropylene composite materials. Part I. Development and investigation of surface treatments. **Compos. Part A: Appl. Sci. Manufact.** 33: 1083-1093.

APPENDIX A

ASPECT RATIO OF NATURAL FIBERS IN

PP COMPOSITES AFTER PROCESSING

Table A1 Aspect ratio of vetiver fiber in PP composite after processing.

No.	Length (μm)	Diameter (μm)	L/D
1	218.66	38.15	5.73
2	179.69	41.19	4.36
3	190.57	40.07	4.76
4	209.19	39.38	5.31
5	177.63	49.88	3.56
6	215.32	30.56	7.05
7	146.11	40.99	3.57
8	140.63	50.73	2.77
9	202.41	58.73	3.45
10	306.79	50.55	6.07
11	209.25	35.75	5.85
12	394.95	92.75	4.26
13	157.85	51.39	3.07
14	225.27	55.68	4.05
15	281.03	49.26	5.71
16	183.56	24.78	7.41
17	173.50	57.54	3.02
18	151.22	45.17	3.35
19	191.42	48.91	3.91
20	163.36	40.84	4.00
21	187.87	54.24	3.46
22	154.42	58.1	2.66
23	193.66	68.96	2.81

Table A1 Aspect ratio of vetiver fiber in PP composite after processing (Continued).

No.	Length (μm)	Diameter (μm)	L/D
24	143.18	65.77	2.18
25	185.48	40.46	4.58
26	213.06	38.47	5.54
27	140.88	35.88	3.93
28	263.41	63.87	4.12
29	304.73	34.93	8.72
30	218.05	56.47	3.86
31	263.24	52.05	5.06
32	178.24	50.59	3.52
33	169.81	53.61	3.17
34	237.14	33.76	7.02
35	235.84	61.83	3.81
36	182.36	43.22	4.22
37	262.47	49.88	5.26
38	382.97	37.91	10.10
39	264.23	45.84	5.76
40	315.44	34.70	9.10
41	289.54	60.17	4.81
42	183.10	53.66	3.41
43	146.10	33.98	4.30
44	194.40	44.63	4.36
45	361.66	37.99	9.52
46	228.22	41.68	5.48

Table A1 Aspect ratio of vetiver fiber in PP composite after processing (Continued).

No.	Length (μm)	Diameter (μm)	L/D
47	172.49	39.68	4.35
48	106.88	44.14	2.42
49	201.25	28.50	7.06
50	117.00	50.21	2.33
51	161.02	36.23	4.44
52	168.88	46.38	3.64
53	169.91	49.45	3.44
54	169.18	35.70	4.74
55	150.75	42.67	3.53
56	254.62	54.80	4.65
57	201.25	49.00	4.11
58	200.77	43.93	4.57
59	267.43	26.96	9.92
60	381.47	49.35	7.73
61	239.28	27.25	8.78
62	232.04	46.18	5.03
63	157.16	44.98	3.49
64	158.03	66.07	2.39
65	229.63	89.23	2.57
66	145.31	29.70	4.89
67	165.38	52.50	3.15
68	273.47	54.92	4.98
69	192.50	40.25	4.78

Table A1 Aspect ratio of vetiver fiber in PP composite after processing (Continued).

No.	Length (μm)	Diameter (μm)	L/D
70	153.69	49.19	3.12
71	203.19	44.84	4.53
72	101.08	53.06	1.91
73	133.10	34.13	3.90
74	195.05	18.27	10.68
75	198.13	48.91	4.05
76	161.73	42.33	3.82
77	215.28	33.12	6.50
78	212.62	81.38	2.61
79	199.32	39.53	5.04
80	155.66	47.19	3.30
81	255.70	45.84	5.58
82	201.76	68.25	2.96
83	232.03	97.58	2.38
84	336.88	46.38	7.26
85	215.37	60.20	3.58
86	212.38	44.59	4.76
87	199.73	43.09	4.64
88	245.41	25.38	9.67
89	133.14	45.79	2.91
90	416.50	40.25	10.35
91	263.00	30.22	8.70
92	148.71	23.88	6.23

Table A1 Aspect ratio of vetiver fiber in PP composite after processing (Continued).

No.	Length (μm)	Diameter (μm)	L/D
93	217.89	33.26	6.55
94	183.47	53.97	3.40
95	220.11	38.38	5.74
96	165.75	50.30	3.30
97	353.26	74.87	4.72
98	148.56	50.36	2.95
99	144.36	16.35	8.83
100	218.86	20.35	10.76
Average	**209.75**	**46.44**	**4.94**
S.D.	**63.83**	**14.42**	**2.15**

Table A2 Aspect ratio of rossells fiber in PP composite after processing.

No.	Length (μm)	Diameter (μm)	L/D
1	369.87	19.19	19.27
2	428.28	49.88	8.59
3	213.35	45.63	4.68
4	244.71	15.77	15.52
5	199.30	21.94	9.10
6	294.32	14.14	20.82
7	442.54	37.64	11.76
8	334.64	37.12	9.02
9	242.00	41.09	5.89
10	370.55	19.66	18.85
11	221.24	45.68	4.84
12	474.61	33.49	14.17
13	423.81	36.26	11.69
14	378.40	19.97	18.95
15	318.78	38.74	8.23
16	228.92	34.67	6.60
17	314.33	23.80	13.21
18	324.79	23.25	13.97
19	265.82	27.35	9.72
20	646.00	34.04	18.98
21	505.30	32.48	15.56
22	632.10	60.68	10.42
23	609.29	30.94	19.70

Table A2 Aspect ratio of rossells fiber in PP composite after processing (Continued).

No.	Length (μm)	Diameter (μm)	L/D
24	472.93	24.07	19.65
25	656.28	30.94	21.21
26	251.69	19.43	12.95
27	533.44	71.94	7.42
28	367.85	23.48	15.67
29	352.77	26.25	13.44
30	284.26	17.50	16.24
31	371.69	36.32	10.52
32	480.00	31.61	15.19
33	218.80	27.48	7.96
34	427.68	102.58	4.17
35	381.16	21.88	17.42
36	402.53	45.77	8.80
37	406.29	48.32	8.41
38	581.57	51.69	11.25
39	447.83	39.94	11.21
40	327.37	24.5	13.36
41	501.62	49.53	10.13
42	455.21	26.26	17.34
43	216.47	17.26	12.54
44	538.47	73.30	7.35
45	316.19	23.80	13.29
46	319.33	21.88	14.60

184

Table A2 Aspect ratio of rossells fiber in PP composite after processing (Continued).

No.	Length (μm)	Diameter (μm)	L/D
47	447.56	67.24	6.66
48	438.55	43.55	10.07
49	340.61	27.18	12.532
50	196.31	25.48	7.70
51	419.42	31.50	13.32
52	503.87	47.97	10.50
53	482.53	50.58	9.54
54	629.41	25.24	24.94
55	313.06	41.13	7.61
56	475.39	62.18	7.65
57	372.54	31.72	11.75
58	385.35	39.18	9.84
59	395.79	22.03	17.97
60	408.53	32.13	12.72
61	432.59	33.50	12.91
62	292.63	17.85	16.40
63	491.95	33.43	14.72
64	382.13	46.70	8.19
65	314.08	83.80	3.75
66	506.74	13.01	38.95
67	599.19	28.46	21.06
68	462.99	41.87	11.06
69	306.13	21.61	14.17

Table A2 Aspect ratio of rossells fiber in PP composite after processing (Continued).

No.	Length (μm)	Diameter (μm)	L/D
70	276.77	31.56	8.77
71	498.71	39.68	12.57
72	446.82	37.99	11.77
73	380.06	46.20	8.23
74	370.26	36.43	10.16
75	407.13	24.39	16.70
76	273.75	16.99	16.11
77	230.59	26.71	8.63
78	249.99	19.66	12.72
79	455.79	30.96	14.72
80	246.75	23.63	10.44
81	533.31	69.17	7.71
82	358.50	32.95	10.88
83	318.16	28.34	11.23
84	358.18	22.31	16.06
85	475.13	27.79	17.10
86	314.40	19.19	16.38
87	215.08	28.88	7.45
88	445.70	21.88	20.37
89	490.14	41.87	11.71
90	409.02	30.94	13.22
91	417.70	58.94	7.09
92	481.94	24.66	19.54

Table A2 Aspect ratio of rossells fiber in PP composite after processing (Continued).

No.	Length (μm)	Diameter (μm)	L/D
93	299.27	25.44	11.76
94	298.12	19.84	15.03
95	440.30	48.54	9.07
96	458.09	27.22	16.83
97	494.81	43.23	11.45
98	430.73	17.50	24.61
99	372.19	56.88	6.54
100	513.45	34.65	14.82
Average	**393.53**	**34.80**	**12.83**
S.D.	**109.80**	**15.82**	**5.26**

Table A3 Aspect ratio of sisal fiber in PP composite after processing.

No.	Length (μm)	Diameter (μm)	L/D
1	408.82	70.53	5.80
2	313.25	34.13	9.18
3	345.56	80.67	4.29
4	533.75	34.17	15.62
5	267.16	64.09	4.17
6	719.60	39.57	18.19
7	356.77	41.46	8.61
8	315.44	60.95	5.18
9	441.32	61.65	7.16
10	858.39	84.23	10.191
11	503.59	65.04	7.74
12	395.65	69.17	5.72
13	311.56	64.83	4.81
14	753.08	64.09	11.75
15	425.26	60.89	6.98
16	355.69	45.68	7.79
17	419.10	87.29	4.80
18	307.41	50.09	6.14
19	879.24	78.15	11.25
20	675.44	40.26	16.78
21	456.49	24.52	18.62
22	455.75	48.22	9.45
23	466.50	50.27	9.280

Table A3 Aspect ratio of sisal fiber in PP composite after processing (Continued).

No.	Length (μm)	Diameter (μm)	L/D
24	426.66	49.75	8.58
25	385.10	40.37	9.54
26	566.26	49.75	11.38
27	455.44	40.29	11.30
28	541.63	67.38	8.04
29	468.21	57.62	8.13
30	493.86	58.28	8.48
31	603.12	45.94	13.13
32	494.94	57.40	8.62
33	440.14	62.22	7.07
34	684.76	42.00	16.30
35	865.58	84.59	10.233
36	946.54	89.62	10.56
37	689.10	51.39	13.41
38	300.60	56.74	5.30
39	660.86	73.96	8.94
40	698.11	46.33	15.07
41	684.63	47.02	14.56
42	432.93	37.08	11.68
43	401.88	43.45	9.25
44	561.55	60.65	9.26
45	541.51	74.46	7.27
46	356.53	45.50	7.83

Table A3 Aspect ratio of sisal fiber in PP composite after processing (Continued).

No.	Length (μm)	Diameter (μm)	L/D
47	269.30	62.66	4.30
48	553.14	86.50	6.40
49	727.81	42.07	17.30
50	545.57	68.68	7.94
51	535.20	53.21	10.06
52	481.65	40.70	11.83
53	755.43	69.13	10.93
54	531.87	46.44	11.45
55	498.29	46.61	10.69
56	496.52	111.66	4.45
57	480.52	93.53	5.14
58	671.75	64.38	10.43
59	324.41	44.72	7.26
60	780.23	42.09	18.54
61	590.40	58.94	10.02
62	532.41	79.99	6.66
63	593.64	56.44	10.52
64	580.21	52.68	11.01
65	848.18	74.91	11.32
66	688.30	43.52	15.82
67	620.57	57.26	10.84
68	509.48	28.57	17.83
69	540.13	73.39	7.36

Table A3 Aspect ratio of sisal fiber in PP composite after processing (Continued).

No.	Length (μm)	Diameter (μm)	L/D
70	602.73	72.33	8.33
71	452.23	41.57	10.88
72	651.12	52.22	12.47
73	452.29	63.18	7.16
74	687.71	33.43	20.57
75	532.76	47.68	11.17
76	501.67	42.09	11.92
77	348.53	59.73	5.84
78	701.46	70.53	9.95
79	372.63	80.9	4.61
80	415.03	43.73	9.49
81	384.57	38.03	10.11
82	500.88	126.95	3.95
83	541.55	47.04	11.51
84	440.53	35.53	12.40
85	751.83	69.4	10.83
86	666.03	59.22	11.25
87	667.77	69.68	9.58
88	487.57	80.24	6.08
89	638.17	74.99	8.51
90	589.25	61.26	9.62
91	562.33	40.25	13.97
92	442.35	95.66	4.62

Table A3 Aspect ratio of sisal fiber in PP composite after processing (Continued).

No.	Length (μm)	Diameter (μm)	L/D
93	595.79	52.69	11.31
94	635.75	77.91	8.16
95	760.12	53.66	14.17
96	375.30	81.35	4.61
97	477.76	34.04	14.04
98	308.21	26.32	11.71
99	477.76	34.04	14.04
100	308.21	26.32	11.71
Average	**531.50**	**57.92**	**9.96**
S.D.	**151.600**	**18.77**	**3.71**

APPENDIX B

PRESENTATIONS, PABLICATIONS, AND AWARD

PRESENTATIONS

Usa Somnuk, Yupaporn Ruksakulpiwat, Nitinat Suppakarn, and Wimonlak Sutapun. (10-11 August 2004). Characterization of chemical treated vetiver grass. **The 3rd Thailand Material Science and Technology Conference**, Miracle Grand Convention Hotel, Bangkok, Thailand.

Usa Somnuk, Wimonlak Sutapun, Nitinat Suppakarn, Pranee Phinyocheep, and Yupaporn Ruksakulpiwat. (18-20 October 2005). Effect of processing conditions on shear-induced crystallization of vetiver grass polypropylene composites. **The 31st Congress on Science and Technology of Thailand**, Technopolis, Suranaree University of Technology, Nakhon Ratchasima, Thailand.

Yupaporn Ruksakulpiwat, Jongrak Kluengsamrong, **Usa Somnuk**, Wimonlak Sutapun, and Nitinat Suppakarn. (18-20 October 2005). Comparison of rheological properties and mechanical properties of polypropylene composites from various types of natural fibers. **The 31st Congress on Science and Technology of Thailand**, Technopolis, Suranaree University of Technology, Nakhon Ratchasima, Thailand.

Usa Somnuk, Nitinat Suppakarn, Wimonlak Sutapun, and Yupaporn Ruksakulpiwat (5-9 February 2006). Injcetion molding of vetiver grass-polypropylene composites: Effect of particle sizes on rheological, thermal and mechanical Properties. **The 28th Australasian Polymer Symposium and Australasian Society for Biomaterials 16th Annual Conference**, Rotorua, New Zealand.

Yupaporn Ruksakulpiwat, **Usa Somnuk**, Pranee Phinyocheep, Nitinat Suppakarn, and Wimonlak Sutapun (5-9 February 2006). Effect of particle sizes of vetiver grass on shear-induced crystallization of injection molded vetiver grass-polypropylene composites.**The 28th Australasian Polymer Symposium and Australasian Society for Biomaterials 16th Annual Conference**, Rotorua, New Zealand.

Yupaporn Ruksakulpiwat, **Usa Somnuk**, Pranee Phinyocheep, Nitinat Suppakarn, and Wimonlak Sutapun (7-11 May 2006). Shear-induced crystallization of natural fiber-polypropylene composites. **SPE Annual Technical Conference 2006 (ANTEC 2006)**, Charlotte, North Carolina, USA.

Usa Somnuk, Pranee Phinyocheep, Nitinat Suppakarn, Wimonlak Sutapun, and Yupaporn Ruksakulpiwat (28-31 May 2006). Effect of processing conditions on crystallization of vetiver grass-polypropylene composites. **The 4th East-Asian Polymer Conference 2006**, Tianjin, China.

อุษา สมนึก, ปราณี ภิญโญชีพ, นิธินาถ ศุภกาญจน์, วิมลลักษณ์ สุตะพันธ์, ยุพาพร รักสกุลพิวัตน์ (24-25 พฤษภาคม 2550). การศึกษาการใช้ประโยชน์จากหญ้าแฝกเป็นสารตัวเติมในพอลิโพรพิลีนคอมพอสิท, **การประชุมวิชาการ เรื่อง 80 พรรษา พัฒนาวิชาการหญ้าแฝก** กรมพัฒนาที่ดิน กรุงเทพมหานคร

PUBLICATIONS

Usa Somnuk, Gerhard Eder, Pranee Phinyocheep, Nitinat Suppakarn, Wimonlak Sutapun, and Yupaporn Ruksakulpiwat. Quiescent crystallization of natural fibers-polypropylene composites (2007). **Journal of Applied Polymer Science** Issue 5, Vol. 106, 2997-3006.

Usa Somnuk, Nitinat Suppakarn, Wimonlak Sutapun, and Yupaporn Ruksakulpiwat. Shear-induced crystallization of injection molded vetiver grass-polypropylene composites. **Journal of Applied Polymer Science** (Submitted).

AWARD

Certificate of Excellence for the King of Thailand Vetiver Award-ICV4 (2006) in the topic of "An investigation of using vetiver grass in polypropylene composites". **The Forth International Conference on Vetiver-ICV4**, Caracas, Venezuela.

BIOGRAPHY

Miss Usa Somnuk was born on July 13, 1977 in Bangkok, Thailand. She received her Bachelor's Degree in Science (Chemistry) from Mahidol University in 1999. She then earned her Master's Degree in Polymer Science from Petroleum and Petrochemical College, Chulalongkorn University in 2001. After that, she continued with her graduate study in Polymer Engineering Program, Institute of Engineering, Suranaree University of Technology. Her expertise is in the field of polymer processing, polymer characterization, and polymer composites. During her doctoral degree study, she presented four papers in Thailand and four papers in aboard. She also published two papers in Journal of Applied Polymer Science as shown in Appendix B. In addition, she received a "Certificate of Excellence for the King of Thailand Vetiver Award-ICV4" in the topic of "An investigation of using vetiver grass in polypropylene composites" from Chaipattana Foundation (see Appendix B).